

DISSERTATION

zur Erlangung des Doktorgrades der Fakultät für
Chemie und Pharmazie der Ludwig Maximilians
Universität München

HIGH-RESOLUTION STRUCTURE OF THE HUMAN TRANSLATION TERMINATION COMPLEX

Sarah Matheisl

aus
Deggendorf, Deutschland

2016

Erklärung

Diese Dissertation wurde im Sinne von § 7 der Promotionsordnung vom 28. November 2011 von Herrn Prof. Dr. Roland Beckmann betreut.

Eidesstattliche Versicherung

Diese Dissertation wurde eigenständig und ohne unerlaubte Hilfe erarbeitet.

München, den 08.06.2016

Sarah Matheisl

Dissertation eingereicht am 10.06.2016

1. Gutachter: Prof. Dr. Roland Beckmann
2. Gutachter: Dr. Daniel Wilson

Mündliche Prüfung am 04.08.2016

I. Table of Contents

I.	Table of Contents	02
II.	List of Abbreviations	05
1.	Introduction	10
1.1	The Ribosome	10
1.1.1	An Overview	10
1.1.2	The Three Kingdoms of Life	12
1.2	The Eukaryotic Translation Cycle	13
1.2.1	Initiation	14
1.2.2	Elongation	18
1.2.3	Termination and Recycling	24
1.2.4	<i>In vitro</i> Translation Systems	32
1.2.5	Co- and Post-translational Protein Folding	32
1.3	Translational Arrest by Nascent Polypeptides	34
1.3.1	Features and Functions	34
1.3.2	The Human Cytomegalovirus gp48/UL4 uORF2 Nascent Polypeptide	38
1.3.3	Stalling as Tool for Programming Ribosomes <i>in vitro</i>	40
1.4	Structural Analysis of Macromolecular Complexes: Cryo-Electron Microscopy in the New Era	41
1.5	Aims of the Thesis	44
2.	Materials and Methods	46
2.1	Molecular Cloning	46
2.1.1	Plasmids and Strains	46
2.1.2	Polymerase Chain Reaction-based Methods	47
2.1.3	Purification of DNA Fragments	53
2.1.4	Enzymatic Digestion with DpnI	54
2.1.5	Ligation	54
2.1.6	Preparation of Chemical Competent <i>Escherichia coli</i> Cells	54
2.1.7	Transformation and Plasmid Isolation	54
2.1.8	DNA Sequencing Reaction	55
2.2	Protein Analysis	56
2.2.1	Determination of Protein Concentration	56
2.2.2	Protein Precipitation	56
2.2.3	Sodium Dodecyl Sulfate-polyacrylamide Gel Electrophoresis	56
2.2.4	Semi-dry Western Blotting	57
2.2.5	Mass Spectrometry	58
2.3	Protein Expression and Purification	58
2.3.1	General Procedures	59
2.3.2	Human Δ(1-46)Jmjd4	60
2.3.3	Human eRF1	60
2.3.4	Human eRF1 Co-expression with Δ(1-46)Jmjd4 for <i>in vivo</i> Hydroxylation	61
2.3.5	Human Δ(1-138)eRF3a	61

2.3.6	Guanosine Triphosphatase Deficient Mutants of Human Δ(1-138)eRF3a	62
2.3.7	Human eRF3a Full Length	62
2.3.8	Human eRF1:eRF3a Complex Formation	62
2.3.9	Co-purification of the Human eRF1:Δ(1-138)eRF3a Complex (Co-expressed with Δ(1-46)Jmjd4 for <i>in vivo</i> Hydroxylation)	63
2.3.10	Co-purification of the Human eRF1:eRF3a Full Length Complex (Co-expressed with Δ(1-46)Jmjd4 for <i>in vivo</i> Hydroxylation)	64
2.3.11	Human ABCE1	64
2.4	Human Cell Culture	65
2.4.1	Human Embryonic Kidney 293T Cells	65
2.4.2	HeLa S3 Suspension Cells	66
2.5	Establishing a Human <i>in vitro</i> Expression System for Obtaining Stalled 80S Ribosomes	66
2.5.1	T7 Polymerase-based <i>in vitro</i> Transcription	66
2.5.2	HeLa S3 Extract-based <i>in vitro</i> Translation	67
2.6	Preparation of Human Stalled Ribosome-nascent Chain Complexes	68
2.7	Binding Assay of Translation Termination Complexes	69
2.8	Electron Microscopy	70
2.8.1	Negative Stain Electron Microscopy Sample Preparation and Data Analysis	71
2.8.2	Cryo-electron Microscopy Sample Preparation	71
2.8.3	Cryo-electron Microscopy Data Collection	71
2.8.4	Cryo-electron Microscopy Data Analysis of Tecnai G2 Spirit (<i>FEI Company</i>) Derived Datasets	72
2.8.5	Cryo-electron Microscopy Data Analysis of a Titan Krios (<i>FEI Company</i>) Derived Dataset	72
2.8.6	Molecular Model Building, Validation and Interpretation	75
2.8.7	Figure Preparation	76
2.8.8	Cryo-electron Microscopy Data Processing Software	76
3.	Results	77
3.1	Obtaining Human Cytomegalovirus gp48/UL4 uORF2 (hCMV)-stalled Ribosome-nascent Chain Complexes	77
3.1.1	Establishment of a Human <i>in vitro</i> Translation Extract	77
3.1.2	Purification of Homogenously Stalled Ribosome-nascent Chain Complexes	79
3.2	<i>In vitro</i> Reconstitution of Ribosome Complexes Involved in Translation Termination	81
3.2.1	Purification of Protein Components	81
3.2.2	Preparation of Natively heRF1 Containing Ribosome-nascent Chain Complexes	89
3.2.3	Preparation of Natively heRF1 Containing Ribosome-nascent Chain Complexes bound to Guanosine Triphosphatase-deficient heRF3a	90
3.2.4	Preliminary Analysis: Binding Assays and Negative Staining	91
3.2.5	Tecnai G2 Spirit Derived Reconstructions	92

3.3	High-resolution Structure of Human eRF1 Bound to the Human 80S Ribosome	93
3.3.1	Data Processing and the Resulting Cryo-Electron Microscopy Reconstruction	93
3.3.2	Interactions of Human eRF1 with the Human Ribosome and Comparisons to Previous Human eRF1 Structures	98
3.3.3	The Human Cytomegalovirus gp48/UL4 uORF2 (hCMV) Stalling Mechanism	100
3.3.4	Involvement of Known heRF1 Motifs in Interactions with the Messenger and Ribosomal RNAs	106
3.3.5	The Stop Codon Resembles a UNR-type U-turn Geometry	108
4.	Discussion	110
4.1	Sample Generation	110
4.1.1	Establishment of a Human <i>in vitro</i> Translation System	110
4.1.2	Utilization of Viral mRNA Sequences for Modulating Initiation and Stalling in the Human <i>in vitro</i> Translation System	110
4.1.3	Protein Purification, Complex Formation and Ribosomal Binding	113
4.2	Cryo-Electron Microscopy as Method of Choice	115
4.3	Molecular Mechanism of hCMV-peptide Mediated Stalling of the Human Ribosome	116
4.4	Molecular Mechanism of UAA(A) Stop Codon Decoding	119
5.	Summary and Outlook	128
6.	References	130
7.	Appendix	158
7.1	Plasmid Constructs for Protein Expression	158
7.1.1	pCDNA3.1 3xFLAG-hABCE1	159
7.1.2	pET-28a (His) ₆ -Δ(1-46)Jmjd4	161
7.1.3	pET-32a TRX-(His) ₆ -TEV-heRF3a Full Length	163
7.1.4	pETDuet-1 heRF1	166
7.1.5	pETDuet-1 (His) ₈ -3C-heRF1	168
7.1.6	pETDuet-1 Δ(1-138)heRF3a	170
7.1.7	pRSFDuet-1 Δ(1-138)heRF3a-3C-(His) ₈	172
7.1.8	pRSFDuet-1 (His) ₈ -3C-Δ(1-138)heRF3a	174
7.1.9	pETDuet-1 heRF3a Full Length	176
7.1.10	pETDuet-1 heRF3a Full Length-3C-(His) ₈	178
7.1.11	pETDuet-1 (His) ₈ -3C-heRF3a Full Length	180
7.2	Plasmid Construct for the Human <i>in vitro</i> Translation System	182
7.2.1	pT7CFE1 CrPV IGR IRES-linker-(His) ₆ -3C-HA-hCMV-p(A) ₂₆ with TAA(A).	183
8.	Acknowledgements	184

II. List of Abbreviations

(His) ₆ /(His) ₈	hexahistidine/oktahistidine
°C	degree Celsius
µg	microgram (10^{-6} gram)
µL	microliter (10^{-6} liter)
2D	two-dimensional
2OG	2-oxoglutarate
3D	three-dimensional
5'-m ⁷ G	5'-7-methyl guanosine
A	adenine
Å	angstrom
A ₂	adenine at position 2 of the stop codon
A ₃	adenine at position 3 of the stop codon
A ₄	adenine at the position following the stop codon (4)
aa	amino acid(s)
AAP	arginine attenuator peptide
ABC	adenosine triphosphate-binding cassette
ABCE1	adenosine triphosphate-binding cassette E1
AdoMetDC	S-adenosylmethionine decarboxylase
ADP	adenosine diphosphate
ADRB2	adrenoceptor β-2 (or β-2 adrenergic receptor)
Amp	ampicillin
AMPPNP	adenosine 5'-(β,γ-imido)triphosphate lithium salt hydrate
anti-SD	anti-Shine-Dalgarno
AP	accessory protein
APS	ammonium persulfate
A-site	aminoacyl-transfer ribonucleic acid binding site
ATP	adenosine triphosphate
ATPase	adenosine triphosphatase
A _{xxx}	absorption at xxx nanometer
C	cytosine
Ca	calcium
Cam	chloramphenicol
cAMP	cyclic adenosine 3',5'-monophosphate
CCD	charge-coupled device
CF	cystic fibrosis
CFTR	cystic fibrosis transmembrane conductance regulator
CGS1	cystathionine-γ-synthase 1
Cl	chlorine
CO ₂	carbon dioxide
conc	concentration
CP	central protuberance
CPS-A	small subunit of the arginine-specific carbamoyl-phosphate synthetase
CRISPR	clustered, regularly interspaced, short palindromic repeat
CrPV	cricket paralyses virus
cryo-EM	cryo-electron microscopy
CTF	contrast transfer function
CTT	C-terminal tail
CV	column volume
<i>D. melanogaster</i>	<i>Drosophila melanogaster</i>

DC	decoding center
DDD	direct electron detection device
ddH ₂ O	double distilled H ₂ O
DENR	density-regulated protein
DF	difluorotoluene
DMD	Duchenne muscular dystrophy
DMEM	Dulbecco's Modified Eagle Medium
DNA	deoxyribonucleic acid
dNTP	deoxynucleoside triphosphate
DPAPB	dipeptidyl aminopeptidase B
DQE	detective quantum efficiency
ds	double stranded
DTT	1,4-dithiothreitol
e ⁻	electron
<i>E. coli</i> , <i>Ec</i>	<i>Escherichia coli</i>
ECL	enhanced chemiluminescence
EDTA	ethylenediaminetetraacetic acid
eEF1A, 2	eukaryotic elongation factor 1A, 2
EF-G	elongation factor G
EF-Tu	elongation factor thermo unstable
eIF1, 1A, 2, 2B, 4, 5, 5B, 6	eukaryotic initiation factor 1, 1A, 2, 2B, 4, 5, 5B, 6
EJC	exon junction complex
EM	electron microscopy
EMD	Electron Microscopy Data Bank
ER	endoplasmatic reticulum
eRF1, 3	eukaryotic release factor 1, 3
ES	expansion segment
E-site	transfer ribonucleic acid exit-site
F	fluorine
FCS	fetal calf serum
FEG	field emission gun
fl	full length
FLuc	firefly luciferase
fMet	N-formylmethionine
FSC	Fourier shell correlation
fwd	forward
G	Gibbs free energy
G	guanine
G ₂	guanine at position 2 of the stop codon
G ₃	guanine at position 3 of the stop codon
GADD34	growth-arrest- and DNA-damage-induced transcript 34
GDP	guanosine diphosphate
GEF	guanine nucleotide exchange factor
GMPPCP	guanosine 5'-[β,γ-methyleno]triphosphate sodium salt
GMPPNP	guanosine 5'-[β,γ-imido]triphosphate trisodium salt hydrate
GTP	guanosine triphosphate
GTPase	guanosine triphosphatase
h	hour(s)
h	human
h#	helix # of ribosomal small subunit
H#	Helix # of ribosomal large subunit
<i>H. marismortui</i>	<i>Haloarcula marismortui</i>

<i>H. sapiens</i> , <i>Hs</i>	<i>Homo sapiens</i>
HA	human influenza hemagglutinin amino acids 98 - 106
HBB	hemoglobin subunit beta gene
H-bonding	hydrogen bonding
hCMV	human cytomegalovirus gp48/UL4 upstream open reading frame 2
HCV	hepatitis C virus
HEPES	4-(2- hydroxyethyl)piperazine-1- ethanesulfonic acid
heRF1	human eukaryotic release factor 1
heRF3a fl	human eukaryotic release factor 3a full length
HMG	high mobility group
HRP	horseradish peroxidase
HSP70	heat shock protein 70 kDa
IF1, 2, 3	initiation factor 1, 2, 3
IGR	intergenic region
IPTG	isopropyl β -D-1- thiogalactopyranoside
IRES	Internal Ribosome Entry Site
ITAF	Internal Ribosome Entry Site-transacting factor
Kan	kanamycin
kb	kilo base pair (10^3 base pairs)
kDa	kilodalton (10^3 dalton)
KOD	recombinant <i>Thermococcus kodakaraensis</i> KOD1 deoxyribonucleic acid polymerase
L	liter
LB	Luria Bertani
LCF	local density correlation function
LSU	large subunit
M	molar
MAP	mitogen-activated protein
MCS	multiple cloning site
MCT-1	multiple copies in T-cell lymphoma-1
MDa	megadalton (10^6 dalton)
MEGAWHOP	megaprimer polymerase chain reaction of whole plasmid (cloning)
Mg	magnesium
MifM	membrane insertion and folding monitor
min	minute(s)
mL	milliliter (10^{-3} liter)
mM	millimolar (10^{-3} molar)
mRNA	messenger ribonucleic acid
MTF	modulation transfer function
mTOR	mechanistic target of rapamycin
MWCO	molecular weight cut-off
N ₂	nitrogen
Na	sodium
NAC	nascent polypeptide-associated complex
NBD	nucleotide binding domain
NC	nitrocellulose
NGD	no-go (mediated) messenger ribonucleic acid decay
NMD	nonsense-mediated messenger ribonucleic acid decay
NMR	nuclear magnetic resonance (spectroscopy)
NSD	non-stop (mediated) messenger ribonucleic acid decay
nt	nucleotide(s)
NTT	N-terminal tail

O ₂	oxygen
OAc	acetate
Oc	<i>Oryctolagus cuniculus</i>
OD ₆₀₀	optical density at $\lambda = 600$ nm
OH	hydroxide
OL	overlapping
ORF	open reading frame
PAA	polyacrylamide
PABP	poly(A)-binding protein
PCR	polymerase chain reaction
PDB	Protein Data Bank
PEI	polyethylenimine
P _i	inorganic phosphate
PIC	pre-initiation complex
PK	pseudoknot
PMSF	phenylmethylsulfonylfluorid
POST	post-translocation state
PRE	pre-translocation state
P-site	peptidyl-transfer ribonucleic acid binding site
PTC	peptidyl transferase center
PTC	premature termination codon
PTM	post-translational modification
px	pixel
RAC	ribosome-associated complex
RACK1	receptor for activated C kinase 1
RBS	ribosome binding site
rev	reverse
RF1,2	release factor 1, 2
RfBEM	restriction-free blunt end mutagenesis (cloning)
RNA	ribonucleic acid
rpm	rounds per minute
r-proteins	ribosomal proteins
RRF	ribosome recycling factor
RRL	rabbit reticulocyte lysate
rRNA	ribosomal ribonucleic acid
RT	room temperature
rut	rho utilisation site
S	sedimentation coefficient (Svedberg unit)
<i>S. cerevisiae</i>	<i>Saccharomyces cerevisiae</i>
SD	Shine-Dalgarno
SDS	sodium dodecyl sulfate
SDS-PAGE	sodium dodecyl sulfate-polyacrylamide gel electrophoresis
sec	second(s)
SecM	secretion monitor
SMEM	Spinner Minimum Essential Medium
SNR	signal-to-noise ratio
SOX10	sex-determining region Y-related high mobility group-box
SPIDER	System for Processing Image Data from Electron microscopy and Related fields
SRL	sarcin-ricin loop
SRY	sex-determining region Y
SSU	small subunit

SU	subunit
T	thymine
T _a	annealing temperature
TBS	tris(hydroxymethyl)aminomethane- buffered saline
TBS-T	tris(hydroxymethyl)aminomethane- buffered saline with tween
TC	ternary complex
TCA	trichloroacetic acid
TCP 1	T-complex protein 1
TEM	transmission electron microscopy
TEMED	tetramethylethylenediamine
TEV	tobacco etch virus
TF	trigger factor
<i>Thermus, Tt</i>	<i>Thermus thermophilus</i>
TI ^{POST}	post-translocational intermediate
TI ^{PRE}	pre-translocational intermediate
T _m	melting temperature
TnaC	tryptophanase leader peptide
Tris	tris(hydroxymethyl)aminomethane
tRNA	transfer ribonucleic acid
trunc	truncated
TRX	thioredoxin
TS	transition state
U	uracil
U ₁	uracil at position 1 of the stop codon
uORF	upstream open reading frame
Upf1	up-frameshift 1
UTR	untranslated region
UV	ultraviolet
V	volt
v/v	volume per volume
VPg	viral protein genome-linked
w/v	weight per volume
WG	wheat germ
WT	wild-type
XBP1u	unspliced form of X-box-binding protein 1
XNDI	X-linked nephrogenic diabetes insipidus
ZBP1	Z-deoxyribonucleic acid- binding protein 1
β-gal	β-galactosidase
Δ(1-138)heRF3a	truncated (at amino acids 1 - 138) human eukaryotic release factor 3a

1. Introduction

The genetic information of each organism is stored in its double-stranded deoxyribonucleic acid (DNA). According to the central dogma of molecular biology (Crick, 1970) gene expression and therefore the synthesis of proteins, which are encoded in the genetic information, is constituted of two processes: In the first process called transcription, ribonucleic acid (RNA) polymerases utilize one DNA strand as template to make RNA. Such RNA can directly fulfill several functions in the cell as transfer RNA (tRNA) (Berg and Offengand, 1958; Giegé, 2006) and ribosomal RNA (rRNA) or can be used as template as messenger RNA (mRNA) for the second process called translation. In eukaryotes, the transcribed mRNA is processed prior to its usage in translation: Processing steps involve the addition of a 5'-7-methyl guanosine (5'-m⁷G) cap (capping), the addition of a poly(A) tail at the 3' end (polyadenylation) and RNA splicing to remove intervening sequences termed introns. Then, the mRNA is read (decoded) in nucleotide triplets, termed codons (Crick *et al.*, 1961), to assemble the corresponding amino acids (aa) to a polypeptide chain composing the functional protein. The ribosome, a large molecular machine first described in 1955 (Palade, 1955) functions as platform for the four-step translation cycle. Newly from the ribosome emerging polypeptide chains require folding into their three-dimensional (3D) protein structures ('native state') to fulfill their cellular function properly which already occurs co-translationally and is facilitated by chaperons. In rather rare cases, the newly translated polypeptide chain leads to arrest in translation, resulting in a stalled polypeptide-bound ribosome residing on the mRNA. Large parts of today's comprehension on ribosome-mediated processes have been generated by biochemical and structural data. Especially recently, due to new technological advances, high-resolution structures from both, x-ray crystallography and cryo-electron microscopy (cryo-EM), have revealed novel and enlightening insights into the intricate molecular networks underlying the ribosome's functions in the translation cycle.

1.1 The Ribosome

1.1.1 An Overview

All ribosomes are conserved in their function to catalyze protein synthesis. In prokaryotes and eukaryotes, they are often referred to as 70S and 80S particles, respectively based on their particular sedimentation coefficient (in the Svedberg unit S). Ribosomes are all composed of two unequally sized subunits (SUs) which accordingly are called small (30S in prokaryotes, 40S in eukaryotes) and large (50S in prokaryotes, 60S in eukaryotes) subunit (SSU and LSU, respectively). Each subunit has its distinct structure and function: The SSUs from different organisms have similar shapes revealing the head, body, platform, beak and shoulder landmarks (see Figure 1A) (Wimberly *et al.*, 2000). The mRNA is situated in a channel (mRNA channel) which it enters between the ribosomal head and shoulder, it twines around the neck and exits between the head and the platform (Jenner *et al.*, 2010; Yusupova *et al.*, 2001). The mRNA-contained information is read in the conserved decoding center (DC) on the SSU interface surface (see Figure 1B).

The LSU has an overall crown-like shape comprising the prominent central protuberance (CP), the L1-stalk at the tRNA exit-site and the acidic L7/L12-stalk (P1/P2-stalk in eukaryotes) serving as factor 'landing platform' (see Figure 1C). The peptidyl transferase center (PTC), where peptide-bond formation between the aa is catalyzed, is located in the LSU. It is entirely comprised of rRNA, which exclusively conducts the catalytic reaction, leading to the designation ribozyme (Cech, 2000). To convey information from the DC to the PTC, tRNAs are utilized as adapters where the mRNA codon is

read by the tRNA anticodon in the DC. The tRNA binding sites are on the interface sides of both SUs and are named according to the tRNA state in the elongation cycle: Aminoacyl- (A-), peptidyl- (P-) or exit- (E-)site. The participating tRNA traverses from the A- via the P- to the E-site. Each tRNA is only charged by a specific aa corresponding to its anticodon sequence (Berg and Offengand, 1958; de Duve, 1988; Lengyel, 1966) ensuring incorporation of the cognate aa. Reading in nucleotide triplets results in 4^3 possible codons (three of which function as stop codons), yet only 20 different canonical aa are encoded leading to a degenerate code (Lagerkvist, 1978). Initial binding of the aminoacyl-tRNA occurs partly to the A-site where its anticodon is matched to the displayed mRNA codon before complete accommodation, whereas the hitherto synthesized polypeptide chain is linked to the P-site tRNA. Peptide-bond formation transfers the peptide chain to the A-site, why both tRNAs have to be moved to resume the original arrangement of a P-site peptidyl-tRNA. The deacylated tRNA in the P-site is shifted to the E-site being regarded as ready for exiting the ribosome. Due to the 5' to 3' reading direction of the mRNA, proteins are synthesized from their N- to the C-terminus (Dintzis, 1961). The PTC is located at the heart of the ribosome, hence newly synthesized polypeptides have to pass through an \sim 80 angstrom (\AA) long and 10 - 20 \AA wide exit tunnel (Frank *et al.*, 1995) before being exposed to the cellular environment (see Figure 1B). The tunnel is predominantly composed of rRNA (Nissen *et al.*, 2000) explaining its electronegative potential (Lu *et al.*, 2007). \sim 30 \AA from the PTC the so called central constriction, a narrowing of the tunnel between uL4 and uL22, is apparent (Nissen *et al.*, 2000). Further down, at the tunnel exit (folding vestibule), the eukaryote-specific protein L39e resides whereas the extension of L23 takes its place in prokaryotes (Harms *et al.*, 2001). Tunnel components have been demonstrated to interact with the newly synthesized peptide.

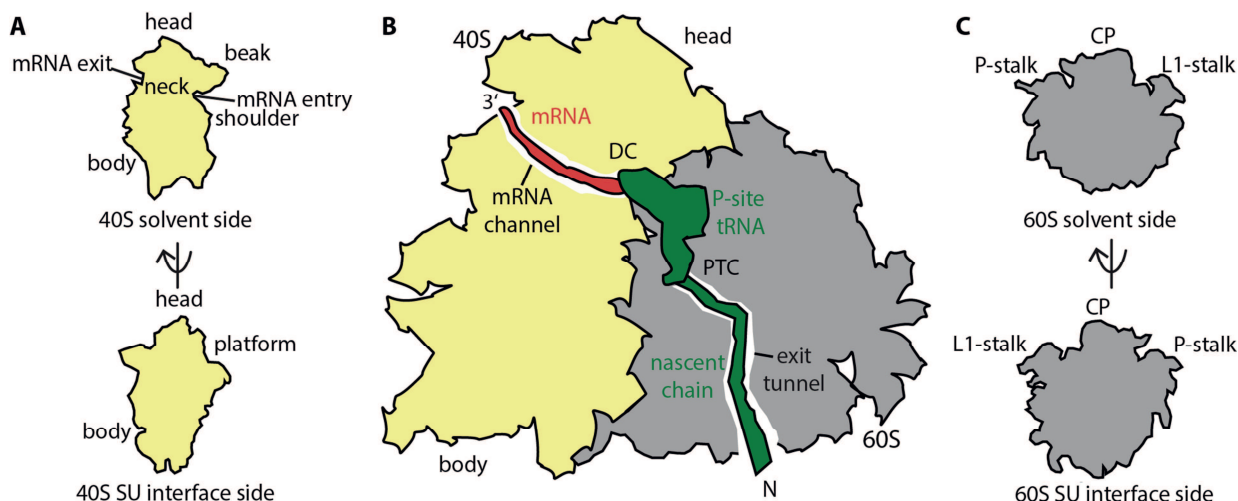


Figure 1: Schematic Representation of the Ribosome.

(A) The human 40S subunit (SU) (yellow) with head, body, platform, beak and shoulder indicated. **(B)** The human 80S ribosome (40S SU (yellow) and 60S SU (gray)) with mRNA channel, exit tunnel, decoding center (DC) and peptidyl-transferase center (PTC) indicated. The mRNA is depicted in red whereas the P-site peptidyl-tRNA in green. **(C)** The human 60S SU (gray) in its crown-shape with the central protuberance (CP), the L1-stalk at the tRNA exit site and the acidic P1/P2- or simply P-stalk (L7/L12-stalk in prokaryotes) indicated.

Generally, maximization of reaction accuracy combined with high efficiency puts conflicting demands on enzymes. The eukaryotic ribosome is a precise enzyme with an error rate of 2×10^{-4} to 6×10^{-6} (Stansfield *et al.*, 1998) while incorporating \sim 5 aa/sec (Olofsson *et al.*, 1987). Profiling data (Yang *et al.*, 2014) showed diminishing of this conflict by slow elongation with higher accuracy of rather

important residues whereas accuracy is sacrificed at other residues to gain speed. Such delicately modulated trade-off corroborates the multi-level regulation of ribosomal translation for optimized cellular function.

1.1.2 The Three Kingdoms of Life

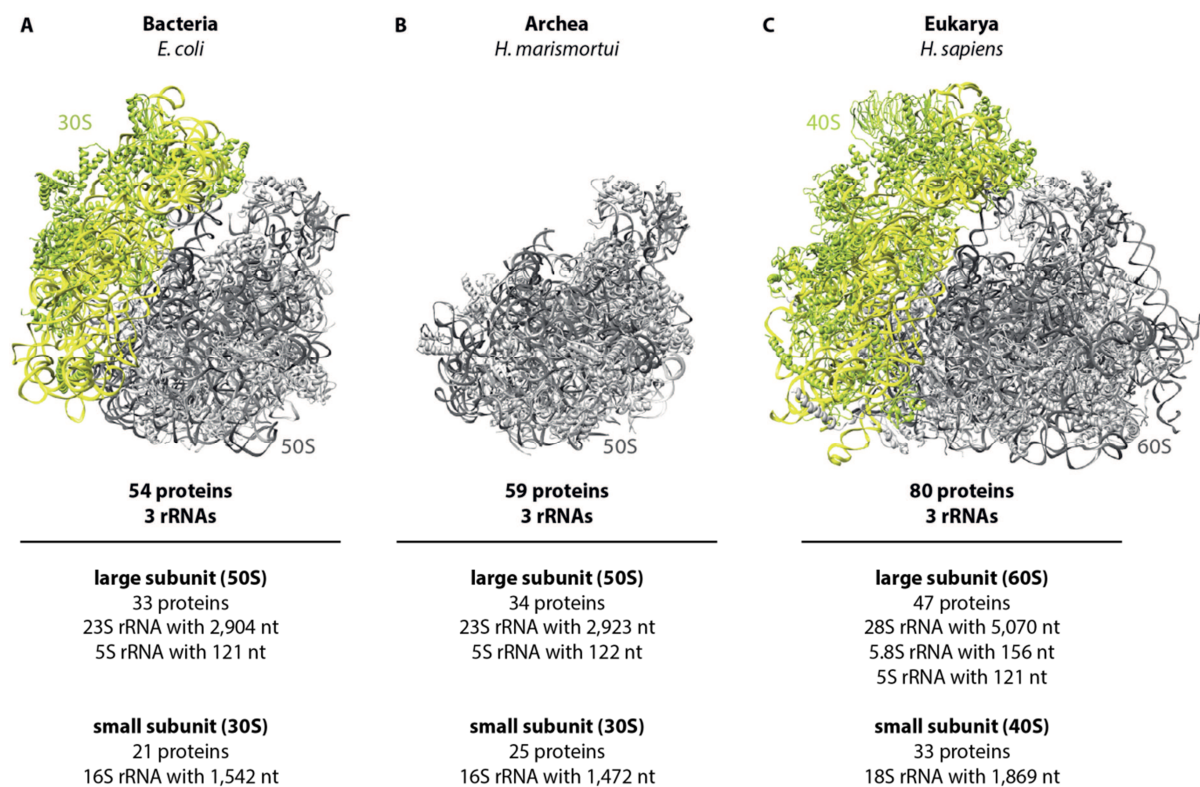


Figure 2: Comparison of the Bacterial *Escherichia coli*, Archaeal *Haloarcula marismortui* and Eukaryotic *Homo sapiens* Ribosomes.

(A) 2.4 Å resolution structure of the bacterial *Escherichia coli* (*E. coli*) 70S ribosome (Noeske *et al.*, 2015) with the 30S small subunit (SSU) colored in yellow and the 50S large SU (LSU) colored in gray (PDB-code: 4YBB). (B) 2.4 Å resolution structure of the archaeal *Haloarcula marismortui* (*H. marismortui*) 50S LSU (Gabdulkhakov *et al.*, 2013) colored as in (A) (PDB-code: 4HuB). (C) 3.6 Å resolution structure of the eukaryotic *Homo sapiens* (*H. sapiens*) 80S ribosome (Khatter *et al.*, 2015). The 40S SSU and the 60S SSU are colored as in (A) (PDB-code: 4ug0).

The contained amount of nucleotides (nt) of ribosomal RNA and the amount of ribosomal proteins are indicated below the structures.

As aforementioned, the ribosome always consists of two subunits whereat ribosomes from all three kingdoms of life contain a common conserved core (~4,400 nucleotides (nt), 34 ribosomal proteins (r-proteins)) (Melnikov *et al.*, 2012). Irrespective of this, their composition varies tremendously amongst different species, as visualized in high-resolution structures (see Figure 2) (Gabdulkhakov *et al.*, 2013; Khatter *et al.*, 2015; Noeske *et al.*, 2015): The bacterial *Escherichia coli* (*E. coli*, *Ec*) (LSU: 23S, 5S rRNA, 33 r-proteins; SSU: 16S rRNA, 21 proteins), the archaeal *Haloarcula marismortui* (*H. marismortui*) (LSU: 23S, 5S rRNA, 34 proteins; SSU: 16S rRNA, 25 proteins) and the eukaryotic *Homo sapiens* (*H. sapiens*) (LSU: 28S, 5.8S, 5S rRNAs and 47 r-proteins; SSU: 18S rRNA and 33 proteins) ribosomes differ in mass of up to 2 megadalton (MDa) (*E. coli* vs. *H. sapiens*). Such differences are mainly attributed to additional rRNA expansion segments (ESs), (Spahn *et al.*, 2001),

variable rRNA regions (Cannone *et al.*, 2002) as well as 13 (12 in yeast) eukaryote-specific proteins (Halic *et al.*, 2005; Sengupta *et al.*, 2004; Spahn *et al.*, 2001; Taylor *et al.*, 2009) and protein-extensions of the conserved proteins (Armache *et al.*, 2010a, 2010b). These compositional discrepancies demand a consistent system for r-protein nomenclature which has been established recently and will be adhered to hereupon (Ben-Shem *et al.*, 2011).

In the eukaryotic LSU the additional mass can be found in two clusters indicating an intertwined co-evolution (Yokoyama and Suzuki, 2008) of rRNA and r-proteins. The extra rRNA mass can be found as long ES helices protruding from the ribosome into the cytosol (Armache *et al.*, 2010b; Ben-Shem *et al.*, 2011). Even though rRNA ESs are largely responsible for the increased mass in eukaryotic ribosomes, a particular function for their enormous length could not have been assigned with certainty to date (Armache *et al.*, 2010b; Ben-Shem *et al.*, 2011; Houge *et al.*, 1993, 1995; Sweeney *et al.*, 1994). The eukaryote-specific r-proteins contain long unusual tails and are mainly situated at the solvent surface of the ribosome forming wide-ranging interactions (Ben-Shem *et al.*, 2011; Klinge *et al.*, 2011). The additional protein layer basically fulfills three functions: First, it seems to stabilize the long bulged ESs whose lengths increase with complexity of the eukaryotic organism, whereat ES27¹ is the most dramatic with 200 nt length in *Saccharomyces cerevisiae* (*S. cerevisiae*) and 850 nt in *H. sapiens* (Anger *et al.*, 2013; Cannone *et al.*, 2002). Second, eukaryote-specific proteins participate in interactions between the two SUs mainly at the periphery (Ben-Shem *et al.*, 2010, 2011; Selmer, 2006; Yusupov, 2001). These so-called intersubunit bridges are of dynamic composition, changing with each conformational rearrangement of the ribosome (Balagopal and Parker, 2011). Compared to prokaryotes, the interaction surface is nearly doubled in eukaryotes where additional bridges are mostly abundant at the periphery (Ben-Shem *et al.*, 2011). Third, particularly on the SSU, eukaryote-specific proteins were suggested to assist in the much more complex process of eukaryotic translation initiation. Eukaryote-specific eS31 and eS30 for example were shown to interact with the initiation factor eIF1A (Weisser *et al.*, 2013) or eS1, eS13, eS26 and eS27 all anchor the huge multimeric eIF3 complex to the 40S SU (Hajnsdorf and Boni, 2012; Hashem *et al.*, 2013). eS6, another eukaryote-specific r-protein, plays a role in translational control due to its phosphorylation by the S6-kinase which is activated by the mechanistic target of rapamycin (mTOR) pathway in response to nutritional and environmental cues (Meyuhas and Dreazen, 2009; Ruvinsky and Meyuhas, 2006). Also, the receptor for activated C kinase 1 (RACK1), a scaffolding-protein (Nilsson *et al.*, 2004; Sengupta *et al.*, 2004), plays a putative role in SU joining via indirect eIF6 phosphorylation (Ceci *et al.*, 2003) or the recruitment of specific mRNAs (e.g. β -actin mRNA/Z-DNA binding protein (ZBP1)) (Ceci *et al.*, 2012) why it might allow ribosome positioning for localized translation (Sasaki *et al.*, 2010). Additionally, RACK1 was shown to be necessary for hepatitis C virus (HCV) Internal Ribosome Entry Site (IRES)-mediated translation initiation (Majzoub *et al.*, 2014).

1.2 The Eukaryotic Translation Cycle

Translation, the process where mRNA is decoded in order to produce polypeptide chains, is mediated via the ribosome in all living cells. Generally, translation appears as cycle composed of four phases: Initiation, elongation, termination and recycling (see Figure 3) (Kapp and Lorsch, 2004; Rodnina and Wintermeyer, 2009). In bacteria polypeptide synthesis is mediated in the cytoplasm whereas in eukaryotes it occurs in the cytoplasm or across the endoplasmatic reticulum (ER) membrane. Especially during the initiation and termination phases eukaryotes employ a far more complex regulatory system which the focus is set on henceforth.

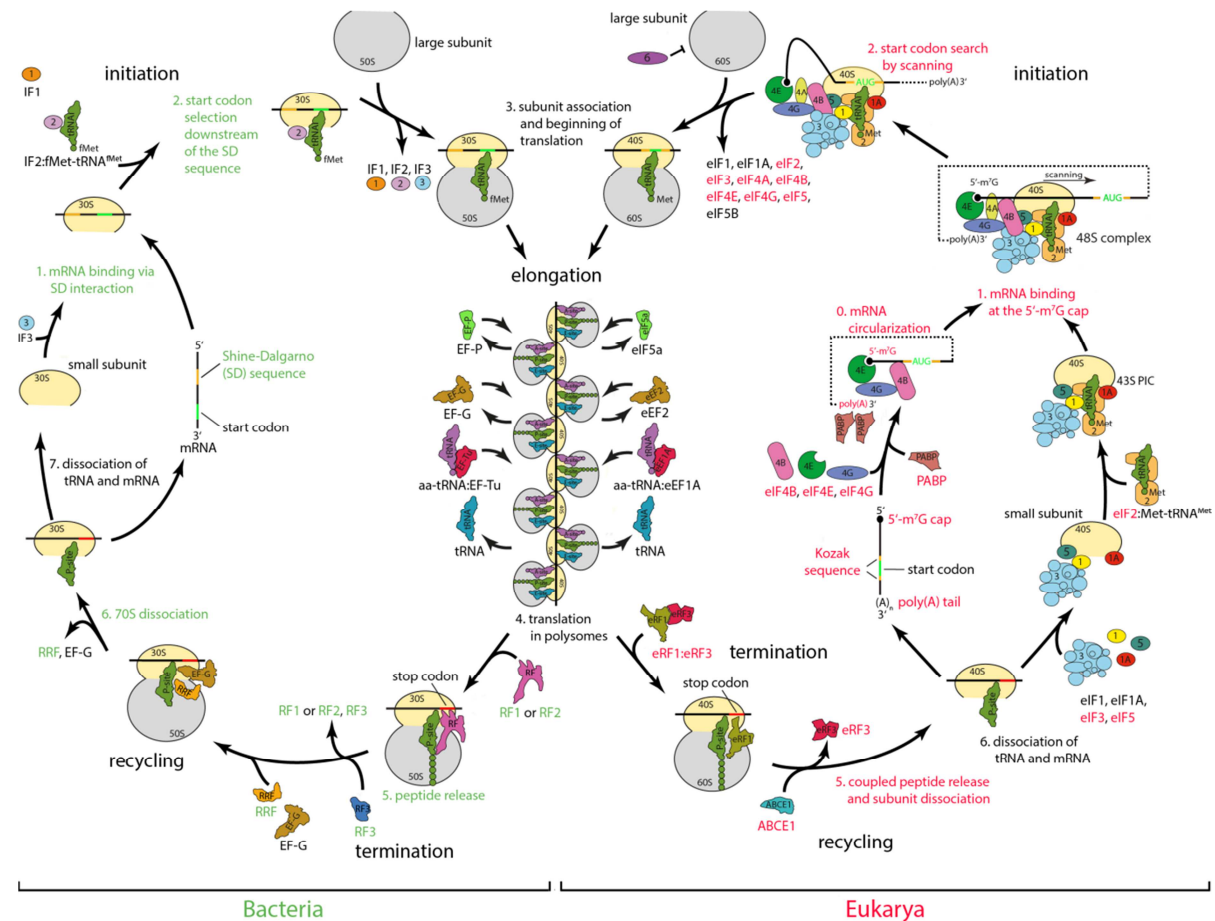


Figure 3: Schematic of the Bacterial and Eukaryotic Translation Cycles.

The translation process is realized in a four-step cycle consisting of initiation, elongation, termination and recycling. On the left-hand side, the translation cycle and its required protein factors are indicated for bacteria, whereas on the right-hand side for Eukarya. Factor names in black are homologous, in green are bacteria-specific and in red are eukaryote-specific.

Figure was based on Melnikov *et al.* (Melnikov *et al.*, 2012). Abbreviations see II.

1.2.1 Initiation

The initiation process intends the assembly of an elongation-competent ribosome with an mRNA AUG start codon in its SSU P-site, bound to an initiator tRNA (fMet-tRNA_i^{fMet} in prokaryotes and Met-tRNA_i^{Met} in eukaryotes).

In prokaryotes the Shine-Dalgarno (SD) sequence, located 7 - 10 nt upstream of the mRNA AUG start codon, plays a profound role in AUG positioning (Shine and Dalgarno, 1974). The SD sequence base pairs with the anti-Shine-Dalgarno (anti-SD) sequence in the 3' end of the 16S rRNA, positioning the AUG codon in the 30S P-site (Kaminishi *et al.*, 2007). Three initiation factors (IF1, 2 and 3) promote binding of the fMet-tRNA_i^{fMet} (IF2), control mRNA binding (IF3), block the ribosomal A-site (IF1) and monitor subunit joining (IF2 and 3) to form an initiating complex.

In eukaryotes, on the contrary, this initiation process is by far more intricate relying on an mRNA scanning mechanism and on 13 core initiation factors (eIFs) which are termed eIF1 - 6 and of which numerous are even multimeric complexes (reviewed in Aitken and Lorsch, 2012; Hinnebusch, 2014;...

Voigts-Hoffmann *et al.*, 2012). Such complexity renders this process highly regulated (Sonenberg and Hinnebusch, 2009), yet beclouds our understanding of the detailed molecular processes.

Canonical Initiation

The first step in eukaryotic translation initiation is the assembly of a ternary complex (TC): The trimeric (α , β , γ) guanosine triphosphatase (GTPase) eIF2 recognizes the unique structure of the Met-tRNA_i^{Met} which binds with high affinity to guanosine triphosphate (GTP)-bound eIF2 (see Figure 4) (Kolitz and Lorsch, 2010). Notably, phosphorylation of eIF2 α on Ser51 in response to various stress-stimuli, as key mechanism of translational control, inhibits guanosine diphosphate (GDP) to GTP nucleotide exchange by its guanine nucleotide exchange factor (GEF) eIF2B, retaining eIF2 incompetent for Met-tRNA_i^{Met} binding (Jackson *et al.*, 2010; Schmitt *et al.*, 2010).

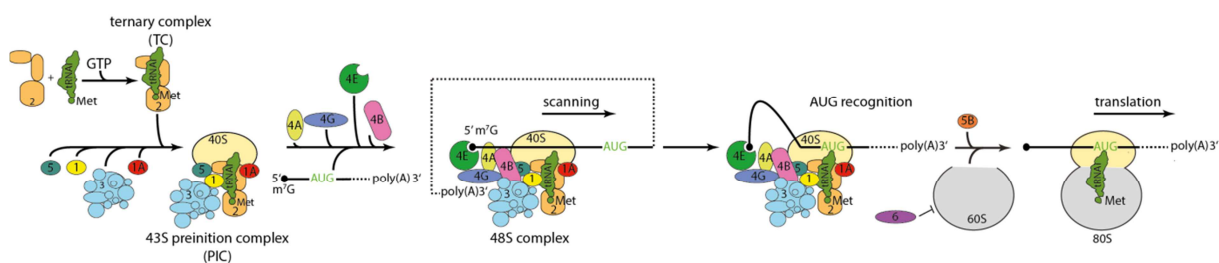


Figure 4: Canonical Translation Initiation in Eukaryotes.

During canonical translation initiation in eukaryotes, ribosomal scanning is inevitable for AUG start codon recognition. Here, 13 core protein factors (called eIF1 - 6) are required. First, ternary complex (TC) formation of eIF2, the initiator tRNA Met-tRNA_i^{Met} and guanosine triphosphate (GTP) is performed. Subsequently, the TC joins eIF1, 1A, 3, 5 and the 40S subunit (SU) to form the 43S preinitiation complex (PIC). Interactions with 5' mRNA-bound eIF4F (consisting of eIF4A, E, G) and eIF4B enable PIC binding to the mRNA which results in the 48S complex. Unwinding of the mRNA allows scanning in 5' to 3' direction until encounter of an AUG start codon, where the 60S SU is joined to result in the 80S initiation complex which is enhanced by eIF5 and 5B. Premature 60S SU binding is prevented by eIF6. Finally, initiation factors are evicted rendering the 80S ribosome ready for translation elongation.

eIF1, 1A, 3 and 5 binding to the 40S SU all promote association with the TC to form a 43S preinitiation complex (PIC) (Algire *et al.*, 2002; Asano *et al.*, 2001; Kolupaeva *et al.*, 2005; Majumdar *et al.*, 2003). eIF1, 1A and 3 are thought to have already bound to the 40S SU during the recycling process to prevent subunit re-joining (Jackson *et al.*, 2012). Structural and biochemical data have delivered insights into the positioning of the eIFs on the 40S SU: eIF1 binds in proximity to the P-site (Lomakin *et al.*, 2003; Rabl *et al.*, 2011). eIF1A binding to the A-site was revealed by homology modeling based on its prokaryotic homolog IF1 (Carter, 2001), protruding with its C-terminal tail (CTT) into the P-site (Olsen *et al.*, 2003) and therefore blocking full tRNA accommodation. The eIF1A N-terminal tail (NTT) interacts with eIF2 and 3, directly stabilizing TC binding to the 43S PIC (Olsen *et al.*, 2003). The large multimeric eIF3-complex (13 SU in mammals (a - m), 6 in yeast (a, b, c, g, i, j)) (Jackson *et al.*, 2010) reveals a 5-lobed shape (Querol-Audi *et al.*, 2013; Siridechadilok *et al.*, 2005; Sun *et al.*, 2011), localizes uniquely at the solvent-exposed side of the 40S SU and was reported to span from the mRNA entry to the exit channel (Chiu *et al.*, 2010; Pisarev *et al.*, 2008; Querol-Audi *et al.*, 2013; Siridechadilok *et al.*, 2005). Further, it can interact with each component of the 43S PIC (Asano *et al.*, 2000; Kolupaeva *et al.*, 2005; Pisarev *et al.*, 2008; Valasek, 2003) possibly coordinating its assembly. Both terminal domains of eIF5 interact with eIF2 (β and γ) (Alone and Dever, 2006;

Asano *et al.*, 1999; Das *et al.*, 2001; Paulin *et al.*, 2001; Yamamoto *et al.*, 2005), however, its precise localization, as well as its time of binding, is still under debate.

eIF1 and 1A jointly promote the ‘open’, scanning-competent conformation of the 43S PIC (Pestova *et al.*, 1998). Here, the tRNA_i is not fully accommodated (P_{out} state), yet (Saini *et al.*, 2010). As mentioned, eIF1A’s CTT extends into the P-site to prevent full tRNA_i acceptor stem loop (ASL) accommodation, keeping it rather in a P/E state (Dunkle *et al.*, 2011; Saini *et al.*, 2010). Further, based on the crystal structure of the eIF1-bound 40S SU from *Tetrahymena thermophile*, eIF1 promotes an unlocked mRNA ‘latch’ (open mRNA entry channel between the 40S body (h18) and head (h34 and uS3)) likewise keeping the tRNA in the metastable P_{out} state (Passmore *et al.*, 2007). In addition, in mammals eIF3 was suggested to be non-dispensable for the ‘open’ 43S PIC conformation (Chaudhuri *et al.*, 1999; Kolupaeva *et al.*, 2005; Majumdar *et al.*, 2003).

The 5'-m⁷G-capped mRNA is redundantly bound to the eIF4F complex consisting of eIF4A, E and G: eIF4A is an adenosine triphosphate (ATP)-dependent, non-processive DEAD-box helicase (Liu *et al.*, 2008; Lorsch and Herschlag, 1998; Sengoku *et al.*, 2006) and the least conserved factor eIF4B (mammals) or eIF4H (plants) promotes its activity (Bi *et al.*, 2000; Cheng *et al.*, 2008; Özeş *et al.*, 2011; Rogers *et al.*, 2001, 2002; Rozovsky *et al.*, 2008). eIF4F catalyzes mRNA unwinding directly at the 5' mRNA end for 43S PIC loading (Pestova and Kolupaeva, 2002) whereupon evidence accumulates for the necessity of more potent helicases (e.g. Dhx29 (mammals), Ded1 (yeast)) to catalyze mRNA unwinding of more complex secondary structures during mRNA scanning (Abaeva *et al.*, 2011; Pisareva *et al.*, 2008). 5'-m⁷G cap recognition, mediated by eIF4E, which is least abundant under the eIFs, represents the rate-limiting step in initiation and consequently is highly regulated upon cellular stimuli (Duncan *et al.*, 1987; Hiremath *et al.*, 1985; reviewed in Raught and Gingras, 1999). eIF4G acts as scaffold. It is known to interact with the poly(A)-binding protein (PABP) bound to the 3'-poly(A) tail and to simultaneously interact with eIF4E bound to the 5'-m⁷G cap which results in bridging and therefore circularization of the mRNA. This locally brings the recycling and initiation steps closer together, accelerating the passage to the next round of the translation cycle (Uchida *et al.*, 2002). Furthermore, in mammals eIF4G activates eIF4A’s helicase activity (Rogers *et al.*, 2002; Schütz *et al.*, 2008) and directly interacts with eIF3 (part of the 43S PIC) which assigns a role in 43S PIC recruitment and consequently 48S complex (43S PIC and mRNA) assembly (LeFebvre *et al.*, 2006).

Once recruited, the 43S PIC scans 5' to 3', base by base with ~8 bases/sec during which codon sampling in the P-site is realized (Berthelot *et al.*, 2004; Vassilenko *et al.*, 2011). Only in the right sequence surrounding the first AUG encounter leads to start codon recognition. If there is sufficient deviation from the ideal Kozak sequence 5'-(A/G)NNAUGG-3' (Kozak, 1986), leaky scanning leads to start codon omitting, resulting in initiation at an ensuing AUG-codon. Upon start codon recognition the complex engages its ‘closed’, scanning arrested conformation (Maag *et al.*, 2005). eIF1, situated at the critical intersubunit bridge B2a (Rabl *et al.*, 2011), blocks premature binding of the 60S SU. For tRNA_i accommodation, domain rearrangements in eIF1 and 1A are a prerequisite to clear the P-site (Yu *et al.*, 2009). Especially, eIF1 (which is functionally homologous to the prokaryotic IF3 in maintaining proper start codon selection) (Lomakin *et al.*, 2006) dissociation is of major importance and is enhanced by eIF5 (Nanda *et al.*, 2009; Pisarev *et al.*, 2006) triggering a cascade: GTP hydrolysis by eIF2 can now be followed by eIF5-mediated inorganic phosphate (P_i) release (Algire *et al.*, 2005; Maag *et al.*, 2005) resulting in full accommodation of the tRNA_i in the P-site (P_{in} state) (Maag *et al.*, 2005) which stabilizes the Met-tRNA_i^{Met} - mRNA interaction and is accompanied by 40S head rotation

which locks the Met-tRNA_i^{Met} (Lomakin and Steitz, 2013). In a described model, displacement of eIF1A CTT could confer movement to eIF5 (Maag *et al.*, 2006) which then interacts with the eIF1A CTT to consequently allow P_i release (Aitken and Lorsch, 2012). However, detailed domain positioning at this stage is not known.

Next, eIF2:GDP together with eIF5 dissociate from the complex (Shin *et al.*, 2002; Singh *et al.*, 2006, 2007) freeing the eIF1A CTT for the mediation of SU joining (Acker *et al.*, 2006; Marintchev *et al.*, 2003; Olsen *et al.*, 2003). Premature 80S assembly is likewise impeded on the 60S SU by the anti-associative eIF6 protein which is bound to the LSU GTPase center and has to dissociate (Brina *et al.*, 2011; Gartmann *et al.*, 2010; Greber *et al.*, 2012; Klinge *et al.*, 2011, 2012). 60S recruitment, facilitated by another GTPase called eIF5B (structurally homologous to IF2) (Pestova *et al.*, 2000) evicts the remaining eIFs from the 40S SU (Acker *et al.*, 2006) rendering the complete 80S ribosome competent for translation elongation (Aitken and Lorsch, 2012).

Internal Ribosome Entry Site-mediated Initiation

Compared to the highly regulated, multi-step process of eukaryotic initiation (see Figures 4 and 5A), many viruses have evolved alternative mechanisms to circumvent host control and even compromise or sabotage the host's canonical translation (by targeted proteolysis (Castelló *et al.*, 2009; Chau *et al.*, 2007; Etchison *et al.*, 1982), eIF modification (Feigenblum and Schneider, 1993; McInerney *et al.*, 2005; Mulvey *et al.*, 2003) or overproduction of competing 5'-m⁷G cap-binding proteins (Marcotrigiano *et al.*, 1999)).

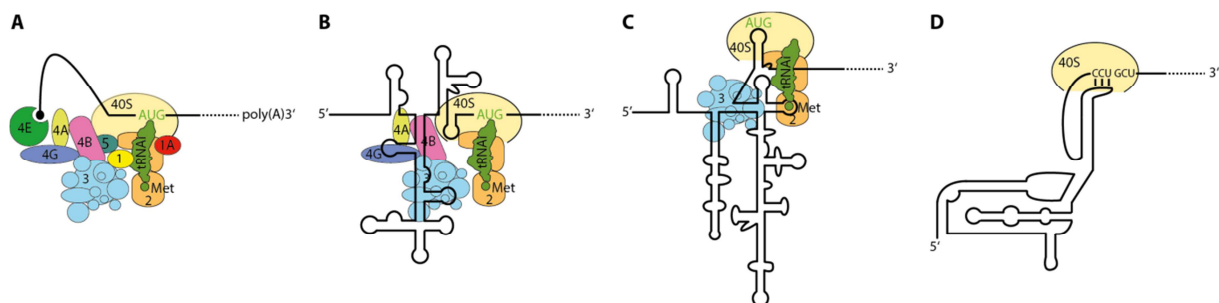


Figure 5: Comparison of the Canonical and Several Internal Ribosome Entry Site-mediated Translation Initiation Processes.

(A) The canonical 5'-m⁷G cap-dependent 48S initiation complex is assembled (as described in Figure 4 in more detail) which allows for mRNA scanning. **(B)** Encephalomyocarditis virus (EMCV) Internal Ribosome Entry Site (IRES) mediated initiation. Direct interaction between the EMCV IRES and the eukaryotic initiation factor eIF4G circumvents the necessity for eIF4E by direct recruitment of the 43S preinitiation complex to the IRES. Therefore, eIF1, 1A and 4E are not needed in the initiation process. **(C)** Hepatitis C virus (HCV) IRES mediated initiation. Here, direct interaction of the HCV IRES with the 40S subunit (SU), as well as with eIF3, removes the need for further eIFs. Since the AUG start codon is directly placed into the peptidyl-tRNA site of the 40S SU, no scanning is necessary either. Yet, Met-tRNA_i^{Met} positioning by eIF2 is still required. **(D)** Cricket paralysis virus (CrPV) intergenic region (IGR) IRES mediated initiation. In this particular case neither Met-tRNA_i^{Met} nor eIFs are required by directly recruiting the 40S SU. Protein synthesis is initiated from the aminoacyl-tRNA binding site GCU codon by jump-starting elongation.

Color scheme see Figure 4.

The utilization of IRES-sequences, cis-acting mRNA whose 3D structure is of utter importance for its function, allows viral translation to by-pass the canonical initiation pathway eliminating the need for some (or even all) of the cellular eIFs (Fernández-Miragall *et al.*, 2009; reviewed in Holcik and

Sonenberg, 2005; Jang *et al.*, 1988; Pelletier and Sonenberg, 1988). IRES-dependent translation is known to be 5' cap-independent, why for instance positive strand viral RNA of *Picornaviridae* instead contain a viral protein genome-linked (VPg) covalently attached to the 5' end of their genome. IRES classification is mainly based on their dependency on the canonical initiation factors: The class of *Type I* IRES comprises entero- and rhinovirus genomes (Jackson *et al.*, 1990; Nomoto *et al.*, 1976) whereas the oldest class of *Type II* IRES comprises cardio- and aphthovirus genomes all of the *Picornaviridae* family with the most characterized IRES being the encephalomyocarditis virus (EMCV) IRES (see Figure 5B) (Jang *et al.*, 1988). For both types I and II, many of the canonical initiation factors are needed except for eIF4E and the N-terminal region of eIF4G (reviewed in Hanson *et al.*, 2012). *Type III* IRES are present in the *Flaviviridae* family whose mRNA directly binds to the 40S SU and eIF3 why no 5'-m⁷G cap-binding eIFs are needed and are exemplified by the HCV IRES (see Figure 5C) (Tuller *et al.*, 2010; Zhou *et al.*, 2013). All IRES types mentioned so far additionally utilize non-canonical initiation factors called IRES-transacting factors (ITAFs) further circumventing their dependency on the targeted host eIFs (Morley *et al.*, 2005). Cricket paralyses virus (CrPV) IRES (see Figure 5D), the prototypical example for a *type IV* IRES, is independent of any cellular initiation factors and occurs in the family of *Dicistroviridae* (Wilson *et al.*, 2000).

The natural CrPV IRES is located at an intergenic region (IGR) of a dicistronic message (Wilson *et al.*, 2000). Whereas initiation via the HCV IRES still requires proper positioning of the Met-tRNA_i^{Met} on the AUG start codon in the P-site, the CrPV IGR IRES even eliminates such need by starting translation from the A-site: The mRNA binds directly to the 40S SU, recruiting the 60S SU for hijacking the complete 80S ribosome. Cryo-EM studies (Fernández *et al.*, 2014; Muhs *et al.*, 2015; Schüler *et al.*, 2006) revealed that the CrPV IGR IRES pseudoknot I (PKI) mimics the tRNA/mRNA interaction in the A-site DC rather resembling the pre-translocation (PRE) state of the ribosome than any initiation state. Further, eukaryotic elongation factor 2 (eEF2) requirement for translocation to subsequently obtain the first open reading frame (ORF) codon (GCU) in the A-site argues for a jump-started elongation rather than initiation by this type of IRES (Fernández *et al.*, 2014).

1.2.2 Elongation

Compared to translation initiation and termination, the elongation cycle (see Figure 6) is highly conserved between eukaryotes and bacteria. Most studies in this context therefore were conducted in the easier approachable model system of bacteria, yet the obtained key findings should be likewise applicable for eukaryotic organisms.

After successful initiation, the ribosome harbors an initiator tRNA in its P-site and contains an empty A-site displaying the next ORF codon for tRNA sampling. Delivery of the aminoacyl-tRNA is mediated as ternary complex together with the GTP-bound elongation factor EF-Tu (eEF1A in eukaryotes). Solely cognate aminoacyl-tRNA binding results in GTP-hydrolysis, subsequent EF-Tu dissociation and progression towards rapid peptide-bond formation to elongate the nascent peptide chain by one aa. A finalizing translocation step, facilitated by EF-G (eEF2 in eukaryotes), moves the mRNA and the bound tRNAs by one codon displaying the next ORF codon in the empty A-site for anew tRNA delivery in a sequential manner.

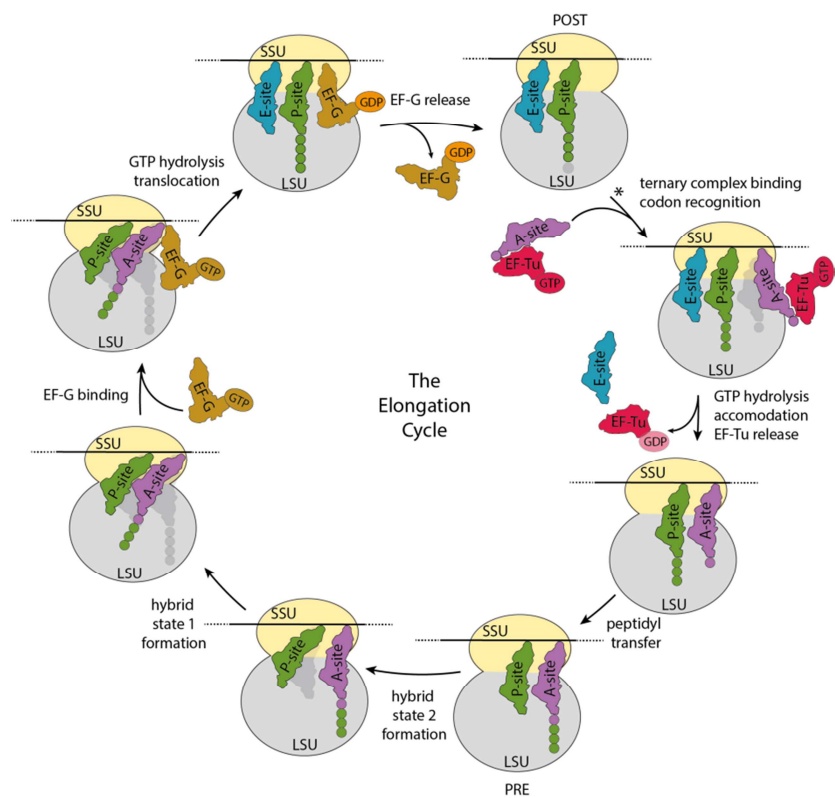


Figure 6: The Elongation Cycle.

The small ribosomal subunit (SSU) is depicted in yellow, the large ribosomal subunit (LSU) in gray. The description start is indicated by a '*': Amino-acid-bound tRNA (purple) delivery to the ribosomal aminoacyl-tRNA binding site (A-site) is mediated by the elongation factor EF-Tu (red) as ternary complex with guanosine triphosphate (GTP). Subsequent GTP hydrolysis to guanosine diphosphate (GDP) (light pink) is followed by tRNA accommodation and GDP:EF-Tu release. At which point the deacylated tRNA in the exit site (E-site) (blue) vacates the ribosome is uncertain. Concomitant to peptide-bond formation, the nascent chain is transferred from the peptidyl-tRNA binding site (P-site) (green) to the A-site (purple) tRNA which results in the pre-translocation (PRE) state. In hybrid state 2, the P-site tRNA is in a hybrid P/E state (first letter corresponding to its position on the SSU, second letter to its position on the LSU). In the subsequent hybrid state 1, additionally the A-site peptidyl-tRNA is found in a hybrid A/P state. Elongation factor EF-G (brown) binding and GTP hydrolysis promote translocation of the tRNAs into the P/P and E/E states. The release of GDP:EF-G results in the post-translocation (POST) state which is ready for the next round of elongation.

Decoding and tRNA Accommodation

Efficient and precise decoding is required for high fidelity rates of elongation while performing at high speed. To increase the local concentration of the ternary aminoacyl-tRNA:EF-Tu:GTP complex, multiple EF-Tu proteins were suggested to interact simultaneously with the L7/L12-stalk (P1/P2-stalk or P-stalk in eukaryotes) proteins located at the tRNA entry side (Blanchard *et al.*, 2004; Diaconu *et al.*, 2005; Rodnina *et al.*, 1996). tRNA binding to the A-site not only results in Watson-Crick base-pairing interactions of the tRNA anticodon arm with the mRNA codon, but also induces conformational changes in the highly conserved rRNA residues *Ec* A1492 (*Hs* A1824), *Ec* A1493 (*Hs* A1825) and *Ec* G530 (*Hs* G626) which interact with the minor groove of the formed codon-anticodon helix at position 1 and 2 (not at 3 which is consistent with the 'wobble hypothesis' (Crick, 1966)) to form an A-minor interaction (Ogle *et al.*, 2001). Unexpectedly, the Watson-Crick base-pairing geometry (instead of wobble-pair geometry) was reported also for near- or non-cognate tRNA binding in crystal structures (Ratje *et al.*, 2010) which even was accompanied by similar rRNA

positioning and interaction patterns as for cognate tRNA binding. Yet, such enforced and unfavorable nucleotide conformation results in high energy loss and is therefore thought to be responsible for tRNA discrimination and the absence of elongation progression due to lacking energy for near- and non-cognate tRNA binding. This results in a model for codon discrimination where the ribosome rather provides a geometric highly restrictive environment coupled to energy loss for near- or non-cognate tRNAs than performs specific sampling of right Watson-Crick base-pairing conformations for cognate tRNAs which would lead to unique rRNA interactions. Nevertheless, a close-by rRNA nucleotide in Helix 69 (H69), *Ec* A1913 (*Hs* A3731) was reported to acquire different conformations upon cognate versus near-cognate tRNA binding to the A-site (Demeshkina *et al.*, 2012; Selmer, 2006).

Subsequent to cognate tRNA binding, the resulting energy is transferred to conformational changes (Pape *et al.*, 1999): Ribosomal domain closure (a large scale SSU rotation towards the LSU) (Ogle *et al.*, 2002, 2003), distortion of the tRNA body in the anticodon- and the D-stem to fit the A/T state (state where the aminoacyl-tRNA is bound to the A-site of the SSU, yet not to the LSU) (Moazed and Noller, 1989; Schmeing *et al.*, 2009; Stark *et al.*, 1997; Valle *et al.*, 2002) and EF-Tu domain rearrangement to prevent clashing into the 23S rRNA sarcin-ricin loop (SRL) (Voorhees and Ramakrishnan, 2013). These conformational rearrangements all contribute to GTPase activation of EF-Tu in which the phosphate of *Ec* A2662 (in the SRL) (Voorhees *et al.*, 2010) and a conserved His (*Ec* His84) of EF-Tu itself (Daviter *et al.*, 2003) were suggested to play a major role. The SRL opens a 'hydrophobic gate' (Berchtold *et al.*, 1993; Schuette *et al.*, 2009; Sengupta *et al.*, 2008; Villa *et al.*, 2009; Vogeley *et al.*, 2001; Voorhees *et al.*, 2010) accompanied by the stabilization of an active *Ec* His84 conformation coordinating an H₂O to catalyze hydrolysis of the GTP γ-phosphate (Berchtold *et al.*, 1993; Daviter *et al.*, 2003; Knudsen *et al.*, 2001). P_i release is followed by domain rotation of EF-Tu (Berchtold *et al.*, 1993) which disrupts important interaction sites (Schmeing *et al.*, 2009) and leads to dissociation of GDP:EF-Tu. At this point, the tRNA is solely bound via its Watson-Crick base-pairing interactions which, as mentioned above, are stronger for cognate tRNAs. This serves as another, independent step of proof-reading (Blomberg *et al.*, 2009; Gromadski and Rodnina, 2004; Thompson and Stone, 1977). Now, the aminoacyl-tRNA acceptor stem can accommodate into the PTC to allow rapid peptide-bond formation. Interestingly, Zaher *et al.* (Zaher and Green, 2009) reported further proof-reading even after the aa has already been incorporated. The codon-anticodon helix in the P-site is monitored, resulting in complete translation termination for discovered mismatches, once again increasing fidelity of the process.

Peptidyl Transfer

As mentioned in 1.1.1, the PTC is solely comprised of rRNA (Ban, 2000; Nissen *et al.*, 2000; Selmer, 2006; Voorhees *et al.*, 2009) providing the environment for the nucleophilic attack of the A-site primary amine to the P-site peptidyl-tRNA aminoacyl-ester to elongate the polypeptide chain by one aa (see Figure 7). This reaction concomitantly transfers the whole nascent chain from the P-site tRNA to the A-site aminoacyl-tRNA. Importantly, spontaneous ester-bond hydrolysis during translation is omitted by steric exclusion of H₂O via the PTC residues *Ec* A2486 (*Hs* A4394) and *Ec* C2063 (*Hs* C3880) on the one side and *Ec* U2585 (*Hs* U4493) on the other (Schmeing *et al.*, 2005a).

A-site aminoacyl-tRNA accommodation results in an induced fit mechanism remodeling the PTC residues *Ec* G2583 - U2585 (*Hs* G4491 - U4493) and *Ec* U2506 (*Hs* U4414) (Schmeing *et al.*, 2005a; Voorhees *et al.*, 2009) as well as in re-positioning of the carbonyl carbon of the P-site ester-bond to

facilitate the catalyzed reaction (Schmeing *et al.*, 2005b). Simultaneous proper arrangement of the A-site α -amino group in close proximity reveals a major contribution of the PTC to the reaction's catalysis by substrate positioning why the ribosome is thought to function as 'entropy trap' (Sievers *et al.*, 2004). Notably, the ribosome enhances the nucleophilic attack by seven orders of magnitude indicating further contribution besides proper substrate positioning. Prime candidates for direct participation in the chemical reaction are the N3 of *Ec* A2451 (*Hs* A4359) (Muth, 2000; Nissen *et al.*, 2000) or the 2' OH of the P-site A76 ribose (Hansen *et al.*, 2002). The importance of these residues however, has been challenged by numerous studies. *Ec* A2451 (*Hs* A4359) for example was shown to be dispensable for peptide-bond formation (Youngman *et al.*, 2004) and replacement of the A76 ribose 2' OH by 2' H or 2' fluoride (F) revealed only moderate decrease in the catalysis rate (Zaher *et al.*, 2011). Further, the A76 ribose 2' OH was suggested to be involved in a fully concerted 8-membered proton-shuttle mechanism (in the transition state (TS)) (Kuhlenkoetter *et al.*, 2011) which is contradictory to studies that rather propose a 2-step mechanism involving a tetrahedral TS (Hiller *et al.*, 2011). Although the precise catalytic mechanism of peptide-bond formation, as well as the contribution of individual residues, still remains to be elucidated, a ribosomal role beyond substrate positioning is evident due to its large catalytic power compared to the un-catalyzed reaction (Sievers *et al.*, 2004).

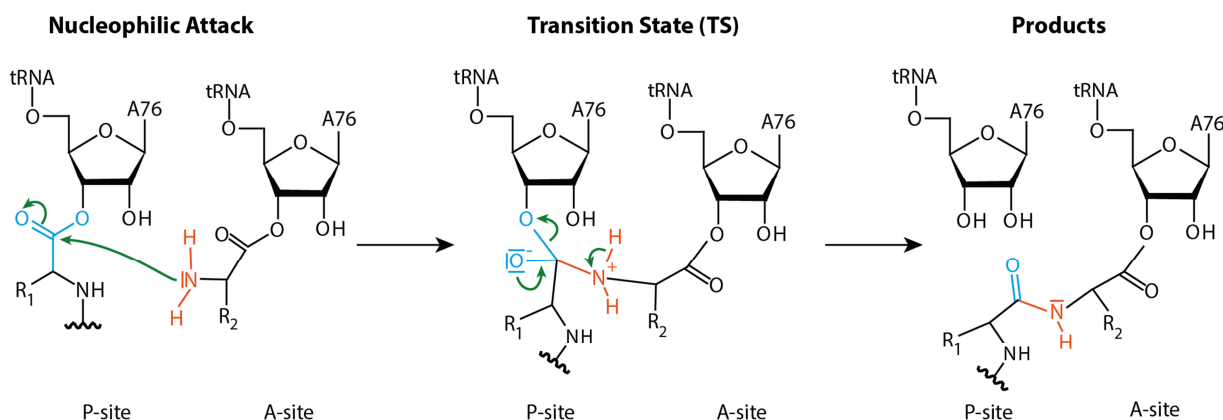


Figure 7: Peptide-bond Formation.

Chemical mechanism of the peptide-bond formation reaction between the amino acid (aa) delivered to the aminoacyl-tRNA binding site (A-site) and the nascent peptide chain bound to the tRNA in the peptidyl-tRNA binding site (P-site). The free electron pair of the primary amine of the A-site aa (red) acts as nucleophile which attacks the carbonyl carbon of the ester-bond (blue) in the P-site. Break down of the transition state (TS) results in a deacylated tRNA in the ribosomal P-site and transfer of the nascent peptide chain to the A-site tRNA (Beringer and Rodnina, 2007; Rodnina, 2013; Schmeing *et al.*, 2005b).

The reaction mechanism was drawn with ChemSketch (ACD/Labs).

Translocation

Successful peptide-bond formation results in an elongated nascent peptide chain attached to the A-site tRNA, whereas the deacylated tRNA is localized in the P-site. To render the A-site accessible for the next tRNA, translocation (the movement of the mRNA and tRNAs by nearly 50 Å) from the ribosomal PRE to the post-translocation (POST) state is required (see Figure 8). To this end, first a hybrid state is adopted by the tRNAs, where only their counterparts in the LSU move to the P- and E-sites resulting in an A/P and P/E hybrid state 1 (Bretscher, 1968; Moazed and Noller, 1989). Such hybrid state was suggested to be promoted by peptide-bond formation (Semenkov *et al.*, 2000; Sharma *et al.*, 2004) or can occur spontaneously (Agirrezabala *et al.*, 2008; Julián *et al.*, 2008) where

the P/E state precedes formation of the A/P state (Pan *et al.*, 2007; Walker *et al.*, 2008) even resulting in a short-lived hybrid state 2 intermediate. Hybrid state formation is facilitated by counter-clockwise rotation of the SSU relative to the LSU (ratcheting) resulting in the rotated PRE state (Frank and Agrawal, 2000).

Since the ribosome itself was observed to allow tRNA movement in both directions (Konevega *et al.*, 2007; Shoji *et al.*, 2006), directionality (Frank, 2012; Frank and Gonzalez, 2010), as well as precision (to exactly keep the reading-frame), is mediated by EF-G (eEF2 in eukaryotes). GTP-bound EF-G mimics the ternary aminoacyl-tRNA:EF-Tu:GTP complex and inserts its domain IV into the DC of the SSU (Agrawal *et al.*, 1998; Nissen *et al.*, 1995) disrupting the delicate hydrogen bonding (H-bonding) network and preventing back-translocation (Chen *et al.*, 2013; Connell *et al.*, 2007; Gao *et al.*, 2009; Khade *et al.*, 2013; Ratje *et al.*, 2010; Tourigny *et al.*, 2013). This induces SSU head movement of 18° toward the E-site relative to the SSU body (head swiveling) (Schuwirth *et al.*, 2005) thought to facilitate tRNA movement in a yet unknown way (Guo and Noller, 2012; Ratje *et al.*, 2010; Zhang *et al.*, 2009b).

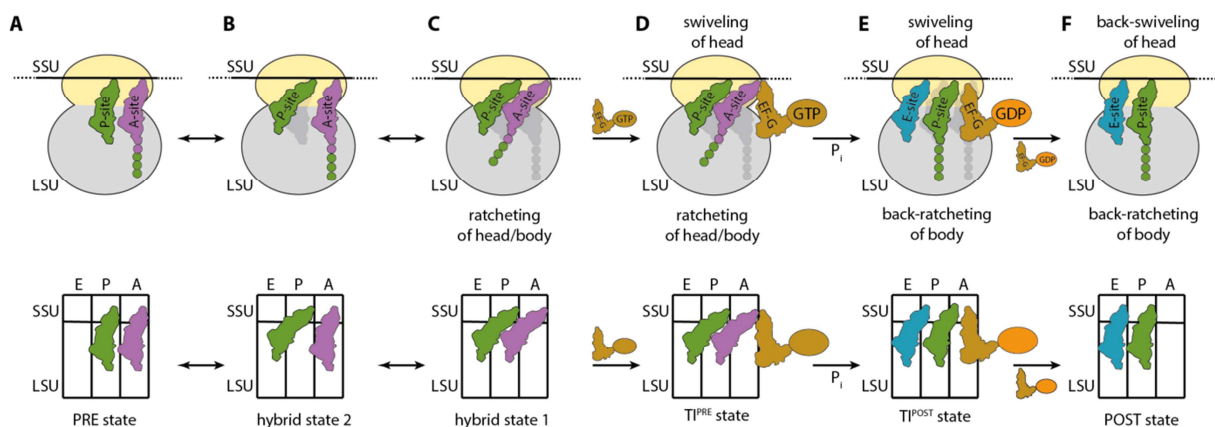


Figure 8: tRNA Positioning in the Ribosomal Head and Body during Translocation.

The small ribosomal subunit (SSU) is depicted in yellow, the large ribosomal subunit (LSU) in gray. In the lower schematic, the tRNA exit-site (E-site), the peptidyl-tRNA binding site (P-site) and the aminoacyl-tRNA binding site (A-site) are marked with E, P and A, respectively. **(A)** The pre-translocation (PRE) state is highly dynamic where both tRNAs can either exist in the classical A/A and P/P states or spontaneously fluctuate to hybrid states in which the tRNA(s) are moved relative to the LSU like in **(B)**, the hybrid state 2, where the P-site tRNA is moved to the P/E state or in **(C)**, the hybrid state 1, where the A-site tRNA is additionally moved to the A/P state. **(D)** Subsequently, guanosine triphosphate (GTP):EF-G (brown) binding stabilizes the ratcheted pre-translocational intermediate (TI^{PRE}) state with a moderately swiveled SSU head. **(E)** Due to further head swiveling and back-ratcheting after GTP to guanosine diphosphate (GDP)-hydrolysis, the additional movement of the tRNAs relative to the LSU to the ap/P and pe/E states follows, resulting in the post-translocational intermediate (TI^{POST}) state. **(F)** GDP:EF-G dissociation completes translocation with the ribosome in the unratcheted post-translocation (POST) state in which a back-swiveled SSU head results in the classical P/P and E/E tRNA states.

Crystallization of the *Thermus thermophilus* (*Thermus*, *Tt*) 70S PRE ribosome bound to an L9-fused EF-G protein visualized a compacted EF-G conformation where its domains III - V are oriented away from the A-site of the SSU (Lin *et al.*, 2015). It was hypothesized that SSU rotation allows GTP-independent elongation of the factor positioning domain III next to domain I. Subsequent GTP-hydrolysis might further extend EF-G putting domain IV into the DC of the SSU. The fully extended EF-G conformation was observed for L9-fused EF-G bound to the POST state. Interestingly, EF-G not only resembles the ternary complex of aminoacyl-tRNA:EF-Tu:GTP, but recently a similar role for a

highly conserved His (*Ec* His91) in coordinating an H₂O molecule for GTP-hydrolysis in context with the SRL has been observed, highlighting even more similarities to EF-Tu's function on the ribosome (Voorhees *et al.*, 2010). A recent cryo-EM structure of an *E. coli* 70S ribosome bound to a His91Ala EF-G mutant protein demonstrated strong contacts of EF-G to S12 and L11 only with the rotated PRE (as opposed to the non-rotated POST) state restricting EF-G's conformation (Li *et al.*, 2015). S12 contacts stabilized domain III which properly positions the domain in vicinity to switch I. This was stated to be a prerequisite for GTP hydrolysis.

By solving two differently rotated cryo-EM reconstruction of the *Thermus* ribosome bound to fucidic-acid-stalled EF-G, which cannot undergo the rearrangements upon GTP hydrolysis, two novel hybrid states were discovered (Ratje *et al.*, 2010): After EF-G binding, the pre-translocational intermediate (Tl^{PRE}) state is engaged with tRNAs in the A/P and P/E states where the 30S SU head is moderately swiveled and the body ratcheted by 7°. Further swiveling, yet back-rotation of the body to only 4° lead to the Tl^{POST} state with tRNAs in the intra-subunit ap/P and pe/E states. This Tl^{POST} state was suggested to be stabilized by EF-G domain IV which interacts with h34 leading to 'latch' opening of the mRNA channel. EF-G-catalyzed mRNA and tRNA movements (Ermolenko and Noller, 2011; Savelbergh *et al.*, 2003; Studer *et al.*, 2003) in the SSU are coupled to complete back-ratcheting of the SSU to the classical POST state leaving the ribosome with a peptidyl-tRNA in the P-site and a deacylated tRNA in the E-site (Ermolenko and Noller, 2011) which has to dissociate for completion of one elongation cycle (Chen *et al.*, 2011; Uemura *et al.*, 2010). Sequential elongation steps are performed until an mRNA stop codon is displayed in the A-site.

Recent cryo-EM analysis of native, translating human 80S ribosomes revealed a significant population of the POST state and hence its high-resolution structure (Behrmann *et al.*, 2015). Authors suggest a stoichiometric E-site tRNA which contacts the LSU 28S rRNA with its acceptor stem and CCA-end. A tight binding pocket excludes aminoacyl-tRNAs, yet unlike in prokaryotes C75 interacts with eukaryote-specific eL44. Due to further E-site tRNA abundance in the unrotated PRE state, authors reason that it is the rotation which leads to E-site tRNA destabilization resulting in its subsequent release. Although the prevalent model for translocation includes EF-G binding, GTP-hydrolysis and subsequent mRNA/tRNAs movement coupled to ribosome unlocking followed by relocking steps, the sequential order of ribosome movement and translocation is still a hot topic in the field, leaving discussions about causes and consequences.

Despite of being highly regulated the steps of tRNA delivery or translocation can be erroneous which results in stalled ribosomes blocking further progression. Here, EF4 (former LepA), which contains six domains, (four of which are homologous to EF-G (Evans *et al.*, 2008b)) can produce relief. The crystal structure of *Thermus*-bound EF4 revealed its function in back-translocation or in helping to displace the EF-Tu delivered A-site tRNA. Remodeling of the DC is accompanied by a clockwise rotation of the SSU relative to LSU and is thought to ensure that ribosomes don't remain stalled during elongation (Gagnon *et al.*, 2014). A corresponding counterpart has not been discovered in eukaryotes (yet).

Eukaryotic Peculiarities

Even though the general process of translation elongation is highly conserved, some specific features have evolved for eukaryotes:

For example, E-site tRNA clearance after successful translocation is facilitated by the yeast- or fungal-specific adenosine triphosphatase (ATPase) eEF3 (Andersen *et al.*, 2006; Gagnon *et al.*, 2014) which, however, lacks homologues in higher eukaryotes.

Further, in eukaryotes eEF2 is post-translationally modified from His to diphthamide on the tip of its functionally important domain IV which was suggested to play a crucial role during development (Chen and Behringer, 2004; Liu *et al.*, 2006; Webb *et al.*, 2008) and to positively influence frame-accurate translocation (Ortiz *et al.*, 2006) by disrupting the mRNA - tRNA duplex interaction in the SSU DC (Taylor *et al.*, 2007). In addition, a regulatory phosphorylation at Thr56 by the eEF2 kinase was reported to inhibit eEF2 binding to the ribosome (Carlberg *et al.*, 1990) blocking total protein translation. Since translation elongation consumes the vast majority of energy in the eukaryotic cell (Rennie, 2005), eEF2 kinase regulation by the mitogen-activated protein (MAP) kinase and mTOR signaling pathways (Knebel *et al.*, 2001; Redpath *et al.*, 1996; Wang *et al.*, 2001) couples various cellular stimuli like mitogens, growth factors or G-protein coupled receptor antagonists to translation elongation via the eEF2-phosphorylation status, rendering eEF2 a key player in eukaryotic translation regulation.

eIF5A (EF-P in bacteria) does not represent a eukaryote-specific factor, however, is uniquely modified on a conserved lysine to hypusine (Park *et al.*, 2010). Its involvement in the elongation cycle by promoting the sophisticated poly-proline synthesis especially is important in the context of ribosomal stalling. As the quantity of genome-wide poly-proline motifs increases with complexity of the eukaryotic organism, a role for eIF5A in eukaryotic evolution has been suggested (Mandal *et al.*, 2014).

Reaching higher structural resolution and therefore increasing sensitivity for subtle changes and structural insights, Budkevich *et al.* (Budkevich *et al.*, 2014) have recently not only discovered propensity towards a rotated PRE-state during mammalian elongation, but also a novel 40S movement during tRNA accommodation from the A/T to the A/A state which is absent in bacteria. Such subunit rolling is concomitant with an altered binding site and interaction pattern for the ternary aminoacyl-tRNA:eEF1A:GTP complex. Even though the overall process of elongation seems to be conserved, subtle, yet crucial changes have evolved for eEF1A in order to adapt to a changed eukaryotic ribosomal interaction partner.

1.2.3 Termination and Recycling

Whenever the mRNA displays one of the three stop codons UAA (ochre), UAG (amber) or UGA (opal) in the ribosomal A-site during translation, generally speaking, no matching tRNA is abundant (Brenner *et al.*, 1965; Weigert and Garen, 1965). In rare cases, due to translational recoding, UAG can lead to selenocysteine incorporation (Chambers *et al.*, 1986; Zinoni *et al.*, 1986) and in methanogenic archaea as well as in bacteria UGA can lead to pyrrolysine incorporation (Kavran *et al.*, 2007; Yanagisawa *et al.*, 2006; Yuan *et al.*, 2010). Yet, typically stop codon recognition is mediated by class-I release factors (RFs) (Capecchi, 1967; Frolova *et al.*, 1994) which catalyze peptide-release, whereupon peptide-synthesis is completed. Sequence similarities between eukaryotic and prokaryotic class-I RFs are rarely present, however, they all mimic a tRNA-like shape and are known to bind to the ribosomal A-site where they fulfill their functions.

Prokaryotic Termination

Prokaryotes utilize two class-I release factors (RF1 and RF2) (see Figures 9A, B) (Capecchi, 1967) with mixed specificities for recognizing the three stop codons. UAA and UAG are recognized by RF1, whereas UAA and UGA by RF2. In biochemical studies, the PxT- (RF1, residues *Ec* 188 - 190 (*Tt* 184 - 186)) and SPF-motifs (RF2, residues *Ec* 205 - 207 (*Tt* 206 - 208)) were suggested to directly decode the three bases of the stop codon with the three aa residues upon binding (Anderson *et al.*, 2000), yet several crystal structures of RF1/2-bond 70S ribosomes enlightened us with a more complicated network of interactions (Jin *et al.*, 2010; Korostelev *et al.*, 2008, 2010; Laurberg *et al.*, 2008; Weixlbaumer *et al.*, 2008; reviewed in Zhou *et al.*, 2012). In all structures, the RFs bound in their extended conformation connecting the DC with the PTC in the respective SUs. The two factors are similarly composed of four domains 1 - 4, where domain 1 contacts class-II RF and L11 (Pallesen *et al.*, 2013), domains 2 and 4 co-fold for forming the decoding region and domain 3 is involved in peptide-hydrolysis via its conserved GlyGlyGln (GGQ) motif. Strikingly, the high-resolution structures revealed conformational changes in the ribosomal DC upon RF binding: Unlike during A-site tRNA binding (see 1.2.2 Decoding), RF1/2 binding is concomitant with *Ec/Tt* A1492 (*Hs* A1824) bulging out of helix 44 (h44) to engage in stabilizing interactions with *Ec/Tt* G530 (*Hs* G626). *Ec/Tt* A1493 (*Hs* 1825) remains in h44 and stacks on *Ec/Tt* A1913 (*Hs* A3731) (in H69) resuming the original place of *Ec/Tt* A1492 (*Hs* A1824). If *Ec/Tt* A1913 (*Hs* A3731) resided in its non-stacking position, RF1/2 binding would sterically clash. The mRNA stop codon bases 1 and 2 are positioned similarly to sense codon bases during decoding (Demeshkina *et al.*, 2012), yet interestingly base 3 is rotated away from its usual base pairing position due to RF1/2 loop insertion between bases 2 and 3 (also see Figure 53D). RF1/2 further contact mRNA bases 4 and 5 whose identities have been shown to influence termination efficiency (Tate and Mannerling, 1996).

How can the two RFs result in such high termination accuracy of 10^{-5} without any proof-reading mechanism (Freistroffer *et al.*, 2000)? Generally, stop codon recognition relies on an H-bonding network and van-der-Waals stacking interactions (see Figures 9C - J). A conserved Gly (RF1: *Ec* Gly120 (*Tt* Gly116) (Korostelev *et al.*, 2008, 2010); RF2: *Ec* Gly137 (*Tt* Gly138) (Laurberg *et al.*, 2008; Weixlbaumer *et al.*, 2008)) packs against Uracil at position 1 of the stop codon (U_1) sterically hindering larger purines to bind. Further H-bonding to the backbone N of a glutamic acid (RF1: *Ec* Glu123 (*Tt* Glu119); RF2: *Ec* Glu140 (*Tt* Glu141)) excludes cytosine due to its inverted H-bonding capacity. RF1, containing the PxT-motif, uses *Ec* Thr190 (*Tt* Thr186) to discriminate U_1 and the adenine at position 2 (A_2) by donating an H-bond to the 4-keto oxygen of U_1 and by accepting an H-bond from the N6-amino group of A_2 (see Figures 9C, D). This would not be possible with a guanine at position 2 (G_2) harboring a keto-group instead of an amino group at its position 6. RF2, containing the SPF-motif, can donate and accept an H-bond either from A_2 or G_2 with *Ec* Ser205 (*Tt* Ser206) (see Figures 9E, F). For RF1, H-bonding to both types of purines in position 3 is possible with *Ec* Gln185 (*Tt* Gln181) and *Ec* Thr198 (*Tt* Thr194) (see Figures 9G, H). Stacking on *Ec/Tt* G530 discriminates smaller pyrimidines for both RFs. RF2 however, uses the H-bonding capacity of *Ec* Thr214 (*Tt* Thr216) that can only act once as H-bond donor excluding guanine at position 3 (G_3) (see Figures 9I, J). Consequently, the two motifs previously suggested only play a partial role in specific codon recognition: Merely *Ec* Thr190 (*Tt* Thr186) (PxT) and *Ec* Ser205 (*Tt* 206) (SPF) in RF1 and RF2, respectively directly interact with the stop codon. The Pro residues (PxT, SPF) are rather responsible for proper loop-conformation whereas Ala (x in *E.coli* PxT), Val (x in *Thermus* PxT) and Phe (SPF) provide non-specific van-der-Waals contacts.

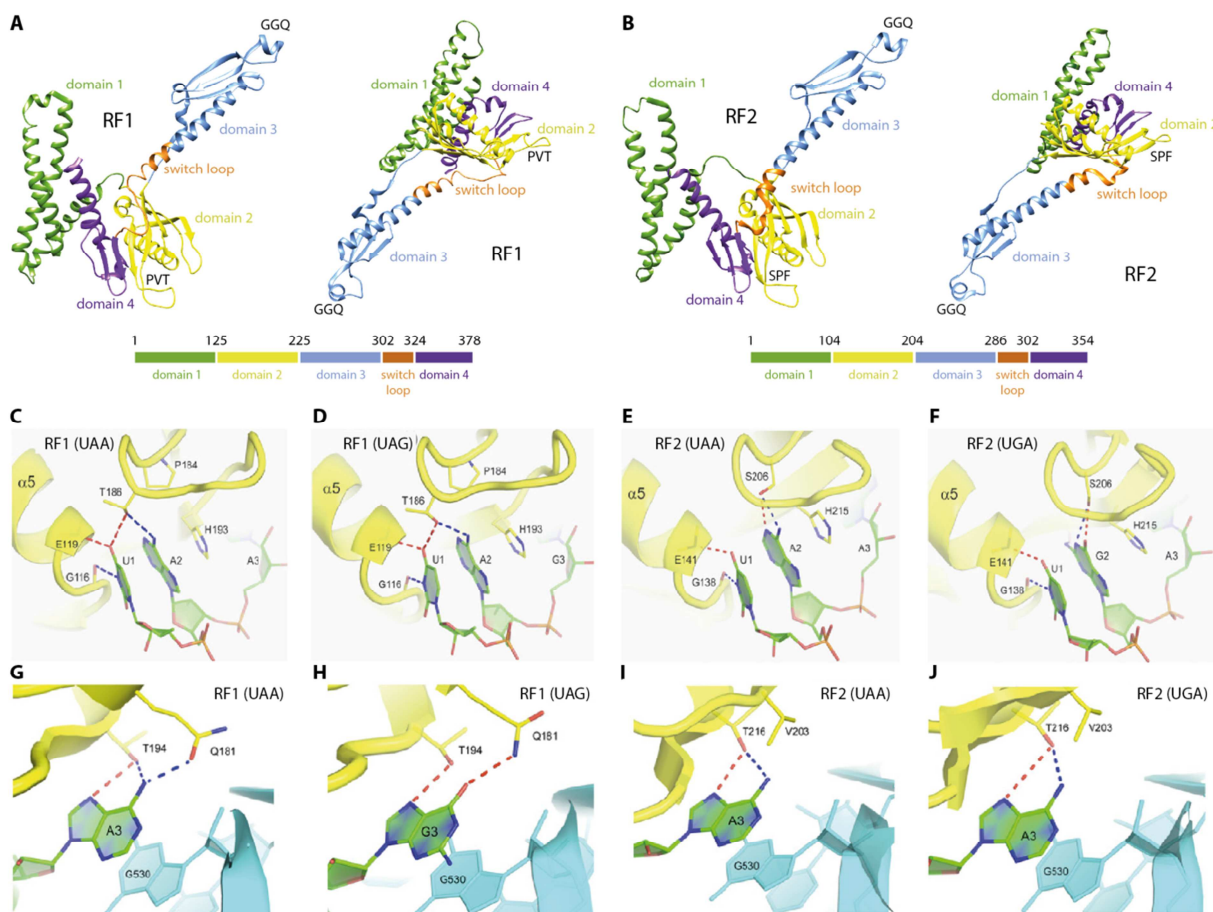


Figure 9: Stop Codon Decoding by the Prokaryotic Class-I Release Factors RF1 and RF2.

(A) Crystal structure of the *Thermus thermophilus* (*Thermus*) ribosome-bound class-I release factor RF1 (decoding the UAA stop codon) (Laurberg *et al.*, 2008) with its domains 1 (green), 2 (yellow), 3 (blue) and 4 (purple) colored distinctively. The switch loop is colored in orange (PDB-code: 3D5A). (B) Crystal structure of the *Thermus* ribosome-bound class-I release factor RF2 (decoding the UAA stop codon) (Korostelev *et al.*, 2008) colored as in (A) (PDB-code: 3F1E). (C) Recognition of uracil at position 1 (U_1) and adenine at position 2 (A_2) of the UAA stop codon by RF1 (Laurberg *et al.*, 2008). (D) Recognition of U_1 and A_2 of the UAG stop codon by RF1 (Korostelev *et al.*, 2010). (E) Recognition of U_1 and A_2 of the UAA stop codon by RF2 (Korostelev *et al.*, 2008). (F) Recognition of U_1 and guanine at position 2 (G_2) of the UGA stop codon by RF2 (Weixlbaumer *et al.*, 2008). (G) Recognition of adenine at position 3 (A_3) of the UAA stop codon by RF1 (Laurberg *et al.*, 2008). (H) Recognition of guanine at position 3 (G_3) of the UAG stop codon by RF1 (Korostelev *et al.*, 2010). (I) Recognition of A_3 of the UAA stop codon by RF2 (Korostelev *et al.*, 2008). (J) Recognition of A_3 of the UGA stop codon by RF2 (Weixlbaumer *et al.*, 2008).

Release factors are indicated in yellow, the 16S rRNA in cyan and the mRNA in green with its heteroatoms colored distinctively. Figures (C) - (J) taken from Korostelev (Korostelev, 2011).

Subsequent to peptide-release RF1/2, the deacylated P-site tRNA and the mRNA are still bound to the ribosome. Class-II release factor RF3 ensures efficient release of RF1/2 in a GTP-coupled manner (Freistroffer *et al.*, 1997; Grentzmann *et al.*, 1998). The RF3 GTPase is structurally related to EF-G (see Figure 10A) and likewise interacts with the SRL (Gao *et al.*, 2007), however, here the aforementioned His residue (see 1.2.2) (Voorhees *et al.*, 2010) important for catalyzing GTP hydrolysis is situated more than 8 Å away from the γ -phosphate likely not taking part in the reaction as observed in two crystal structures (Jin *et al.*, 2010; Zhou *et al.*, 2012b). Interestingly, RF3 was suggested to bind in its GDP-bound state whereupon nucleotide exchange (Zavialov *et al.*, 2001) leads to ribosome inter-

subunit rotation and head movement causing a clash of the 30S head and the L11-stalk with RF1/2 (reviewed in Klaholz, 2011; Zhou *et al.*, 2012a). This, together with a hinge movement in RF3, was proposed to promote RF1/2 release resulting in the post-termination complex. According to cryo-EM reconstructions of the RF3-bound 70S ribosome the deacylated tRNA resides in a P/E hybrid state (Jin *et al.*, 2010; Zhou *et al.*, 2012b). Such observation explains why RF3 only functions after peptide release since only deacylated tRNAs can be moved to the E-site.

Prokaryotic Ribosome Recycling

To prepare for the next round of translation, the post-termination complex has to be further dissociated into its components: mRNA, deacylated tRNA and the ribosomal SUs. This process is mediated by the ribosome recycling factor (RRF) (Janosi *et al.*, 1996), likewise a structural mimicry of a tRNA (see Figure 10B) (Kim *et al.*, 2000; Selmer, 1999; Toyoda *et al.*, 2000; Yoshida *et al.*, 2001), in concert with GTP-bound EF-G (Barat *et al.*, 2007; Hirashima and Kaji, 1973; Peske *et al.*, 2005). Precise interactions of the two factors are still a matter of debate. Moreover, when and how the tRNA and mRNA are released has also not been established (Nakamura and Ito, 2011). As connection to the initiation process, IF3 is thought to bind to the 30S SU employing its anti-associative potential to keep the SUs separate (Peske *et al.*, 2005; Zavialov *et al.*, 2005) until a new round of translation is heralded (Hirokawa *et al.*, 2008; Karimi *et al.*, 1999).

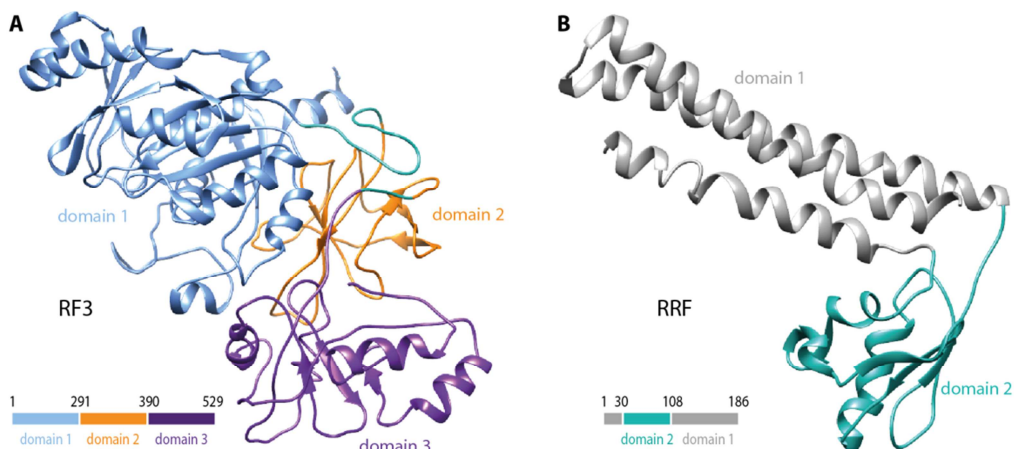


Figure 10: Crystal Structures of Ribosome-bound RF3 and RRF.

(A) Crystal structure of ribosome-bound *Escherichia coli* class-II release factor RF3 with its domains 1 (blue), 2 (orange) and 3 (purple) colored distinctively (PDB-code: 4V89). **(B)** Crystal structure of ribosome-bound *Thermus thermophilus* ribosome recycling factor (RRF) with its domains 1 (gray) and 2 (turquoise) colored distinctively (PDB-code: 4v46).

Eukaryotic (Premature) Termination

Conversely, a single class-I release factor termed eRF1 was discovered to perform decoding of all three stop codons in eukaryotes. eRF1 is composed of three domains (Frolova *et al.*, 2000; Song *et al.*, 2000): The N domain which is suggested to interact with the stop codon (Bertram *et al.*, 2000), the M domain which harbors the conserved GGQ motif (Frolova *et al.*, 1999; Seit-Nebi *et al.*, 2001) and the C domain which interacts with GTP-bound eRF3 likely for approaching the ribosome in a ternary complex or with ATP binding cassette E1 (ABCE1) for ribosome recycling (Cheng *et al.*, 2009; Ebihara and Nakamura, 1999). Numerous biochemical studies suggested many eRF1 residues to be directly involved in stop codon interactions, yet evidence has accumulated for the participation of the TAS-NIKS (residues 58 - 64), the YxCxxxF (residues 125 - 131) and the GTS (residues 31 - 33)

motifs located within the N domain (Bulygin *et al.*, 2010; Chavatte *et al.*, 2002; Conard *et al.*, 2012; Frolova *et al.*, 2002; Seit-Nebi *et al.*, 2002; Wong *et al.*, 2012). In addition, nuclear magnetic resonance (NMR) and x-ray crystallography-derived structures delivered proposed modes of action for eRF1 (Cheng *et al.*, 2009; Ivanova *et al.*, 2007; Mantsyzov *et al.*, 2010; Polshakov *et al.*, 2012; Song *et al.*, 2000). As opposed to the prokaryotic RFs, eRF1 is delivered to the ribosome by eRF3 (see Figures 11A, B), the class-II RF thought to stimulate eRF1 activity on the ribosome and therefore to increase termination efficiency (Cheng *et al.*, 2009; Frolova *et al.*, 1999). eRF3 is composed of an N terminal domain which is non-essential for termination (Kushnirov *et al.*, 1988), however, was reported to interact with the PABP bound to the 3' poly(A) tail of the mRNA (Cosson *et al.*, 2002; Hoshino *et al.*, 1999). This interaction likely enhances termination efficiency (Cosson *et al.*, 2002; Ivanov *et al.*, 2008). Further, eRF3 consists of the GTP-binding G domain as well as the β -barrel domains 2 and 3 which are homologous to EF-Tu and eEF1A (Kong *et al.*, 2004).

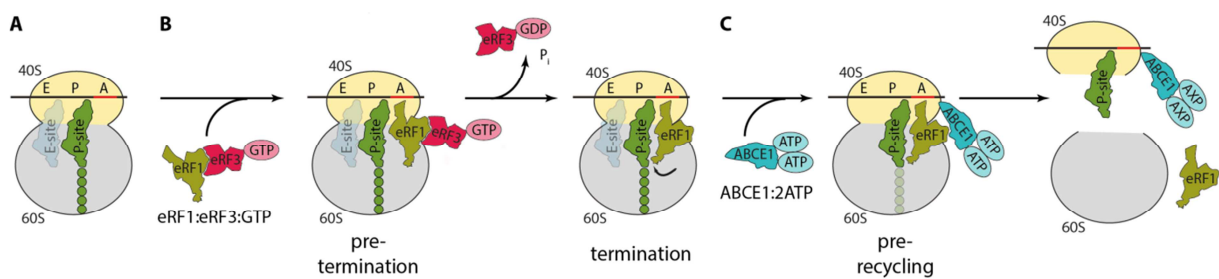


Figure 11: Schematic of Eukaryotic Termination and Recycling.

The 40S ribosomal subunit (SU) is depicted in yellow, the 60S ribosomal SU in gray. Further, the tRNA exit-site (E-site), the peptidyl-tRNA binding site (P-site) and the aminoacyl-tRNA binding site (A-site) are marked with E, P and A, respectively. **(A)** When the ribosome encounters a stop codon (red) in the A-site decoding center, usually translation termination is sought. **(B)** For the formation of the pre-termination complex, the eRF1:eRF3:guanosine triphosphate (GTP) ternary complex binds to the A-site. eRF1 universally decodes all three stop codons whereupon GTP is hydrolyzed by the guanosine triphosphatase eRF3 which subsequently dissociates from the ribosome. Conformational changes in eRF1 result in its elongated conformation where its M Domain is positioned in the peptidyl-transferase center. Here, peptide-release is mediated by the universally conserved GGQ motif. **(C)** Recycling factor ABCE1 binding to 2 adenosine triphosphates (ATPs) can assist in the release mechanism and eventually leads to recycling of the 60S SU, eRF1 and the 40S SU (still bound to the deacylated tRNA and ABCE1). The state of the ABCE1-bound nucleotides after ribosome recycling is still unknown.

Upon ribosome encounter in the ternary complex, eRF1 was shown to perform stop codon decoding, however, to not engage in its active and elongated conformation, yet. Therefore, the GGQ motif is still bound to eRF3 as opposed to the PTC where peptide-bond hydrolysis takes place (des Georges *et al.*, 2014; Preis *et al.*, 2014; Taylor *et al.*, 2012). eRF3 interactions with eRF1 and the ribosome were demonstrated to be a prerequisite for GTP hydrolysis (Frolova *et al.*, 1996) upon which eRF3 dissociation leads to structural rearrangements in eRF1 (Salas-Marco and Bedwell, 2004) to position the eRF1 M domain within the PTC to hydrolyze the ester-bond in a similar manner to its prokaryotic counterpart (see Figure 11B) (Muhs *et al.*, 2015). The basic steps of eukaryotic translation termination were visualized in medium-resolution cryo-EM structures of the eRF1:eRF3:GMPPNP containing pre-termination complex (des Georges *et al.*, 2014; Preis *et al.*, 2014; Taylor *et al.*, 2012), the eRF1-containing termination complex (Muhs *et al.*, 2015) and the eRF1:ABCE1:AMPPNP containing pre-recycling complex (Preis *et al.*, 2014), yet, due to lacking resolution and ambiguous

biochemical results the molecular mechanism of stop codon decoding has been a matter of debate for decades.

Further significance of comprehending the molecular mechanism of stop codon recognition lies in the association of premature termination codons (PTCs) (nonsense mutations) with ~1/3 of all inherited genetic diseases (Frischmeyer, 1999). The presence of a PTC can lead to exon skipping, decreased mRNA stability or protein truncation (Mort *et al.*, 2008). Generally, for cellular protection potential dominant negative or gain-of-function effects due to protein truncation are prevented by the eukaryotic surveillance mechanism known as nonsense-mediated (mRNA) decay (NMD) (reviewed in Kervestin and Jacobson, 2012; Leeds *et al.*, 1991; Lykke-Andersen and Bennett, 2014; Peltz *et al.*, 1993; Pulak and Anderson, 1993; reviewed in Shoemaker and Green, 2012). Here, the PTC is recognized as such, leading to rapid degradation of the truncated protein as well as the faulty mRNA. The mechanistic understanding of NMD is still poor, yet three basic models have evolved describing the process of how NMD might be triggered: 1) The exon junction complex (EJC) model, 2) the up-frameshift 1 (Upf1) 3'-untranslated region (UTR) sensing and potentiation model and 3) the faux 3'-UTR model (reviewed in He and Jacobson, 2015).

The occurrence of diseases and their phenotypic expressions are associated with varying rationales depending on whether NMD is activated or not. The NMD protection mechanism only grasps if the PTC is positioned at least 50 nt upstream of the most 3' exon-exon junction (reviewed in Maquat, 2004). As briefly mentioned, PTCs which do not provoke NMD can lead to dominant negative effects if the truncated protein interferes with the wild-type (WT) protein. An example for this is the sex-determining region Y (SRY)-related high mobility group (HMG)-box (SOX10) gene whose PTC-containing mRNA causes the Waardenburg-Shah syndrome (Mort *et al.*, 2008). Furthermore, the associated absence of NMD due to a PTC in the last exon of the β -globin gene (HBB) results in a dominant-type of β -thalassemia (Hall and Thein, 1994). The pathogenesis of this disorder involves the dominant-negative dimer formation of the truncated β -globin chain with the α -globin chain hence leading to anemia in the patients (Hall and Thein, 1994; reviewed in Thein, 2013). Another example, where NMD is beneficial is the Marfan Syndrome (Byers, 2004), a connective tissue disorder, where NMD contributes to limiting the severity of the disease. Here, truncated and WT fibrillin-1, a 350 kilodalton (kDa) glycoprotein, interact with each other which disrupts the proper formation of the extracellular microfibrils (Eldadah *et al.*, 1995). Consequently, here NMD and the abolishment of the truncated protein results in a mild phenotype, whereas its expression is associated with severe effects on the patient. However, NMD can also be associated with drawbacks if the truncated protein would retain some activity, but the decay pathway results in complete protein abolishment and loss of function. 10 % of cystic fibrosis (CF) patients with e.g. a W1282X or G542X mutation in the cystic fibrosis transmembrane conductance regulator (CFTR) gene suffer from the consequences (Hamosh *et al.*, 1992; Roberto Gambari, 2015). It was shown that the N-terminal part of the CTFR protein is sufficient to form a functional cyclic adenosine 3',5'-monophosphate (cAMP)-regulated chloride channel (Sheppard *et al.*, 1994) and a small percentage (10 - 15 %) of protein expression would already be sufficient to efficiently milder the patients' disorders (Chu *et al.*, 1992). Further diseases which are caused by PTC-associated NMD are for example the Hurler syndrome (alpha-L-iduronidase deficiency), X-linked nephrogenic diabetes insipidus (XNDI), ataxiatelangiectasia (ATM), cystinosis, Duchenne muscular dystrophy (DMD), Hailey-Hailey disease, factor VII deficiency or infantile neuronal lipofuscinosis (reviewed in Bidou *et al.*, 2012 and Linde and Kerem, 2008). Consequently, high hopes and efforts have been attributed to PTC read through drug

development by outcompeting release factor binding to prevent NMD (reviewed in Bidou *et al.*, 2012; Linde and Kerem, 2008). A detailed mechanistic understanding of how eRF1 binds to the ribosome and especially the mRNA stop codon could serve as starting point to specifically design drugs that successfully compete for stop codon binding. Enabling the translation of merely a small percentage of the full length protein (with a point mutation) would in many cases already be associated with clinical rescue.

So far, potential therapeutics in this context include aminoglycosides and the organic molecule PTC124, yet both are associated with high drawbacks. Aminoglycoside binding to prokaryotic ribosomes was demonstrated to cause *Ec* A1492 (*Hs* A1824) and *Ec* A1493 (*Hs* 1825) to flip out of h44 mimicking tRNA delivery to the A-site and to increase error-prone tRNA selection (François *et al.*, 2005; Tsai *et al.*, 2013). This was suggested to more effectively allow near-cognate aa-tRNA binding to the stop codon (reviewed in Ramakrishnan, 2002). However, this type of antibiotic cannot be used for long-term drug treatment as it has relatively severe side effects due to its nephrotoxicity and ototoxicity (Humes, 1988; Selimoglu, 2007). PTC124 (Ataluren) has been discovered in a high-throughput screen and specifically targets PTCs for read through, however, does not affect canonical termination (Welch *et al.*, 2007). Its effect has been controversial as PTC124 itself was discovered to upregulate firefly luciferase (FLuc) activity which was utilized as read-out for its effectiveness in the initial screening (Auld *et al.*, 2009). *PTC Therapeutics* has stated to have used independent screenings which reassure a role for PTC124 in nonsense-suppression by now (Peltz *et al.*, 2009), yet clinical trials struggle to reveal clear effects (reviewed in Keeling *et al.*, 2014; Kerem *et al.*, 2014). Compared to aminoglycosides, PTC124 has manageable side-effects for the patient and due to unmet medical needs for DMD it has been licensed in Europe under the trade name Translarna™ (*PTC Therapeutics*) for its treatment.

Another therapeutic approach could be the prevention of NMD through increasing the performance of canonical termination instead. Designing drugs with specific effects only on desired targets, however, will most likely prove difficult. General perturbation of NMD would likely result in off-target effects which are associated with intolerable side-effects for the patient hindering the drugs' therapeutic applications (reviewed in Keeling *et al.*, 2014).

Many efforts have been undertaken to develop drugs on the basis of increasing PTC read through, however, no promising candidate has been discovered up to date. Whichever method or compound will lead to safe and efficient treatment of PTC-derived diseases in the end, understanding the molecular mechanism of translation termination and NMD will be crucial to design effective termination or NMD suppressor drugs.

Eukaryotic Ribosome Recycling

Successful canonical termination results in an 80S ribosome associated with an mRNA, eRF1 in the A-site and a deacylated tRNA in the P-site. Consequently, to complete the translation cycle, components have to be disjoint (see Figure 11C).

To this end, the ABC-type ATPase ABCE1 (Rli in yeast) (Barthelme *et al.*, 2011; Pisarev *et al.*, 2010), which consists of two head-to-tail asymmetric ATPase sites (nucleotide binding domains (NBDs)) and two $[\text{Fe}_4\text{-S}_4]^{2+}$ clusters, plays a pivotal role (see Figures 12A, C) (Hung *et al.*, 1998). ABCE1 is essential (Andersen and Leevers, 2007; Dong *et al.*, 2004; Zhao *et al.*, 2004), conserved in eukaryotes and archaea (Dean and Annilo, 2005; Kerr, 2004) and was suggested to also play a role in ribosome

biogenesis (Dong *et al.*, 2004; Yarunin *et al.*, 2005). *In vitro* studies showed that already eRF1-binding by itself can promote recycling, however, the reaction rate is highly stimulated by ABCE1 (Pisarev *et al.*, 2010; Shoemaker and Green, 2011). Cryo-EM studies of yeast eRF1:Rli (Preis *et al.*, 2014) and archaeal (*Pyrococcus furiosus*) Pelota:ABCE1 (Pelota is the surveillance class-I RF and therefore paralog of eRF1) (Becker *et al.*, 2012) revealed four major contact sites of Rli/ABCE1 in the pre-recycling complex, primarily to the SSU. One contact is mediated by the $[\text{Fe}_4\text{-S}_4]^{2+}$ cluster domain which stabilizes the eRF1 C domain (Preis *et al.*, 2014). Why the contact is mediated by such peculiar cluster is still under debate. However, it was suggested to represent a direct link to cellular oxidative stress during which the oxidation of Fe^{2+} could cause ABCE1 inactivation (Alhebshi *et al.*, 2012; Barthelme *et al.*, 2007). Yeast Rli was shown to stimulate termination in an ATP-independent manner (Shoemaker and Green, 2011). Yet, its ATPase activity is required to promote SU splitting, resulting in the 60S SU and a deacylated tRNA:mRNA:40S SU complex.

In general, ABC-type proteins perform a tweezer like motion (Chen *et al.*, 2003; Hopfner, 2003): ATP binding closes a gap between the two NBDs whereas ATP hydrolysis leads to opening and adenosine diphosphate (ADP) and P_i release (see Figure 12B) (Barthelme *et al.*, 2011). In the case of ABCE1, however, it still remains to be elucidated what triggers such motion and how the motion is transferred to ribosome recycling.

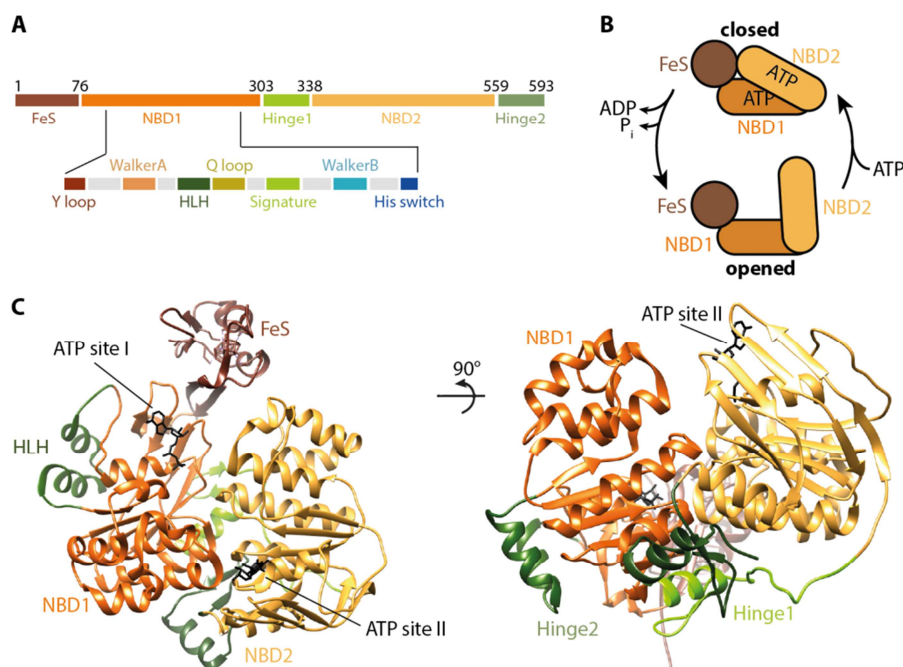


Figure 12: Recycling in Eukaryotes: The Adenosine Triphosphatase ABCE1.

(A) Primary domain structure of the human adenosine triphosphate (ATP)-binding cassette E1 (ABCE1) protein consisting of the conserved FeS domain (FeS) (dark brown), a nucleotide binding domain 1 (NBD1) (dark orange), a first hinge domain (Hinge 1) (light green), a second nucleotide binding domain (NBD2) (light brown) and a second hinge domain (Hinge 2) (green). Further, a more detailed composition of NBD1 is given (the aromatic Y loop (brown), the Walker A and B motifs (orange and light blue), the helix-loop-helix (HLH) (dark green), the Q loop (ocher), the ABC signature motif (Signature) (light green) and the His switch Region (His switch) (dark blue)). **(B)** Schematic of the catalytic cycle of ATP-binding cassette-type ATPases. A tweezer like motion closes or opens a gap between the two NBDs. The conformational changes between the closed and the opened conformations upon ATP binding and hydrolysis, respectively are fundamental for the proteins' functions. **(C)** Crystal structure of *Pyrococcus abyssi* ABCE1 (PDB-code: 3BK7). NBD1 and NBD2 form a cavity into which the two $[\text{Fe}_4\text{-S}_4]^{2+}$ clusters (in the FeS domain) extend. They are positioned adjacent to the ATP site I. As shown, two adenosine diphosphate molecules are bound to the ATP sites I and II.

Figure (C) was modified from Nürenberg *et al.* (Nürenberg and Tampé, 2013).

Similarly to prokaryotes, ribosome dissociation is irreversible due to initiation factor binding to the individual subunits (Jackson *et al.*, 2010). Further, 40S clearance seems to be mediated by eIF1, 1A and 3j (shown *in vitro*) (Pisarev *et al.*, 2007), ligatin/eIF2D (Skabkin *et al.*, 2010) or to a lesser extend multiple copies in T-cell lymphoma-1 (MCT-1) and density-regulated protein (DENR) (Skabkin *et al.*, 2010). ABCE1's interaction with the eIFs tightly couples ribosome recycling and translation initiation which completes and prepares the translation cycle for its efficient re-start.

1.2.4 *In vitro* Translation Systems

In vitro translation systems have been successfully used for more than 50 years (Dvorak *et al.*, 1967; Matthaei and Nirenberg, 1961). Since then, commercially available cell-free translation systems have provided useful tools for protein expression in *E. coli* (S30 Systems (*Promega*), *PURExpress*® (NEB)), RTS (5 Prime), Expressway™ (*ThermoFisher Scientific*)), wheat germ (WG) (TNT® Systems (*Promega*), WEPRO (*CellFree Sciences*), RTS (5 Prime)) or rabbit reticulocyte lysate (RRL (*Promega*), Retic lysate IVT (*ThermoFisher Scientific*)) extracts particularly if the sought protein product interferes with cell viability due to its toxicity or is rapidly degraded by intracellular proteases. These systems are not only useful to characterize synthesized proteins, but also for *in vitro* reconstitution of translation intermediates. To efficiently analyze the intricate translation cycle and dissect individual molecular contributions, such controllable environments can be advantageous. While *E. coli*- (Carlson *et al.*, 2011; Gale and Folkes, 1954; Shimizu *et al.*, 2001, 2005), WG-, insect cell- (such as SF9 or SF21) (Ezure *et al.*, 2006, 2010) or RRL-based extracts (Jackson and Hunt, 1983) are commonly available and protocols are well established, it was not until recently that the human translation system came to the fore (Brödel *et al.*, 2013; Mikami *et al.*, 2010a; Zeenko *et al.*, 2008). Here, the certainty of 'natural' post-translational modifications (PTMs) like phosphorylation or N-glycosylation is an advantage, while such modifications are missing in RRL-derived proteins due to lacking microsomes. The bottle neck however, is reduced initiation efficiency caused by phosphorylation of the initiation factor eIF2 α on Ser51 during extract preparation, still constituting an obstacle for efficient translation. Nonetheless, it is crucial to especially understand translation regulation in the human system, allowing for more precise drug development in the future. This renders the human system ideal for biochemical assays or *in vitro* reconstitutions followed by high-resolution structural studies which can generate profound insights into molecular details of the translation cycle relevant for human health.

1.2.5 Co- and Post-translational Protein Folding

For obtaining functional activity, nascent polypeptide chains have to acquire their 'native state' by 3D folding which is thermodynamically favored in solution. The primary aa sequence defines both the local structure like α -helices or β -sheets (secondary) and the protein's overall 3D (tertiary) structure (Anfinsen *et al.*, 1954). Numerous folding-related studies were conducted *in vitro* on chemically denatured proteins (Brockwell *et al.*, 2000; Herbst *et al.*, 1997; Kubelka *et al.*, 2004), however, cellular influences such as molecular crowding (Ellis and Minton, 2006), molecular chaperones (reviewed in Hartl, 1996), interacting co-factors (Apyo and Wittung-Stafshede, 2002; Bushmarina *et al.*, 2006; Goedken *et al.*, 2000; Pozdnyakova *et al.*, 2000; reviewed in Wilson *et al.*, 2004; Wittung-Stafshede, 2002), translation speed (Chow *et al.*, 2003; Mu *et al.*, 2008) and the influence of the translating ribosome itself (Chattopadhyay *et al.*, 1996; Das *et al.*, 1992; Kudlicki *et al.*, 1997; Phillips, 1967) were demonstrated to cause affected folding funnels *in vivo*. A folding funnel (see Figure 13A) is a model representing potential conformational energy states available *en route* to the 'native state' of the protein (Bryngelson *et al.*, 1995; Dill *et al.*, 1995). Its rugged energy surface was

introduced to account for transiently stable intermediates and restricted conformational space (global minima) when progressing along the folding procedure which can result in kinetically trapped intermediates. Partially folded or misfolded proteins expose hydrophobic aa patches prone to result in amorphous aggregates, oligomers or even amyloid fibrils (Cabrita *et al.*, 2009; David *et al.*, 2010; Demontis and Perrimon, 2010; Eichmann *et al.*, 2010). In this regard, maintaining protein integrity is of particular importance since several abundant diseases including Parkinson's, Alzheimer's and Huntington's diseases are associated with aggregated proteins (reviewed in Chiti and Dobson, 2006; Kayed *et al.*, 2003; Olzscha *et al.*, 2011).

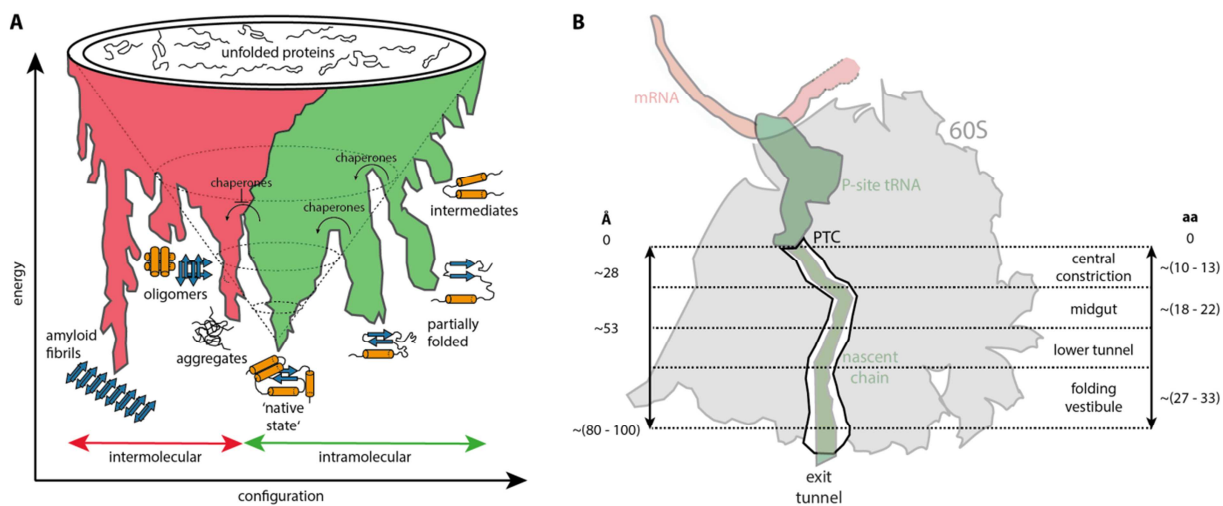


Figure 13: Co- and Post-translational Protein Folding.

(A) Schematic of a folding funnel energy landscape that proteins traverse during folding. The 'native state' is represented by a deep free energy minimum. The roughness of the funnel was introduced to account for partially folded and intermediate states demonstrated by local minima in which proteins can be kinetically trapped. Chaperones assist in surmounting the energy-barriers and in preventing the destabilization of (partially) folded or intermediate states (green). If multiple proteins form intermolecular contacts, amorphous aggregates, toxic oligomers or ordered amyloid fibrils can result (red). **(B)** Architecture of the ribosomal tunnel which is divided into the peptidyl-transferase center (PTC), the central constriction, the midgut, the lower tunnel and the folding vestibule areas. Approximate distances in angstrom (\AA) as well as amino acid (aa) lengths from the PTC are indicated.

Figure (A) based on Hartl *et al.* (Hartl *et al.*, 2011).

The chaperone machinery restricts such potential misfolding or aggregation by promoting folding without being part of the protein's final structure (reviewed in Deuerling and Bukau, 2004; reviewed in Frydman, 2001; reviewed in Hartl and Hayer-Hartl, 2009). The heat shock protein 70 kDa (HSP70) family, DnaK in prokaryotes (reviewed in Mayer and Bukau, 2005) and HSC70 in eukaryotes, (Auluck *et al.*, 2002) comprises chaperones functioning in the cytoplasm which mediate co- or post-translational folding as well as escorting proteins to chaperonins (GroEL (group I) in bacteria (reviewed in Hartl and Hayer-Hartl, 2009; reviewed in Horwich and Fenton, 2009), TRiC (group II) in eukaryotes (Cuéllar *et al.*, 2008)). Moreover, the ribosome itself was suggested to be involved in protein folding (Chattopadhyay *et al.*, 1996; Das *et al.*, 1992; Kudlicki *et al.*, 1997) and certainly serves as platform for chaperones of the HSP70 system: Trigger factor (TF) in prokaryotes (Ferbitz *et al.*, 2004; Hoffmann *et al.*, 2006; Tomic *et al.*, 2006; Wegrzyn and Deuerling, 2005; Witt, 2009) and the nascent polypeptide-associated complex (NAC) (Wiedmann *et al.*, 1994) or MPP11 and HSP70L1 in mammals (ribosome-associated complex (RAC) in yeast) (Gautschi *et al.*, 2001; Leidig *et al.*, 2013)

serve as protective shields for the nascent polypeptide chains. Beyond, during translation ribosomes form distinctly arranged pseudo-helical polysome-complexes which allow for maximized distance and minimized interchain interaction between neighboring newly emerging nascent chains as visualized via cryo-EM tomography (Brandt *et al.*, 2009; Chow *et al.*, 2003). Single-domain proteins can only completely engage their ‘native state’ post-translationally (Chow *et al.*, 2003; Taniuchi and Anfinsen, 1969) and have been observed to successfully do so independently even *in vitro* (Anfinsen and Haber, 1961). However, especially in eukaryotes, larger multi-domain proteins undergo domain-wise folding already co-translationally (Batey *et al.*, 2008; Evans *et al.*, 2008a). Evolution of larger and more complex multi-domain proteins might have been accompanied by slowing the translational speed adapting to co-translational folding. A remarkable finding for translation adjustments, to concomitantly allow for highly optimized protein folding, is the clustering of rare codons (Clarke and Clark, 2008), particularly at inter-domain regions, which causes translational pausing, resulting in synchronization of translation and folding or allowing for interactions with chaperones (Zhang *et al.*, 2009a).

If protein folding is monitored so closely directly after the protein emerges from the ribosome protected exit tunnel (Fulle and Gohlke, 2009; Voss *et al.*, 2006), is it likewise already in the tunnel directly after aa addition in the PTC? The tunnel provides a highly spatially confined area with 80 - 100 Å length (Voss *et al.*, 2006) and 10 Å (at the central constriction) - 20 Å diameter (see Figure 13B) (Ban, 2000). Such confinements don’t allow for tertiary structure formation, however, several biochemical (Ellis *et al.*, 2009; Voss *et al.*, 2006) and computational (Ziv *et al.*, 2005) experiments have been reported for sequence-dependent α -helical propensity of nascent peptides in the tunnel environment. The varying electrostatic potential (Lu and Deutsch, 2005, 2008; Lu *et al.*, 2007) was suggested to be responsible for some tunnel regions to promote α -helix formation more than others (Bhushan *et al.*, 2010a; Kosolapov *et al.*, 2004; Tu and Deutsch, 2010; Tu *et al.*, 2007). However, whether this is due to entropic effects or particular aa interactions with the tunnel wall still has to be investigated.

1.3 Translational Arrest by Nascent Polypeptides

After its discovery in 1982 (Bernabeu and Lake, 1982), the ribosomal exit tunnel was commonly contemplated as static conduit, however, ongoing research has revealed its capacity to actively interact with and even monitor the newly emerging polypeptides (Berndt *et al.*, 2009; Bornemann *et al.*, 2008; Cruz-Vera *et al.*, 2005, 2006; Devaraneni *et al.*, 2011; Dimitrova *et al.*, 2009; Gong and Yanofsky, 2002; Liao *et al.*, 1997; Lin *et al.*, 2012, 2011; Lovett and Rogers, 1996; Lu and Deutsch, 2005; Lu *et al.*, 2011; Mariappan *et al.*, 2010; Morris and Geballe, 2000; Nakatogawa and Ito, 2002; Pool, 2009; Ramu *et al.*, 2011; Robinson *et al.*, 2012; Wang and Sachs, 1997a, 1997b; Yap and Bernstein, 2009). The nascent chain configuration cannot only signal to the tunnel exit influencing extra-ribosomal activities like chaperone-engagement as mentioned above (see 1.2.5), but can also affect its own translation progression by the modulation of PTC residues from within the tunnel. In extreme cases, specific nascent chain interactions with tunnel wall components can lead to ribosomal slow-down or even stalling due to PTC inactivation, termed ribosomal arrest.

1.3.1 Features and Functions

Up to 49 % of all human transcripts (Calvo *et al.*, 2009; Lawless *et al.*, 2009) contain upstream ORFs (uORFs) on their transcript leader sequences. Such abundance reveals the multi-functionality associated with their mode of gene regulation one of which is ribosomal arrest. Random ribosomal

arrest during peptide elongation would be harmful to the cell, demanding for precise cues upon which slow-down or stalling is expedient. Often, the key regulators are small, extrinsic effector molecules like antibiotics (e.g. macrolides for the antibiotic resistance genes ErmCL and ErmAL1 (Ramu *et al.*, 2009)) or a free aa like Trp for the tryptophanase leader peptide TnaC (Gong and Yanofsky, 2002; Wang and Sachs, 1997a, 1997b). But even the nascent chain itself can be sufficient (as reported for the membrane integration and folding monitor (MifM) (Chiba *et al.*, 2009), the secretion monitor SecM (Nakatogawa and Ito, 2002) or the human cytomegalovirus gp48/UL4 uORF2 (hCMV) (Degnin *et al.*, 1993; Geballe *et al.*, 1986)) for the *cis*-specific elements to function in translational arrest by inhibiting peptidyl-transfer (e.g. ErmCL, MifM, SecM), translocation (e.g. cystathionine- γ -synthase 1 (CGS1) contained arrest-peptide (Onouchi *et al.*, 2005)) or their own translation termination (e.g. arginine attenuator peptide (AAP), hCMV (Degnin *et al.*, 1993), TnaC). The arrest-sequences can encompass only as little as 3 aa, but also a wide stretch wherein the critical aa reside. Mostly, only a few residues herein are essential for stalling, however, their exact spacing and therefore positioning in the tunnel are inevitable. Stalling can occur at single sites (e.g. ErmCL, hCMV, TnaC) or over longer stretches and at multiple sites (e.g. MifM, SecM). In prokaryotes, stalling effects are rather positive: For instance, residing ribosomes allow disruption of mRNA secondary structures that expose the SD sequence of the target ORF to enable translation initiation (see Figure 14A). Examples therefor are ErmCL (Ramu *et al.*, 2009), ErmAL1 (Ramu *et al.*, 2009), MifM (Chiba and Ito, 2012; Chiba *et al.*, 2009) or SecM (Ramu *et al.*, 2009). TnaC-mediated regulation takes advantage of coupled transcription and translation in prokaryotes (Gong and Yanofsky, 2003; Proshkin *et al.*, 2010). Here, 70S ribosome stalling blocks access for the transcription termination factor Rho, which allows continued transcription of the downstream genes (Gong *et al.*, 2001), resulting in target ORF expression (see Figure 14B). In eukaryotes, stalled ribosomes rather serve as road-block preventing ribosomal scanning of downstream ORFs which results in their repression. Human AMD1 for example encodes for the S-adenosylmethionine decarboxylase (AdoMetDC) playing an important role in polyamine biosynthesis. Its expression is monitored via a negative feedback loop by its uORF encoding the MAGDIS peptide (Hill and Morris, 1993). Polyamine-dependent stalling of MAGDIS translation termination leads to ribosomal stalling and precludes scanning (Hill and Morris, 1993). Another example for uORF-mediated gene regulation by a small effector molecule is CPS-A (*Neurospora crassa*: arg-2, *S. cerevisiae*: CPA1) which encodes the small subunit of the arginine-specific carbamoyl-phosphate synthetase catalyzing the first step of Arg synthesis. Consequently, cellular Arg levels are coupled to ribosomal stalling by the uORF encoded AAP (Luo and Sachs, 1996): High Arg abundance leads to arrest at uORF translation termination. Here, further ribosomes are not only hindered from scanning (Wang and Sachs, 1997b), however, for the orthologous gene CPA1 in yeast, induction of NMD was shown as consequence (Gaba *et al.*, 2005). Moreover, there are also eukaryotic stalling peptides which intrinsically harbor stalling competency without being modulated by small effector molecules (see Figure 14C): The most characterized hCMV-peptide (see 1.3.2) (Degnin *et al.*, 1993) stalls at its own translation termination.

Discovered stalling sequences differ in composition, are diverse, hardly conserved and therefore presumably lately evolved fine-tuning details in translation modulation. Their ultimate regulatory consequences differ greatly from mRNA cleavage (e.g. CGS1) (see Figure 14D) (Chiba, 1999; Haraguchi *et al.*, 2008; Ominato *et al.*, 2002) to recoding (e.g. 2A peptide) (see Figure 14E) (Atkins *et al.*, 2007; Sharma *et al.*, 2012) and mRNA localization (e.g. SecM, unspliced X-box-binding protein 1 (XBP1u) (see Figure 14F) (Pavitt and Ron, 2012)), yet their common purpose is the regulation of gene expression of an associated ORF.

Cross-linking experiments (e.g. Wu *et al.*, 2012), high-resolution cryo-EM structures of nascent chain harboring ribosomes (Arenz *et al.*, 2014a; Bischoff *et al.*, 2014; Sohmen *et al.*, 2015) and mutational scanning analyzes of aa residues in the stalling peptides (e.g. ErmAL1 (Ramu *et al.*, 2011), ErmCL (Vazquez-Laslop *et al.*, 2008; Vázquez-Laslop *et al.*, 2010), MifM (Chiba and Ito, 2012), SecM (Lawrence *et al.*, 2008; Nakatogawa and Ito, 2002; Yap and Bernstein, 2009), TnaC (Cruz-Vera and Yanofsky, 2008; Cruz-Vera *et al.*, 2005, 2007; Gollnick and Yanofsky, 1990; Gong and Yanofsky, 2002)) provided molecular insights into interaction patterns of several stalling mechanisms. Although very diversely regulated, in all cases the PTC geometry is somehow perturbed. Further, some re-occurring residues have been identified in the upper part of the tunnel predominantly modulating nascent chain interactions: uL4 and uL22, likely due to the constricted nature of their localization, were found to be key players in e.g. APP- (Wu *et al.*, 2012) or MifM-mediated stalling (Sohmen *et al.*, 2015) particularly since peptide stabilization was not observed at the central constriction for non-regulator peptides (Bhushan *et al.*, 2010a). In close proximity, *Ec* A751 (*Hs* A1582) of the 23S (28S in eukaryotes) rRNA was identified upon mutation for MifM and SecM to play a critical role in stalling. Several rRNA residues like *Ec* A2602 (ErmCL, MifM), *Ec* U2585 (AAP, ErmCL, hCMV, MifM, TnaC), *Ec* A2058 (AAP, hCMV, TnaC), *Ec* U2609 (AAP, hCMV, TnaC) and *Ec* A2062 (AAP, ErmCL, hCMV, SecM) (Arenz *et al.*, 2014a, 2014b; Bhushan *et al.*, 2010b, 2011; Bischoff *et al.*, 2014; Sohmen *et al.*, 2015) were reported as re-occurring interaction partners for the stalling peptides, however, uniquely combined for each particular case. PTC-contained residues are prone to be affected due to their critical contribution to translation termination or peptide-bond formation. Importantly, not all contacts observed between the nascent chain residues and the tunnel wall contribute to stalling and not all ribosomal residues shown to be important for stalling (by mutational studies) directly contact the nascent chain. Rather, it seems to be a complex relay mechanism, which propagates signals within the tunnel ultimately up to the PTC, also influencing residues not directly engaging with the nascent chain (Bhushan *et al.*, 2011; Gong and Yanofsky, 2002; Seidelt *et al.*, 2009; Vázquez-Laslop *et al.*, 2010). In some cases, the A-site- or P-site-bound aa influences stalling properties (e.g. ErmAL1 (Ramu *et al.*, 2011), hCMV (Degnin *et al.*, 1993), SecM (Muto *et al.*, 2006)). Especially Pro operates as poor A-site substrate due to its low nucleophilicity and geometric restraints transferred to the PTC (Pavlov *et al.*, 2009). Some peptides efficiently exhibit stalling properties for elongation as well as termination (e.g. AAP, ErmCL, MifM) others are limited to either one of them (e.g. hCMV, SecM, TnaC) once again stressing the individuality rendering each uORF truly unique.

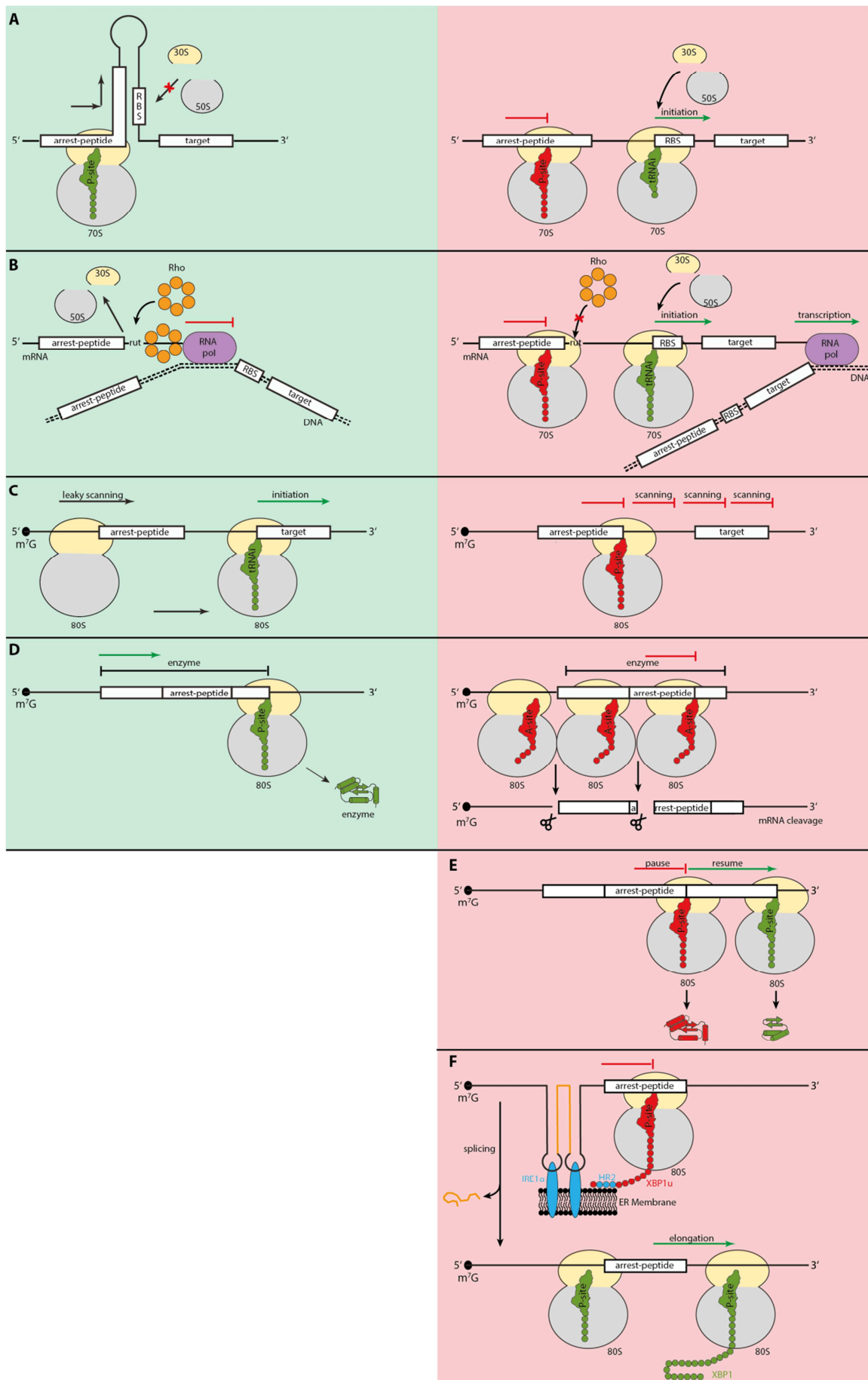


Figure 14: Schematic of Peptide-mediated Stalling Mechanisms and Their Respective Effects.

The small ribosomal subunit is depicted in yellow, the large ribosomal subunit in gray. The initiator tRNA ($tRNA_i$), the peptidyl-tRNA binding site (P-site) and the aminoacyl-tRNA binding site (A-site) tRNAs are marked accordingly. **(A)** The ribosome binding site (RBS) is sequestered in a secondary mRNA structure when the arrest-peptide containing upstream open reading frame (uORF) is translated (left). If stalling occurs, the RBS is exposed leading to downstream initiation and target translation (right) (e.g. MifM, ErmCL, ErmAL1, SecM). **(B)** Arrest-peptide containing uORF translation is terminated leaving the transcription termination factor Rho (orange) binding site, called rho utilization site (rut), accessible which results in transcription termination and therefore 3' truncated mRNA (left). If translation termination is stalled, however, Rho cannot bind, resulting in prolonged mRNA transcription by the RNA polymerase (pol) (purple) and translation of the target sequence (right) (TnaC). **(C)** Leaky scanning of the arrest-peptide containing uORF leads to downstream target translation (left). If uORF translation is initiated, however, the translating 80S ribosome is stalled which prevents downstream target translation (right) (e.g. hCMV, AAP, AdoMetDC). **(D)** If the arrest-peptide containing open reading frame is translated, it results in enzyme expression (left). If translation is stalled, the ribosome acts as road-block for following ribosomes which stack behind. 5' mRNA cleavage by an endonuclease results in fragmented mRNA preventing target expression (right) (CGS1). **(E)** mRNA translation is terminated, paused and re-initiated (right) (2A peptide). **(F)** The stalled ribosome exposes an already translated HR2 protein sequence which localizes the mRNA to the endoplasmatic reticulum (ER) membrane. There, the transmembrane endoribonuclease IRE α mediates mRNA splicing to generate mRNA encoding the active form of the target sequence (right) (XBP1u).

Figure was based on Ito *et. al.* (Ito and Chiba, 2013).

When discussing peptide-mediated arrest as mode of gene regulation, the successful release of stalled ribosomes for re-usage, which certainly temporally influences the anticipated gene regulation, has to be considered. Some arrest sequences (e.g. MifM, SecM, Vemp (Ishii *et al.*, 2015)) are sensitive to force which, when applied, corrects the perturbed PTC leading to release of stalling. As mentioned, other stalling mechanisms are sensitive to extrinsic cues whose altered concentrations result in the formation or perturbation of the composite binding pocket. Other stallers seem to be dead-end stallers which are subjected to the mRNA surveillance pathways. Literature on the involvement of such pathways, especially in eukaryotes, is scarce. Genome-wide analysis in mammalian cells on NMD substrates demonstrated enrichment of uORF-containing transcripts (Mendell *et al.*, 2004). Basic or acidic clusters of aa are known to induce ribosome arrest (Bengtson and Joazeiro, 2010; Ito-Harashima *et al.*, 2007; Kuroha *et al.*, 2009; Matsuda *et al.*, 2014; Wilson *et al.*, 2007) evidenced by non-stop mRNA where translation continues into the mRNA poly(A) tail (encoding poly-lysine) followed by ribosomal stalling. Such stalling however, was reported to induce non-stop mRNA decay (NSD) (Frischmeyer *et al.*, 2002; van Hoof, 2002; Keiler *et al.*, 1996; Parker, 2012). Generally, peptide-mediated stalled ribosomes would rather be a classical target for the no-go mRNA decay (NGD) pathway, (Doma and Parker, 2006; Parker, 2012) yet abundant A-site occupancy in most render this pathway inapplicable. Taken together, as no clear boundaries are set between NGD and NSD, further studies would be beneficial to unravel the role of the mRNA surveillance systems in gene regulation via peptide-mediated arrest.

1.3.2 The Human Cytomegalovirus gp48/UL4 uORF2 Nascent Polypeptide

The human cytomegalovirus is a species of the *Herpesviridae* whose infection usually remains asymptomatic in the healthy population, however, can lead to carcinoma in immunocompromised patients (Geballe *et al.*, 1986; Herbein and Kumar, 2014). Of particular interest in the ribosome stalling context is its UL4 gene which expresses a 48 kDa N- and O-glycosylated protein gp48 (or UL4) and contains three uORFs (Chang *et al.*, 1989; Schleiss *et al.*, 1991). Hereof, uORF2 encodes for a 22 codon peptide (1-MEPLVLSAKKLSSLLTCKYIIPP-22) inhibiting its own translation termination (Degnin *et*

al., 1993) and therefore scanning ribosomes which cannot pass and initiate at the downstream gp48/UL4 ORF in the early stage of infection (see Figure 15) (Degnin *et al.*, 1993; Geballe *et al.*, 1986). To possibly express the gp48/UL4 ORF, the AUG Kozak consensus context of uORF2 is weak causing leaky scanning and occasional omission of its initiation (Cao and Geballe, 1995). On the contrary, both uORF1 and 3 do not appear to have any influence on gp48/UL4 expression (Degnin *et al.*, 1993). Efficient uORF2-mediated stalling was demonstrated in WG, RRL (Bhushan *et al.*, 2010b; Janzen *et al.*, 2002), *Drosophila melanogaster* (*D. melanogaster*) and yeast translation extracts (Bhushan *et al.*, 2010b) indicating the manipulation of a conserved eukaryotic ribosomal feature by the hCMV-peptide for ribosome stalling. This unspecificity for a certain species could also be observed for CGS1 or APP (Fang *et al.*, 2004; Spevak *et al.*, 2010). By contrast, MifM or SecM peptides function in a species-specific manner, as both only stall in gram-positive or gram-negative bacteria, respectively.

Relevant residues for stalling were characterized in mutational studies where uORF2 was cloned upstream of the reporter β -galactosidase (β -gal) whose expression level was monitored: Upon the most critical residues for stalling were the stop codon itself which resides in the ribosomal A-site as well as the ultimate and penultimate Pro residues (22/21) (Degnin *et al.*, 1993). Medium effects were observed for Tyr19, however, more severe effects for Ser12, Ala8 and Ser7 mutations (all bold in the above codon-message) (Alderete *et al.*, 1999; Degnin *et al.*, 1993). In isolated clinical hCMV strains, the six most C-terminal aa residues were identical (Degnin *et al.*, 1993), yet conversely, the N-terminus was more polymorphic (Alderete *et al.*, 1999).

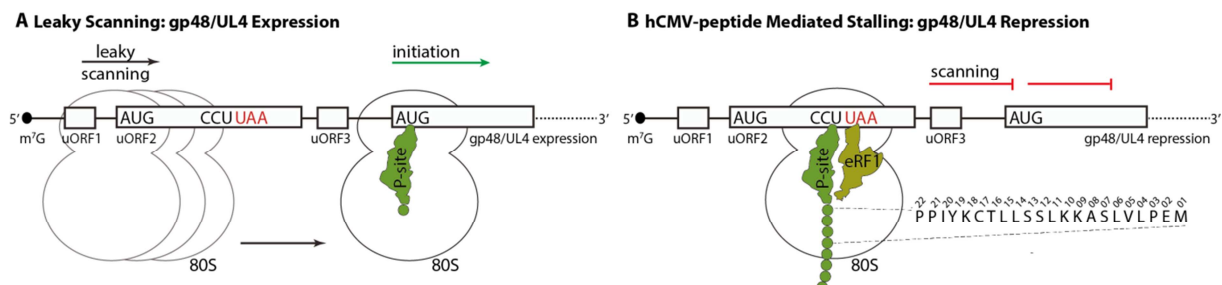


Figure 15: Schematic of hCMV-stalling Mediated Regulation of gp48/UL4 Expression.

(A) Leaky scanning of the AUG codon in the upstream open reading frame 2 (uORF2) leads to initiation at the proximal AUG of the gp48/UL4 open reading frame and consequently its expression. **(B)** Translation of uORF2 however, leads to peptide-mediated stalling at its own translation termination. The stalled ribosome harbors a stop codon (red) in its aminoacyl-tRNA binding site (A-site) where the release factor eRF1 (light green) can bind. The Proline encoding CCU codon is positioned in the ribosomal peptidyl-tRNA binding site (P-site). Arrested ribosomes prevent further 80S scanning, resulting in repression of gp48/UL4.

Figures were modified from Matheisl *et al.* (Matheisl *et al.*, 2015).

Interestingly, Geballe and co-workers discovered that interactions between eRF1 in the ribosomal A-site and the hCMV-peptide contribute to stalling activity and that eRF1 even accumulates on the stalled ribosome (Janzen *et al.*, 2002). Further, eRF1 Gly183 and Gly184 (of the GGQ motif) are both necessary for full inhibition of downstream translation since usage of an AAQ mutant eRF1 in *in vitro* translation assays increased downstream expression in a similar β -gal assay as above. When mutation of stalling-relevant residues was combined with the addition of the AAQ mutant eRF1, downstream translation of the β -gal reporter was even further increased (compared to the mutations only). In the final proposed model, the two N-terminal Pro interact (directly or indirectly) with both Gly of the GGQ motif. It was suggested that eRF1 and the mRNA vacate the ribosome

before the peptidyl-tRNA is hydrolyzed which renders eRF1 irresponsible for the prolonged association of the hCMV peptidyl-tRNA on the ribosome.

In 2010, a cryo-EM reconstruction of a WG CMV-stalled ribosome-nascent chain complex (RNC) with an average resolution of 6.5 Å was published visualizing the hCMV-stalling peptide in the tunnel (Bhushan *et al.*, 2010b). The resolution allowed rough placement of the nascent chain backbone revealing an extended conformation and probable interacting tunnel wall components (Bhushan *et al.*, 2010b). Most likely, an IGG anticodon tRNA resides in the P-site since it is known to decode CCU (and CCC) codons encoding Pro like in the construct (Geballe, 1996). A loop of the ribosomal protein uL16 (L10e) was suggested to interact with the CCA-end of the tRNA and perhaps to be important for stalling activity. Moreover, the C-terminal nascent chain residues were hypothesized to interact with the upper part of the tunnel, namely with *Ec* A2062 (*Hs* A3879) and *Ec* U2585 (*Hs* U4493). Additional contacts are made to *Ec* U2609 (*Hs* U4517) and *Ec* A2058 (*Hs* A3875). At the central constriction area stabilization of the nascent chain around residues 10 - 12 by uL22, uL4 and the *Ec* A751 (*Hs* A1582) region was further hypothesized. Even though placement of the nascent chain might reveal contact sites to the tunnel wall, at this resolution no clear statement could be made about specific molecular interactions not to mention side-chain interactions. Since mutational studies of eukaryotic exit tunnel components could not have been conducted so far, their importance for hCMV-peptide-mediated stalling could also not have been verified biochemically, yet.

1.3.3 Stalling as Tool for Programming Ribosomes *in vitro*

High-resolution structures of empty ribosomes are a useful reference for identifying positions of rRNA nucleotides and r-proteins and for identifying molecular differences during the steps of the translation cycle. Yet, to acquire novel molecular insights into the translation process ribosomes associated with their translated mRNA, tRNA(s) or protein factors are required for highest possible resemblance of the canonical situation. Studying such ribosomal complexes via cryo-EM or x-ray crystallography has preferably required homogenous samples of synchronized ribosomal states for a long time. Consequently, the possibility to halt translation at a particular state due to stalling and to enrich for such ribosomes was exploited as tool to efficiently obtain suitable samples. Generally, arrest can be mediated via stalling peptides as described above (see 1.3.1) or truncated and stem-loop containing mRNAs (Becker *et al.*, 2011; Frauenfeld *et al.*, 2011; Halic *et al.*, 2004) all yielding RNCs. The combination with ligand incubation for *in vitro* reconstitution has proven to be an elegant technique for structural studies (Becker *et al.*, 2011; Preis *et al.*, 2014).

Less than a handful cryo-EM structures of the human 80S ribosome are existent (Anger *et al.*, 2013; Behrmann *et al.*, 2015; Khatter *et al.*, 2015; Quade *et al.*, 2015) which are either non-functional (Anger *et al.*, 2013; Khatter *et al.*, 2015), derived from pullout assays (Behrmann *et al.*, 2015) or are associated with the HCV IRES (Quade *et al.*, 2015) emphasizing the challenges of sample preparation and obtaining large enough quantities required for structural investigations. For the human system and in the context of studies on translation termination, *in vitro* reconstitution by the preparation of hCMV-peptide stalled RNCs was thought to be most ideally suited since the hCMV-peptide is known to successfully and stably stall at its own translation termination in several organisms (Bhushan *et al.*, 2010b; Cao and Geballe, 1998; Preis *et al.*, 2014) and even enrich for eRF1 (Janzen *et al.*, 2002).

1.4 Structural Analysis of Macromolecular Complexes: Cryo-Electron Microscopy in the New Era

In many cases, structural visualization of macromolecular complexes proofed indispensable for the detailed mechanistic understanding of the critical biological processes they fulfill. Relevant functional states delivered explicit insights which contributed to our current knowledge of molecular activities throughout the translation cycle.

Before major technology advances, near-atomic resolution has been reserved to x-ray crystallography which successfully revealed numerous prokaryotic 70S (e.g. Dunkle *et al.*, 2011; Hansen *et al.*, 2002; Schmeing *et al.*, 2005b, 2009; Schuwirth *et al.*, 2005) and archaeal 50S (Gabdulkhakov *et al.*, 2013) ribosomal structures advancing our understanding of key steps in the translation cycle. It was not until recently that the first high-resolution crystal structure of a eukaryotic 80S yeast ribosome was presented at 3.0 Å (Ben-Shem *et al.*, 2011). Further, a *Tetrahymena thermophila* 60S SU at 3.5 Å and a 40S SU at 3.9 Å could be crystallized (Klinge *et al.*, 2011; Weisser *et al.*, 2013) whereas higher eukaryotic structures were denied comparable success likely due to their increasing complexity and lacking homogeneity (Khatter *et al.*, 2014). The best resolution acquired by crystallization of the human ribosome at present is 26 Å (Khatter *et al.*, 2014). Only very recently, attempts for cryo-EM reconstructions on human ribosomes revealed first high-resolution structures in non-functional (5.0 Å and 3.6 Å) (Anger *et al.*, 2013; Khatter *et al.*, 2015) and functional (3.5 Å and 3.9 Å) (Behrmann *et al.*, 2015; Quade *et al.*, 2015) states.

Despite its long-term drawback in obtaining high-resolution, cryo-EM (a form of transmission electron microscopy (TEM)) has always been advantageous in key considerations: Comparably small sample quantities are needed for specimens from 170 kDa (the human γ -secretase (Lu *et al.*, 2014)) to ~75 MDa (the extremophile *Sulfolobus turreted* icosahedral virus (Veesler *et al.*, 2013)) along with sample preparation in a nearly native buffer system. Sample homogeneity plays an important role, however, as opposed to crystallography, was shown to be computationally adjustable nowadays (Amunts *et al.*, 2014; Fernández *et al.*, 2013, 2014; Koh *et al.*, 2014). Especially the combination of lower-resolution cryo-EM structures to visualize the larger interaction context, as well as subunit arrangements, and the docking of high-resolution crystallography or NMR structures has provided valuable insights so far. From its birth in 1984, when methods for convenient sample vitrification in a frozen-hydrated state were introduced (Adrian *et al.*, 1984; Dubochet *et al.*, 1982), increasing resolution for cryo-EM was highly sought (see Figure 16A for the correlation of acquired resolution and increasing observable molecular details). By 1997, the 10 Å limit was overcome visualizing α -helices of the hepatitis B virus (Böttcher *et al.*, 1997). Technical innovations, like the development of the field emission gun (FEG) (Zhou and Chiu, 1993), improved illumination systems (Glaeser *et al.*, 2011), automated data collection (Allegretti *et al.*, 2014; Nickell *et al.*, 2005; Suloway *et al.*, 2005) and robust computational algorithms (Chen and Grigorieff, 2007; Glaeser, 2004; Klug, 2010; Langlois *et al.*, 2011; Pauling and Corey, 1953; Scheres, 2012a, 2012b; Sorzano *et al.*, 2009; Voss *et al.*, 2009; Zhu *et al.*, 2004) all considerably contributed to resolution improvement. By 2010, the first atomic cryo-EM structure of the human adenovirus was reported at 3.6 Å (Liu *et al.*, 2010). In theory, obtaining atomic resolution has been feasible for TEMs for years, yet practical limitations in cryo-EM application on biological samples have limited such achievement. Since biological molecules are built of light elements (carbon, oxygen, nitrogen, phosphor, sulfur and hydrogen), they only scatter electrons (e^-) weakly. Such barrier could be overcome with high e^- dose, however, as opposed to material sciences, biological specimen suffer from radiation damage and beam-induced motion

(Leapman and Sun, 1995) prohibiting the reception of higher signal-to-noise ratios (SNRs) by these means. Fortunately, particularly recent developments in the camera technology leveraged cryo-EM to the long-sought quantum leap in obtaining high resolution which allowed also ribosomal structures to be solved at near-atomic resolution. These achievements herald a new era in which the long-term obstacle of lacking high-resolution is overcome for cryo-EM.

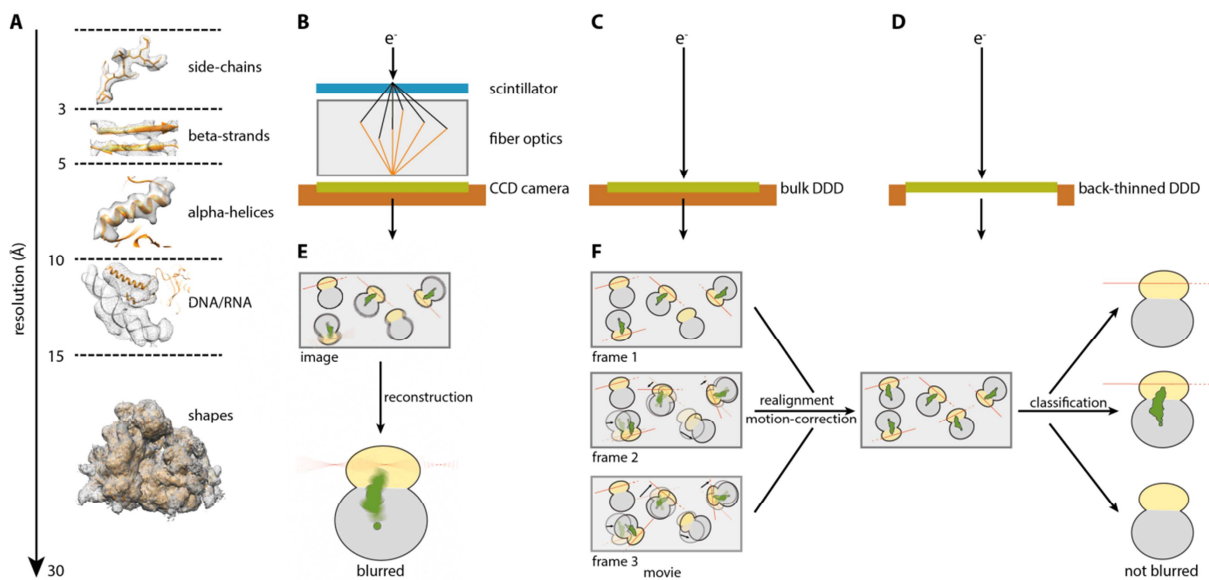


Figure 16: Recent Technology Advances in Cryo-Electron Microscopy.

(A) Correlation of acquired resolution (in angstrom (\AA)) and increasing observable molecular details: General shapes (Tecnai G2 Spirit derived reconstruction of the human 80S ribosome), DNA/RNA (PDB-code: 4v6w, EMD: 5805) (Anger *et al.*, 2013), alpha-helices (PDB-code: 3j3b, EMD: 5592) (Anger *et al.*, 2013), beta-strands (PDB-code: 5a8L, EMD: 3099) (Mattheisl *et al.*, 2015) and side-chains (PDB-code: 5afi, EMD: 2847) (Fischer *et al.*, 2015) can be visualized at increasing resolution. **(B)** Electron (e^-) detection via a charge-coupled-device (CCD) camera. A phosphate scintillator is needed to convert the e^- signals to photons, which are transferred to the camera sensor through fiber optics, leading to indirect e^- detection. **(C)** First, bulk direct electron detection devices (DDDs), where e^- signal conversion was no longer necessary due to direct e^- detection, were introduced. **(D)** Then, novel back-thinned DDDs with less support matrix followed. Here, prevention of e^- back-scattering results in a higher modulation transfer function and therefore higher detective quantum efficiency. **(E)** CCD camera derived blurred-image due to beam-induced motion. In addition, limited sorting and classification could result in heterogeneous reconstructions. **(F)** Image acquisition and processing improved concomitant to DDD development. The read-out is fast enough to record several frames (movie) that can be realigned and corrected for beam-induced motion. Further developments in classification algorithms more easily result in individual homogenous structures due to increased sorting power.

Figures (A) and (B) designed on the basis of Schröder *et al.* (Schröder, 2015). Figure (F) designed on the basis of Binshtein *et al.* (Binshtein and Ohi, 2015) and Bai *et al.* (Bai *et al.*, 2014).

Previously, charge-coupled-device (CCD) cameras were used for signal detection in cryo-EM (see Figure 16B). The CCD camera is composed of a phosphate scintillator to convert the e^- signals to photons which are then transferred to the camera sensor through fiber optics, consequently indirectly recording the e^- image. Now, new technology allows direct detection of e^- on a semiconductor membrane of novel direct e^- detection devices (DDDs) leading to a higher contrast across high spatial frequencies which allows higher resolution at lower magnification (see Figure 16C) (McMullan *et al.*, 2009a, 2009b). The modulation transfer function (MTF) measures the contrast across all spatial frequencies. A measure to specifically calculate and compare camera performances is the detective quantum efficiency (DQE) which analyzes the combined effects of the SNR of the

incoming signal (described by the MTF) and the errors (or noise) which diminish the SNR in the detection process.

Further, removing support matrix of the bulk DDD, called back-thinning, minimized noise from back-scattering e^- (see Figure 16D) (McMullan *et al.*, 2009a). The associated higher SNR requires fewer particles to be collected whereas faster read-out possible due to DDDs (up to 400 frames/sec) enables concomitant fractionation of the applied e^- dose into separate frames. Such frames can be individually corrected for beam-induced motion still opposing a problem whose origin is hardly understood (see Figures 16E, F) (Bai *et al.*, 2013; Brilot *et al.*, 2012; Campbell *et al.*, 2012; Li *et al.*, 2013). Moreover, various frame combinations can be utilized for particle alignment, which requires high SNR, and the final reconstruction, which preferably requires little e^- damage (Baker and Rubinstein, 2010). Possessing much higher DQEs (Li *et al.*, 2013; McMullan *et al.*, 2014; Ruskin *et al.*, 2013) combined with faster read-out, DDDs revolutionized the structural field (Bai *et al.*, 2013). This technical acquisition was accompanied by novel computational algorithms further enhancing final data quality. With improving resolution, subtle conformational changes in the specimen became more and more apparent. Unsupervised 3D classification based on the maximum likelihood estimation (Lyumkis *et al.*, 2013; Scheres, 2010, 2012a; Scheres *et al.*, 2007; Sigworth, 1998; Sigworth *et al.*, 2010), combined with the empirical Bayesian approach (Scheres, 2012b), even rebounded the heterogeneity of some samples to advantage (Elad *et al.*, 2008; Lyumkis *et al.*, 2013; Spahn and Penczek, 2009; Zhang *et al.*, 2008). From one single biochemical preparation multiple conformational states could be separated allowing even deeper mechanistic understanding of the investigated process.

During the past two years, several ribosomal structures were successfully reconstructed to resolutions beyond 4 Å which all delivered novel insights: To only name a few, the prokaryotic TnaC-stalled (3.8 Å) (Bischoff *et al.*, 2014) and SecM-stalled (3.3 – 3.7 Å) (Zhang *et al.*, 2015) 70S ribosomes, the *Plasmodium falciparum* 80S ribosome (3.2 Å) (Wong *et al.*, 2014), the scanning and engaged mammalian-SRP complex (3.75 Å) (Voorhees and Hegde, 2015), the human mitoribosome (3.5 Å) (Amunts *et al.*, 2015), the MifM-stalled *B. subtilis* 70S ribosome (3.9 Å) (Sohmen *et al.*, 2015), the EF-Tu-bound ribosome (2.9 Å) (Fischer *et al.*, 2015), the eIF1:eIF4A-bound 40S preinitiation complex (3.46 Å) (Llácer *et al.*, 2015) the SecYEG-bound translocating ribosome (3.33 Å) (Jomaa *et al.*, 2016) and the EF-4 bound ribosome (3.2 – 3.7 Å) (Zhang *et al.*, 2016) under which very recently structures of the human ribosome like the HCV IRES-bound 80S ribosome (3.9 Å) (Quade *et al.*, 2015) and the non-functional 80S ribosome itself (3.6 Å) (Khatter *et al.*, 2015) were generated.

Although technical and computational progress led to the high pace of advancing cryo-EM, the technique still has its limits. To convincingly visualize ions and side-chains, resolutions better than 3 Å are worth pursuing. Improving computational power and developing tools for efficient model building, refinement and validation are desirable. Stopping beam-induced motion, most likely deriving from structural changes in the carbon support (Russo and Passmore, 2014), will be one of the next obstacles to be tackled by the cryo-EM community. Notably, not all structures will readily reach atomic resolution since conformational flexibility, as likewise for crystallography, limits visualization, but taken together, recent developments provide the feasibility of near-atomic resolution structures of large macromolecular complexes via cryo-EM. As versatile tool, cryo-EM is starting to become as widely used as crystallography, opening the floodgates for answering long-standing questions like the molecular mechanism of stop codon decoding in eukaryotes and beyond.

1.5 Aims of the Thesis

This dissertation aims at unraveling the molecular mechanism underlying stop codon recognition during translation termination in the human ribosome by structural means.

Why spending the enormous effort and not just draw conclusions from high-resolution crystallized prokaryotic termination complexes? Termination and especially stop codon recognition is one of the least conserved processes during translation. In bacteria, two class-I release factors (RF1 and RF2) have evolved with overlapping specificity for two stop codons each (Scolnick *et al.*, 1968). High-resolution structures have already been solved starting from 2008 by the crystallization of an RF1-bound 70S ribosome (Laurberg *et al.*, 2008). Since then, all possible stop codon - RF1/2 combinations have been crystallized to high resolution to elucidate the molecular network of stop codon recognition by the two prokaryotic RFs (Korostelev *et al.*, 2008, 2010; Weixlbaumer *et al.*, 2008). The unrelated eukaryotic eRF1 however, mediates stop codon decoding for all three codons while being structurally diverse from RF1 and RF2. Consequently, the precise underlying mechanism of eukaryotic stop codon decoding is a pressing issue, which can only be solved by a high-resolution structure of the eRF1-bound ribosome, because all hitherto existing genetic and biochemical studies could only reveal contradictory results.

At the start of the project various options were available for biochemical sample preparation of the first human ribosome in a functional state: Native pullouts could have been conducted as in the meantime has been successfully reported by Spahn and co-workers (Behrmann *et al.*, 2015). Gain of this approach is to certainly obtain several natural ribosome states, yet its drawback is limited amounts of particles for each state resulting in compromised resolution. Since particularly the state of translation termination at highest possible resolution was aimed at, *in vitro* reconstitution seemed rather promising in our case. *In vitro* translation combined with subsequent reconstitution has been successfully performed from the yeast (Becker *et al.*, 2011), the WG (Preis *et al.*, 2014) and the RRL (Gogala *et al.*, 2014) *in vitro* translation systems before where efficiently stalled 80S ribosomes were purified and supplemented with the according protein factors.

Recently, a Japanese group (Mikami *et al.*, 2010a) has published a supposedly efficient way for *in vitro* translation extract preparation based on human HeLa cells which has been applied commercially by *Thermo Scientific*. Conversely, testing the latter could not produce reliable, reproducible results. Hence at first, we set out for the establishment of a human translation extract and its optimization due to adjustments to our particular needs.

With this extract in hands, the generation of 80S ribosomes each harboring a peptidyl tRNA in its P-site and a stop codon in its A-site was of necessity. Translation of the human hCMV-stalling sequence resulted in inhibition of termination and effective enrichment of stalled RNCs for *in vitro* reconstitution. hCMV-mediated stalling has been characterized extensively via mutational studies (Alderete *et al.*, 1999; Degnin *et al.*, 1993; Janzen *et al.*, 2002) and has already successfully been used for low-resolution cryo-EM structures (Bhushan *et al.*, 2010b; Preis *et al.*, 2014), yet also here only a high-resolution structure can elucidate the molecular basis of why termination is impeded.

Several approaches for the purification of the participating human proteins eRF1, eRF3 and ABCE1 were undertaken to successfully assemble a termination involved complex. Due to the reluctance of the human ribosome to high-resolution crystallization up to date, cryo-EM presented the method of

choice to acquire the required resolution in this project. To this end, the hCMV-peptide stalled, heRF1-only containing human RNC preparation was subjected to structural investigations by cryo-EM eventually allowing the reconstitution of a 3.8 Å cryo-EM density followed by atomic model building to unravel the molecular mechanism of hCMV-peptide mediated stalling as well as stop codon decoding during human translation termination.

2. Materials and Methods

2.1 Molecular Cloning

2.1.1 Plasmids and Strains

For cloning experiments in this study, several plasmid backbones (see Table 1) were used as basis for modification. After insert cloning, final plasmids were used for protein expression and purification from bacterial *E. coli* or human HEK293T cells and cell-free protein expression experiments.

Table 1: Plasmid Backbones and Their Respective Inserts Used in this Study.

Backbone	Purpose	Cloned Insert	Selection Marker	Manufacturer
pCDNA3.1	Protein expression in mammalian cells	3xFLAG-hABCE1	Amp	<i>Invitrogen</i>
pET-28a	Protein expression in <i>E. coli</i>	(His) ₆ -Δ(1-46)Jmjd4	Kan	<i>Novagen</i>
pET-32a	Protein expression in <i>E. coli</i>	TRX-(His) ₆ -TEV-heRF3a full length (fl)	Amp	<i>Novagen</i>
pETDuet-1	Protein co-expression in <i>E. coli</i>	Differently (His) ₈ -3C-tagged heRF1 and heRF3a fl/ Δ(1-138)heRF3a combinations Tagged/untagged heRF1 only	Amp	<i>Novagen</i>
prSFDuet-1	Protein co-expression in <i>E. coli</i>	(His) ₈ -3C-Δ(1-138) heRF3a WT, H300Q and R371G only	Kan	<i>Novagen</i>
pT7CFE1-NHis	Cell-free protein expression in human translation system	CrPV IGR IRES-linker-(His) ₆ -3C-HA-hCMV-p(A) ₂₆	Amp	<i>Thermo Scientific</i>

E. coli strains (see Table 2) were grown in 1x Luria Bertani (LB) medium (1 % (w/v) bacto tryptone, 0.5 % (w/v) yeast extract, 1 % (w/v) sodium chloride (NaCl) in H₂O) or where indicated in 2x LB (2 % (w/v) bacto tryptone, 1 % (w/v) yeast extract, 1 % (w/v) NaCl in H₂O) under shaking conditions (120 - 140 rounds per minute (rpm)) at 37 °C for plasmid amplification and at various temperatures (18 °C, 20 °C, 30 °C, 37 °C) for protein expression. To determine the growth of liquid cultures, the optical density at a wavelength of $\lambda = 600$ nm (OD₆₀₀) was measured with a BioPhotometer® (*Eppendorf*). Growth on agar plates (1x LB completed with 1.5 % (w/v) agar) was performed at 37 °C overnight. For establishing selection pressure, the corresponding antibiotic kanamycin (50 µg/mL) (Kan) or ampicillin (100 µg/mL) (Amp) (and chloramphenicol (34 µg/mL) (Cam) for the pRARE plasmid containing *E. coli* Rosetta (DE3)) was added.

Table 2: *E. coli* Strains Used in this Study.

Strain	Purpose	Genotype	Manufacturer
<i>E. coli</i> BL21 (DE3)	Protein expression	F ⁻ ompT gal dcm lon hsdSB(rB ⁻ mB ⁻) λ(DE3 [lacI lacUV5-T7 gene 1 ind1 sam7 nin5])	Stratagene
<i>E. coli</i> DH5α	Plasmid amplification	F ⁻ endA1 glnV44 thi ⁻¹ recA1 relA1 gyrA96 deoR nupG Φ80dlacZΔM15 Δ(lacZYA-argF)U169, hsdR17(rK ⁻ mK ⁺), λ ⁻	Stratagene
<i>E. coli</i> ER2566	Protein expression	F ⁻ λ- fhuA2 [lon] ompT lacZ::T7 gene 1 gal sulA11 Δ(mcrC-mrr)114::IS10 R(mcr-73::miniTn10-TetS)2 R(zgb-210::Tn10) (TetS) endA1 [dcm]	NEB
<i>E. coli</i> Rosetta (DE3)	Protein expression	F ⁻ ompT hsdSB(RB- mB-) gal dcm λ(DE3 [lacI lacUV5-T7 gene 1 ind1 sam7 nin5]) pRARE (Cam ^R)	Novagene
<i>E. coli</i> XL1blue	Plasmid amplification	endA1 gyrA96(nalR) thi-1 recA1 relA1 lac glnV44 F' ⁻ [::Tn10 proAB+ lacIq Δ(lacZ)M15] hsdR17(rK- mK+)	Stratagene

2.1.2 Polymerase Chain Reaction-based Methods

Gibson Assembly Cloning (NEB)

Gibson Assembly (GA) (see Figure 17A) is a fast and flexible cloning method which is independent of restriction enzymes. The prerequisite on DNA level are overlapping sequence endings between the fragments to be assembled. In favor of three enzymatic reactions even multiple overlapping DNA fragments can be joined: First, an exonuclease creates single-stranded 3' overhangs to allow annealing between the fragments. Then, a DNA polymerase extends the 3' ends to fill the existing gaps before a DNA ligase seals the remaining nicks.

Table 3: Primers Used for Gibson Assembly Cloning in this Study.

Blue color indicates sequences overlapping with the target vector. Melting temperatures (T_m) are only given for the annealing parts of the sequences and were calculated with the T_m Calculator (NEB) (<http://tmcalculator.neb.com>). Forward (fwd) and reverse (rev) primers are indicated.

Name	Sequence	T_m	Type	Purpose
SM 42	5' cctggccaccacca tatgCTGGAAGTGTGTT TCAGGGGCCGTACCCATACGATGTTCCAG ATTACG3'	66 °C	fwd	Clone(His) ₆ -3C-HA-hCMV-(UAA)G into pT7CFE1-NHis
SM 43	5' gatctcactcgagtgc TTAAGGAGGAATATA TTTGCAGG3'	60 °C	rev	Clone(His) ₆ -3C-HA-hCMV-(UAA)G into pT7CFE1-NHis

For the described GA approach, the plasmid template pT7CFE1-NHis was linearized (with NdeI/NotI) to reduce the background of its transformation. The insert was polymerase chain reaction (PCR) amplified to append sequences contained in the primers (see Table 3) which partly overlap with the target vector. For amplification, a 50 μL sample containing 0.5 μM of each primer, 10 ng of the linearized template plasmid and 50 % (v/v) of the Phusion Flash High-Fidelity Master Mix (Finnzymes) was assembled. Cycling conditions were based on the manufacturer's recommendation with an amplification time of 20 seconds (sec)/kilo base pair (kb) and an annealing temperature (T_a) 2 °C

higher than the lower melting temperature (T_m) of the two primers (annealing sequence < 20 nt). As starting material for the GA reaction, 100 ng vector and 3x molar excess of the amplified insert were incubated in 1x GA Master Mix (NEB) in a total volume of 20 μ L. Samples were incubated at 50 °C for 1 hour (h) to obtain fully assembled DNA and diluted 1:4 prior to their transformation (see 2.1.7).

Megaprimer PCR of Whole Plasmid Cloning

The megaprimer PCR of whole plasmid (MEGAWHOP) cloning method (see Figure 17B) (Miyazaki, 2011) is a further technique to circumvent the classical problem-prone restriction enzyme-based cloning. In this novel kit-independent approach overlapping sequences between two fragments are also required. Therefore, sequences which are homologous to the target site of the plasmid are added to the insert fragment through primer overhangs during a first PCR (PCRI). The amplified product is then used as primer (due to its size called megaprimer) in a second PCR (PCRII) in which the homologous regions prime to the original vector sequence which is replaced during whole-plasmid PCR.

Table 4: Primers Used for Megaprimer PCR of Whole Plasmid Cloning in this Study.

Blue color indicates sequences overlapping with the target vector. Melting temperatures (T_m) are only given for the annealing parts of the sequences and were calculated with the T_m Calculator (NEB) (<http://tmcalculator.neb.com>). Forward (fwd) and reverse (rev) primers are indicated.

Name	Sequence	T_m	Type	Purpose
SM 59	5' cggttatttccaccatatt gAAAGCAAAAT GTTGATCTTGCTTGTAAATAC3'	65 °C	fwd	Clone CrPV IGR IRES-linker into pT7CFE1-(His) ₆ -3C-HA-hCMV-(UAA)G-p(A) ₂₆
SM 60	5' catattatcatcggttttc AGGTAAATTCT TAGGTTTTCGACTACC3'	65 °C	rev	Clone CrPV IGR IRES-linker into pT7CFE1-(His) ₆ -3C-HA-hCMV-(UAA)G-p(A) ₂₆
SM 108	5' taagaaggagatatacc ATGGGTCATCACC ATCACCATCACCATCACGATTACGATATT CCAACGACCCTGGAAGTTCTGTTCCAGG GGCCCGCGGACGACCCAGTGC3'	71 °C	fwd	Clone (His) ₈ -heRF1 in pETDuet-1 (Multiple Cloning Site 1 (MCS1))
SM 109	5' caggcgcgcgcgactcgaattc TTAGTAGTC ATCAAGGTAAAAAAATTATCG3'	68 °C	rev	Clone (His) ₈ -heRF1 in pETDuet-1 (MCS1) Clone heRF1 in pETDuet-1 (MCS1)
SM 110	5' taagaaggagatatacc ATGGCGGACGAC CCCAGTGC3'	71 °C	fwd	Clone heRF1 in pETDuet-1 (MCS1)

DNA amplification during PCRI (primers see Table 4) was performed with the Phusion Flash High-Fidelity Master Mix (Finnzymes) as described for the GA cloning, but with an elongation time of 30 sec – 1 minute (min)/kb and an T_a equal to the lower T_m of the two primers (due to the T_m being in the higher ranges of possible T_m).

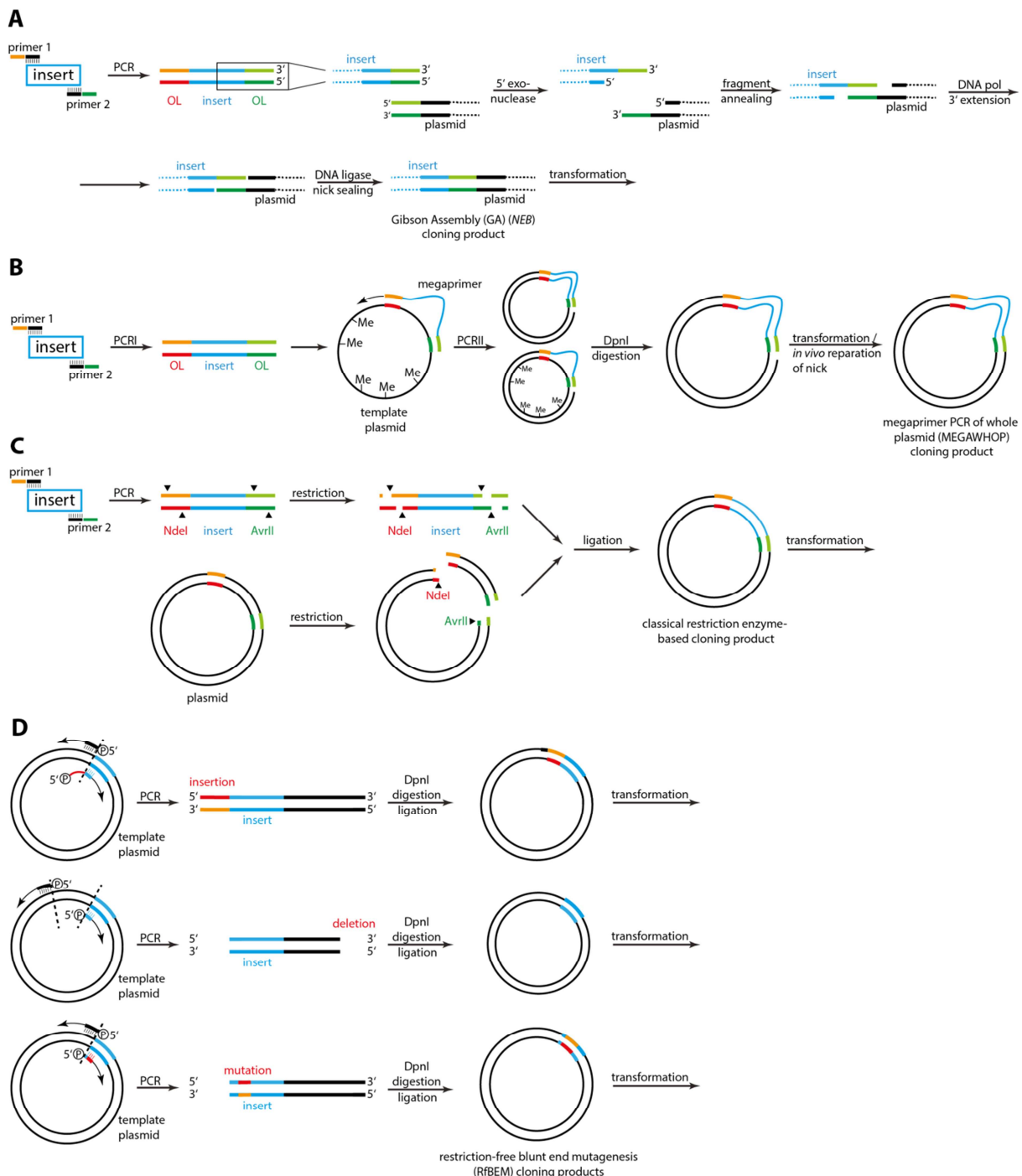


Figure 17: Applied Cloning Strategies.

(A) Gibson Assembly (GA) (NEB) cloning strategy. Overlapping (OL) sequences (red/orange, dark/light green) are added to the insert (light blue) during a polymerase chain reaction (PCR). Subsequent 5' exonuclease treatment and fragment annealing are followed by DNA polymerase (pol) 3' extension and nick sealing resulting in the final product. **(B)** Megaprimer PCR of whole plasmid (MEGAWHOP) cloning strategy color coded as in (A). OL sequences are added to the insert during a first PCR (PRCI). Subsequent usage of this PCR product as megaprimer in a second PCR (PCRII), DpnI digestion of the methylated (Me) plasmid and transformation result in the final product. **(C)** Classical restriction enzyme-based cloning strategy. The PCR product and the vector are digested with the same restriction enzymes (here: NdeI and AvrII) to create sticky or blunt ends. Restriction sites (red/orange, dark/light green) can be added to the insert (light blue) during the PCR. Ligation of the restricted fragments results in the final product. **(D)** Restriction-free blunt end mutagenesis (RfBEM) cloning strategy. 5' phosphorylated primers (P) are used to introduce an insertion (red/orange), deletion or mutation (red/orange) during a PCR. Subsequent DpnI digestion and ligation result in the final products.

For amplification during PCRII, 8 µL of PCRI purified product and 250 ng of the target vector were supplemented with deoxynucleoside triphosphates (dNTPs) (2 millimolar (mM) each, (Merck/Millipore)), 1x KOD Buffer (Merck/Millipore) and the KOD Xtreme™ Hot Start DNA Polymerase (Merck/Millipore). Amplification was performed with two T_a during the following gradient PCR protocol:

94 °C	2 min	
98 °C	8 sec]
50.9 °C and 65.2 °C	30 sec	8x
74 °C	1 min/kb]
98 °C	8 sec]
50.9 °C and 65.2 °C	30 sec	8x
68 °C	1 min/kb]
68 °C	3 min	
12 °C	∞	

Samples were pooled and subjected to DpnI digestion (see 2.1.4) and PCR product purification (see 2.1.3) before transformation (see 2.1.7).

Classical Restriction Enzyme-based Cloning

Cloning into both multiple cloning sites (MCSs) of the Duet-1 co-expression vectors cannot be successfully accomplished by MEGAWHOP cloning due to equal sequences neighboring the MCSs. Therefore, it was reverted to the classical restriction enzyme-based cloning method (see Figure 17C). To this end, restriction enzyme recognition sites were appended to the insert fragments by primer overhangs (see Table 5) during a PCR realized with the Phusion Flash High-Fidelity Master Mix (Finnzymes) as described for template amplification (PCRI) during MEGAWHOP cloning. The PCR purified product (see 2.1.3) was subjected to enzymatic digestion (20 µL PCR purified product, 3 µL 10x CutSmart® Buffer (NEB), 1 µL of each enzyme (NEB) in a total volume of 30 µL) at 37 °C overnight. In parallel, the plasmid was digested with the same restriction enzymes (10 - 20 microgram (µg) plasmid, 5 µL 10x CutSmart® Buffer (NEB), 1.5 µL of each enzyme (NEB) in a total volume of 50 µL). Subsequent ligation (see 2.1.5) and transformation (see 2.1.7) resulted in the final clones.

Table 5: Primers Used for Classical Restriction Enzyme-based Cloning in this Study.

Green color indicates restriction enzyme recognition sites (AvrII: cctagg; NdeI: catatg). Melting temperatures (T_m) are only given for the annealing parts of the sequences and were calculated with the T_m Calculator (NEB) (<http://tmcalculator.neb.com>). Forward (fwd) and reverse (rev) primers are indicated.

Name	Sequence	T_m	Type	Purpose
SM 82	5'CTAG cctagg ttaGTCTTCTCTGGACCAGT TTCAGAA3'	67 °C	rev	Clone (His) ₈ -3C-heRF3a fl in pETDuet-1 heRF1 (Multiple Cloning Site (MCS) 2) Clone Δ(1-138)heRF3a in pETDuet-1 (His) ₈ -heRF1 (MCS2) Clone (His) ₈ -3C-Δ(1-138)heRF3a in pRSFDuet-1 (MCS2)
SM 84	5'GGAATT ccatatg GGTCATCACCACCATC CACCACGATTACGATATTCAACGACCC	70 °C	fwd	Clone (His) ₈ -3C-heRF3a fl in pETDuet-1 heRF1 (MCS2)

	TGGAAGTTCTGTTCCAGGGGCCGATCCGG GCAGTGGCG3'			
SM 88	5'GGAATT <color>catatg</color> TCAGAACCTATTGAAAAT GGAGAGACAG3'	67 °C	fwd	Clone Δ(1-138h)heRF3a in pETDuet-1 (His) ₈ -heRF1 (MCS2)
SM 89	5'GGAATT <color>catatg</color> GGTCATCACCACCATCACC CACCATCACGATTACGATATTCCAACGACCC TGGAAGTTCTGTTCCAGGGGCCCTCAGAACCC TATTGAAAATGGAGAGACAG3'	67 °C	fwd	Clone (His) ₈ -3C-Δ(1- 138)heRF3a in pRSFDuet-1 (MCS2)

Restriction-free Blunt End Mutagenesis Cloning

A cloning method which allows short mutations, insertions or deletions is restriction-free blunt end mutagenesis (RfBEM) cloning (see Figure 17D). Primers need to be 5' phosphorylated and carry the desired mutation or overhang for insertion. During PCR the whole plasmid is amplified resulting in DNA fragments comprising 5' phosphorylated ends which are subjected to ligation.

For amplification, 100 µL sample containing 10 µM of each primer (see Table 6), 15 ng of the template plasmid and 50 % (v/v) of the Phusion Flash High-Fidelity Master Mix (*Finnzymes*) were assembled and equally divided into 8 samples. Cycling conditions were as follows:

98 °C	20 sec		
98 °C	10 sec]	
Gradient: ± 5 °C of calculated T _a	20 sec]	2x
72 °C	6 min]	
98 °C	10 sec]	
Gradient: ± 5 °C of calculated T _a	20 sec]	3x
72 °C	5 min]	
98 °C	10 sec]	
Gradient: ± 5 °C of calculated T _a	20 sec]	18x
72 °C	4.5 min]	
12 °C	∞		

Afterwards, all samples were pooled and subjected to PCR product purification (see 2.1.3), DpnI digestion (see 2.1.4), gel extraction (see 2.1.3), ligation (see 2.1.5) and transformation (see 2.1.7).

Table 6: 5' Phosphorylated Primers Used for Restriction-free Blunt End Mutagenesis Cloning in this Study.

Red color indicates the mutated codons. Melting temperatures (T_m) are only given for the annealing parts of the sequences and were calculated with the T_m Calculator (*NEB*) (<http://tmcalculator.neb.com>). Forward (fwd) and reverse (rev) primers are indicated.

Name	Sequence	T _m	Type	Purpose
SM 96	5'GCACTCGAGTGAGATCTGAC3'	60 °C	fwd	Replacing stop in pT7CFE1 CrPV IGR IRES-linker-(His) ₆ -3C- HA-hCMV-p(A) ₂₆ with ideal stops codons
SM 97	5' <color>TTT</color> AAGGAGGAATATTTGCAGG3'	60 °C	rev	Replacing stop in pT7CFE1 CrPV IGR IRES-linker-(His) ₆ -3C- HA-hCMV-p(A) ₂₆ with UAA(A)

SM 98	5' TTCA AGGAGGAATATATTGCAGG3'	57 °C	rev	Replacing stop in pT7CFE1 CrPV IGR IRES-linker-(His) ₆ -3C-HA-hCMV-p(A) ₂₆ with UGA(A)
SM 99	5' TCTA AGGAGGAATATATTGCAGG3'	57 °C	rev	Replacing stop in pT7CFE1 CrPV IGR IRES-linker-(His) ₆ -3C-HA-hCMV-p(A) ₂₆ with UAG(A)
SM 143	5' CAGAAGAG TTTGTCCCAAATATG3'	62 °C	fwd	Creating GTPase deficient mutant of heRF3a fl or Δ(1-138)heRF3a: H300Q
SM 144	5'GCCAGGGGCATCTAGAATTG3'	66 °C	rev	Creating GTPase deficient mutant of heRF3a fl or Δ(1-138)heRF3a: H300Q
SM 145	5' GGCT ATGAAGAACATGTAAGGAGAAC3'	62 °C	fwd	Creating GTPase deficient mutant of heRF3a fl or Δ(1-138)heRF3a: R371G
SM 146	5'CTCATTGCTCCAATTTACTGTT3'	60 °C	rev	Creating GTPase deficient mutant of heRF3a fl or Δ(1-138)heRF3a: R371G
SM 223	5'AGCACTCGAGTGAGATCTGAC3'	61 °C	fwd	Mutational screening of hCMV-stalling: Stop23Ala
SM 224	5' GGCAGGAGGA ATATATTGCAGG3'	57 °C	rev	Mutational screening of hCMV-stalling: Stop23Ala
SM 225	5'TAAAGCACTCGAGTGAGATC3'	57 °C	rev	Mutational screening of hCMV-stalling: Pro22Ala
SM 226	5' GGCAGGA ATATATTGCAGGTCA3'	56 °C	rev	Mutational screening of hCMV-stalling: Pro22Ala
SM 227	5'CCTTAAAGCACTCGAGTGAG3'	59 °C	fwd	Mutational screening of hCMV-stalling: Pro21Ala
SM 228	5' GGCAATAT ATTGCAGGTCA3'	57 °C	rev	Mutational screening of hCMV-stalling: Pro21Ala
SM 229	5'CCTCCTTAA AGCACTCGAGTG3'	63 °C	fwd	Mutational screening of hCMV-stalling: Ile20Ala
SM 230	5' GGCAT ATTGCAGGTCA3'	64 °C	rev	Mutational screening of hCMV-stalling: Ile20Ala
SM 231	5'ATTCCCTCTAAAGCACTCG3'	60 °C	fwd	Mutational screening of hCMV-stalling: Tyr19Mutation
SM 232	5' GGCTTGCAGGT CAGCAGG3'	60 °C	rev	Mutational screening of hCMV-stalling: Tyr19Ala
SM 233	5' GAATTGCAGGT CAGCAGG3'	60 °C	rev	Mutational screening of hCMV-stalling: Tyr19Phe
SM 234	5'TATATTCCCTCTAAAGCACTCG3'	60 °C	fwd	Mutational screening of hCMV-stalling: Lys18Ala
SM 235	5' GGCGCAGGT CAGCAGGCTG3'	62 °C	rev	Mutational screening of hCMV-stalling: Lys18Ala
SM 236	5'AAATATATTCCCTCTAAAGCACTC3'	59 °C	fwd	Mutational screening of hCMV-stalling: Cys17Ala
SM 237	5' GGCGGT CAGCAGGCTGCTC3'	61 °C	rev	Mutational screening of hCMV-stalling: Cys17Ala
SM 238	5'TGCAAATATATTCCCTCTAAAGCAC TCG3'	69 °C	fwd	Mutational screening of hCMV-stalling: Thr16Ala
SM 239	5' GGCCAGCAGGCTGCTCAG TTTCG3'	71 °C	rev	Mutational screening of

				hCMV-stalling: Thr16Ala
SM 240	5'ACCTGCAAATATATTCCCTCC3'	57 °C	fwd	Mutational screening of hCMV-stalling: Leu15Ala
SM 241	5' GGC CAGGCTGCTCAGTTTTTC3'	60 °C	rev	Mutational screening of hCMV-stalling: Leu15Ala
SM 244	5'CTGCTGACCTGCAAATATATTCC3'	60 °C	fwd	Mutational screening of hCMV-stalling: Ser13Ala
SM 245	5' GGC GCTCAGTTTTTCGCACT3'	63 °C	rev	Mutational screening of hCMV-stalling: Ser13Ala
SM 246	5'AGCCTGCTGACCTGCAAATATATTCC3'	67 °C	fwd	Mutational screening of hCMV-stalling: Ser12Mutation
SM 247	5' GGC CAGTTTTTCGCACTCA3'	67 °C	rev	Mutational screening of hCMV-stalling: Ser12Ala
SM 248	5' GGT CAGTTTTTCGCACTCA3'	67 °C	rev	Mutational screening of hCMV-stalling: Ser12Thr
SM 249	5'AGCAGCCTGCTGACCTGC3'	67 °C	fwd	Mutational screening of hCMV-stalling: Leu11Ala
SM 250	5' GGC TTTTTCGCACTCAGCACCA3'	67 °C	rev	Mutational screening of hCMV-stalling: Leu11Ala
SM 251	5'CTGAGCAGCCTGCTGACC3'	65 °C	fwd	Mutational screening of hCMV-stalling: Lys10Ala
SM 252	5' GGC TTTCGCACTCAGCACCAAG3'	64 °C	rev	Mutational screening of hCMV-stalling: Lys10Ala
SM 253	5'AAACTGAGCAGCCTGCTGAC3'	65 °C	fwd	Mutational screening of hCMV-stalling: Lys9Ala
SM 254	5' GGC CGCACTCAGCACCAAGC3'	63 °C	rev	Mutational screening of hCMV-Stalling: Lys9Ala
SM 255	5'AAAAAACTGAGCAGCCTGC3'	62 °C	fwd	Mutational screening of hCMV-stalling: Ala8Mutation
SM 256	5' CAC ACTCAGCACCAAGCGGTTTC3'	64 °C	rev	Mutational screening of hCMV-stalling: Ala8Val
SM 257	5' GTC ACTCAGCACCAAGCGGTTTC3'	64 °C	rev	Mutational screening of hCMV-stalling: Ala8Asp
SM 258	5'GCGAAAAAACTGAGCAGGCC3'	65 °C	fwd	Mutational screening of hCMV-stalling: Ser7Ala
SM 259	5' GGC CAGCACCAAGCGGTTCC3'	65 °C	rev	Mutational screening of hCMV-stalling: Ser7Ala
SM 260	5'CTGACCTGCAAATATATTCCCTCCTTAA3'	65 °C	fwd	Mutational screening of hCMV-stalling: Leu14Ala
SM 261	5' GGC GCTGCTCAGTTTTTCGCACTC3'	67 °C	rev	Mutational screening of hCMV-stalling: Leu14Ala

2.1.3 Purification of DNA Fragments

Generated PCR products were purified with the QIAquick® PCR Purification Kit (*Qiagen*) according to the manufacturer's instructions and eluted in 30 µL nuclease-free H₂O. For obtaining solely DNA according to a particular size, the DNA fragments were subjected to agarose gel electrophoresis whereupon only the desired fragment was excised from the gel under ultraviolet (UV) light. After weight determination, the DNA was extracted and purified from the agarose gel using the QIAquick®

Gel Extraction Kit (*Qiagen*) following the manufacturer's instructions. Elution was also performed in 30 µL nuclease-free H₂O.

2.1.4 Enzymatic Digestion with DpnI

Previously described cloning methods (see 2.1.2, MEGAWHOP and RfBEM cloning) require incubation with the dam-methylated DNA specific restriction enzyme DpnI to eliminate the template plasmid which is of bacterial origin. PCR amplified DNA remains undigested which yields in higher cloning efficiency. 30 µL purified PCR product was incubated with 20 U DpnI (*NEB*) in NEBuffer-4 (*NEB*) for at least 2 h at 37 °C.

2.1.5 Ligation

After gel extraction, the DpnI digested intermediate of the RfBEM cloning was ligated with 1,200 U T4 DNA ligase (*NEB*) in 1x T4 Reaction Buffer (*NEB*) in a total volume of 40 µL at 16 °C overnight.

For classical restriction enzyme-based cloning, the vector insert ratio had to be considered (see Table 7). Ligation reactions were performed in a total volume of 10 µL containing 400 U T4 DNA ligase (*NEB*) in 1x T4 Reaction Buffer (*NEB*) at 16 °C overnight.

Table 7: Plasmid to Insert Ratios for Ligations during Classical Restriction Enzyme-based Cloning.

Plasmid	Insert	Ratio (Plasmid : Insert)
pETDuet-1 (His) ₈ -3C-heRF1	Δ(1-138)heRF3a	3:1
pETDuet-1 heRF1	(His) ₈ -3C-heRF3a fl	1:2
PRSFDuet-1	(His) ₈ -3C-Δ(1-138)heRF3a	3:1

2.1.6 Preparation of Chemical Competent *Escherichia coli* Cells

A 5 mL LB *E. coli* (strains see 2.1.1) overnight culture was diluted 1:100 in 100 mL 1x LB and grown to an OD₆₀₀ = 0.6 - 0.8 at 37 °C under shaking conditions (140 rpm). In case of *E. coli* Rosetta (DE3), Cam was added to the media. Henceforth, all utilized equipment was pre-cooled at 4 °C. The *E. coli* culture was cooled on ice for 15 min whereupon centrifugation (10 min / 4 °C / 5,000 rpm / GSA (*Sorvall*TM)) was performed. The supernatant was discarded whereas the resulting pellet was resuspended in 50 mL 0.1 molar (M) calcium chloride (CaCl₂). The mixture was incubated for 30 min on ice before centrifugation was conducted as above. Again, the supernatant was discarded whereas the pellet was resuspended in 50 mL 0.1 M CaCl₂ supplemented with 15 % (v/v) glycerol. Subsequently, the competent cells were gently aliquoted, flash frozen in liquid nitrogen and stored at -80 °C until further use.

2.1.7 Transformation and Plasmid Isolation

Competent *E. coli* cells were thawed on ice for 10 min. 50 µL cells were incubated on ice with 40 µL ligation reaction (RfBEM cloning), with 10 µL ligation reaction (classical restriction enzyme-based cloning), with 30 µL PCR purified product (MEGAWHOP cloning) or with 2 - 10 µL of the 1:4 dilution of the GA reaction (GA cloning) for 10 min. A 42 °C heat-shock was performed in an H₂O-bath for 45 sec. Immediate incubation on ice for 1 minute was followed by incubation under shaking conditions (350 rpm) at 37 °C in 900 µL LB without antibiotics for 1 - 2 h. Cells were collected (3 min / RT / 5,000 rpm / 5415D (*Eppendorf*)), 700 µL medium was omitted and the remainder was plated on pre-warmed selective LB-agar plates. Incubation followed at 37 °C overnight.

5 mL 1x LB medium (containing the corresponding antibiotic(s)) each was inoculated with one bacterial colony. Growth was performed at 37 °C overnight before cells were harvested (10 min / 4 °C / 4,500 rpm / Rotanta 46R (*Hettich*)) and plasmids were isolated using the QIAprep® Spin Miniprep Kit (*Qiagen*) according to the manufacturer's protocol. Optional steps were omitted and elution was performed in 30 µL nuclease-free H₂O. Accordingly, 200 mL inoculated 1x LB medium was used as starting material for plasmid isolation using the QIAGEN Plasmid Maxi Kit (*Qiagen*) according to the provided instructions. Plasmids were resuspended in a volume of 200 - 300 µL nuclease-free H₂O.

2.1.8 DNA Sequencing Reaction

The concentration of plasmid preparations was determined spectrophotometrically via light-absorption measurements at a wavelength of $\lambda = 260$ nm (A_{260}) (1 $A_{260} = 50$ µg/µL DNA) using the NanoDrop™ 1000 spectrophotometer (*Thermo Scientific*). 750 - 1500 ng plasmid DNA per 15 µL total volume were provided for sequencing reactions with *Eurofins*. The sequencing primer was added to a final concentration of 30 µM or was optionally provided by the sequencing company (see Tables 8 and 9). Received sequencing results were analyzed and compared using the software ApE (A plasmid editor by M. Wayne Davis).

Table 8: Sequencing Primers (Binding to Plasmid Backbone) Used for Sequencing Reactions.
Forward (fwd) and reverse (rev) primers are indicated.

Plasmid Backbone	Primer Name	Sequencing Primer	Type
pCDNA3.1	pCDNA3_fwd (<i>Eurofins</i>)	5'GGCTAACTAGAGAACCCACTG3'	fwd
	pCDNA3_rev (<i>Eurofins</i>)	5'GGCAACTAGAAGGCACAGTC3'	rev
pET-28a	T7 (<i>Eurofins</i>)	5'TAATACGACTCACTATAGGG3'	fwd
	T7 term (<i>Eurofins</i>)	5'CTAGTTATTGCTCAGCGGT3'	rev
pET-32a	T7 (<i>Eurofins</i>)	5'TAATACGACTCACTATAGGG3'	fwd
	T7 term (<i>Eurofins</i>)	5'CTAGTTATTGCTCAGCGGT3'	rev
pETDuet-1 (sequencing MCS1)	SM 117	5'GATCGATCTCGATCCCG3'	fwd
	SM 92	5'TACGATTACTTCTGTTGA3'	rev
pETDuet-1 (sequencing MCS2)	SM 118	5'GTACACGGCCGCATAATCG3'	fwd
	T7 term (<i>Eurofins</i>)	5'CTAGTTATTGCTCAGCGGT3'	rev
pRSFDuet-1 (sequencing MCS1)	SM 93	5'CATTAGGAAATTAAATACGAC3'	fwd
	SM 92	5'TACGATTACTTCTGTTGA3'	rev
pRSFDuet-1 (sequencing MCS2)	SM 118	5'GTACACGGCCGCATAATCG3'	fwd
	T7 term (<i>Eurofins</i>)	5'CTAGTTATTGCTCAGCGGT3'	rev
pT7CFE1-NHis	SM 49	5'CTCAAGACCCGTTAGAGGC3'	rev

Table 9: Sequencing Primers (Binding to Insert) Used for Sequencing Reactions.
Forward (fwd) primers are indicated.

Insert	Primer Name	Sequencing Primer	Type
3xFLAG-hABCE1	SM 148	5'GACACAGGCAATTGTATGTC3'	fwd
Various heRF1	SM 91	5'CTTTTTGGCACACTCCAAGG3'	fwd
Various heRF3 fl	SM 86 (SM 87 and SM 90: sequences see above)	5'TTCGTGCCAACGTCCACGC3'	fwd
Various Δ (1-138)heRF3	SM 87	5'GGAGGAAGAGGAAATCCC 3'	fwd
	SM 90	5'TGTCCTGGTACATTGGATTAC3'	fwd

2.2 Protein Analysis

2.2.1 Determination of Protein Concentration

Protein absorption at $\lambda = 280$ nm was measured using the NanoDropTM 1000 spectrophotometer (*Thermo Scientific*). To calculate the corresponding protein concentration, the sequence-specific extinction coefficient (in $M^{-1} cm^{-1}$) according to the EXPASy ProtParam Tool (<http://www.expasy.org/tools/>) (Artimo *et al.*, 2012) was taken into account for each protein (see Table 10).

Table 10: Extinction Coefficients (Assuming All Cysteine Residues are Reduced) of Proteins Used in this Study.

Extinction coefficients were calculated with EXPASy ProtParam Tool (<http://www.expasy.org/tools/>) (Artimo *et al.*, 2012).

Protein	Extinction Coefficient	Molecular Weight	Related UniProtKB Entry
(His) ₆ -Δ(1-46)Jmjd4, isoform1	96,370 $M^{-1} cm^{-1}$	49,588.6 Da	Q9H9V9
3xFLAG-hABCE1	45,270 $M^{-1} cm^{-1}$	70,371.6 Da	P61221
heRF1, isoform 1	31,860 $M^{-1} cm^{-1}$	48,996.8 Da	P62495
heRF3a fl, isoform 2 (co-expression)	46,410 $M^{-1} cm^{-1}$	68,413.3 Da	P15170
heRF3a fl, isoform 3 (single expression)	46,410 $M^{-1} cm^{-1}$	68,799.7 Da	P15170
Δ(1-138)heRF3a, isoform 2	40,910 $M^{-1} cm^{-1}$	55,437.4 Da	P15170

2.2.2 Protein Precipitation

For the analysis of diluted protein solutions, great volumes were reduced by the precipitation of contained proteins and their resuspension in a smaller volume. To this end, a final concentration of 6 % (v/v) trichloroacetic acid (TCA) (*Sigma*) and 0.0125 % (w/v) sodium-deoxycholate (*Roth*) (as co-precipitant) were added to the protein solution which was adjusted with double distilled H_2O (dd H_2O) to a final volume of 1,200 μL . Incubation on ice for 30 min was followed by centrifugation (30 min / 4 °C / 14,000 rpm / 5417R (Eppendorf)). Thereupon, the white precipitate was washed with 900 μL 100 % (v/v) ice-cold acetone (*Roth*) and centrifuged again under the same conditions. The acetone was removed completely whereupon the remaining pellet was air-dried at RT and resuspended in 10 μL 1x sodium dodecyl sulfate (SDS) Sample Buffer (SB) (50 mM tris(hydroxymethyl)aminomethane (Tris) / HCl pH 6.8, 2 % (w/v) SDS, 10 % (v/v) glycerol, 0.1 % (w/v) bromophenol blue, 100 mM 1,4-dithiothreitol (DTT)) prior to analysis via SDS-polyacrylamide gel electrophoresis (SDS-PAGE) (see 2.2.3).

2.2.3 Sodium Dodecyl Sulfate-polyacrylamide Gel Electrophoresis

Electrophoresis

For separation of proteins according to their molecular weight, the method of denaturing SDS-PAGE was applied. To this end, discontinuous polyacrylamide (PAA) gels consisting of a 4 % (v/v) stacking (37 mM Tris / pH 6.8, 4 % (w/v) acrylamide-, bis-acrylamide solution (37.5:1) (*Roth*), 0.1 % (w/v) SDS, 0.05 % (v/v) tetramethylethylenediamine (TEMED), 0.1 % (w/v) ammonium persulfate (APS)) and a 15 % (v/v) separating (37 mM Tris / pH 8.6, 15 % (w/v) acrylamide-, bis-acrylamide solution (37.5:1) (*Roth*), 0.1 % (w/v) SDS, 0.05 % (v/v) TEMED, 0.1 % (w/v) APS) gel were used. Protein samples were

completed with SDS SB (see 2.2.2) followed by a heat-denaturing step at 95 °C for 2 min. Electrophoresis was conducted at a constant voltage of 230 volt (V) in SDS-Running Buffer (25 mM Tris, 192 mM glycine, 0.1 % (w/v) SDS) for 45 min. For size determination, either the PageRuler™ Unstained Protein Ladder (10 to 200 kDa) (*Thermo Scientific*) or the PageRuler™ Prestained Protein Ladder (10 to 180 kDa) (*Thermo Scientific*) was used.

Coomassie Brilliant Blue Staining

The conventional method for visualizing protein bands after SDS-PAGE is their staining with Coomassie Brilliant Blue. To this end, the gel was heated in H₂O at 600 W (microwave) twice for 1 min to remove residual salt and SDS. Staining with Coomassie® G-250 solution (SimplyBlue™ SafeStain (*Novex*)) at 600 W for 1 min and shaking at RT for 5 - 10 min was followed by incubation with H₂O until a clear background was obtained. The gels were digitalized using a desk scanner (Perfection 4490 PHOTO, *Epson*) and eventually processed with the Adobe Software Package CS6 (*Adobe Systems Incorporated*).

SYPRO® Orange Staining

For less concentrated protein samples, the more sensitive dye SYPRO® Orange ($\lambda_{Ex(max)} = 300/472$ nm; $\lambda_{Em(max)} = 570$ nm) was applied. The staining procedure included incubation with a 1:5,000 dilution of SYPRO® Orange (*Invitrogen*) in freshly made 10 % (v/v) acetic acid under shaking conditions in the dark for 1 h. Subsequently, the gel was washed 3x with H₂O for 5 min each and digitalized using the Typhoon FLA 900 scanner (Laser: 473 nm, Filter: LBP, adjusted exposure time) (*GE Healthcare*) or the Chemi Doc™ MP Imaging System (Light source: Blue Epi Illumination, Filter: 605/5, adjusted exposure time) (*BIO-RAD*). Digitalized images were processed further as mentioned above.

2.2.4 Semi-dry Western Blotting

Western Blotting

Semi-dry Western blotting was used subsequent to SDS-PAGE in order to qualitatively (or semi-quantitatively) identify proteins. Cropped Whatman® filter-papers, the PAA gel and the nitrocellulose (NC) membrane (*GE Healthcare*) were pre-equilibrated in Blotting Buffer (20 % (v/v) methanol, 48 mM Tris, 39 mM glycine, 0.037 % (w/v) SDS). A semi-dry blotting sandwich was assembled in the blotting apparatus (*PeqLab*) from anode to cathode containing three 3 mm Whatman® filter-papers, the NC membrane, the PAA gel and three further 3 mm Whatman® filter-papers. Protein transfer was achieved by applying a constant current of 1 mA per cm² gel for 55 min. Afterwards, the membrane was stained with amidoblack solution (0.1 % (w/v) naphthol blue black, 7.5 % (v/v) acetic acid, 20 % (v/v) ethanol) for 1 min to check transfer efficiency whereupon destaining was performed in destain solution (40 % (v/v) ethanol, 10 % (v/v) acetic acid) until a white background was obtained. The membrane was incubated shortly in Tris-buffered saline (TBS) (20 mM Tris / HCl pH 7.6 / 4 °C, 150 mM NaCl) for pH neutralization and digitalized (Perfection 4490 PHOTO, *Epson*).

Antibody Detection

To saturate unspecific binding sites, the membrane was incubated for 1 h at 4 °C in 5 % (w/v) milk powder dissolved in TBS. Incubation with the primary antibody solution was performed according to specifically pre-tested and optimized conditions for each antibody (see Table 11). After washing 3x for 10 min at 4 °C with TBS, TBS-T (TBS supplemented with 0.1 % (v/v) Tween) and TBS to remove unbound antibodies, the horseradish peroxidase (HRP)-coupled secondary antibody solution was

applied also in its ideal concentration. Three washing steps at 4 °C with TBS-T each for 10 min followed.

In the case of the α -FLAG®HRP antibody, the primary antibody was already coupled to HRP. Therefore, the protocol was adjusted to blocking for 1 h at RT in 5 % (w/v) milk powder dissolved in TBS-T. The washing steps were also performed in TBS-T, 2x for 5 min each. After primary antibody incubation, washing was performed with TBS-T again 6x for 5 min each.

Table 11: Antibodies for Protein Identification on Western Blot Membranes Used in this Study.

1 st Antibody	Dilution	Incubation Condition	2 nd Antibody	Dilution	Incubation Condition
goat- α -eRF3a (Santa Cruz)	1:100	2 % (v/v) BSA/TBS, RT, 1.5 h	donkey- α -goat IgG-HRP (Santa Cruz)	1:10,000	5 % (v/v) milk/TBS, 4 °C, 1 h
mouse- α -eRF1 (Santa Cruz)	1:2,000	5 % (v/v) BSA/TBS, RT, 1 h	goat- α -mouse IgG-HRP (Santa Cruz)	1:2,500	5 % (v/v) milk/TBS, 4 °C, 1.5 h
mouse- α - FLAG®HRP (Sigma)	1:1,000	TBS-T, RT, 1 h	-----	-----	-----
mouse- α -HA (Sigma)	1:1,000	2 % (v/v) BSA/TBS, 4 °C, overnight	goat- α -mouse IgG-HRP (Santa Cruz)	1:2,500	5 % (v/v) milk/TBS, 4 °C, 1 h

The signal was produced by providing enhanced chemiluminescence (ECL) substrate (Enhanced Chemi Luminescence Detection Kit for Western blot (*AppliChem*)) to the bound HRP according to the manufacturer's recommendations. Signal detection was performed on LucentBlue X-ray film (*advansta*) which was exposed until an appropriate signal to noise ratio was obtained. The film was fixed using a developing device (Optimax Type TR, *PROTEC*) whereupon image digitalization and processing was performed as mentioned in 2.2.3.

2.2.5 Mass Spectrometry

To monitor the post-translational side-chain C4 hydroxylation of lysine 63 of differently treated heRF1 protein samples, they were subjected to SDS-PAGE, excised from the gel and provided to Thomas Fröhlich (Gene Center, LMU). Subsequently, gel extraction and enzyme digestion with chymotrypsin or trypsin were performed before analysis via mass spectrometry. Here, also possible secondary hydroxylation sites were monitored. Data evaluation was performed via the Scaffold 4 software (*Proteome Software, Inc.*).

2.3 Protein Expression and Purification

Throughout the protein expression and purification procedures appropriate volumes of intermediate steps were taken for analysis via SDS-PAGE. These samples were all stored at -20 °C.

Several strategies (see Figure 18) were pursued concurrently in order to obtain the human eRF1:eRF3a protein complex. Protein purification was based on metal affinity chromatography via the introduced histidine (His)-tag and on subsequent size exclusion chromatography via an ÄKTA Purifier FPLC system (*GE Healthcare*) if necessary. Only the approaches which lead to proteins or protein complexes ending up as potential high-resolution cryo-EM sample are elaborated below.

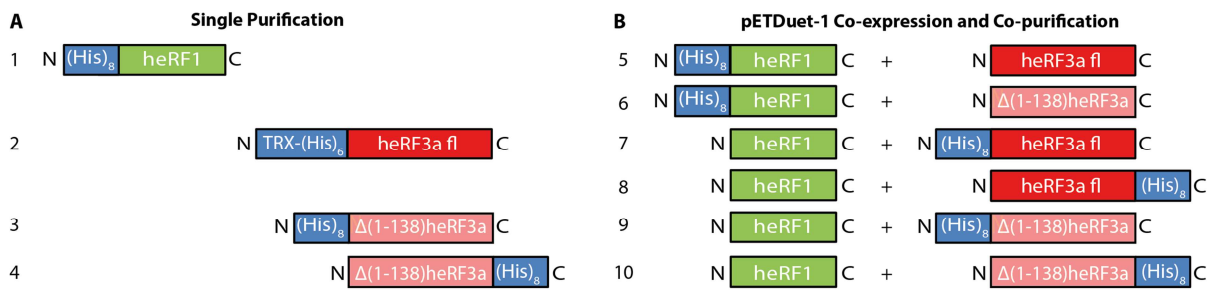


Figure 18: Schematic Overview of Purification Strategies for the Human eRF1:eRF3a:GMPPCP Complex.

Several purification strategies for the class-I release factor eRF1 and the class-II release factors $\Delta(1-138)$ heRF3a and heRF3a full length (fl) were conducted in parallel: **(A)** Single purification of **1**: N-terminally (N) octahistidine ((His)₈)-tagged heRF1, **2**: N-terminally Thioredoxin (TRX)-hexahistidine ((His)₆)-tagged heRF3a fl, **3**: N-terminally (His)₈-tagged $\Delta(1-138)$ heRF3a, **4**: C-terminally (C) (His)₈-tagged $\Delta(1-138)$ heRF3a. **(B)** Co-expression and co-purification of **5**: N-terminally (His)₈-tagged heRF1 and untagged heRF3a fl, **6**: N-terminally (His)₈-tagged heRF1 and untagged $\Delta(1-138)$ heRF3a, **7**: Untagged heRF1 and N-terminally (His)₈-tagged heRF3a fl, **8**: Untagged heRF1 and C-terminally (His)₈-tagged heRF3a fl, **9**: Untagged heRF1 and N-terminally (His)₈-tagged $\Delta(1-138)$ heRF3a and **10**: Untagged heRF1 and C-terminally (His)₈-tagged $\Delta(1-138)$ heRF3a.

2.3.1 General Procedures

Testing Protein Expression Conditions in *Escherichia coli* Cells

All protein expression conditions in *E. coli* which were not based on previous publications were tested in matters of induction time (1 h, 3 h, overnight) and expression temperature (18 °C, 30 °C, 37 °C) in a culture volume of 20 mL by the addition of 1 mM isopropyl β -D-1-thiogalactopyranoside (IPTG). Further, different *E. coli* expression strains (*E. coli* BL21 (DE3), Rosetta (DE3), ER2566) were tested for suitable expression conditions.

Escherichia coli Cell Harvest and Lysis

After ideal large-scale protein expression was performed in *E. coli*, cells were harvested (15 min / 4 °C / 6,000xg / SLC-6000 (*Sorvall*TM)) and the resulting cell pellet was washed once with H₂O before flash freezing the dry pellet in liquid nitrogen and storage at -80 °C. All following steps during protein purification were either performed on ice or at 4 °C. To continue, the pellet was thawed and resuspended in Lysis Buffer (composition individually indicated for each purification). Lysis was conducted with three passes through the Microfluidizer® (*Microfluidics*) at a pressure of 15,000 psi (103 MPa). Finally, the lysate (L) was cleared from cellular debris (P) (30 min / 4 °C / 13,500 rpm / SS-34 (*Sorvall*TM)).

Testing Protein Stability

After each protein purification procedure, the stability of the final protein was tested via centrifugation (15 min / 4 °C / 14,000 rpm / 5417R (*Eppendorf*)) and subsequent analysis of the resulting supernatant and pellet fractions via SDS-PAGE. Furthermore, an equal sample was flash frozen in liquid nitrogen, thawed and similarly analyzed to ensure stability of the protein when undergoing the freeze-thaw cycle.

Increasing Protein Concentration

To increase protein concentration during its purification, centrifugal filter units (Amicon Ultra-50 or Ultra-15 (*Millipore*)) with a molecular weight cut-off (MWCO) of at least half of the protein's size

were used. Membranes were pre-equilibrated with the corresponding protein buffer whereupon spinning speed and time were adjusted to obtain the desired protein concentration, never exceeding a speed of 3,000xg to ensure the protein's integrity.

2.3.2 Human Δ (1-46)Jmjd4

Construct: pET-28a (His)₆- Δ (1-46)Jmjd4

Expression Conditions

An overnight culture of transformed *E. coli* BL21 (DE3) was diluted to an $OD_{600} = 0.1$ in 5 L 1x LB_{Kan}. Cells were grown to an $OD_{600} = 0.8$ at 37 °C and temperature adjusted (4 °C, 30 min) for subsequent expression at 18 °C overnight. Induction of protein expression was performed by the addition of 0.5 mM IPTG. After 18.5 h, cells were harvested, flash frozen in liquid nitrogen and stored at -80 °C.

Protein Purification

After cell lysis (L) (see 2.3.1) (50 mM 4-(2-hydroxyethyl)piperazine-1-ethanesulfonic acid (HEPES) / potassium hydroxide (KOH) pH 7.5 / 4 °C, 500 mM NaCl, 5 mM imidazole, 1 pill/50 mL ethylenediaminetetraacetic acid (EDTA)-free complete protease inhibitor (Roche)), the *E. coli* cell material was incubated with pre-equilibrated 7.5 mL 50 % (w/v) TALON® Metal Affinity Resin (Clontech) at 4 °C under rotation for 1.25 h. The bead-lysate mixture was transferred to an Econo-Pac® Chromatography Column (BIO-RAD). The flow through (FT) was collected via gravity-flow whereupon the beads were washed 6x with 35 mL High Salt Wash Buffer (W₁ - W₆) (50 mM HEPES / KOH pH 7.5 / 4 °C, 500 mM NaCl, 20 mM imidazole, 5 mM β -mercaptoethanol). Elution was performed with a step gradient of 5x 8 mL Elution Buffer (50 mM HEPES / KOH pH 7.5 / 4 °C, 500 mM NaCl) each supplemented with 50 (E₅₀), 100 (E₁₀₀), 150 (E₁₅₀), or 2x 250 mM (E_{250/1} and E_{250/2}) imidazole. Appropriate samples were pooled, concentrated and possible aggregates were removed (15 min / 4 °C / 14,000 rpm / 5417R (Eppendorf)) before performing gel filtration on a Superdex 75 (10/300) GL (GE Healthcare) column. The appropriate fractions were pooled and concentrated to 1.00 μ g/ μ L. Aliquots were prepared, flash frozen in liquid nitrogen and stored at -80 °C.

2.3.3 Human eRF1

Construct: pETDuet-1 (His)₈-3C-heRF1

Expression Conditions

An overnight culture of transformed *E. coli* BL21 (DE3) was diluted to an $OD_{600} = 0.1$ in 1 L 1x LB_{Amp}. Cells were grown to an $OD_{600} = 0.6$ at 37 °C and temperature adjusted (4 °C, 30 min) for subsequent expression at 18 °C overnight. Induction of protein expression was performed by the addition of 1 mM IPTG. After 20 h, cells were harvested, flash frozen in liquid nitrogen and stored at -80 °C.

Protein Purification

After cell lysis (L) (see 2.3.1) (50 mM HEPES / KOH pH 7.5 / 4 °C, 500 mM NaCl, 5 mM imidazole, 5 mM β -mercaptoethanol, 1 pill/50 mL EDTA-free complete protease inhibitor (Roche)), the *E. coli* cell material was incubated with pre-equilibrated 1.5 mL 50 % (w/v) TALON® Metal Affinity Resin (Clontech) at 4 °C under rotation for 1 h. The bead-lysate mixture was transferred to a Poly-Prep® Chromatography Column (BIO-RAD). The flow through (FT) was collected via gravity-flow whereupon the beads were washed 6x with 7.5 mL High Salt Wash Buffer (W₁ - W₆) (see 2.3.2). Elution was performed via 3C-protease cleavage (final concentration (conc) 0.5 μ g/ μ L) of the (His)₈-tag (E_{3C}) at 4 °C for 1 h (50 mM HEPES / KOH pH 7.5 / 4 °C, 200 mM NaCl, 1 mM imidazole, 5 mM

β -mercaptoethanol, 2.5 mM magnesium chloride ($MgCl_2$)). Further elution possibilities were tested to ensure quantitative elution of the tag-free protein. Aliquots were prepared, flash frozen in liquid nitrogen and stored at -80 °C.

***In vitro* Hydroxylation**

Purified heRF1 was subjected to *in vitro* hydroxylation of the lysine 63 side-chain C4 by the 2-oxoglutarate and Fe(II)-dependent oxygenase JmjD4. Therefore, incubation of 40 μ g (8.5 μ M) heRF1 with 4 μ g (0.85 μ M) Δ (1-46)JmjD4 (50 mM HEPES / KOH 7.5 / 4 °C, 200 mM NaCl, 6.76 μ M 2-oxoglutarate, 42.2 μ M $NH_4FeSO_4 \cdot 6H_2O$) was performed at 4 °C overnight. Further, quenching efficiency with 10 mM EDTA (pH 8.0) for 5 min on ice was tested to prevent potential hydroxylation of secondary sites. Hydroxylation efficiency for heRF1 Lys63 was monitored via mass spectrometry (see 2.2.5).

2.3.4 Human eRF1 Co-expression with Δ (1-46)JmjD4 for *in vivo* Hydroxylation

Constructs: pETDuet-1 (His)₈-3C-heRF1 and pET-28a (His)₆- Δ (1-46)JmjD4

Expression Conditions

Co-expression of heRF1 and Δ (1-46)JmjD4 was performed in 5 L 1x LB_{Amp/Kan} *E. coli* BL21 (DE3) as described for the heRF1 only expression (see 2.3.3).

Protein Purification

Expression and purification were also performed as described in 2.3.3, however, up-scaled accordingly due to the usage of 5 L *E. coli* culture as starting material. Also here, the hydroxylation efficiency for heRF1 Lys63 was monitored via mass spectrometry (see 2.2.5).

2.3.5 Human Δ (1-138)eRF3a

Construct: pRSFDuet-1 (His)₈-3C- Δ (1-138)heRF3a

Expression Conditions

An overnight culture of transformed *E. coli* BL21 (DE3) was diluted to an $OD_{600} = 0.1$ in 2 L 1x LB_{Kan}. Cells were grown to an $OD_{600} = 0.6$ at 37 °C. Induction of protein expression was performed by the addition of 1 mM IPTG. After 21 h at 30 °C, cells were harvested, flash frozen in liquid nitrogen and stored at -80 °C.

Protein Purification

Subsequent to cell lysis (L) (see 2.3.1) (50 mM HEPES / KOH pH 7.5 / 4 °C, 500 mM NaCl, 10 % (v/v) glycerol, 0.1 % (v/v) Nonidet P40, 10 mM imidazole, 2 mM β -mercaptoethanol, 1 mM phenylmethylsulfonylfluorid (PMSF), 1 pill/50 mL EDTA-free complete protease inhibitor (Roche)) the *E. coli* cell material was incubated with pre-equilibrated 1.5 mL 50 % (w/v) TALON® Metal Affinity Resin (Clontech) at 4 °C under rotation for 1 h. The bead-lysate mixture was transferred to a Poly-Prep® Chromatography Column (BIO-RAD). The flow through (FT) was collected via gravity-flow whereupon the beads were washed 5x with 8.5 mL High Salt Wash Buffer (W₁ - W₅) (50 mM HEPES / KOH pH 7.5 / 4 °C, 500 mM KCl, 10 mM imidazole). Elution (E_{3C}) was performed via 3C-protease cleavage (final conc 0.5 μ g/ μ L) of the (His)₈-tag at 4 °C for 1 h (50 mM HEPES / KOH pH 7.5 / 4 °C, 50 mM KCl, 2 mM β -mercaptoethanol). Further elution possibilities were tested to ensure quantitative elution of the tag-free protein. Aliquots were prepared, flash frozen in liquid nitrogen and stored at -80 °C.

2.3.6 Guanosine Triphosphatase Deficient Mutants of Human Δ(1-138)eRF3a

Constructs: pRSFDuet-1 (His)₈-3C-Δ(1-138)heRF3a H300Q and R371G

According to Salas-Marco *et al.* (Salas-Marco and Bedwell, 2004) the yeast eRF3 mutants His348Gln and Arg419Gly are deficient in GTP hydrolysis while maintaining the capability of GTP binding. The corresponding mutations His300Gln (H300Q) and Arg371Gly (R371G) in human Δ(1-138)eRF3a were therefore introduced via RfBEM cloning and mutant protein was expressed and purified as described for the truncated human eRF3a (Δ(1-138)heRF3a protein (see 2.3.5).

2.3.7 Human eRF3a Full Length

Construct: pET-32a TRX-(His)₆-TEV-heRF3a fl

Expression Conditions

Here, the initial overnight culture of transformed *E. coli* BL21 (DE3) was grown in 30 mL 2x LB_{Amp} medium at RT without shaking overnight. Subsequently, it was transferred to 37 °C, grown to an OD₆₀₀ = 0.6 under shaking conditions and diluted 1:80 in 1 L 2x LB_{Amp} again. After further growth to an OD₆₀₀ = 0.6 - 0.7 at 37 °C, the culture was temperature adjusted (4 °C, 30 min) and protein expression was induced with 0.25 mM IPTG. After incubation at 20 °C for 18 h, cells were harvested, frozen in liquid nitrogen and stored at -80 °C.

Protein Purification

After cell lysis (L) (see 2.3.1) (70 mM Tris / HCl pH 8.0 / 4 °C, 300 mM KCl, 10 % (v/v) glycerol, 1 % (v/v) Triton™ X-100 (v/v), 1 mM β-mercaptoethanol, 1 mM PMSF, 1 pill/50 mL EDTA-free complete protease inhibitor (Roche)), the *E. coli* cell material was incubated with pre-equilibrated 1.5 mL 50 % (w/v) TALON® Metal Affinity Resin (Clontech) at 4 °C under rotation for 1 h. The bead-lysate mixture was transferred to an Econo-Pac® Chromatography Column (BIO-RAD). The flow through (FT) was collected via gravity-flow whereupon the beads were washed 3x with 15 mL Wash Buffer 1 (W₁ – W₃) (50 mM Tris / HCl pH 7.5 / 4 °C, 2 M KCl, 10 % (v/v) glycerol, 1 mM β-mercaptoethanol), 1x with 7.5 mL Wash Buffer 2 (W₄) (like Wash Buffer 1, but containing 800 mM KCl) and 1x with 7.5 mL Wash Buffer 3 (W₅) (like Wash Buffer 1, but containing 100 mM KCl). Elution (E_{TEV}) was performed via tobacco etch virus (TEV)-protease cleavage (50 µL (home-made) in 5 mL total volume) of the thioredoxin (TRX)-(His)₆-tag at 4 °C overnight (50 mM HEPES / KOH pH 7.5 / 4 °C, 100 mM KCl, 10 % (v/v) glycerol, 2.5 mM MgCl₂, 1 mM DTT). Aliquots were prepared, flash frozen in liquid nitrogen and stored at -80 °C.

For optimization of heRF3a full length (fl) purification that was intended for individual use (no ternary complex formation), the elution strategy was changed to an imidazole step-gradient (3x 150 mM and 3x 250 mM) (E_{150/1}, E_{150/2}, E_{150/3}, E_{250/1}, E_{250/2}, E_{250/3}) of 2 mL each. Adequate fractions were pooled and supplemented with TEV-protease (50 µL, home-made) before dialysis (Spectra/Por® MWCO 12 - 14 kDa (SPECTRUM)) at 4 °C overnight. Subsequently, the retentate was loaded onto 1.5 mL 50 % (w/v) TALON® Metal Affinity Resin (Clontech) again. The flow through (FT₂) was collected and concentrated (Final), aliquots were flash frozen in liquid nitrogen and stored at -80 °C.

2.3.8 Human eRF1:eRF3a Complex Formation

Human eRF1 and Δ(1-138)eRF3a

For complex formation, equimolar amounts of individually purified heRF1 and Δ(1-138)heRF3a were incubated together with 1 mM β,γ-methyleneguanosine 5'-triphosphate (GMPPCP) (Sigma) for

10 min at 20 °C in Buffer CF (50 mM HEPES, pH 7.5 / 4 °C, 100 mM NaCl, 26 mM KCl, 1.5 mM β-mercaptoethanol, 2.5 mM MgCl₂). Possible aggregates were removed (30 min / 4 °C / 14,000 rpm / 5417R (*Eppendorf*)) before the sample was loaded onto the analytical size exclusion column S200 (150/5) Increase GL (*GE Healthcare*) (50 mM HEPES, pH 7.5 / 4 °C, 125 mM KCl, 1 mM β-mercaptoethanol, 2.5 mM MgCl₂). Successful complex formation was monitored by an absorption profile at λ = 280 nm as well as by SDS-PAGE of the obtained, concentrated fractions. Adequate samples were aliquoted, flash frozen in liquid nitrogen and stored at -80 °C.

Human eRF1 and eRF3a Full Length

Here, for complex formation heRF1 was applied in excess to ensure quantitative binding of human heRF3a fl and therefore circumvent the challenge of heRF3a fl separation from the heRF1:heRF3a fl complex via size exclusion chromatography due to the insufficient difference in size. Samples were assembled and treated as mentioned above for complex formation (50 mM HEPES / KOH pH 7.5 / 4 °C, 40 mM KCl, 120 mM NaCl, 4 % (v/v) glycerol, 0.4 mM DTT, 3 mM β-mercaptoethanol, 2.5 mM MgCl₂) and loaded onto an S200 (10/300) (*GE Healthcare*) size exclusion column. Successful complex formation was monitored by an absorption profile at λ = 280 nm as well as by SDS-PAGE. Adequate samples were concentrated, aliquoted, flash frozen in liquid nitrogen and stored at -80 °C. Complex stability after concentration and freezing was monitored by an absorption profile at λ = 280 nm as well as by SDS-PAGE of the obtained fractions from sample application on an analytical S200 (150/5) Increase GL (*GE Healthcare*) size exclusion column.

2.3.9 Co-purification of the Human eRF1:Δ(1-138)eRF3a Complex (Co-expressed with Δ(1-46)Jmjd4) for *in vivo* Hydroxylation)

Constructs: pETDuet-1 (His)₈-3C-eRF1 Δ(1-138)heRF3a and pET-28a (His)₆-Δ(1-46)Jmjd4

Expression Conditions

An overnight culture of transformed *E. coli* BL21 (DE3) was diluted to an OD₆₀₀ = 0.1 in 8 L 1x LB_{Amp/Kan}. Cells were grown to an OD₆₀₀ = 0.6 at 37 °C. Induction of protein expression was performed by the addition of 1 mM IPTG. After 3 h at 37 °C, cells were harvested, flash frozen in liquid nitrogen and stored at -80 °C

Protein Purification

After cell lysis (L) (see 2.3.1) (50 mM HEPES / KOH pH 7.5 / 4 °C, 100 mM NaCl, 5 mM imidazole, 5 mM β-mercaptoethanol, 2.5 mM MgCl₂, 1 pill/50 mL EDTA-free complete protease inhibitor (*Roche*)), the *E. coli* cell material was incubated with pre-equilibrated 5 mL 50 % (w/v) TALON® Metal Affinity Resin (*Clontech*) at 4 °C under rotation for 1 h. The bead-lysate mixture was transferred to an Econo-Pac® Chromatography Column (*BIO-RAD*). The flow through (FT) was collected via gravity-flow whereupon the beads were washed 6x with 25 mL Low Salt Wash Buffer (W₁ - W₆) (50 mM HEPES / KOH pH 7.5 / 4 °C, 100 mM NaCl, 20 mM imidazole, 5 mM β-mercaptoethanol, 2.5 mM MgCl₂). Elution was performed via 3C-protease cleavage (E_{3C}) (final conc 0.5 µg/µL) of the (His)₈-tag at 4 °C for 1 h (50 mM HEPES / KOH pH 7.5 / 4 °C, 100 mM NaCl, 1 mM β-mercaptoethanol, 2.5 mM MgCl₂). 1 mM GMPPCP (*Sigma*) was added to the sample which was incubated at 20 °C for 10 min before performing size exclusion chromatography on a Superdex 200 (10/300) GL (*GE Healthcare*) column. The appropriate fractions were pooled and concentrated to 0.96 µg/µL. Aliquots were made, flash frozen in liquid nitrogen and stored at -80 °C. Lastly, also here the hydroxylation status of heRF1 Lys63 was analyzed via mass spectrometry (see 2.2.5).

2.3.10 Co-purification of the Human eRF1:eRF3a Full Length Complex (Co-expressed with Δ(1-46)Jmjd4) for *in vivo* Hydroxylation)

Constructs: pETDuet-1 eRF1 (His)₈-3C-eRF3a fl and pET-28a (His)₆-Δ(1-46)Jmjd4

Expression Conditions

An overnight culture of transformed *E. coli* BL21 (DE3) was diluted to an OD₆₀₀ = 0.1 in 1 L 1x LB_{Amp/Kan}. Cells were grown to an OD₆₀₀ = 0.6 at 37 °C. Induction of protein expression was performed by the addition of 1 mM IPTG. After 3 h at 30 °C, cells were harvested, flash frozen in liquid nitrogen and stored at -80 °C

Protein Purification

After cell lysis (L) (see 2.3.1 for lysis and 2.3.9 for the corresponding buffer) the *E. coli* cell material was incubated with pre-equilibrated 1 mL 50 % (w/v) TALON® Metal Affinity Resin (Clontech) at 4 °C under rotation for 1 h. The bead-lysate mixture was transferred to a Bio-Spin® Chromatography Column (BIO-RAD). The flow through (FT) was collected via gravity-flow whereupon the beads were washed 6x with 5 mL Low Salt Wash Buffer (W₁ - W₆) (see 2.3.9). Elution was performed with a step gradient of 6x 1 mL Elution Buffer (50 mM HEPES / KOH pH 7.5 / 4 °C, 2 mM β-mercaptoethanol, 2.5 mM MgCl₂, 100 mM NaCl) each supplemented with 0 (E₀), 50 (E₅₀), 100 (E₁₀₀), 150 (E₁₅₀), 200 (E₂₀₀) or 250 (E₂₅₀) mM imidazole. Appropriate samples were pooled, concentrated to 2.29 µg/µL and 1 mM GMPPCP (Sigma) was added before incubation at RT for 10 min. Analytical size exclusion chromatography on a Superdex S200 (150/5) Increase GL (GE Healthcare) column followed where complex formation was monitored by an absorption profile at λ = 280 nm as well as by SDS-PAGE of the obtained fractions.

2.3.11 Human ABCE1

(Construct: pCDNA3.1 3xFLAG-hABCE1)

Expression Conditions and Cell Lysis

Expression of human ABCE1 has failed in *E. coli* cells, why it was expressed in human HEK293T cells. Ten 154 cm² dishes with HEK293T cells were transfected as described in 2.4.1. After 48 h, cells were washed off the plates with DPBS (Gibco) (5 min / 4 °C / 1,600 rpm / Rotanta 46R (Hettich)) and the resulting dry pellet was flash frozen in liquid nitrogen before storage at -80 °C. Here, lysis was performed by incubation with NP-40 Substitute Lysis Buffer (50 mM HEPES / KOH pH 7.5 / 4 °C, 100 mM potassium acetate (KOAc), 1 mM DTT, 5 mM MgCl₂, 0.5 % (v/v) NP-40 Substitute, 1 pill/50 mL EDTA-free complete protease inhibitor (Roche)) at 4 °C under rotation for 30 min.

Protein Purification

The HEK293T cell lysate was cleared (15 min / 4 °C / 14,000 rpm / 5417R (Eppendorf)) whereupon the supernatant (L) was incubated with pre-equilibrated 200 µL 50 % (v/v) ANTI-FLAG® M2 beads (Sigma) at 4 °C for 2 h. Then, the bead-lysate mixture was transferred to a Bio-Spin® Chromatography Column (BIO-RAD). The flow through (FT) was collected via gravity-flow whereupon the beads were washed 3x with 2 mL Lysis Buffer (W₁ - W₃), 3x with 2 mL High Salt Wash Buffer (W₄ - W₆) (50 mM HEPES / KOH pH 7.5 / 4 °C, 400 mM KOAc, 1 mM DTT, 5 mM Mg(OAc)₂, 0.1 % (v/v) Triton™ X-100) and 1x with 2 mL Elution Buffer without 3xFLAG®-peptide (W₇) (50 mM HEPES / KOH pH 7.5 / 4 °C, 100 mM KOAc, 1 mM DTT, 5 mM Mg(OAc)₂). Elution was performed by step-wise incubation with 5x 200 µL Elution Buffer with 0.2 µg/µL 3xFLAG®-peptide (Sigma) (E₁ - E₅) each at 4 °C for 10 min. Low binding tubes (Bioscience Scientific) were used to prevent binding of the eluted protein to the tube wall. To

dispose the 3xFLAG® peptide (*Sigma*) from the final sample, the solution was repeatedly diluted 1:4 in Elution Buffer without 3xFLAG®-peptide and concentrated to a final conc of 0.51 µg/µL. Samples were not stable upon freezing why they had to be stored in low binding tubes at 4 °C overnight until further usage.

2.4 Human Cell Culture

2.4.1 Human Embryonic Kidney 293T Cells

Cell Culture

Adherent human embryonic kidney 293T (HEK293T) cells were cultured at a density of 10 - 90 % confluence in Dulbecco's Modified Eagle Medium (DMEM) (*Gibco*) supplemented with 10 % (v/v) heat-inactivated fetal calf serum (FCS) (*Gibco*), 100 U/mL Penicillin / 100 µg/mL Streptomycin (*Gibco*) and 1x GlutaMAX (*Gibco*) at 37 °C and 5 % carbon dioxide (CO₂) using 58 - 154 cm² dishes.

Transient Transfection

~18 h prior to transient transfection HEK293T cells were seeded to a density of 20 - 30 % confluence in 30 mL supplemented medium in 154 cm² dishes (see Figure 19). As transfection reagent, the stable cationic polymer polyethylenimine (PEI) (*Sigma*) was used. The amount of the required PEI (c = 1 mg/mL) /DMEM (without supplements) mixture was calculated by the

$$\text{number of dishes} \times \mu\text{g of transfected DNA} \times 2.5 \text{ (PEI factor)},$$

assembled and incubated for 5 min at RT. A second mixture of 30 µg DNA in 1 mL DMEM (without supplements) per 154 cm² dish was prepared. Then, the PEI/DMEM and the DNA/DMEM mixtures were combined and incubated for 20 min at RT. Subsequently, 2 mL solution were carefully applied in a dropwise manner and evenly distributed onto the liquid surface of each 154 cm² dish. Transfected cells were incubated for 48 h prior to harvesting.

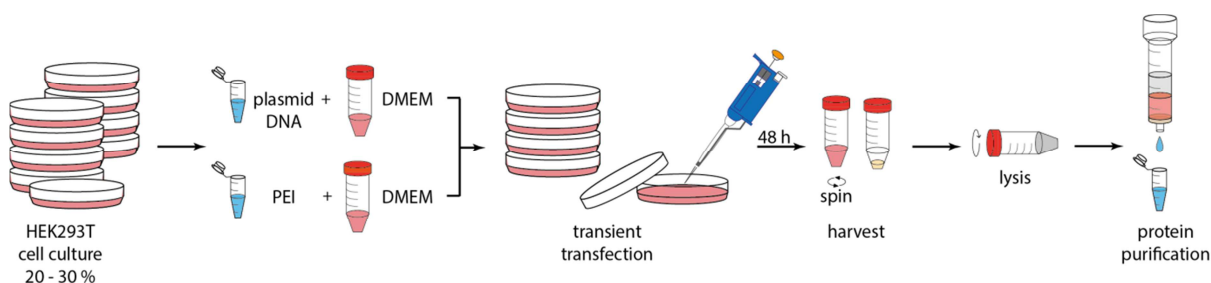


Figure 19: Application of HEK293T Cell Culture.

Human embryonic kidney 293T (HEK293T) cells were cultured adherently in cell culture dishes and seeded at a density of 20 - 30 % confluence 18 hours (h) prior to transient transfection. The cell confluence was determined optically under a light microscope. Transient transfection of plasmid DNA was achieved via the stable cationic polymer polyethylenimine (PEI) in Dulbecco's Modified Eagle Medium (DMEM). 48 h later, gentle centrifugation resulted in a cell pellet that was subjected to cell lysis (see 2.3.1) and protein purification (see 2.3.11).

2.4.2 HeLa S3 Suspension Cells

Cell Culture

HeLa S3 suspension cells were cultured at a density of $3.0 - 6.0 \times 10^5$ cells/mL in Spinner Minimum Essential Medium Eagle (SMEM) (Sigma) supplemented with 10 % (v/v) heat-inactivated FCS (Gibco), 100 U/mL Penicillin / 100 µg/mL Streptomycin (Gibco) and 1x GlutaMAX (Gibco) at 37 °C and 5 % CO₂ using 58 cm² and 154 cm² dishes for small volumes or a spinner flask (40 rpm) for a volume of up to 7.0 L (see Figure 20).

Cell Concentration Determination

Cell counting was performed with a Neubauer cell chamber, Depth 0.100 mm (Marienfeld). The cells were mixed 1:1 with 0.4 % (w/v) Trypan Blue solution (Sigma) before introduction into the chamber. Counting was performed in 4 - 8 big squares visualized under the light microscope TELAVAL31 (ZEISS). To calculate the cell concentration, the following formula was used:

$$\begin{aligned} \text{Concentration } \left(\frac{\text{cells}}{\text{mL}} \right) &= \frac{\text{Average number of cells per square}}{\text{Volume per square [mL]}} \times \text{dilution factor} \\ &= \frac{\text{Total number of cells} \times 10,000}{\text{Number of big squares}} \times 2 \end{aligned}$$

The volume of one big square was calculated to $0.1 \text{ cm} \times 0.1 \text{ cm} \times 0.1 \text{ cm} = 0.0001 \text{ cm}^3 = 0.0001 \text{ mL} = 10,000^{-1}$ resulting in a factor of 10,000. The dilution factor corresponds to the Trypan Blue dilution resulting in a factor of 2.

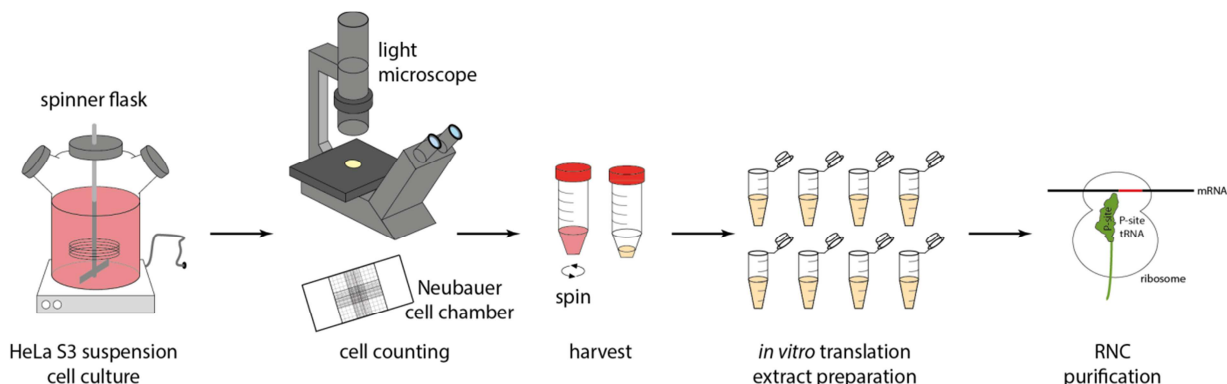


Figure 20: Application of HeLa S3 Suspension Cell Culture.

HeLa S3 suspension cells were cultured in a spinner flask up to a volume of 7.0 liters. Their concentration was determined by cell counting with a Neubauer cell chamber under a light microscope. Gentle centrifugation resulted in a cell pellet that was subjected to extract preparation (see 2.5.2) and subsequent ribosome-nascent chain complex (RNC) purification (see 2.6).

2.5 Establishing a Human *in vitro* Expression System for Obtaining Stalled 80S Ribosomes

2.5.1 T7 Polymerase-based *in vitro* Transcription

Solely sequenced plasmids were used as template for *in vitro* transcription to ensure accuracy on DNA-level. Plasmids were linearized with SpeI-HF (NEB) in 10x CutSmart® Buffer (NEB) at 37 °C

overnight to later obtain a defined mRNA 3' end and were subjected to purification (QIAquick® PCR Purification Kit (*Qiagen*), according to 2.1.3). *In vitro* transcription was performed in a total volume of 100 µL in Transcription Buffer (40 mM Tris / HCl pH 7.0 / 4 °C, 20 mM MgCl₂, 0.01 % (v/v) Triton™ X-100, 2.5 mM Spermidine, 5 mM DTT, 6.25 mM ATP, 6.25 mM CTP, 6.25 mM GTP, 6.25 mM UTP, 0.2 U/mL Anti-RNase (*Ambion*®)) with home-made T7 RNA polymerase and 0.015 µg/µL mRNA at 37 °C for 4 h. After 1 h incubation and a short spin (1 min / RT / 13,000 rpm / 5415D (*Eppendorf*)) to remove accumulated pyrophosphate, fresh T7 RNA polymerase was added. The final mRNA construct encoded for a CrPV IGR IRES sequence for translation initiation, N-terminal HA- and (His)₆-tags, parts (DP75) of the well characterized dipeptidyl aminopeptidase B (DPAPB) (Beckmann *et al.*, 2001), the human hCMV-stalling sequence (Schleiss *et al.*, 1991) and a 26 nt poly(A) tail (p(A)₂₆). The resulting mRNA was LiCl precipitated for purification, analyzed via agarose gel electrophoresis, flash frozen in liquid nitrogen and stored at -80 °C.

2.5.2 HeLa S3 Extract-based *in vitro* Translation

Extract Preparation

The human *in vitro* translation extract was prepared on the basis of Mikami *et al.* (Mikami *et al.*, 2010a) with significant adjustments resulting in the protocol schematically depicted in Figure 21. Here, HeLa S3 suspension cells were grown to a density of 3.0 - 5.5x10⁵ cells/mL as described in 2.4.2. Thereupon, cells were harvested (2 min / RT / 650xg / Rotanta 46R (*Hettich*)), washed 3x in Washing Buffer (35 mM HEPES / KOH pH 7.5 / 4 °C, 140 mM NaCl, 11 mM Glucose) and 1x in Extraction Buffer (20 mM HEPES / KOH pH 7.5 / 4 °C, 45 mM KOAc, 45 mM KCl, 1.8 mM Mg(OAc)₂, 1 mM DTT). The resulting pellet was resuspended in Extraction Buffer to obtain a density of 1.2x10⁹ cells/mL. For maintaining extract activity, gentle cell disruption via nitrogen pressure (30 min / 4 °C / 300 psi) in a cell disruption vessel (*Parr Instrument*) was necessary. The extruding extract was mixed with 1/29 volume High Potassium Buffer (20 mM HEPES / KOH pH 7.5 / 4 °C, 945 mM KOAc, 945 mM KCl, 1.8 mM Mg(OAc)₂, 1 mM DTT), incubated for 5 min on ice and very briefly centrifuged (20 sec / 14,000 rpm / 4 °C). Aliquoting was performed quickly and strictly on ice whereupon the aliquots were flash frozen in liquid nitrogen and stored at -80 °C until further usage.

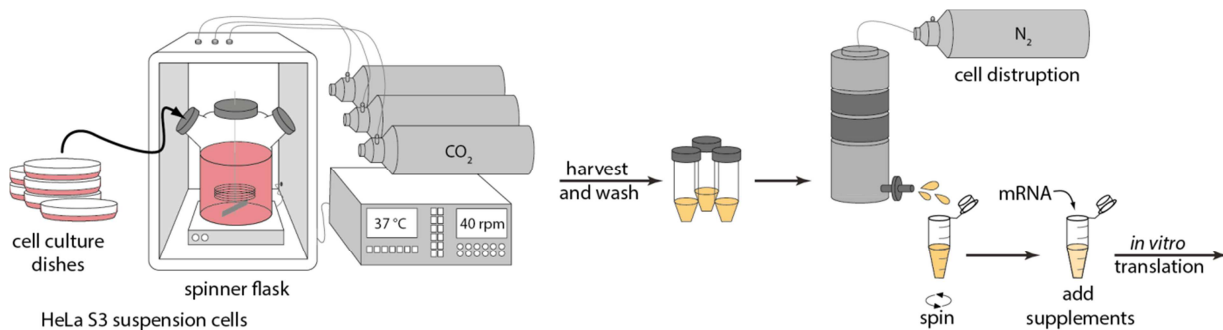


Figure 21: Schematic of *in vitro* Translation Extract Preparation.

Small volumes of HeLa S3 suspension cells were cultured in cell culture dishes. To grow large volumes, cells were transferred into a spinner flask and grown up to 7.0 liters at 37 °C and 40 rounds per minute (rpm) under 5 % carbon dioxide (CO₂). Cells were harvested and immediately subjected to nitrogen (N₂) pressure for gentle cell lysis upon pressure release. Fast centrifugation resulted in the extract to be supplemented and subjected to the *in vitro* translation reaction of the target mRNA.

Optimization of Translational Stalling

Ribosome stalling conditions had to be optimized individually for each batch of translation extract since they differed considerably. First, several translation times (5 min intervals within 60 min translation time) were tested in small test-translation reactions (total volume of 12 μ L each). Then, nine differently concentrated Mg(OAc)₂ solutions resulting in 0.25 mM steps in the range of 2.5 - 4.5 mM were tested. Knowing the ideal Mg(OAc)₂ concentration this was used to test eight KOAc concentrations resulting in 600 mM steps in the range of 600 - 4,800 mM. For each test, 4 μ L of the sample were analyzed via SDS-PAGE, Western blotting and anti-body detection.

In vitro Translation Reaction

In vitro translation was performed in Translation Buffer (24 mM HEPES / KOH pH 7.5 / 4 °C, optimized mM KOAc, 20.1 mM KCl, optimized mM Mg(OAc)₂, 2.5 mM DTT, 0.25 mM GTP, 1.56 mM ATP, 16 mM Creatine Phosphate (*Roche*), 0.45 μ g/ μ L Creatine Kinase (*Roche*), 50 μ g/mL yeast tRNA, 0.4 mM Spermidine, 0.12 mM aa mixture complete (*Promega*) and 0.885 U/ μ L Anti-RNase (*Ambion*®)) with 50 % (v/v) extract. This mixture was supplemented with a final concentration of 0.17 μ g/ μ L mRNA before incubation for 20 - 60 min (depending on the extract) at 30 °C followed.

Mutational Scanning Analysis

For the mutational screening of the hCMV-peptide sequence, the *in vitro* translation reaction volume was also downscaled to 12 μ L. 4 μ L of the sample were analyzed via SDS-PAGE, Western blotting and anti-body detection to monitor stalling efficiency of the mutated peptide chain.

2.6 Preparation of Human Stalled Ribosome-nascent Chain Complexes

Purification of Human CMV-stalled and Truncated CMV Control Ribosome-nascent Chain Complexes

Human 80S ribosomes were stalled via the hCMV-peptide (see 1.3.2) and the resulting ribosome-nascent chain complexes (RNCs) were purified. To this end, the human *in vitro* translation reaction was stopped by the addition of 25 μ g/mL cycloheximide (*Sigma*) which hindered translocation. The reaction (T) was layered onto a sucrose cushion (50 mM Tris / HCl pH 7.0 / 4 °C, 500 mM KOAc, 25 mM Mg(OAc)₂, 5 mM β -mercaptoethanol, 750 mM sucrose, 10 μ g/mL cycloheximide (*Sigma*), 0.1 % (w/v) Nikkol, 1/1,000 EDTA-free complete protease inhibitor (*Roche*)) and centrifuged (45 min / 4 °C / 100,000 rpm / TLA120.2 (*Beckman Coulter*)). The supernatant (SN₁) was quickly and completely removed. The resulting pellet (P) was resuspended in Buffer A (50 mM Tris / HCl pH 7.0 / 4 °C, 250 mM KOAc, 25 mM Mg(OAc)₂, 5 mM β -mercaptoethanol, 250 mM sucrose, 10 μ g/mL cycloheximide (*Sigma*), 0.1 % (w/v) Nikkol, 1/1,000 EDTA-free complete protease inhibitor (*Roche*), 0.1 % (v/v) Anti-RNase (*Ambion*®)) and was shortly centrifuged again to remove residual extract parts (R_{spin} Sup and R_{spin} P) (1 min / 4 °C / 13,000 rpm / 5417R (*Eppendorf*)). The remaining solution was subjected to TALON®-affinity purification. The Co²⁺-matrix TALON® Metal Affinity Resin (*Clontech*) was pre-equilibrated and subsequently pre-exposed to a yeast tRNA mixture (10 μ g/mL) in Buffer A to minimize unspecific RNA binding. The RNC-containing solution was incubated with the beads for 15 min at RT before the beads were washed 1x with 8 column volumes (CVs) (W₁) and 2x with 5 CVs Buffer A (without Anti-RNase) (W₂ - W₃). The final wash 1x with 3 CVs Buffer B (W₄) (50 mM Tris / HCl pH 7.0 / 4 °C, 500 mM KOAc, 25 mM Mg(OAc)₂, 5 mM β -mercaptoethanol, 250 mM sucrose, 0.1 % (w/v) Nikkol, 1/1,000 EDTA-free complete protease inhibitor (*Roche*)) was followed by the elution of the His-tagged RNCs by incubation with 3 CVs Buffer A supplemented with 150 mM imidazole at RT for 15 min. The eluate was loaded onto a sucrose cushion (see above) and centrifuged (60 min / 4 °C

/ 100,000 rpm / TLA 110 (*Beckman Coulter*)). The supernatant (SN_2) was again removed quickly and completely. The pellet was resuspended in an appropriate volume of Buffer C (50 mM Tris / HCl pH 7.0 / 4 °C, 100 mM KOAc, 6 mM Mg(OAc)₂, 1 mM DTT, 1/200 EDTA-free complete protease inhibitor (*Roche*), 0.2 U/mL Anti-RNase (*Ambion*®)) on ice for at least 1 h, briefly centrifuged (RNC_p and RNC_{final}) (1 min / 4 °C / 13,000 rpm / 5417R (*Eppendorf*)), aliquoted, flash frozen in liquid nitrogen and stored at -80 °C. The final ribosome concentration was determined by measuring the absorbance at $\lambda = 260$ nm (1 $A_{260} \approx 20$ pmol for human ribosomes) using a BioPhotometer® (*Eppendorf*). Appropriate sample sizes were taken throughout the purification procedure to monitor purification efficiency of the individual steps via SDS-PAGE and Western blot analyses.

Truncated hCMV-RNCs without a stop codon in the A-site were prepared accordingly as control.

Analytical Sucrose Gradient

To analyze the mono- and polysome fractions in the RNC preparation, the eluate of the TALON® Metal Affinity Resin (*Clontech*) was directly loaded onto a 10 - 40 % sucrose gradient in Buffer D (50 mM Tris / HCl pH 7.0 / 4 °C, 100 mM KOAc, 6 mM Mg(OAc)₂, 1 mM DTT, 1/200 EDTA-free complete protease inhibitor (*Roche*), 10 - 40 % (w/v) sucrose). Gradients were centrifuged (19 h / 4 °C / 16,500 rpm / SW 40 (*Beckman Coulter*)) whereupon they were collected from top to bottom (Gradient Station ip, *BioComp*) while continuously recording the absorption profile at $\lambda = 254$ nm (Econo UV Monitor, *BIO-RAD*).

2.7 Binding Assay of Translation Termination Complexes

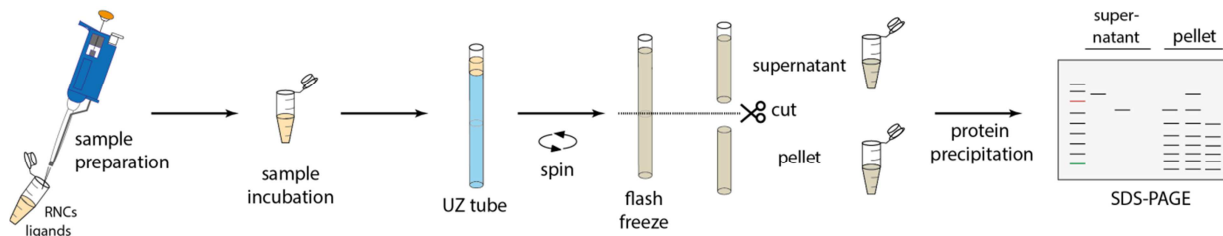


Figure 22: Schematic of the Conducted Binding Assay Studies.

For sample preparation, ribosome-nascent chain complexes (RNCs) were incubated with the respective ligands under various buffer conditions. Ultracentrifugation (UZ) resulted in separation of free ligands (supernatant) or RNC-bound ligands (pellet). The flash frozen centrifugation tubes and their contents were separated between the two fractions by cutting whereupon pellet and supernatant were separately subjected to protein precipitation (see 2.2.2). Sodium dodecyl sulfate-polyacrylamide gel electrophoresis (SDS-PAGE) revealed abundance of the ligands in the respective fractions allowing conclusions about their RNC-binding abilities.

To test ligand binding to the purified RNCs, binding assay studies were performed (see Figure 22). To this end, the ligand containing input was centrifuged (15 min / 4 °C / 14,000 rpm / 5417R (*Eppendorf*)) after thawing to remove possible aggregates. Solely the resulting supernatant was used further. To assure similar binding conditions, compensation buffers were calculated (final buffer conditions, see Table 12) and mixed to 1 pmol RNCs and 5 - 10x molar ligand excess. Samples were incubated for 20 min at RT and for 10 min on ice in a total volume of 12.5 µL to simulate molecular crowding conditions comparable to cryo-EM grid conditions. Ultra-Clear™ tubes (4x21 mm) (*Beckman Coulter*) were filled with 550 µL sucrose cushion (750 mM sucrose in respective binding conditions) and overlaid with the sample. Centrifugation followed (3 h / 4 °C / 40,000 rpm / SW55Ti (*Beckman Coulter*)) whereupon the filled tubes were flash frozen in liquid nitrogen. Subsequent cutting of the tubes and their contents 2 cm from the bottom of each tube resulted in separated

supernatant and pellet fractions which were thawed and concentrated (see 2.2.2) individually. Analysis via SDS-PAGE and SYPRO® Orange Staining (see 2.2.3) followed.

Table 12: Final Buffer Conditions for Conducted Binding Assay Studies.

Buffer condition 1 was used for ligand binding to ribosome-nascent chain complexes (RNCs), buffer condition 2 for natively heRF1 containing RNCs.

Buffer Condition 1		Buffer Condition 2	
20 mM	HEPES pH 7.4 / 4 °C	50 mM	Tris pH 7.0 / 4 °C
100 mM	KOAC	100 mM	KOAC
2.5 mM	Mg(OAc) ₂	6 mM	Mg(OAc) ₂
2 mM	DTT	1 mM	DTT
0.25 mM	Spermidine	0.2 U/mL	Anti-RNase (<i>Ambion</i> ®)
		1/200	EDTA-free complete protease inhibitor (<i>Roche</i>)

2.8 Electron Microscopy

For structural analysis of the hitherto prepared biochemical samples, the method of electron microscopy was used. The material was applied on carbon-coated grids and either stained with uranyl acetate for negative stain EM or plunge frozen for cryo-EM. Data collection, processing and analysis lead to the final reconstruction (see Figure 23).

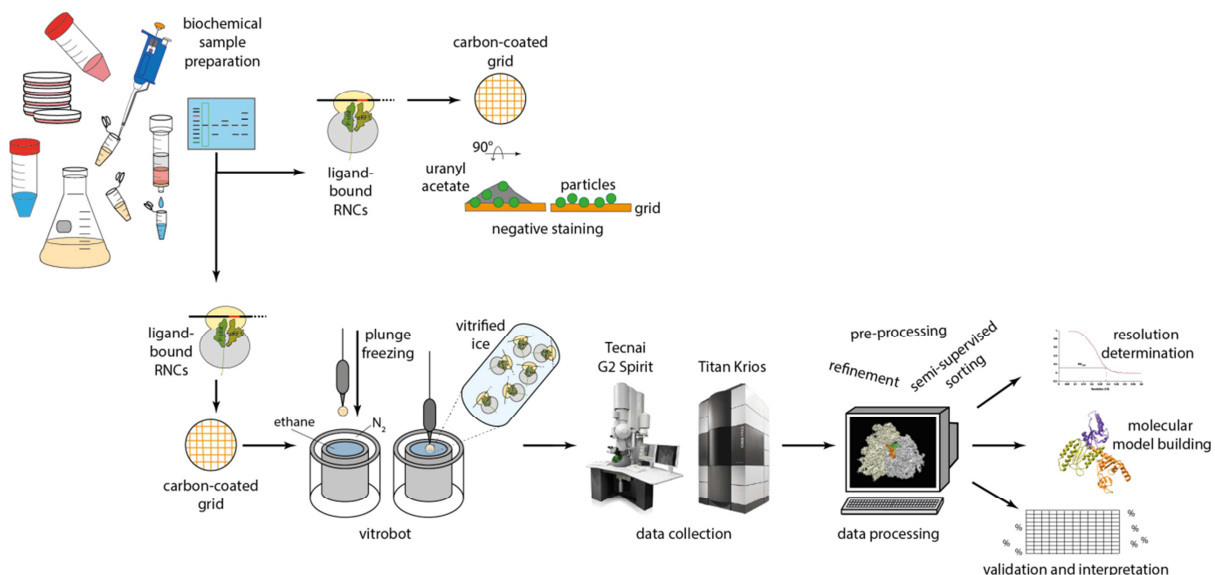


Figure 23: Schematic from the Biochemical Sample Preparation to the Final Cryo-Electron Microscopy-based Molecular Model.

Individually prepared ligands and ribosome-nascent chain complexes (RNCs) were mixed for sample preparation. Subsequently, sample condition and particle density were screened via negative stain electron microscopy (EM). Here, the sample was applied on a carbon-coated grid and stained with uranyl acetate. Ideal conditions were chosen for subsequent cryo-EM sample preparation where the sample-containing carbon-coated grid was vitrified in liquid ethane using a vitrobot. Data collection for low- or high-resolution data was performed with a Tecnai G2 Spirit (Figure from FEI Company) or a Titan Krios (Figure from FEI Company), respectively. Data processing resulted in the final cryo-EM volume which could be used for molecular model building and interpretation.

2.8.1 Negative Stain Electron Microscopy Sample Preparation and Data Analysis

Potential samples for cryo-EM were pre-checked for particle condition and density on negative stain grids (see Figure 23). To this end, the holey carbon-supported grid was glow discharged in a plasma cleaner (Basic Plasma Cleaner, *Harrick Plasma*) at 2.2×10^{-1} torr for 30 sec to ionize the hydrophobic carbon film. Then, the pre-incubated (20 min at RT) sample (3.5 μ L total volume of RNCs with or without 5 - 10x molar ligand excess) was applied to the grid. Different concentrations were tested for each sample whereof the best and final are listed in Table 13. It was incubated at RT for 45 sec before it was washed with 5 - 6 drops of H₂O and stained with 3.5 μ L 2 % (w/v) uranyl acetate (*Ted Pella, Inc.*) which was immediately blotted off and substituted by fresh 3.5 μ L 2 % (w/v) uranyl acetate. Incubation was performed for 15 sec and residual staining was blotted off whereupon the grid dried for at least 5 min at RT. Negative staining grids were monitored with a 100 kV Morgagni electron microscope (*FEI Company*).

2.8.2 Cryo-Electron Microscopy Sample Preparation

The in Table 13 summarized samples were applied on 2 nm pre-coated R3/3 holey carbon supported grids (*Quantifoil*), vitrified in liquid ethane using a Vitrobot Mark IV (*FEI Company*) (see Figure 23) (Grassucci *et al.*, 2007; Wagenknecht *et al.*, 1988) by Charlotte Ungewickell and Susanne Rieder and stored in liquid nitrogen until further usage.

Table 13: Final Ribosome-nascent Chain Complex and Ligand Concentrations in the Cryo-Electron Microscopy Samples.

Detailed buffer conditions are provided in Table 12.

Dataset	Ribosome-Nascent Chain Complex Concentration	Molar Ligand Excess	Buffer
heRF1	5 A ₂₆₀ /mL (0.10 pmol/ μ L)	5x excess	Condition 1
heRF1 + hABCE1	4 A ₂₆₀ /mL (0.08 pmol/ μ L)	5x excess	Condition 1
heRF1 + hABCE1	5 A ₂₆₀ /mL (0.10 pmol/ μ L)	10x excess	Condition 1
heRF1:Δ(1-138)heRF3a	6 A ₂₆₀ /mL (0.12 pmol/ μ L)	5x excess	Condition 1
Natively heRF1-containing	5 A ₂₆₀ /mL (0.10 pmol/ μ L)	None	Condition 2

2.8.3 Cryo-Electron Microscopy Data Collection

Tecnai G2 Spirit (*FEI Company*)

For low-resolution reconstructions, data was collected on a Tecnai G2 Spirit TEM (*FEI Company*) at 120 kV and a calibrated magnification which resulted in a pixel size of 3.17 Å on the object scale. Data was provided with different defocus values between 0.85 μ m and 7.5 μ m and recorded on the Eagle 2K CCD camera (2,048x2,048 pixel, 30x30 μ m) (*FEI Company*). Data collection was performed by Charlotte Ungewickell and Susanne Rieder.

Titan Krios (*FEI Company*)

For high-resolution reconstructions, data was collected on the in-hose Titan Krios TEM (*FEI Company*) equipped with a Falcon II direct electron detection device (*FEI Company*). The acceleration voltage amounted to 300 kV and the magnification settings resulted in a pixel size of 1.062 Å on the object scale. The dataset was provided with the semi-automatic software EPU (*FEI Company*) in a series of seven frames (numbered 0 - 6) with a dose of 5 e⁻/Å² per frame for frames 0 - 3 and 10 e⁻/Å² per frame for frames 4 - 6. Data collection was performed by Dr. Otto Berninghausen.

For the final reconstruction, frames 3 - 6 were excluded for limitation of the effective dose. The three remaining frames were aligned and summed up using the Motion Correction Software MotionCorr (Li *et al.*, 2013).

2.8.4 Cryo-Electron Microscopy Data Analysis of Tecnai G2 Spirit (*FEI Company*) Derived Datasets

Since data analysis is less complicated for data collected on the Tecnai G2 Spirit (*FEI Company*) than on the Titan Krios (*FEI Company*), detailed description for the processing procedure is given only for the latter (see 2.8.5). Dataset specific particle distribution during sorting for data which was collected with the Tecnai G2 Spirit is provided in Table 14. Sorting for non-ribosomal particles (edge-sorting) was followed by sorting against an intrinsically derived structure obtained during initial refinement. Lastly, focused sorting on the ribosomal A-site followed. The same sorting scheme was applied to each dataset to ensure comparability. Yet, for sorting of the natively heRF1 containing RNCs additional sorting (*) was done to assure quantitative heRF1-binding to the ribosome in this case.

Table 14: Particle Distribution of Tecnai G2 Spirit (*FEI Company*) Derived Datasets.

Particle numbers which were sorted out at each step are shown. Corresponding percentage is given in parenthesis.

Dataset	Starting Particles	Particles (Edge Sorting)	Particles (Self-sorting)	Particles (Focused Sorting)	Final Particles	Final Resolution
heRF1 (10x) + hABCE1 (10x)	34,648 (100 %)	3,758 (11 %)	16,101 (46 %)	7,125 (21 %)	7,664 (22 %)	20.9 Å
heRF1 (5x)	14,067 (100 %)	3,978 (28 %)	5,907 (42 %)	1,553 (11 %)	2,629 (19 %)	22.3 Å
heRF1 (5x) + hABCE1 (5x)	31,498 (100 %)	4,214 (13 %)	12,054 (38 %)	6,674 (21 %)	8,556 (27 %)	21.0 Å
heRF1: Δ(1-138)heRF3a complex (5x)	26,534 (100 %)	5,583 (21 %)	2,738 (10 %)	8,330 (31 %)	heRF1:Δ(1-138) heRF3a complex: 9,883 (37 %) heRF1: 4,837 (18 %)	21.0 Å 25.2 Å
Natively heRF1 containing	19,524 (100 %)	4,767 (24 %)	5,734 (29 %)	6,181 (32 %)	5,187 (26 %) *Sorted further: 2,842 (14 %)	21.9 Å *Sorted further: 22.5 Å

2.8.5 Cryo-Electron Microscopy Data Analysis of a Titan Krios (*FEI Company*) Derived Dataset

Pre-processing

For System for Processing Image Data from Electron microscopy and Related fields (SPIDER)-based processing (Frank *et al.*, 1996), microscope- and dataset-specific parameters are required which have to be adjusted and provided in a params file (see Table 15) prior to processing.

Table 15: Parameters Used for Titan Krios Derived Data Processing in this Study.

Number	Parameter	Value
1	Zip flag 0: Do not unzip, 1: Needs to be unzipped	0.0000
2	File format 0: SPIDER, 1: HiScan tif, 2: Perkin elmer, 3: ZI scanner	1.0000
3	Picture dimensions (width) [pixel]	12,288
4	Picture dimensions (height) [pixel]	12,288
5	Pixel size [Å]	1.062
6	Electron energy [kV]	300
7	Spherical aberration [mm]	2.7
8	Source size [Å ⁻¹]	5.00000x10 ⁻³
9	Defocus spread [Å]	0.0000
10	Astigmatism [Å]	0.0000
11	Azimuth [degree]	0.0000
12	Relative amplitude contrast	0.0700
13	Gaussian envelope half width [Å ⁻¹]	10,000
14	--- (reserved)	0.0000
15	--- (reserved)	0.0000
16	--- (reserved)	0.0000
17	Box size [pixel]	420.00
18	Particle diameter [pixel]	330.00
19	Interpolation, decimation factor	3.000/2.000/1.000
20	Actual box size (in decimation)	140/210/420

Data output of the Motion Correction Software (Li *et al.*, 2013) was set to be in .mrc format. Import and conversion to SPIDER format by the command **CP FROM MRC** (Copy from MRC File to SPIDER File) followed. A list, which contains all micrographs in consecutive order (micsuse), was created which is adjusted throughout pre-processing to exclude non-adequate micrographs. The command **TF ED** (Transfer Function - Estimate Defocus from Image Power Spectrum) was used to calculate the contrast transfer functions (CTFs) and to retrieve the correct defocus values. Power spectra, which show the micrograph intensity as square of the amplitude plotted against the special frequency, were created using the command **PW** (Power Spectrum - Amplitudes of Fourier Transform).

Detailed visual evaluation based on power spectrum and micrograph quality using the JWEB software (Shaikh *et al.*, 2008) was performed for each micrograph. Micrographs with power spectra depicting poor information content, drift or astigmatism were excluded. Micrographs showing aggregated or burnt particles, bad ice quality, blurry images or other impurities were also discarded.

Automated particle picking was performed using the program SIGNATURE based on a two-dimensional (2D) template matching method (Chen and Grigorieff, 2007): Particle correlations to 2D-projections from a previously calculated human 80S reference were computed using optimized parameters (pixel size: 4x1.062, box size: 420 pixel (px), particle size: 180 px, particle distance: 15 px, margin: 80 px and local density correlation function (LCF): 0.41) for particle finding. Particle SIGNATURE coordinates were converted to SPIDER coordinates (from center of particle to top left of the window), normalized by providing an internal noise-file, contrast inverted and windowed out using the command **WI** (Window Image/Volume).

For computational advantage, grouping of micrographs according to similar defoci was performed. Such grouping additionally enhances the SNR when creating 3D volumes and allows for facilitated application of the CTF-correction. In this calculation, 283 defocus groups with up to 900 particles each were introduced, omitting micrographs which were recorded at lower defocus than 1.0 μm or higher defocus than 2.7 μm to ensure a defocus spread smaller than 150 nm in each group. Micrographs which belonged to power spectra with cross-correlation values to themselves (when turning the power spectra by 90°) lower than 0.6 were additionally excluded.

Henceforth, data processing and single particle analysis was done using the SPIDER software package. The initial alignment was done on 3-fold decimated data for 255,253 particles. The command **AP MQ** (Alignment - Multi-reference, Shift and Rotation) allowed a cross-correlation based projection matching technique to determine particle orientation: A previously calculated human 80S ribosome was filtered with the **FQ NP** (Filter Quick, no Pad) command (Butterworth low-pass, lower and upper limiting frequencies corresponding to 19.5 Å and 20 Å) and used as initial reference whereof 83 2D projections were generated by the command **PJ 3Q** (Project - 3D Volume Using Eulerian Angles, Trilinear Interpolation) resulting in an angular accuracy of 15°. For re-processing of the dataset, the final volume of the first calculation was filtered accordingly and similarly provided as initial reference. Each single particle was then matched to the best fitting projection leading to the assignment of an individual cross-correlation, translational shifts (x- and y-shifts) and three Eulerian angles to each particle.

Refinement and Semi-supervised Sorting

To improve the resolution of the initially obtained volume, the iterative process of refinement was applied to gradually increase accuracy of the assigned Eulerian angles, the x- and the y-shifts. For each defocus group, particles were refined in parallel: They were aligned (commands: **AP MD** (Alignment - Multi-reference, Rotation) (no shifts, 360° search range, with mirror check) and **AP MQ** (Alignment - Multi-reference, Shift and Rotation) (1 px shift, with mirror check)) to the output volume of the previous round (for the first round, the same reference was used as for the initial alignment) whilst the angular search range was gradually narrowed with proceeding rounds. Back projection (combination of 2D particles to reconstruct the 3D structure) was performed in Fourier space (bp32f algorithm) to obtain sub-volumes for each defocus group. Such sub-volumes were weighted according to the number of particles in the group and subjected to CTF correction (usage of a Wiener filter which squares the amplitudes and flips the phases) via the **TF CTS** (Transfer function - CTF correction 2D and 3D) command before being combined to the final output volume of the round (and input volume for the next round). For this reconstruction, the reference input was never subjected to a Butterworth low-pass filter higher than the frequencies which correspond to 8 Å.

To generate a high-resolution structure, the dataset was sorted from a heterogeneous to a homogenous population. Again, a cross-correlation based method was used, however, here projection matching was competitive: Two reference volumes were offered to which each particle was aligned to, resulting in the calculation of two correlation values. To achieve successful sorting, the particle was assigned to the particle class of the reference where its alignment resulted in a higher cross-correlation. Both resulting particle subsets were back-projected individually as described above and each calculated volume was used as input for the subsequent round of sorting. This was again performed iteratively, until the amount of particles remained stable in each class. Generally spoken, during sorting increasing structural details from global to local differences are considered

starting with ‘edge sorting’ to remove fractional and non-ribosomal particles or noise (here: 35,062 particles; 14.3 %).

For this dataset, after removing noisy particles, particles comprising a significantly lower cross-correlation than other particles of the same defocus group were discarded from the dataset (64,659 particles, 26.4 %) leading to resolution improvement.

Further sorting with a reference from a very early refinement round (which still contained rough features) resulted in the removal of empty 80S and CrPV IGR IRES containing 80S ribosomes (50,952 particles, 20.8 %). To sort for small but critical differences, ‘focused sorting’ was performed, where only a restricted area (defined by a provided mask) was used for the calculation of the cross-correlation and therefore solely determined to which of the two classes the particle was assigned to, leading to removal of further 61,415 particles (25.0 %). The final volume contained 33,165 particles (13.5 %).

Resolution Determination

Two semi-independent sub-volumes (each calculated from either all evenly or oddly numbered particles) were created every round and used for Fourier shell correlation (FSC)-based resolution determination with the **RF 3** (Phase Residual and Fourier Shell Correlation, 3D) command.

Since, as described above, throughout the refinement and sorting process frequencies higher than corresponding to 8 Å were omitted to prevent potential overfitting, the resolution was estimated by the FSC = 0.143 criterion according to Scheres *et al.* (Scheres and Chen, 2012). Obeying this criterion, the average resolution was determined to 3.8 Å with a local resolution extending to 3.6 Å in the core of the ribosome. The local resolution was determined using ResMap (Kucukelbir *et al.*, 2014).

2.8.6 Molecular Model Building, Validation and Interpretation

The heRF1-bound RNC complex was B-factor sharpened using the program EM-BFACTOR (Fernández *et al.*, 2008). For interpretation of the acquired electron density, molecular models were initially rigid body fitted with UCSF Chimera (Pettersen *et al.*, 2004) and, where appropriate, manually adjusted according to the electron density with Coot (Emsley and Cowtan, 2004). Ribosomal RNA and proteins, which contacted heRF1 or comprised the exit tunnel wall and the PTC, were based on the cryo-EM reconstruction of the human 80S POST state by Behrmann *et al.* (Behrmann *et al.*, 2015) (PDB-code: 5AJ0). The human eRF3-bound crystal structure of the eRF1 protein (PDB-code: 3E1Y) by Cheng *et al.* (Cheng *et al.*, 2009) was taken as groundwork for its modeling according to the EM-density. The missing heRF1 Mini Domain, as well as the C-terminal tail residues 421 – 437, was incorporated from the NMR solution structure of the heRF1 C-terminal domain (PDB-code: 2KTV) by Mantsyzov *et al.* (Mantsyzov *et al.*, 2010).

Modeling was followed by refinement using Coot (Emsley and Cowtan, 2004) and the real-space refine tool of the PHENIX software package (Adams *et al.*, 2010) with the default settings of the PHENIX command ‘phenix.real_space_refine model.pdb map ccp4’. To validate the fit of the refined structure to the experimentally acquired data, cross-correlation values between the heRF1 cryo-EM density and a density molmap (width proportional to the resolution and amplitude proportional to the atomic number) generated from the refined molecular heRF1 model or from the initial eRF1 crystal structure were calculated using UCSF Chimera (Pettersen *et al.*, 2004). The cross-correlation values increased when comparing the initial model (domains of the human eRF1 crystal structure

were docked into the isolated density individually) with the refined model: 0.73 to 0.76 for the N domain; 0.66 to 0.68 for the M domain, 0.39 to 0.70 for the C domain.

2.8.7 Figure Preparation

Figures depicting electron densities or molecular models were produced with UCSF Chimera (Pettersen *et al.*, 2004).

2.8.8 Cryo-electron Microscopy Data Processing Software

All software used for cryo-EM data processing and evaluation is summarized in Table 16.

Table 16: Software Used for Cryo-electron Microscopy Data Processing.

Software	Reference
Coot	Emsley and Cowtan, 2004
EM-BFACTOR	Fernández <i>et al.</i> , 2008
Gnuplot	Janert, 2009
JWEB	Shaikh <i>et al.</i> , 2008
MotionCorr	Li <i>et al.</i> , 2013
PHENIX	Adams <i>et al.</i> , 2010
ResMap	Kucukelbir <i>et al.</i> , 2014
SIGNATURE	Chen and Grigorieff, 2007
SPIDER	Frank <i>et al.</i> , 1996
UCSF Chimera	Pettersen <i>et al.</i> , 2004

3. Results

One of the most fundamental questions which has remained without answer for the eukaryotic translation cycle concerns the process of translation termination. Besides tremendous efforts and a great variety of biochemical and structural studies, the molecular mechanism of how stop codon decoding is performed by only one single factor (eRF1) could not have been elucidated so far. Hence, to investigate how eRF1 realizes stop codon decoding, particularly in human translation termination, this study comprises the establishment of a human *in vitro* translation system. Further purification of hCMV programmed human ribosomes for *in vitro* reconstitution of versatile termination complexes was the starting point for high-resolution structural studies solving the long-standing question of eukaryotic stop codon decoding and beyond.

3.1 Obtaining Human Cytomegalovirus gp48/UL4 uORF2 (hCMV)-stalled Ribosome-nascent Chain Complexes

3.1.1 Establishment of a Human *in vitro* Translation Extract

For the generation of stalled human ribosomes, it was set out to establish a human *in vitro* translation extract based on HeLa S3 suspension cells. Prepared extracts were supplemented with *in vitro* transcribed target mRNA upon which its translation was performed. Efficiency was optimized directly with the hCMV-stalling construct rather than a read-out optimized construct such as GFP or luciferase since the latter are both aiming at high translation speed and protein production. The chosen approach ensures ideal conditions for hCMV-mediated translational stalling, which only requires one round of initiation per mRNA and subsequent stabilization of the translation intermediates, rather than high efficiency of protein production for which in contrast multiple rounds of initiation would be beneficial.

mRNA *in vitro* transcription has always been performed separately from translation to introduce an additional layer of control. Solely sequenced and linearized plasmids were used as template for transcription to ensure accuracy on DNA-level. The final template comprised a 5' CrPV IGR IRES sequence for translation initiation. This differs from all other recommended modes of translation initiation in commercially available eukaryotic translation systems. For instance, for the RRL System (*Promega*) a 5' capped or uncapped mRNA is suggested as template. However, such mRNAs could not be successfully translated in the here established human system (see Figure 24A). In the commercially available human system (*Thermo Scientific*) the 5' EMCV IRES sequence is utilized, however, requires supplementation of accessory protein factors (like K3L or hGADD34) for functional initiation (Mikami *et al.*, 2006). During the optimization of the human translation system all efforts towards purification and effective supplementation of these protein factors did not result in sufficient translation why the EMCV IRES sequence was substituted for the CrPV IGR IRES sequence due to its independence of any cellular initiation factors. A further advantage of using the CrPV IGR IRES for translation initiation is the simultaneous incapability to translate canonical mRNAs in the extract why cellular resources like ribosomes and aminoacyl-tRNAs remain available for specific target translation. Accordingly, S7 nuclease treatment of the extract to eliminate cellular mRNAs did not affect adjacent translation efficiency why this step was omitted in the extract preparation protocol.

Different linker sequences between the CrPV IGR IRES 3' terminal CCT codon and the ATG start codon resulted in various stalling efficiencies (see Figure 24B) whereof the most active was used henceforth.

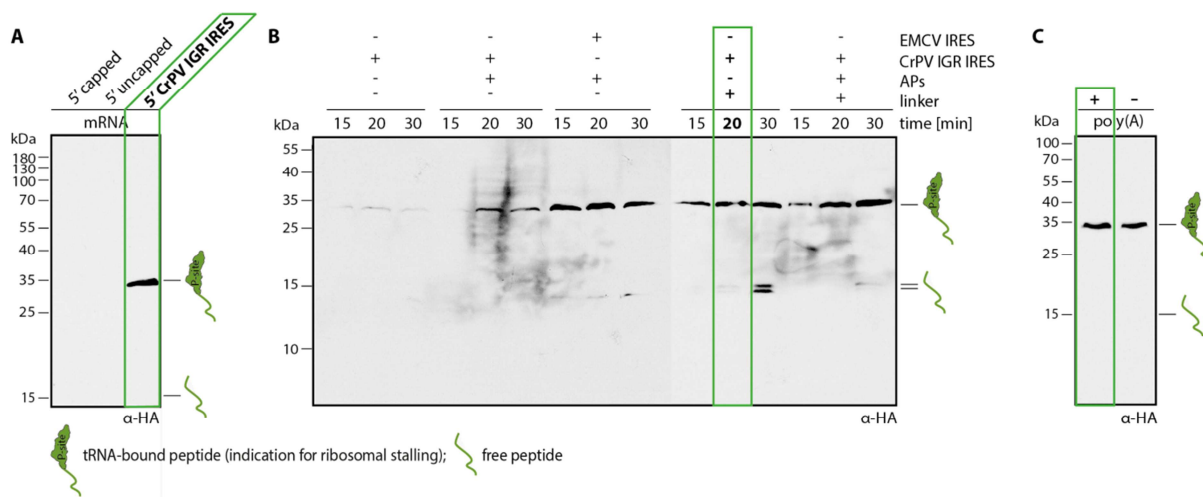


Figure 24: Optimization of the mRNA Sequence for Translation in the Human *in vitro* System.

Anti-hemagglutinin (α -HA) antibody detection of the target translation product. **(A)** Translation and stalling efficiency of various 5' mRNA ends: 5' capped, 5' uncapped or 5' cricket paralysis virus (CrPV) intergenic region (IGR) Internal Ribosome Entry Site (IRES) containing mRNAs were tested. The most efficient 5' end is highlighted in green. **(B)** Translation efficiency of the 5' CrPV IGR IRES mRNA with and without the most active linker sequence to the target open reading frame and of the 5' encephalomyocarditis virus (EMCV) IRES mRNA were tested. Further, each mRNA was translated in the presence of the accessory proteins (APs) from the *in vitro* translation system by *Thermo Scientific*. The combination used further is highlighted in green. **(C)** Necessity of the 3' poly(A) tail for CrPV IGR IRES initiated hCMV-stalling was tested. The condition used further is highlighted in green.

Moreover, the DNA template contained a (His)₆-tag encoding sequence for RNC purification and a human influenza hemagglutinin (HA)-tag (aa 98 - 106) for Western blot detection of either the translated free peptide or the peptidyl-tRNA. Tag-specific antibodies revealed a double band at \sim 15 kDa (theoretically: 14.8 kDa) corresponding to the free peptide only under suboptimal conditions. The vast majority of hCMV-stalled ribosomes remained stable under the extract conditions represented by a signal at \sim 36 kDa since the stalling peptide is still bound to the P-site tRNA causing the \sim 19 kDa shift in its SDS-PAGE running behavior. Further encoding sequence, the DP75 DPAPB (Beckmann *et al.*, 2001) sequence, which has been successfully translated before in home-made *D. melanogaster* extracts, was used. The hCMV sequence was utilized for species-accurate stalling meeting the requirement for a stop codon in the ribosomal DC. Finally, at the 3' end a 26 nt poly(A) tail was encoded, which is not particularly necessary for the CrPV IGR IRES containing construct (see Figure 24C), however, likely increases the stability of mRNAs (Dreyfus and Régnier, 2002; Eckmann *et al.*, 2010) and ensures closer resemblance of the canonical termination state in the *in vitro* reconstituted complexes.

Translational stalling was tested at 30 °C (based on Mikami *et al.*, 2010), 33 °C (based on Brödel *et al.*, 2013) and 37 °C whereof 30 °C was most efficient in all tested extracts. Particularly the ideal time interval of translation, the KOAc concentration and the Mg(OAc)₂ concentration varied for each extract and were optimized anew for each prepared batch (see Figure 25).

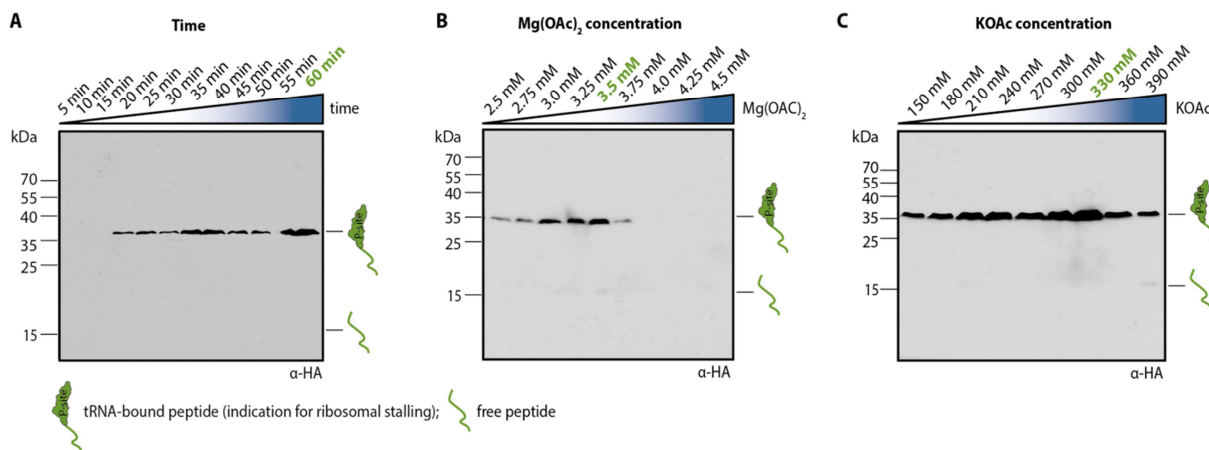


Figure 25: Example of Stalling Optimization in the Human Translation Extract.

Each newly prepared extract was optimized for (A) translation time (B) magnesium acetate (Mg(OAc)_2) and (C) potassium acetate (KOAc) concentration using Western blotting and the anti-hemagglutinin (α -HA) antibody for detection of tRNA-bound human hCMV-peptide or free hCMV-peptide. Optimal conditions varied for each extract. Best conditions for this extract example are highlighted in green.

Figures were modified from Matheisl *et al.* (Matheisl *et al.*, 2015).

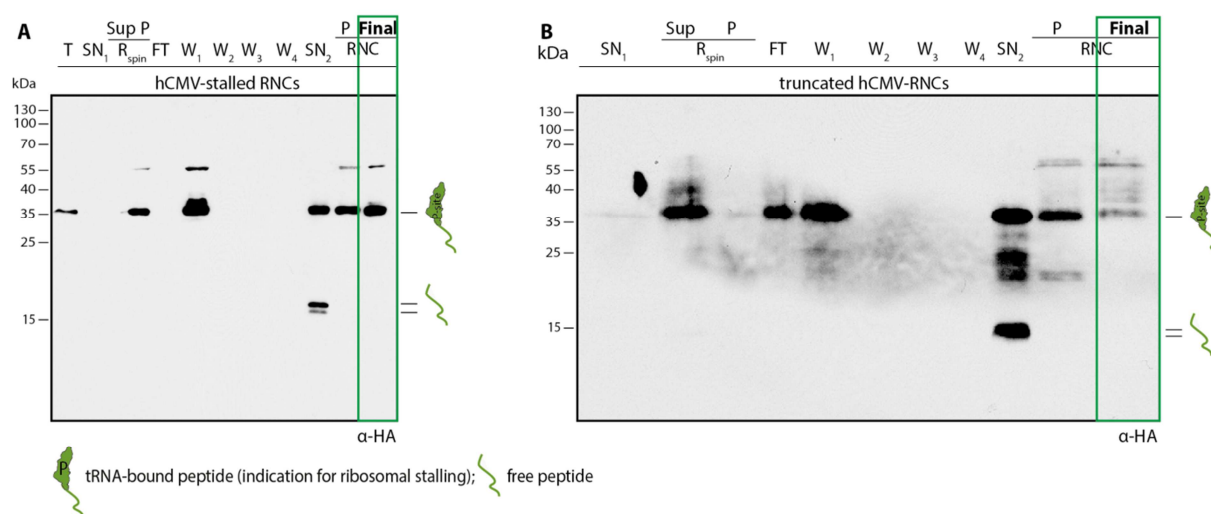
3.1.2 Purification of Homogenously Stalled Ribosome-nascent Chain Complexes

The RNC purification procedure had to be adjusted from published protocols (Beckmann *et al.*, 2001; Bhushan *et al.*, 2011; Halic *et al.*, 2004; Seidelt *et al.*, 2009) in several aspects: The resuspension of ribosomal pellets after concentration via ultra-centrifugation proved rather protracted why it was partially performed under shaking conditions. Additionally, due to the high concentrations of the extracts themselves ($A_{260} \sim 180 - 250$), cellular parts were carried along during the RNC preparation which had to be separated repeatedly via short centrifugation steps for complete removal. Furthermore, prolonged washing steps and higher imidazole concentration for (His)₆-tagged RNC elution resulted in increased purity and greater yields, respectively. As mentioned above (see 3.1.1), successful stalling can be visualized via antibody detection subsequent to Western blotting by a shifted peptide-signal. In the final RNC sample (see Figure 26A, lane 'Final') a homogenously stalled RNC population and no free hCMV-peptide was evident.

One limitation for obtaining great quantities of RNCs was the volume of HeLa S3 suspension cells which could only be grown up to 7.0 L to a maximum density of 6×10^5 cells/mL without aggregation or sedimentation in the utilized set-up. Volume restrictions during extract preparation itself were only present by the cell disruption vessel (30 mL), however, can merely be encountered by harvesting a 15 L HeLa S3 cell culture. After *in vitro* translation, ribosomes were concentrated via centrifugation through a sucrose cushion. Hereafter, measuring the absorption at $\lambda = 260$ nm (A_{260}) represented a good estimation of the ribosome quantity in the extract: On average ($n = 3$) 118 A_{260} /preparation. Measuring the A_{260} for purified RNCs in the final sample an average ($n = 3$) of 1.34 A_{260} /preparation remained. This corresponds to 0.98 % of all ribosomes present during the initial *in vitro* translation reaction. The bottle neck for high yields in RNC preparations therefore rather was the stalling efficiency likely due to challenged initiation of translation and loss during RNC purification. Examples for preparation efficiencies are given in Table 17.

Table 17: Examples for Efficiencies of Human *in vitro* Translation Extract Preparations and Ribosome-nascent Chain Complex Purifications.

Starting Culture Volume	Starting Cell Amount	Final Extract Volume	Cells/mL Extract	RNCs/mL Extract	RNCs/L Cell Culture	Extract Absorption Values
5.6 L	2.4x10 ⁹	5,400 μ L	4.44x10 ⁸	Not applicable	Not applicable	$A_{260} = 228$ $A_{280} = 162$
5.2 L	2.9x10 ⁹	5,935 μ L	4.89x10 ⁸	Not applicable	Not applicable	$A_{260} = 251$ $A_{280} = 172$
7.0 L	1.9x10 ⁹	7,600 μ L	2.50x10 ⁸	TAA(A) stop codon: 33.5 pmol	36.4 nmol	$A_{260} = 177$ $A_{280} = 123$
4.7 L	1.7x10 ⁹	5,140 μ L	3.31x10 ⁸	TAA(A) stop codon: 25.65 pmol	28.1 nmol	$A_{260} = 189$ $A_{280} = 140$
6.0 L	2.0x10 ⁹	4,930 μ L	4.06x10 ⁸	TAA(G) stop codon: 51.3 pmol/mL TAG(A) stop codon: 58.8 pmol	42.2 nmol 48.3 nmol	$A_{260} = 200$ $A_{280} = 140$

**Figure 26: Purification of hCMV-stalled and Truncated hCMV-Ribosome-nascent Chain Complexes.**

Anti-hemagglutinin (α -HA) antibody detection of samples taken throughout the ribosome-nascent chain complex (RNC) purification procedures of (A) human hCMV-stalled RNCs and (B) truncated (trunc) hCMV-RNCs. The free peptide has an apparent mass of ~ 15 kilodalton (kDa) and appears as double band. The peptidyl-tRNA-bound peptide, an indicator for stalled RNCs, of ~ 35 kDa. A band of unknown identity is visible at ~ 55 kDa. Note that the trunc hCMV-RNCs are less stable resulting in a greater variety of bands in the supernatant 2 ('SN2') fraction and less yield in the final RNC ('Final') fraction. The final fractions are highlighted in green for both preparations.

As a result of the limited yields, sucrose gradient purification was omitted in the RNC purification procedure (like usually done for stalled 70S ribosome samples for cryo-EM (Arenz *et al.*, 2014a, 2014b; Bischoff *et al.*, 2014; Sohmen *et al.*, 2015)). However, to assess the fraction of polysomes, an analytical gradient purification (see Figure 27A) was performed whereof the absorption profile at $\lambda = 254$ nm was recorded (see Figure 27B). The vast majority of the absorption signal originated from ribosomes that were singly bound to the mRNA and were evident as monosome 80S peak (shaded in

gray). The area below the absorption curve for ribosomal polysomes was comparably small and was estimated to be < 10 %.

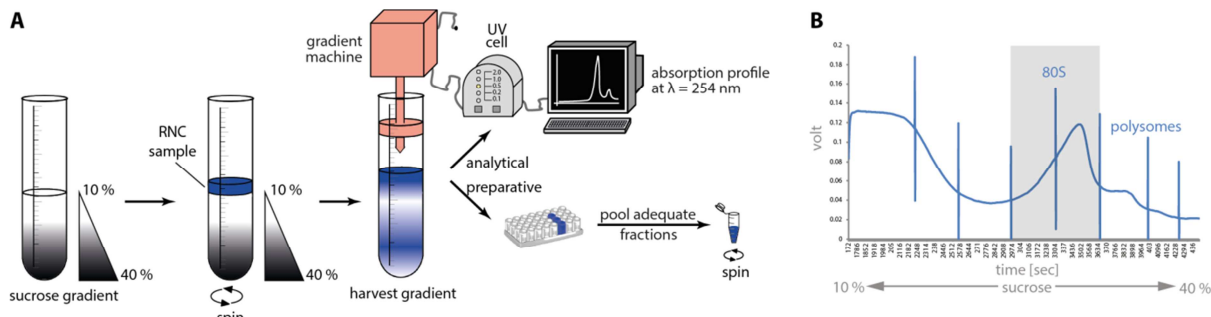


Figure 27: Analytical Sucrose Gradient of Affinity-Purified Ribosome-nascent Chain Complexes.

The polysome-state of the purified ribosome-nascent chain complexes (RNCs) was analyzed via an analytical sucrose gradient from 10 - 40 %. **(A)** Affinity purified RNCs (blue) were layered on top of the gradient (gray) whereupon it was subjected to ultracentrifugation. Subsequent collection of the gradient from top to bottom while recording the absorption at $\lambda = 254$ nm allowed identification of **(B)** monosome 80S (gray-shaded) and polysome fractions in the sample.

To ensure specific assembly of the termination-involved complexes, control RNCs were prepared without harboring a stop codon in the ribosomal A-site. Since the stop codon is a prerequisite for hCMV-mediated peptide stalling (also see Figure 47) (Degnini *et al.*, 1993), it could not be simply abolished by mutation into a sense codon. Therefore, the control construct was truncated after the Pro22 codon (trunc hCMV) which also lead to successful ribosomal stalling, however, less stably as evident in the supernatant 2 (see Figure 26B, lane 'SN2') fraction where increased amounts of unbound peptide were present.

In the wealth of existent mutational studies contradictory conclusions about interactions between eRF1 and the mRNA stop codon have been postulated. Particularly interesting is the varying effect of eRF1 mutations on decoding efficiencies of the three abundant stop codons UAA, UAG and UGA. Also, the mRNA nucleotide at position 4 is known to be influential on termination efficiency which might explain the discrepancy in mutational studies. To investigate interactions of eRF1 while decoding each of the three stop codons and ascertain the role of the nucleotide at position 4, RNCs containing either a UAA(A), UAG(A), UGA(A) or UAA(G) stop codon were prepared similarly.

3.2 *In vitro* Reconstitution of Ribosome Complexes Involved in Translation Termination

3.2.1 Purification of Protein Components

For *in vitro* reconstitution of termination-involved complexes, the corresponding human protein factors were purified. Particularly for the purification of the ternary heRF1:heRF3a:GMPPCP complex several strategies were exploited simultaneously to ensure great yield combined with high purity of the resulting samples (also see Figure 18).

Human eRF1

heRF1 was designed with an N-terminal 3C-protease-cleavable (His)₈-tag and successfully expressed and purified from *E. coli* cells. Extensive high salt washes combined with elution of the protein via 3C-protease cleavage of the (His)₈-tag resulted in great yields (see Table 21) and high purity which is

evident from one single band in the elution fraction after SDS-PAGE analysis (see Figure 28A, lane 'E_{3C}'). Purified heRF1 was used for *in vitro* hydroxylation studies and as negative control of the hydroxylation status of the heRF1 Lys63 side-chain C4 in mass spectrometry analyses (see next section).

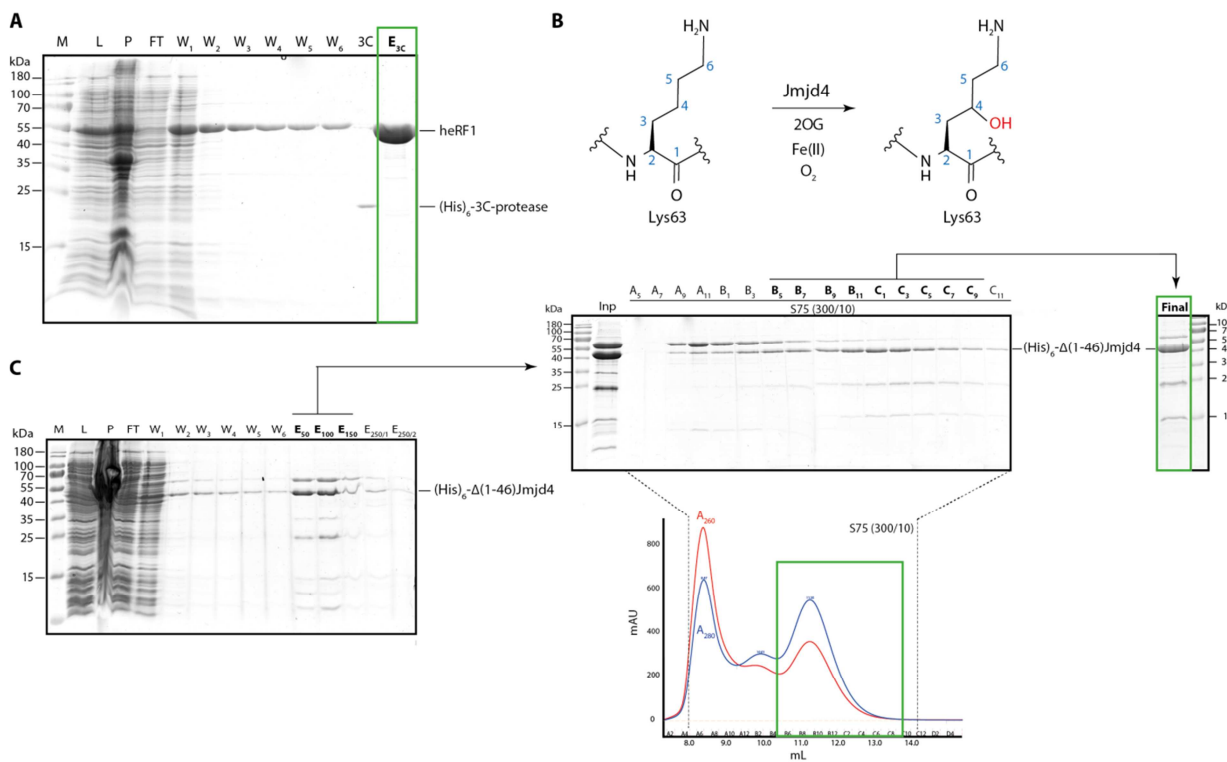


Figure 28: Purification of the heRF1 and the (His)₆-Δ(1-46)Jmjd4 Proteins from *Escherichia coli* Cells.

(A) Sodium dodecyl sulfate-polyacrylamide gel electrophoresis (SDS-PAGE) of samples taken throughout the heRF1 purification procedure. The final 3C-protease cleaved elution sample ('E_{3C}') is highlighted in green revealing high yield of pure heRF1. Also, a sample of the hexahistidine ((His)₆)-tagged 3C-protease was applied. **(B)** Hydroxylation reaction of the heRF1 Lys63 side-chain C4 catalyzed by the oxygenase Jmjd4. Necessary co-factors are 2-oxoglutarate (2OG), Fe(II) and oxygen (O₂). **(C)** SDS-PAGE of samples taken throughout the (His)₆-tagged Δ(1-46)Jmjd4 purification procedure. Subsequent to affinity purification appropriate elutions ('E₅₀', 'E₁₀₀' and 'E₁₅₀') were subjected to size exclusion chromatography on an S75 (300/10) column. Samples 'B₅' - 'C₉' were pooled and concentrated. The final sample ('Final') is highlighted in green revealing high yield of (His)₆-Δ(1-46)Jmjd4 only containing few impurities or degradation products.

Human eRF1 Hydroxylation

Feng *et al.* (Feng *et al.*, 2014) demonstrated the importance of the eRF1 Lys63 side-chain C4 hydroxylation of the TAS-NIKS motif (see Figure 28B) in termination efficiency. Since Lys63 is known to be a key-player in termination (Chavatte *et al.*, 2002), this PTM was assigned great importance. For its *in vitro* hydroxylation, purified heRF1 was incubated with the 2-oxoglutarate and Fe(II)-dependent oxygenase Jmjd4 which was also purified successfully in this study (see Figure 28C, lane 'Final'). Hereupon, heRF1 was analyzed via mass spectrometry to assess the efficiency of the enzymatically catalyzed reaction. The hydroxylation-status was monitored with and without quenching of the reaction with EDTA to prevent potential secondary hydroxylations to occur (see Tables 18 and 19).

In parallel, *in vivo* hydroxylation of heRF1 was anticipated by co-expression of heRF1 and Jmjd4 in *E. coli*. After similar (as to single expression of heRF1) purification and tag-cleavage, co-expressed heRF1 was likewise analyzed via mass spectrometry. A full quantitative analyses was not realized since the obtained results regarding differences in Lys63 side-chain C4 hydroxylation efficiency between the two methods were unambiguous (see Table 18). Comparison and normalization to other, via mass spectrometry analyzed peptides ((a) the FANNYKKF signal and (b) the FHTTEALTALLSDDSK signal), were made which allowed approximate percentages to be assigned for each hydroxylation method (see Table 19).

Table 18: Mass Spectrometry Results for the heRF1 Lys63 Side-chain C4 Hydroxylation Status.

heRF1	Peptide: LADEFGTASNIK*SRVN	
	Intensity of Lys63 C4 Hydroxylated	Intensity of Lys63 C4 Non-hydroxylated
<i>In vivo</i> hydroxylation	1.14x10 ⁶	-----
No hydroxylation	-----	1.44x10 ⁷
<i>In vitro</i> hydroxylation (quenched)	8.60x10 ⁵	6.93x10 ⁶
<i>In vitro</i> hydroxylation (not quenched)	5.14x10 ⁵	4.59x10 ⁶

heRF1	Peptide: MLADEFGTASNIK*	
	Intensity of Lys63 C4 Hydroxylated	Intensity of Lys63 C4 Non-hydroxylated
<i>In vivo</i> hydroxylation	2.21x10 ⁷	-----
No hydroxylation	-----	2.77x10 ⁸
<i>In vitro</i> hydroxylation (quenched)	1.71x10 ⁷	1.75x10 ⁸
<i>In vitro</i> hydroxylation (not quenched)	1.00x10 ⁷	8.18x10 ⁷

Table 19: Normalized Mass Spectrometry Results for the heRF1 Lys63 Side-chain C4 Hydroxylation Status.

heRF1	Peptide: LADEFGTASNIK*SRVN	
	Normalized Intensity of Lys63 C4 Hydroxylated	Normalized Intensity of Lys63 C4 Non-hydroxylated
<i>In vivo</i> hydroxylation	3.69x10 ⁵ (100 %)	----- (0 %)
No hydroxylation	----- (0 %)	3.15x10 ⁶ (100 %)
<i>In vitro</i> hydroxylation (quenched)	2.20x10 ⁵ (60 %)	1.77x10 ⁶ (56 %)
<i>In vitro</i> hydroxylation (not quenched)	1.95x10 ⁵ (53 %)	1.74x10 ⁶ (55 %)

n = 1, normalized with (a) the FANNYKKF signal

heRF1	Peptide: MLADEFGTASNIK*	
	Normalized Intensity of Lys63 C4 Hydroxylated	Normalized Intensity of Lys63 C4 Non-hydroxylated
<i>In vivo</i> hydroxylation	2.21x10 ⁷ (100 %)	----- (0 %)
No hydroxylation	----- (0 %)	2.77x10 ⁸ (100 %)
<i>In vitro</i> hydroxylation (quenched)	1.71x10 ⁷ (61 %)	1.75x10 ⁸ (74 %)
<i>In vitro</i> hydroxylation (not quenched)	1.00x10 ⁷ (54 %)	8.18x10 ⁷ (51 %)

n = 1, normalized with (b) the FHTTEALTALLSDDSK signal

For the *in vitro* hydroxylation method, efficiency was comparable to previously published results of ~60 % (Feng *et al.*, 2014). *In vivo* hydroxylation resulted in quantitative Lys63 hydroxylation since no corresponding peptide without Lys63 hydroxylation could be detected. To ensure specificity of the reaction, secondary hydroxylation sites on all heRF1 Lys residues were monitored whereat no hydroxylation could be detected. Due to the high efficiency, Jmjd4 was also co-expressed for *in vivo* hydroxylation in the following heRF1:heRF3a co-purification strategies.

Human $\Delta(1-138)$ eRF3a

The N-terminal 138 aa of eRF3 are known to be non-essential for ternary complex formation with GTP and eRF1 (Kushnirov *et al.*, 1988) and in this regard truncated eRF3 has been successfully used for termination studies before (des Georges *et al.*, 2014; Pisareva *et al.*, 2006; Preis *et al.*, 2014; Taylor *et al.*, 2012). Considering heRF3a full length protein purification is known to be challenging N-terminally truncated heRF3a was expressed and purified from *E. coli* cells for a start. Extensive high salt washes and specific elution due to (His)₈-tag cleavage via the attached 3C-protease cleavage site resulted in high amounts of stable protein (see Table 21) with only slight contaminations as evident after SDS-PAGE analysis (see Figure 29A, lane 'E_{3C}').

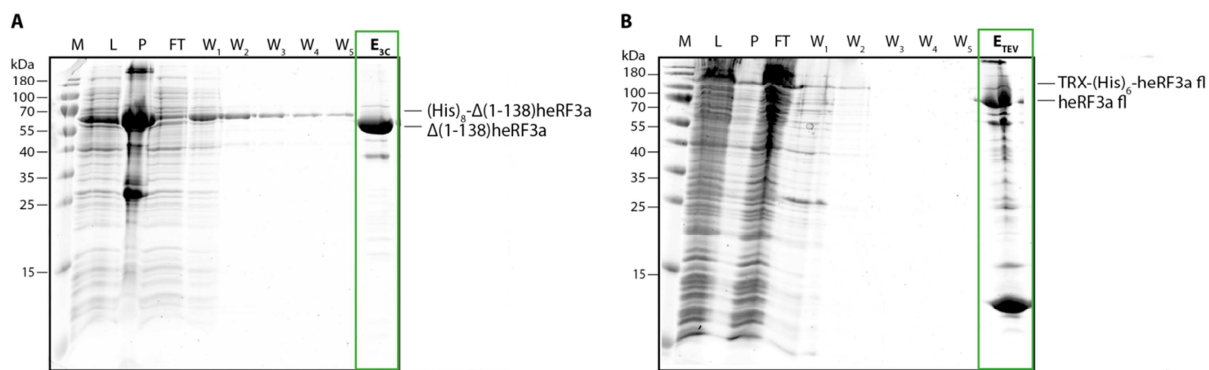


Figure 29: Purification of the $\Delta(1-138)$ heRF3a and the heRF3a Full Length Proteins.

(A) Sodium dodecyl sulfate-polyacrylamide gel electrophoresis (SDS-PAGE) of samples taken throughout the $\Delta(1-138)$ heRF3a purification procedure. Octahistidine ((His)₈)-tagged $\Delta(1-138)$ heRF3a protein could be expressed. The final 3C-protease-cleaved elution sample ('E_{3C}') is highlighted in green revealing high yield of tag-free protein and minor impurities. **(B)** SDS-PAGE of samples taken throughout the heRF3a fl purification procedure. Thioredoxin (TRX) and hexahistidine ((His)₆)-tagged heRF3a fl protein could be expressed. The final TEV-protease cleaved elution sample ('E_{TEV}') is highlighted in green revealing low yield and numerous impurities.

Human Full Length eRF3a

heRF3a full length has only been demonstrated to be stably expressed in the baculovirus/insect system (Frolova *et al.*, 1998) or as TRX-fusion protein in *E. coli* (Kononenko *et al.*, 2010) before. Thus, based on the expression and purification strategy described in Kononenko *et al.*, human eRF3a fl was purified from *E. coli* cells. The N-terminal stability-conferring TRX-tag was fused to a (His)₆-tag required for purification. Both tags could be removed collectively via TEV-cleavage. The yield and grade of purity after cleavage of the tags for elution were only moderate (see Table 21 and Figure 29B, lane 'E_{TEV}' respectively) nevertheless, since heRF3a fl was used for ternary complex formation and adjacent size exclusion chromatography to separate the formed complex from the individual components, it was considered sufficiently pure to proceed.

To optimize for heRF3a fl purity rather than quantity for its individual usage in biochemical assays, the elution strategy was changed to an imidazole step-elution followed by imidazole- and tag-removal via dialysis and TEV-cleavage, respectively. Residual uncleaved protein, as well as the TRX-(His)₆-tag, was removed by another TALON®-affinity purification step, resulting in heRF3a fl protein which was more pure (see Figure 30, lane 'Final'). However, exact comparisons of yields were challenging since impurities falsified the measured protein concentrations.

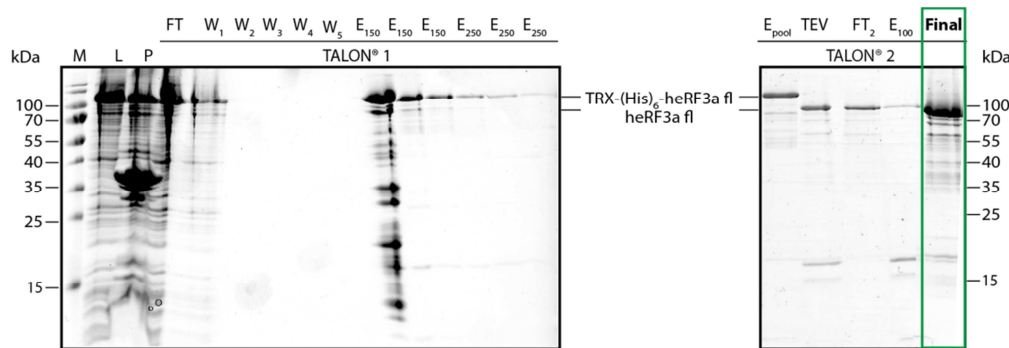


Figure 30: Purification of the Human eRF3a Full Length Protein for Individual Usage.

Sodium dodecyl sulfate-polyacrylamide gel electrophoresis of samples taken throughout the heRF3a fl purification procedure. Thioredoxin (TRX) and hexahistidine ((His)₆)-tagged heRF3a fl protein could be expressed. The final sample after TEV-protease cleavage and two TALON®-affinity purification procedures ('Final') is highlighted in green revealing high yield and some impurities.

Ternary Complex Formation of heRF1, heRF3a and GMPPCP: Co-purification versus *in vitro* Assembly

Like for A-site tRNA delivery by the translational GTPase eEF1A and GTP, the A-site binding factor eRF1 was described to interact with the GTPase heRF3a and GTP. This pre-assembled ternary complex is thought to approach the ribosome for translation termination (Nakamura *et al.*, 1996). To closely resemble this process, *in vitro* complex-assembly was performed by incubation of the purified proteins heRF1 and heRF3a at 25 °C (described as ideal thermodynamic parameter for complex formation in Kononenko *et al.* (Kononenko *et al.*, 2010)) together with the non-hydrolysable GTP-analog GMPPCP for stabilization of ribosomal binding of the complex due to prevention of nucleotide-hydrolysis and heRF3 dissociation. Successful complex formation of heRF1:(Δ1-138)heRF3:GMPPCP could be monitored by its increased molecular weight compared to the single proteins which is apparent by an altered migration behavior during size exclusion chromatography (see Figure 31A) and by the SDS-PAGE analysis of the obtained fractions. Resulting fractions 'B₅' - 'B₈' contained the heRF1 and Δ(1-138)heRF3a proteins in a stoichiometric manner without major impurities. Efficiencies of individual protein purifications and subsequent *in vitro* complex assembly are summarized in Table 21.

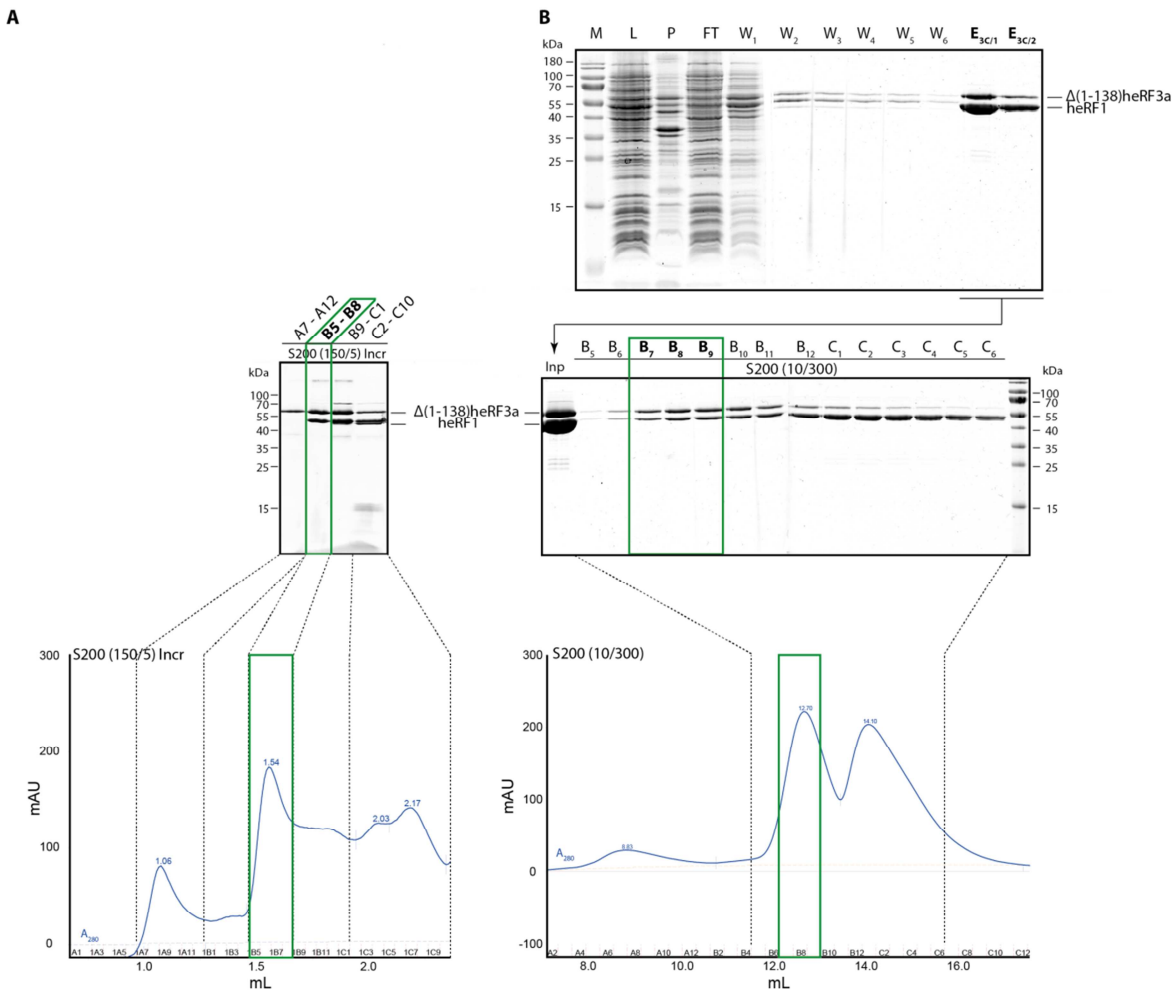


Figure 31: *In vitro* Assembly and Co-purification of the heRF1:Δ(1-138)heRF3a:GMPPCP Complex.

Sodium dodecyl sulfate-polyacrylamide gel electrophoresis of samples taken throughout the ternary complex purification approaches of heRF1, Δ(1-138)heRF3a and GMPPCP. The acquired absorption profiles during size exclusion chromatography are also depicted. **(A)** Incubation of individually purified heRF1 and Δ(1-138)heRF3a with GMPPCP was followed by size exclusion on an S200 (150/5) Increase (Incr) GL column to separate the formed ternary complex from the individual components. The final samples ('B₅'-'B₈') are highlighted in green revealing a stoichiometric, well concentrated complex. **(B)** Co-purification of heRF1 and Δ(1-138)heRF3a resulted in their non-stoichiometric abundance in the 3C-protease-cleaved elution samples ('E_{3C1}' and 'E_{3C2}'). Subsequent size exclusion chromatography of the input (Inp) on an S200 (10/300) column to separate the formed complex from the individual components resulted in a highly concentrated and purified complex (highlighted in green).

In parallel, co-purification of the heRF1:Δ(1-138)heRF3a complex from *E. coli* was performed. N-terminally (His)₈-tagged heRF1 did not result in untagged heRF3 co-purification whereas N-terminally (His)₈-tagged (Δ1-138)heRF3a and untagged heRF1 could be co-purified. To ensure complex stability, washing only occurred under low salt conditions. Again, elution by (His)₈-tag cleavage resulted in pure fractions of the complex (see Figure 31B, lanes 'E_{3C1}' and 'E_{3C2}') which were incubated with GMPPCP before purification and analysis via size exclusion chromatography and SDS-PAGE (see Figure 31B, S200 (10/300)). Indicated fractions 'B₇' - 'B₉' stoichiometrically contained both proteins and were used for binding studies and cryo-EM analysis. Final co-purification yields are provided in Table 21.

For co-purification of the heRF1:Δ(1-138)heRF3a complex (after co-expression with Jmjd4), the heRF1 hydroxylation status was also monitored via mass spectrometry to ascertain the occurrence of *in vivo* hydroxylation on the Lys63 side-chain C4 even if heRF1 is already associated with Δ(1-138)heRF3a in the cell. Results are summarized in Table 20 again revealing full hydroxylation of the Lys63 side-chain C4. Also, no secondary hydroxylation could be detected for any heRF1 Lys residue.

Table 20: Mass Spectrometry Results for the heRF1 Lys63 Side-chain C4 Hydroxylation Status after Co-expression with Δ(1-138)heRF3a and Jmjd4.

heRF1	Peptide: LADEFGTASNIK*SRVN	
	Intensity of Lys63 C4 Hydroxylated	Intensity of Lys63 C4 Non-hydroxylated
<i>In vivo</i> hydroxylation (co-expressed with Δ(1-138)heRF3a and Jmjd4)	3.4x10 ⁵	-----
heRF1	Peptide: MLADEFGTASNIK*	
	Intensity of Lys63 C4 Hydroxylated	Intensity of Lys63 C4 Non-hydroxylated
<i>In vivo</i> hydroxylation (co-expressed with Δ(1-138)heRF3a and Jmjd4)	1.76x10 ⁷	-----

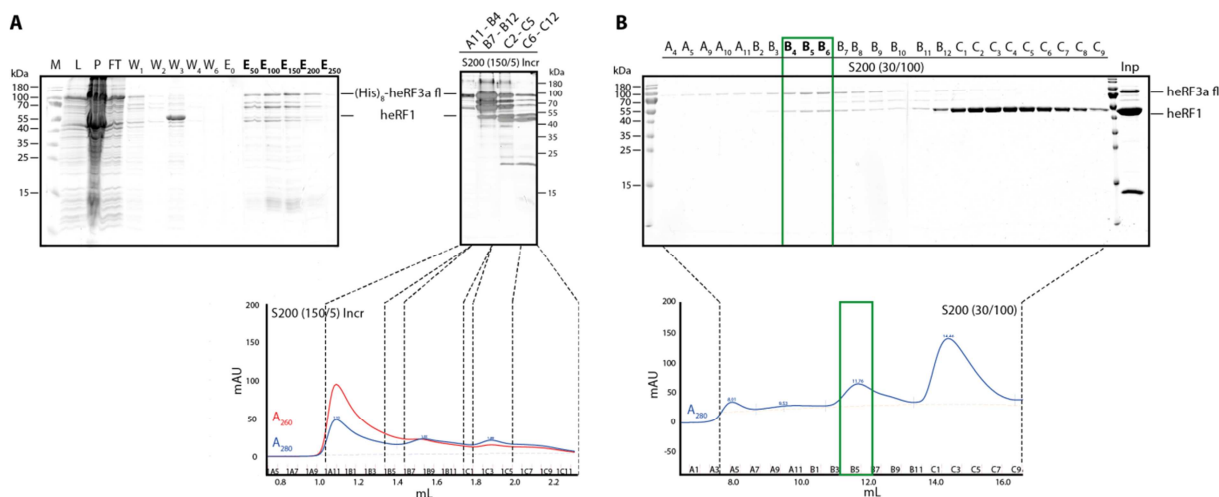


Figure 32: *In vitro* Assembly and Co-purification of the heRF1:heRF3a full length:GMPPCP Complex.

Sodium dodecyl sulfate-polyacrylamide gel electrophoresis (SDS-PAGE) of samples taken throughout the ternary complex purification approaches of heRF1, heRF3a fl and eRF1 could be expressed. The acquired absorption profiles during size exclusion chromatography are also depicted. **(A)** The final samples ('E₅₀' - 'E₂₅₀') after co-purification of heRF1 and heRF3a fl contained impurities (likely heRF3a degradation products). Subsequent size exclusion chromatography on an S200 (150/5) Increase (Incr) GL column to separate the formed ternary complex from the individual components resulted in no fraction that only contained the purified complex. **(B)** Incubation of individually purified heRF1 and heRF3a fl with GMPPCP was followed by size exclusion chromatography on an S200 (30/100) column to separate the formed ternary complex from the individual components. A sample of the input (Inp) was also applied. The final samples ('B₄' - 'B₆') are highlighted in green revealing a stoichiometric, pure ternary complex.

Considering the successful co-purification of the N-terminally truncated heRF3a protein and heRF1, this strategy was also applied for complex formation of heRF1 with the aggregation-prone heRF3a fl protein. Here, after extensive low salt washing steps the elution could only be successfully performed

with imidazole which resulted in impurities in the elution samples (see Figure 32A, lanes 'E₅₀' - 'E₂₅₀'). Especially contaminations being of similar size to the eRFs were present, likely presenting degradation products of heRF3a fl, which could not be separated during size exclusion chromatography (see Figure 32A, S200 (150/5) Incr).

Consequently, *in vitro* assembly of the heRF3a fl containing complex was conducted as for the N-terminally truncated heRF3a protein. Size exclusion chromatography which was analyzed via subsequent SDS-PAGE (see Figure 32B) resulted in low, but feasible amounts of pure termination complex evident in the two stoichiometric bands in the final fractions 'B₄' - 'B₆'.

Human 3xFLAG-ABCE1

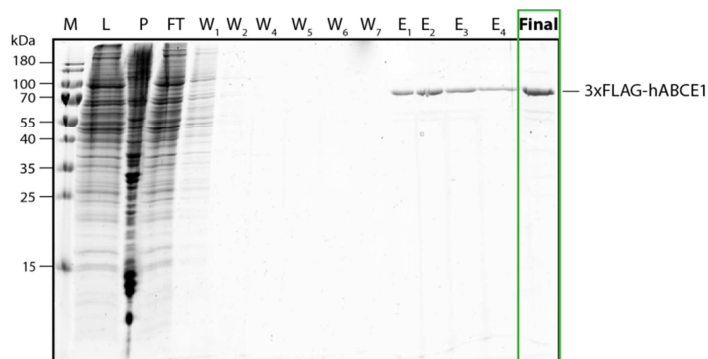


Figure 33: Purification of the 3xFLAG-hABCE1 Protein from Human HEK293T Cells.

Sodium dodecyl sulfate-polyacrylamide gel electrophoresis of samples taken throughout the 3xFLAG-hABCE1 purification procedure. The final concentrated sample ('Final') is highlighted in green revealing high purity.

Attempts to purify hABCE1 from *E. coli* have failed. Thus, expression was performed in human HEK293T cells. Elution via 3C-cleavage and 3xFLAG-tag removal lead to protein instability for which reason elution was performed by incubation with 3xFLAG peptide instead. 3xFLAG peptide removal was achieved by sequential dilution and concentration to avoid falsified determination of protein concentration and surface coverage of the EM-grid. Considerable amounts of 3xFLAG-ABCE1 (see Table 21) were obtained in high purity (see Figure 33, lane 'Final'). Stability of the protein was challenged by sorption to the solid phase of the Eppendorf cup and precipitation during the freeze-thaw cycle even after the addition of cryo-protectant. Remedial measures were storage in low binding Eppendorf cups at 4 °C for one day before usage for *in vitro* reconstitution and EM analysis.

Protein Purification Efficiencies

Table 21: Overview of Protein Purification Efficiencies.

Protein	Strategy	Starting Material	Final concentration	Final amount	Amount of protein per 1 L <i>E. coli</i>
heRF1	Single purification	1 L (<i>E. coli</i>)	0.78 µg/µL	3,627 µg	3,627 µg
(His) ₆ -Δ(1-46) Jmjd4	Single purification	5 L (<i>E. coli</i>)	1.00 µg/µL	1,000 µg	200 µg
heRF1	Single purification (co-expression with (His) ₆ -Δ(1-46)Jmjd4)	5 L (<i>E. coli</i>)	2.76 µg/µL	24,990 µg	4,995 µg
Δ(1-138)heRF3a	Single purification	2 L (<i>E. coli</i>)	1.01 µg/µL	4,747 µg	2,374 µg
heRF3a fl	Single purification (for individual usage)	2 L (<i>E. coli</i>)	0.65 µg/µL	266 µg	133 µg
heRF3a fl	Single purification (for complex-formation)	1 L (<i>E. coli</i>)	3.20 µg/µL, strong impurities	Not assignable due to strong impurities	
heRF1: Δ(1-138)heRF3a: GMPPCP Complex	Co-purification (co-expressed with (His) ₆ -Δ(1-46)Jmjd4)	8 L (<i>E. coli</i>)	0.96 µg/µL	9,360 µg	1,170 µg
heRF1: heRF3a fl: GMPPCP Complex	Single purification and subsequent complex formation	heRF1 (828 µg) heRF3a fl (640 µg)	0.24 µg/µL	30 µg	Not applicable
3xFLAG-hABCE1	Single purification from human HEK293T	Ten 15.4 cm ² dishes (30 - 40 % confluence)	0.51 µg/µL	68 µg	Not applicable

3.2.2 Preparation of Natively heRF1 Containing Ribosome-nascent Chain Complexes

During the establishment of the human RNC purification protocol comparisons of the RNC protein pattern to empty human 80S ribosomes (Anger *et al.*, 2013) on PAA gels revealed an additional band in the RNC preparation at the height of eRF1. For identification, the area of the additional band, containing 3 visible bands (see Figure 34A, green box), was subjected to mass spectrometry. Top hits contained tubulin, T-complex protein 1 (TCP 1), the ribosomal proteins L3 and L4 and eRF1 whereof the latter has been shown to natively bind to RRL hCMV-stalled 80S ribosomes before (Janzen *et al.*, 2002). Increased salt-concentrations of up to 1 M KOAc during washing did not enhance the amount of unbound RNCs which would have been advantageous for more quantitative binding of the heRF1:heRF3:GMPPCP complex during *in vitro* reconstitution. Hence, the amount of natively bound heRF1 and its specificity for hCMV-stalled RNCs was assessed via Western blotting (see Figure 34B). The distinct and specific signal, which only occurred for hCMV-stalled RNCs and not for truncated hCMV-RNCs (control, without a stop codon in the A-site), rendered this sample suitable for cryo-EM analysis.

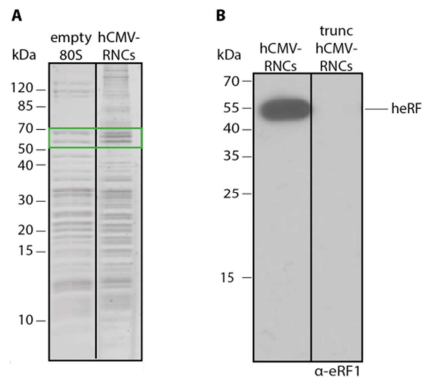


Figure 34: Identification of the Additionally Bound Protein in the Purified hCMV-stalled Ribosome-nascent Chain Complex.

(A) Comparison of the human 80S ribosome preparation from Anger *et al.* (Anger *et al.*, 2013) (left) and the hCMV-stalled ribosome-nascent chain complex (RNC) (right) protein patterns on poly-acrylamide gels revealed additional bands for the RNC preparation. The region of interest, which was subjected to mass spectrometry, is highlighted in green, demonstrating heRF1 abundance. **(B)** Western blot to assess the natively bound heRF1 and its specificity for hCMV-stalled RNCs compared to truncated (trunc) hCMV-RNCs via anti-eRF1 (α -eRF1) antibody detection.

Figure (B) was modified from Matheisl *et al.* (Matheisl *et al.*, 2015).

3.2.3 Preparation of Natively heRF1 Containing Ribosome-nascent Chain Complexes bound to Guanosine Triphosphatase-deficient heRF3a

Stable binding of Δ (1-138)heRF3a to the natively containing heRF1 RNCs was attempted by the addition of the GTPase deficient heRF3 mutants His300Gln or Arg371Gly. Supplementation to the *in vitro* translation reaction was speculated to efficiently trap the pre-termination complex. However, after similar RNC purification and likewise after only applying low-salt washing steps during RNC purification, presence of eRF3a in the final sample could not be determined via Western blotting (see Figure 35).

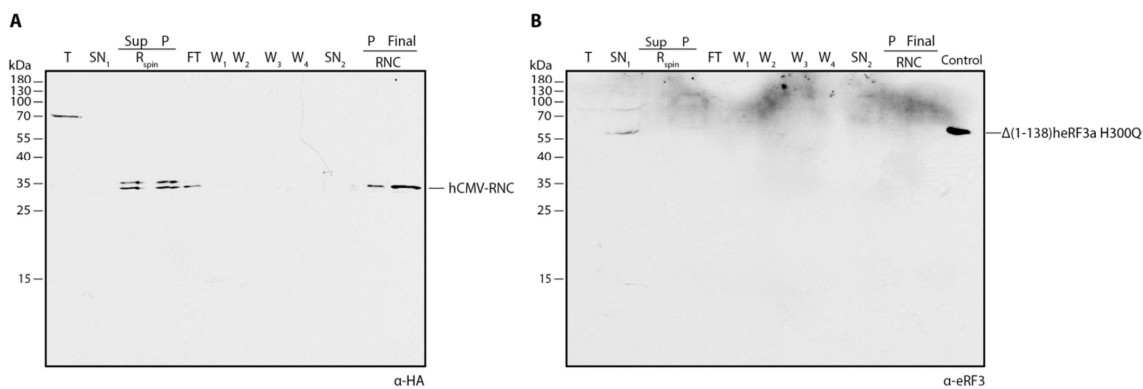


Figure 35: Ternary Complex Formation during Ribosome-nascent Chain Complex Preparation Attempted with Guanosine Triphosphatase-deficient heRF3a.

Western blots of samples taken throughout the ribosome-nascent chain complex (RNC) purification procedure that was supplemented with guanosine triphosphatase-deficient Δ (1-138)heRF3a H300Q protein for its co-purification. **(A)** The stalling efficiency was assessed by anti-hemagglutinin (α -HA) antibody detection. **(B)** The Δ (1-138)heRF3a abundance was monitored by incubation with an eRF3-specific antibody (α -eRF3). No co-purification of the wildtype or mutant eRF3 protein could be detected.

3.2.4 Preliminary Analysis: Binding Assays and Negative Staining

Prior to cryo-EM analysis specific stoichiometric binding of the purified protein factors to hCMV-stalled RNCs was assessed. Particularly adequate buffer conditions could be identified by means of a binding assay. In such assay ribosomes and their potential binding partners were incubated at RT to allow for interactions to occur. Subsequently, complex formation was monitored by pelleting of the sample through a sucrose cushion. Ribosomes by themselves and together with their stably bound interaction partners could migrate through the sucrose cushion and resided in the pellet fraction. Unbound proteins remained in the supernatant due to their limited molecular weight.

The identification of specific binding conditions was started with the heRF1:Δ(1-138)heRF3a:GMPPCP complex. Numerous buffer compositions were tested before (specific) interaction could be detected. As demonstrated in Figure 36A, the ternary complex bound to hCMV-stalled RNCs in an approximately stoichiometric manner (green box), however, did not bind to stop codon deficient truncated hCMV-RNCs (red box) when applied in 5x molar excess. Notably, the ternary complex did not bind to similarly obtained hCMV-stalled RNCs purified from RRL (see Figure 36B), which are evolutionarily very closely related to human ribosomes, showing high specificity for the ternary complex ribosome interaction.

The same buffer conditions were applied for samples containing RNCs with 5x molar excess of hydroxylated eRF1 only. The assessment of adequate binding conditions for heRF1, 3xFLAG-hABCE1 and AMPPCP together provided challenges. Known to sorb the Eppendorf cup surface, the 3xFLAG-hABCE1 protein also interacted with the ultracentrifuge tube during the binding assay studies wherefore it could neither be detected in the pellet nor in the supernatant fraction. Consequently, the same buffer conditions as for the heRF1:Δ(1-138)heRF3a:GMPPCP complex were applied for subsequent negative staining and cryo-EM analysis.

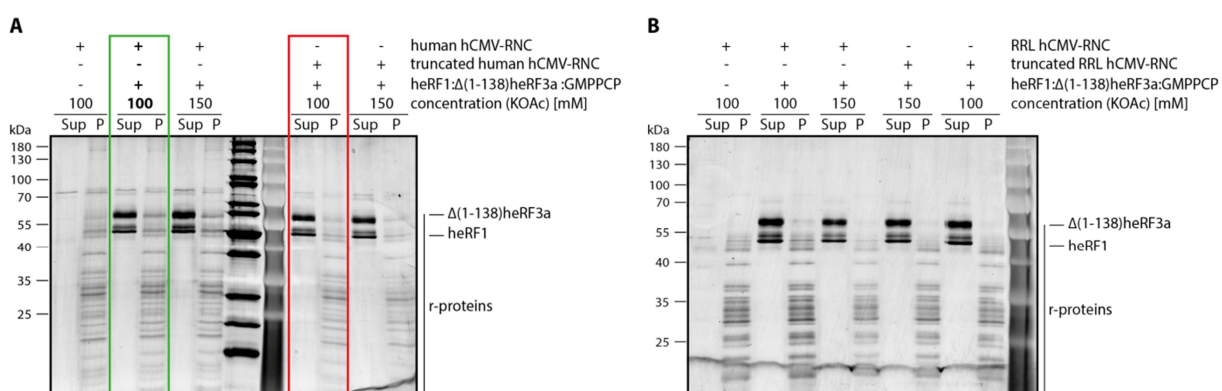


Figure 36: Assay to Assess Binding of the heRF1:Δ(1-138)heRF3a:GMPPCP Complex to Ribosome-nascent Chain Complexes.

Sodium dodecyl sulfate-polyacrylamide gel electrophoresis of supernatant (Sup) and pellet (P) fractions of the binding assays: **(A)** Conducted with hCMV-stalled RNCs or truncated hCMV-RNCs (both from human) and the heRF1:Δ(1-138)heRF3a:GMPPCP complex under different buffer conditions with either 100 mM or 150 mM KOAc. Specific complex binding to hCMV-stalled RNCs revealed final buffer conditions used for subsequent cryo-EM studies (highlighted in green). Highlighted in red is the decreased interaction with the truncated hCMV-RNCs. **(B)** Conducted with hCMV-stalled RNCs or truncated hCMV-RNCs from rabbit reticulocyte lysate (RRL) and the heRF1:Δ(1-138)heRF3a:GMPPCP complex under buffer conditions as in (A). Absent binding of the complex to RRL hCMV-stalled RNCs revealed binding specificity of the human complex to human RNCs under the chosen buffer conditions.

Furthermore, ideal grid-coverage of RNCs was examined during negative staining EM. Various concentrations ranging from 4 - 8 A₂₆₀/mL (0.08 – 0.16 pmol/μL) were tested for each sample. Negative staining data displayed typical 80S particles which were slightly contaminated (see Figure 37A, red box). As illustrated in Figure 37, 4 - 5 A₂₆₀/mL RNCs yielded in sufficient particles aiming at high-resolution reconstructions while yet preventing aggregation. Compared to *E. coli* 70S ribosomes, the critical concentration which led to ribosome aggregation was much lower for human 80S ribosomes due to their higher molecular weight (~2.5 MDa versus ~4.5 MDa) (Yusupova and Yusupov, 2015) and the presence of extruding GC-rich expansion segments (Anger *et al.*, 2013) which both demand for a precise titration of the applied RNC concentration.

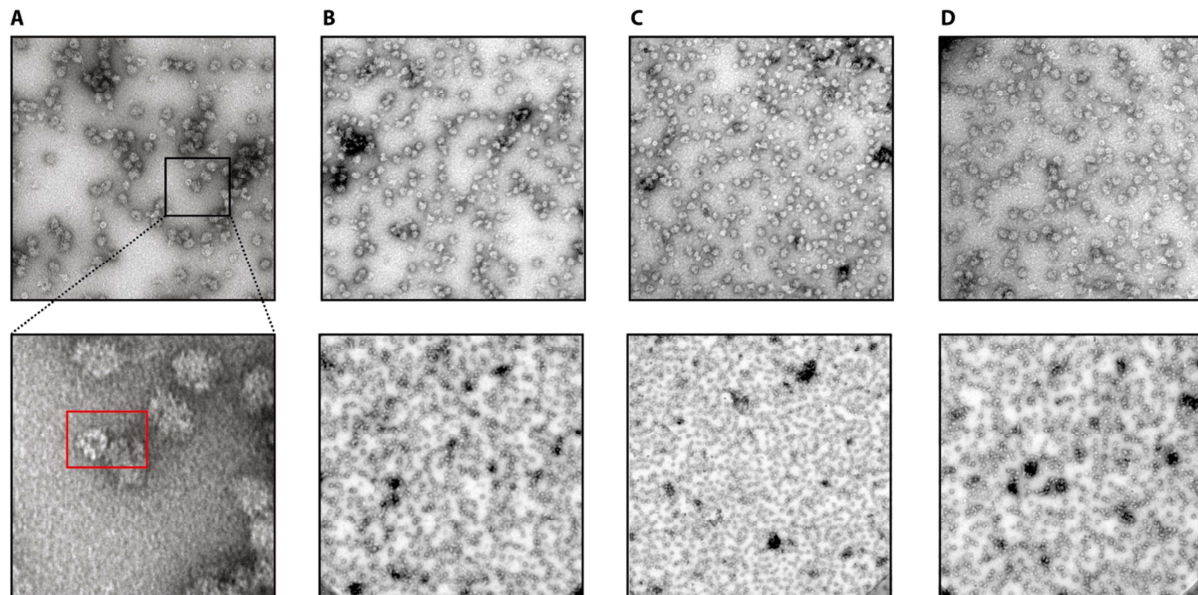


Figure 37: Negative Staining Electron Microscopy Images.

Negative staining electron microscopy (EM) images of: (A) hCMV-stalled ribosome-nascent chain complexes (RNCs) at a final concentration of 4 A₂₆₀ (absorption at $\lambda = 260\text{nm}$)/mL with 5x molar excess of the heRF1:Δ(1-138)heRF3a:GMPPCP complex. One of the co-purified impurities is highlighted in red in a close up of the indicated area. (B) RNCs at a final concentration of 5 A₂₆₀/mL with 5x molar excess of heRF1. (C) RNCs at a final concentration of 5 A₂₆₀/mL with 10x molar excess of heRF1, 3xFLAG-hABCE1 and AMPPNP. (D) Natively heRF1 containing RNCs at a final concentration of 5 A₂₆₀/mL.

3.2.5 Tecni G2 Spirit Derived Reconstructions

To evaluate the percentage of ligand-occupancy in the different complexes, low-resolution cryo-EM reconstructions were calculated. Computational sorting was performed until a homogenous population was obtained for each assembled complex. The reconstructed densities, their corresponding resolutions and ligand occupancies are depicted in Figure 38. Detailed statements about ligand interacting residues could not be made at these resolutions, however, suitability and the required amount of collected data for high-resolution cryo-EM could be pre-assessed.

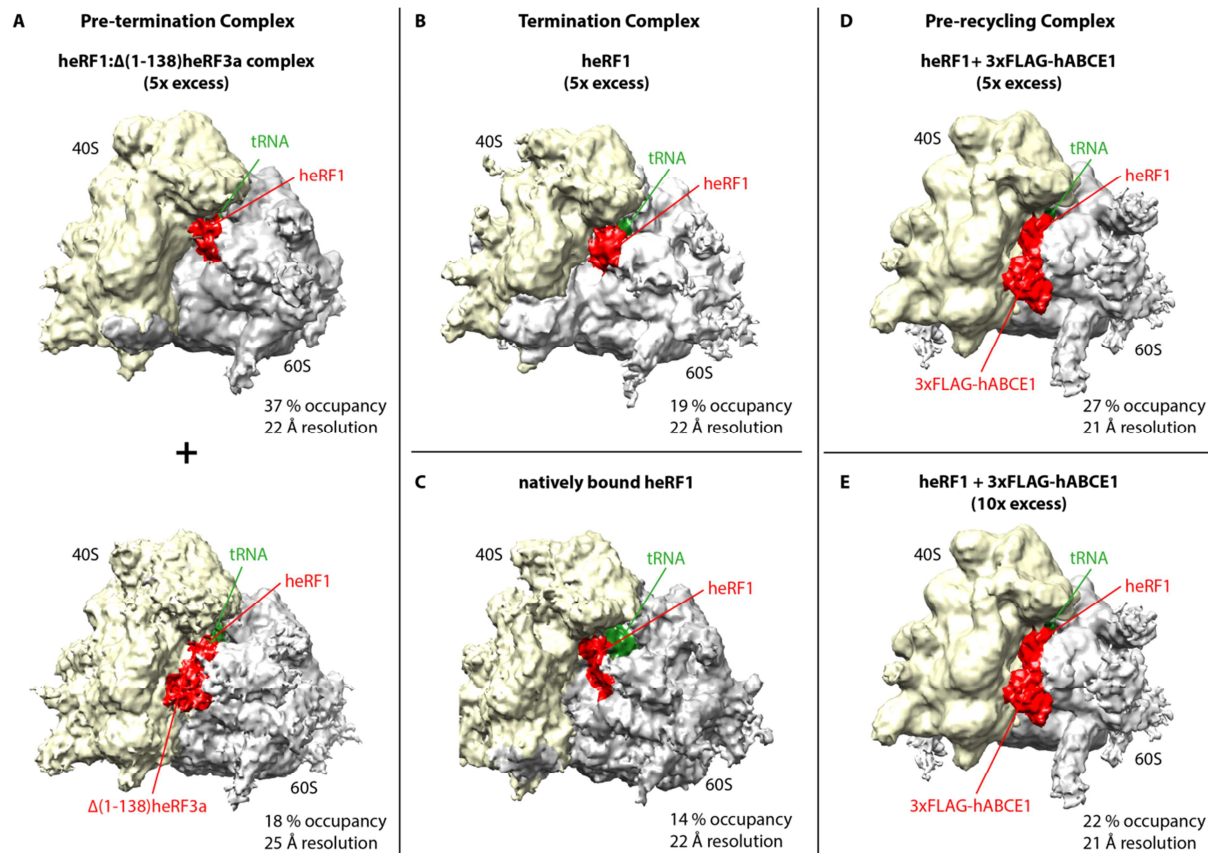


Figure 38: Overview of Cryo-Electron Microscopy Reconstructions from Data Collected with the Tecnai G2 Spirit.

The 40S subunit (SU) is indicated in yellow, the 60S SU in gray. The tRNA is colored in green whereas the protein factors in red. **(A)** Cryo-electron microscopy reconstruction of the pre-termination complex resulted in an eRF1-only containing ribosomal structure with 37 % occupancy and a final resolution of 22 angstrom (\AA). Further sorting, however, revealed a complex containing heRF1 and $\Delta(1-138)\text{heRF3a}$. Here, 18 % occupancy resulted in a final resolution of 25 \AA . In both volumes, a tRNA in the peptidyl-tRNA binding site (P-site) is additionally visible. **(B)** The termination complex containing a P-site tRNA and heRF1. 19 % occupancy resulted in a final resolution of 22 \AA . **(C)** Reconstruction of the ribosome-nascent chain complex (RNC) natively containing heRF1 and a P-site tRNA. 14 % occupancy resulted in a final resolution of 22 \AA . **(D)** The pre-recycling complex assembled with 5x molar excess of heRF1, 3xFLAG-hABCE1 and AMPPNP. Also here, a P-site tRNA is visible. 27 % occupancy resulted in a final resolution of 21 \AA . **(E)** The pre-recycling complex assembled with 10x molar excess of heRF1, 3xFLAG-hABCE1 and AMPPNP. Also here, a P-site tRNA is visible. 22 % occupancy resulted in a final resolution of 21 \AA .

3.3 High-resolution Structure of Human eRF1 Bound to the Human 80S Ribosome

3.3.1 Data Processing and the Resulting Cryo-Electron Microscopy Reconstruction

To elucidate the structural basis of stop codon decoding by heRF1 as well as the hCMV-stalling mechanism at high resolution, single particle analysis of cryo-EM data (starting with 245,253 particles) collected on the in-house Titan Krios TEM equipped with a Falcon II direct electron detector was performed on the most promising termination complex.

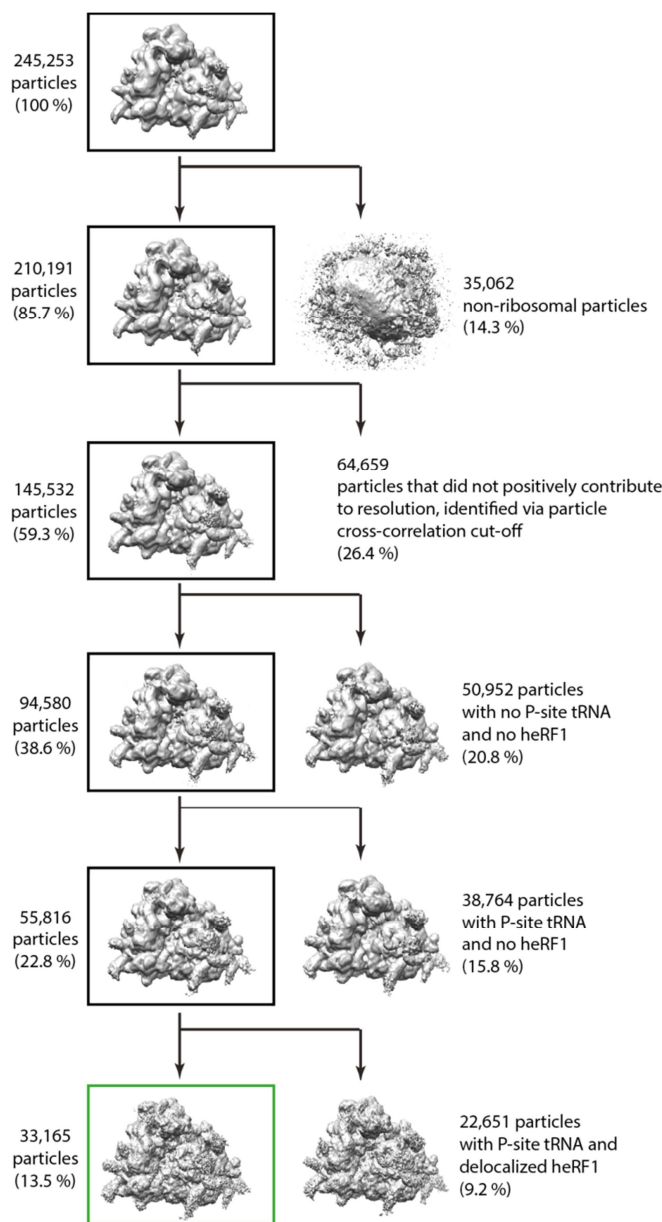


Figure 39: Particle Sorting Scheme of the Termination Complex Cryo-Electron Microscopy Reconstruction.

Number of particles and percentage of starting particles are given for each sorting step. Figure was modified from Mattheisl *et al.* (Mattheisl *et al.*, 2015).

As described in 'Materials and Methods' (see 2.8.5) and depicted in Figure 39, several *in silico* sorting steps with the SPIDER software package were of necessity to result in the final homogenous set of particles. For resolution improvement, the dataset was processed twice: The final volume of the first calculation was used as template for the initial particle alignment and the initial refinement round in the second calculation. Early omitting of particles that did not positively contribute to resolution was realized directly after removing the non-ribosomal particles. Here, cross-correlation values (cc-values) were assigned to each particle resembling its fit to the 3D reconstruction. Cut-off values for each defocus group were based on visual inspection in dependency on the average cc-value of the corresponding defocus group. Further unfocused and focused semi-supervised sorting against intrinsically derived reconstructions resulted in the final reconstruction of 33,165 particles (see

Figures 39, green box and 40). Further, neither RELION-based 3D refinement nor movie processing (Scheres, 2014, 2012a) of the final particles improved the calculated resolution or map quality.

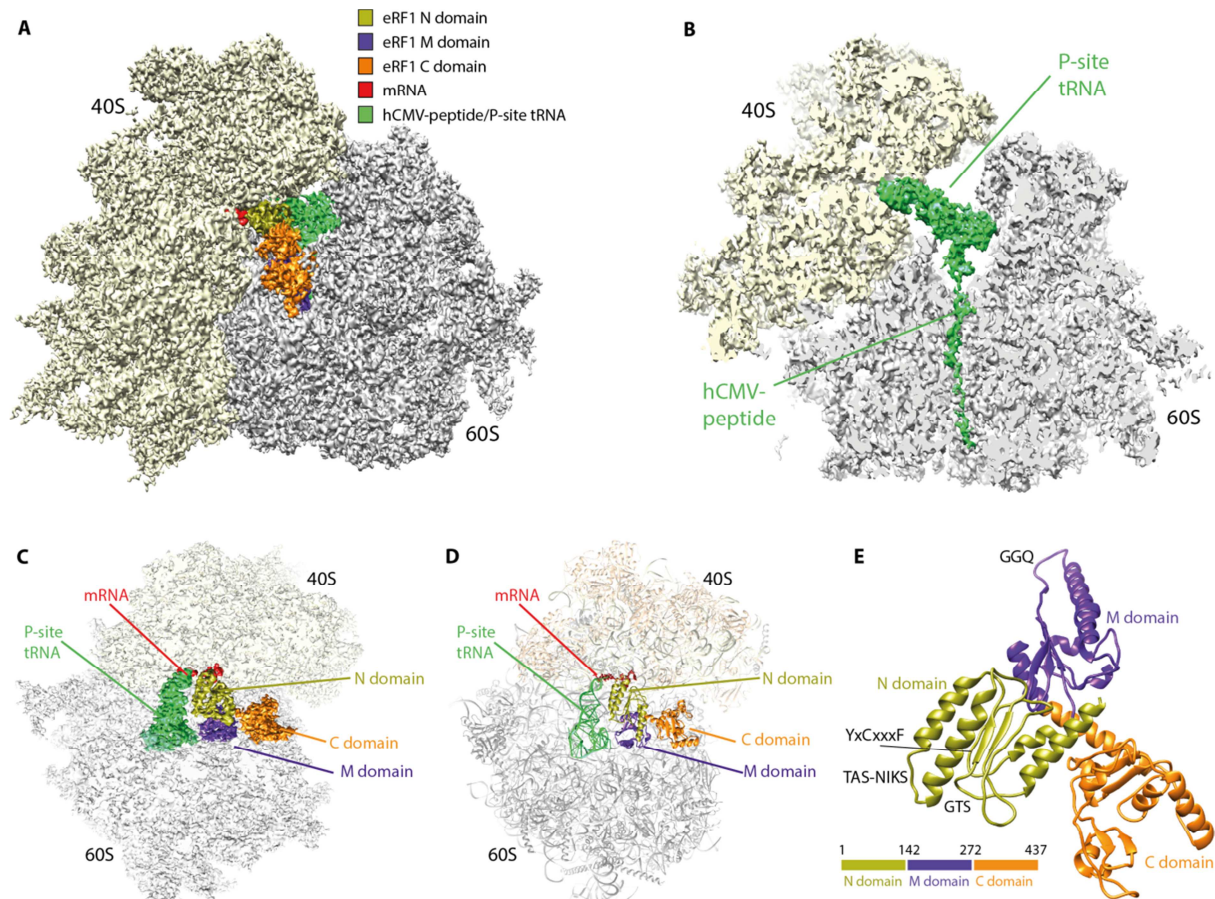


Figure 40: Final Cryo-Electron Microscopy Reconstruction of the eRF1-bound hCMV-stalled Ribosome-nascent Chain Complex.

(A) Final cryo-electron microscopy reconstruction containing the mRNA (red), tRNA (green) and eRF1 (N domain: light green, M domain: purple, C domain: orange). **(B)** Transverse section focusing on the peptidyl-tRNA (green) in the peptidyl-tRNA binding site (P-site). **(C)** Transverse section color coded as in (A). **(D)** Molecular model for (C). **(E)** Molecular model of human eRF1 when bound to the human ribosome color coded as in (A). Most important motifs (GGQ, GTS, TAS-NIKS and YxCxxxF) are indicated.

Figures were modified from Mattheisl *et al.* (Mattheisl *et al.*, 2015).

Data was collected with 7 frames (corresponding to $31.2 \text{ e}^-/\text{\AA}^2$) whereof only the motion-corrected and aligned frames 1 - 4 were used for the initially conducted refinement and sorting steps. Selection of the right frames for reconstruction always is a balancing act between their beneficial effect by increasing the contrast and their harmfulness owing to accumulating electron damage. The smaller, final particle set allowed motion-correction (Cheng *et al.*, 2009) only for the remaining micrographs which was utilized for testing different frame combinations. Particles were picked anew for each frame-combination with the originally determined coordinates. Undecimated refinement resulted in the final reconstructions of each frame-combination. Corresponding resolutions are listed in Table 22 and depicted in Figure 41 whereof frames 0 - 2 visually turned out to be the best compromise revealing an average resolution of 3.8 \AA at $\text{FSC}_{0.143}$ (see Figure 42A).

Table 22: Tested Frame Combinations for the Cryo-Electron Microscopy Reconstruction of the heRF1-bound hCMV-stalled Ribosome-nascent Chain Complex and Their Resulting Average Resolutions.

Frame Combination	Exposed Electron Dose	Resolution (FSC _{0.143})
0 - 1	9.6 e ⁻ /Å ²	3.84 Å
0 - 2	14.4 e ⁻ /Å ²	3.77 Å
0 - 3	19.2 e ⁻ /Å ²	3.73 Å
0 - 4	21.6 e ⁻ /Å ²	3.75 Å
1 - 4	26.4 e ⁻ /Å ²	3.81 Å
1 - 6	31.2 e ⁻ /Å ²	3.81 Å

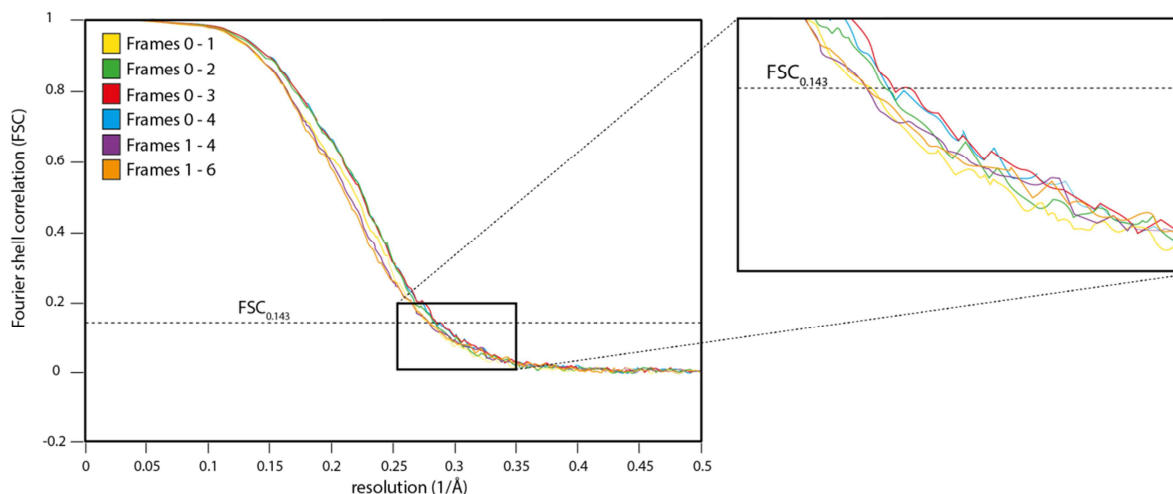


Figure 41: Average Resolutions of the heRF1-bound hCMV-stalled Ribosome-nascent Chain Complex Reconstructions Depending on the Tested Frame Combinations.

The average resolution was based on the Fourier shell correlation (FSC) cut-off criterion at 0.143 (dotted line). A close-up reveals differences in the calculated resolutions that are numerically listed in Table 22.

Low-pass filtering at frequencies lower than corresponding to 8 Å throughout processing was adhered to avoid possible overfitting and therefore noise accumulation potentially interpretable as high-resolution features, which is conform to the application of the resolution criterion at FSC_{0.143}. Local resolution calculations (see Figure 42B) revealed a well-resolved ribosomal core region and more flexible regions at the outer layer mostly consisting of the rRNA ES. Clear density could be assigned to the P-site tRNA linked to the continuous density of the nascent chain reaching from the PTC throughout the upper part of the tunnel to the central constriction formed by uL4 and uL22 (see Figure 40B). Hereafter, only discontinuous density was observable in the lower part of the tunnel. Further, additional density could be assigned to heRF1 whose resolution was of major importance displaying similarly resolved N and M domains and a slightly less well resolved C domain (see Figure 42C).

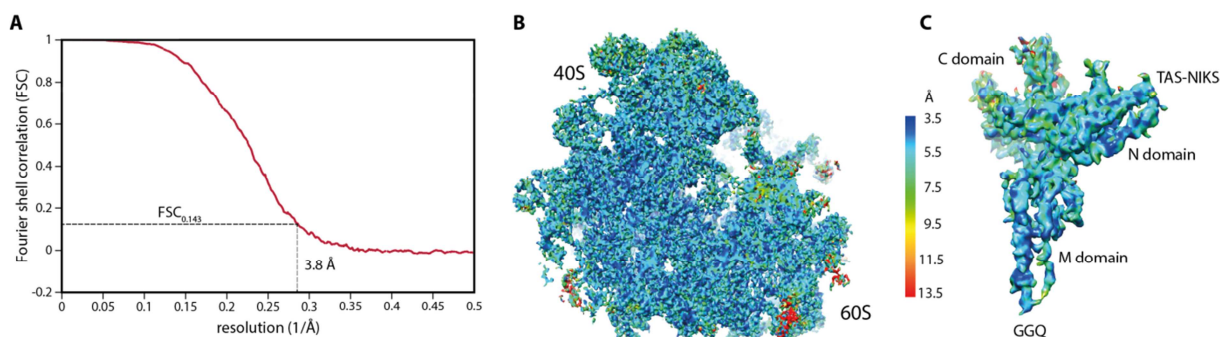


Figure 42: Average and Local Resolutions of the heRF1-bound hCMV-stalled Ribosome-nascent Chain Complex Reconstruction.

(A) The average resolution was based on the Fourier shell correlation (FSC) cut-off criterion at 0.143 (dotted line) and calculated to 3.8 Å. Local resolution for (B) the heRF1-bound hCMV-stalled ribosome-nascent chain complex and for (C) the heRF1 protein as calculated by ResMap (Kucukelbir *et al.*, 2014). Figures were modified from Mattheisl *et al.* (Mattheisl *et al.*, 2015).

For molecular interpretations, rigid body docking of the molecular model of the human 80S POST state (Behrmann *et al.*, 2015) was performed being in agreement with the acquired electron density resembling such POST state. Observed distinct features like the presence of density for bulky side-chains or for the pitch of α -helices and β -strand separation are in accordance with the calculated average resolution (examples see Figure 43). For heRF1, the X-ray crystallography-based molecular model (Cheng *et al.*, 2009) was docked. Due to the different overall conformation of heRF1 in the heRF3-bound crystal structure, each heRF1 domain was fitted separately. From this starting point, the missing Mini Domain, as well as the missing C-terminal tail (residues 420 - 437), was added from the NMR structure (Mantsyzov *et al.*, 2010) and modeled according to the obtained cryo-EM density. Further, individual residues of heRF1 and their ribosomal interaction partners were adjusted to the experimental data. The nascent chain was built *de novo*, yet starting from the central constriction area (hCMV-peptide residue Leu6) the interrupted density only allowed backbone tracing.

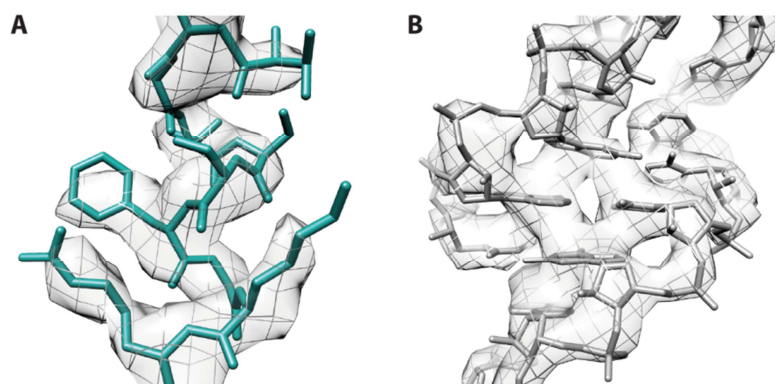


Figure 43: Representative Electron Densities of the Cryo-Electron Microscopy Reconstruction.

Selected electron densities (gray mesh) for (A) a ribosomal protein and (B) ribosomal RNA of the large subunit. Figures taken from Mattheisl *et al.* (Mattheisl *et al.*, 2015).

3.3.2 Interactions of Human eRF1 with the Human Ribosome and Comparisons to Previous Human eRF1 Structures

Crystallized unbound human eRF1 (see Figure 44A) (Song *et al.*, 2000) showed an increased distance of ~ 98 Å between the TAS-NIKS motif, which was proposed in numerous studies to be involved in stop codon recognition in the DC (Chavatte *et al.*, 2002; Frolova *et al.*, 2002), and the GGQ motif, which is the only conserved RF motif and was shown to be engaged in bacterial peptide release in the PTC (Jin *et al.*, 2010; Korostelev *et al.*, 2008, 2010; Laurberg *et al.*, 2008; Weixlbaumer *et al.*, 2008). Consequently, when considering eRF1's accommodation into the ribosome, conformational changes have to occur to meet the distance from the DC located in the SSU to the PTC located in the LSU (~ 85 Å). In the eRF1:eRF3 crystal structure (see Figure 44B), where eRF1 is in the ribosome-unbound state, it engages in a tRNA resembling conformation. In lower resolution cryo-EM reconstructions (des Georges *et al.*, 2014; Preis *et al.*, 2014; Taylor *et al.*, 2012) of the pre-termination complex where the eRF1:eRF3 complex is bound to the 80S ribosome eRF1 was shown to adopt a similar conformation: It is bound to the ribosomal A-site, however, its GGQ motif is locked by its interaction with eRF3. Recently, Muhs *et al.* (Muhs *et al.*, 2015) have demonstrated also by cryo-EM that eRF1-only binding to the 80S ribosome renders the termination factor in its active, elongated conformation with the GGQ motif already positioned in the PTC. This is also in accordance with biochemical release assays showing virtually complete peptide release if only eRF1 is present (Alkalaeva *et al.*, 2006). Indeed, consistent with these postulations, our structure of the termination complex revealed a similar overall orientation of eRF1 on the human ribosome. It is located in the ribosomal A-site mimicking the shape of a tRNA (see Figures 44C, D) reaching from the A-site mRNA DC into the PTC in its elongated state.

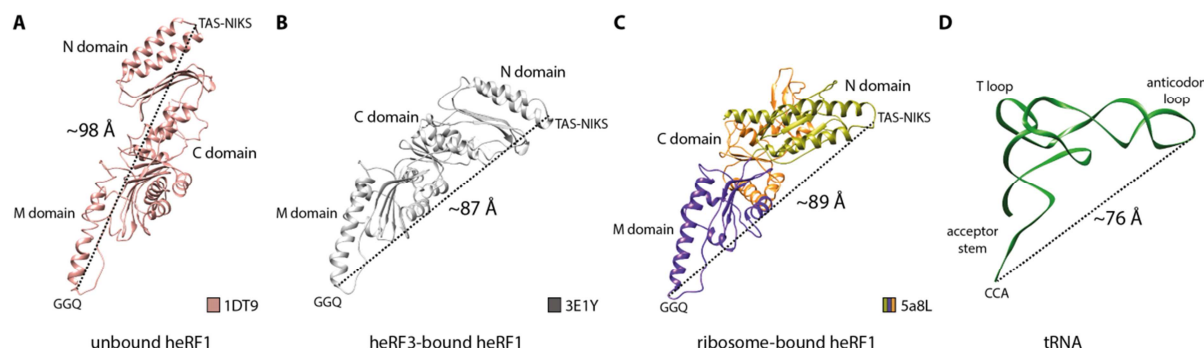


Figure 44: Structural Comparison of Molecular Models: Human Unbound eRF1, eRF3-bound eRF1, Ribosome-bound eRF1 and a P-site tRNA.

(A) Crystal structure of the unbound heRF1 protein (PDB-code: 1DT9) with a distance of ~ 98 Å from the TAS-NIKS motif (Lys63) to the GGQ motif (Gln185) (Song *et al.*, 2000). (B) Crystal structure of the heRF3-bound heRF1 protein (PDB-code: 3E1Y) with a distance of ~ 87 Å from the TAS-NIKS motif (Lys63) to the GGQ motif (Gln185) (Cheng *et al.*, 2009). (C) Ribosome-bound heRF1 protein (PDB-code: 5a8L) with a distance of ~ 89 Å from the TAS-NIKS motif (Lys63) in the decoding center (DC) to the GGQ motif (Gln185) in the peptidyl-transferase center (PTC). (D) Human P-site tRNA with a distance of ~ 76 Å from the anticodon (position 3) in the DC to the CCA-end (A76) in the PTC.

As expected, more detailed comparisons of our molecular model (see Figure 45A) to the human eRF3-bound crystal structure (see Figure 45B) revealed a shifted GGQ motif when their alignment was based on the C domain (see Figure 45C). Notably, even when the alignment was performed on the basis of the GGQ-containing M domain, the tip of the distal loop comprising the GGQ motif is oriented differently (see Figure 45D). Not only is it shifted by ~ 6 Å, but furthermore the Gln side-chain is turned by 180° pointing towards the peptidyl-tRNA ester-bond in our reconstruction.

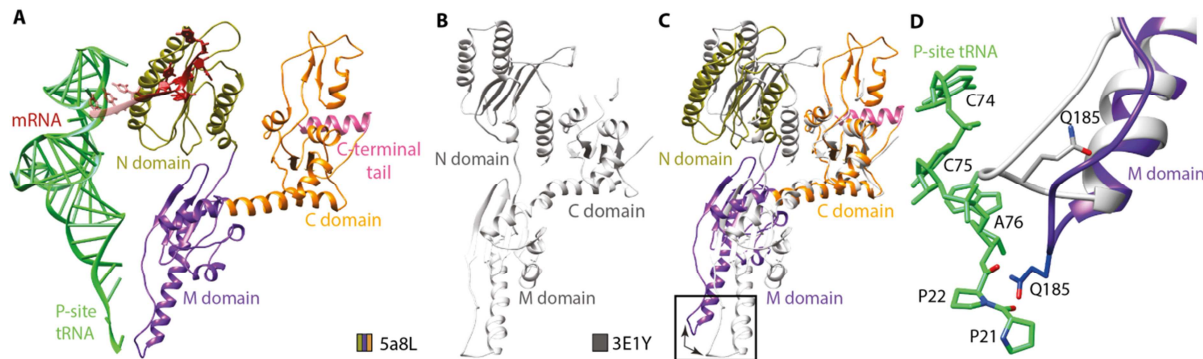


Figure 45: Structural Comparison of Molecular Models: The Human eRF3-bound eRF1 versus the Obtained Human Ribosome-bound eRF1.

(A) Molecular model of the ribosome-bound peptidyl-tRNA binding site (P-site) tRNA (green) and the heRF1 protein with its domains colored distinctively (N domain: light green, M domain: purple, C domain: orange) (PDB-code: 5a8L). The C-terminal tail is indicated in pink. **(B)** Crystal structure of heRF3-bound heRF1 (PDB-code: 3E1Y) (Cheng *et al.*, 2009). **(C)** Overlay of (A) and (B) revealing the additional C-terminal tail in the ribosome-bound model as well as the shifted GGQ-containing loop (black box). **(D)** Close up, on the GGQ-loop additionally showing the rotated side-chain of Gln185 (Q185).

Figures were modified from Matheisl *et al.* (Matheisl *et al.*, 2015).

Moreover, the crystal structure lacks density for the Mini Domain (which contacts eS31 at the 40S head only in the eRF3-bound pre-termination complex (Muhs *et al.*, 2015)) and the C-terminal protein tail (residues: 420 - 437), both located in the C domain. Positioning of the α -helical protein tail into our filtered (4 Å) density (see Figures 46A, B) revealed displacement of the uL11 loop (residues 28 - 40) towards the intersubunit space (see Figure 46C). Further, the α -helical protein tail contacts the ribosomal protein eS27. In this region, heRF1 binding causes the ribosomal stalk base (H43/H44) to move inwards consistent with the pre-recycling complex (Behrmann *et al.*, 2015; Preis *et al.*, 2014). In heRF1's extended conformation the N domain, which harbors the well-studied TAS-NIKS (residues 58 - 64), YxCxxxF (residues 125 - 131) and GTS (residues 31 - 33) motifs, interacts with ribosomal RNA as well as the mRNA stop codon. More detailed molecular interactions for all three heRF1 domains predominantly involving rRNA are depicted in Figure 46D or are discussed in 3.3.4.

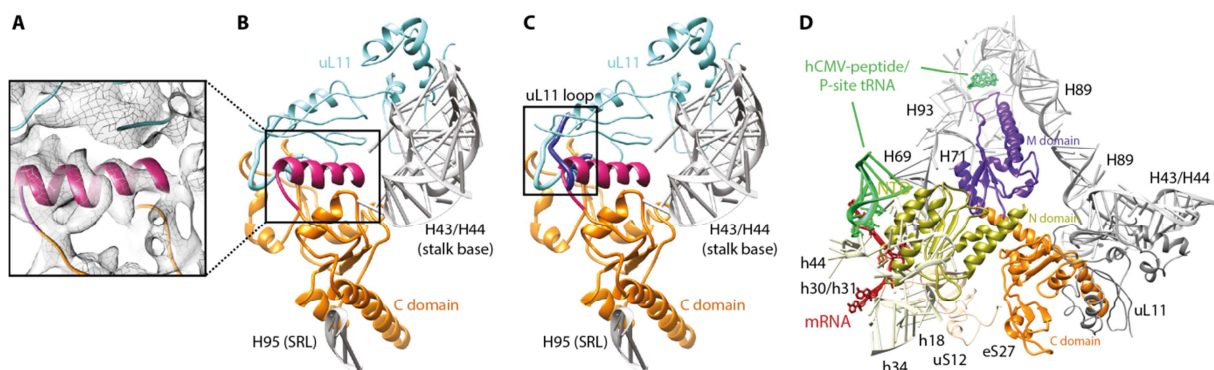


Figure 46: Contacts of heRF1 to the 80S Ribosome.

(A) Density-containing (gray mesh) close up of **(B)** which shows the additional C-terminal heRF1 helix of residues 420 - 437 in pink. The remaining heRF1 C domain is colored in orange, the ribosomal RNA (rRNA) helices 95 (H95) (sarcin-ricin-loop (SRL)) and H43/H44 in gray and the uL11 protein in light blue. **(C)** The displacement of the uL11 loop (residues 28 - 40) color coded as in (B) is highlighted (black box). The original position of the uL11 loop in the ribosomal post-translocation (POST) state (Behrmann *et al.*, 2015) is indicated in dark blue. **(D)** Overview of heRF1 contact sites to the 80S ribosome mainly involving rRNA residues (helices indicated) and the ribosomal proteins eS27 and uL11. heRF1 domains are colored distinctively (N domain: light green, M domain: purple, C domain: orange).

Figures were modified from Matheisl *et al.* (Matheisl *et al.*, 2015).

3.3.3 The Human Cytomegalovirus gp48/UL4 uORF2 (hCMV) Stalling Mechanism

The human cytomegalovirus is a double stranded deoxyribonucleic acid (dsDNA) herpes virus with a 230 kb genome encoding ~200 genes (Schleiss *et al.*, 1991). The UL4 gene is present on a transcript comprising three uORFs and encodes a 48 kDa glycoprotein (gp48/UL4). Expression regulation is mediated in *cis* by the 22-codon uORF2 whose peptide product inhibits its own translation termination (Degnin *et al.*, 1993) preventing scanning 80S ribosomes from translation initiation at the downstream AUG start codon of the gp48/uL4 ORF (also see 1.3.2 and Figure 15).

Meeting the requirement for inhibition of translation termination the hCMV-stalling sequence was employed to stably capture 80S ribosomes with a stop codon in their A-site. Because of their impairment in peptide-release, differences in nucleotide positioning in the conserved PTC, compared to bacterial termination complexes, could provide a hint for participating residues in the reaction. Furthermore, at the intended resolution understanding the molecular mechanism of hCMV-stalling was anticipated.

To strategically analyze the importance of the individual aa residues in hCMV-peptide mediated stalling, mutational analysis was performed exchanging each residue from position 23 (stop codon) to position 7 (Ser) with an Ala (or for selected residues additionally with other relevant aa). In accordance with published results (Degnin *et al.*, 1993; Janzen *et al.*, 2002), mutation of the stop codon as well as the ultimate and penultimate Pro residues resulted in complete abolishment of the stalling mechanism in our *in vitro* translation system (see Figure 47). When Tyr19 was mutated to Ala, few free peptide was apparent, but when mutated to Phe, stalling efficiency was as for the WT emphasizing the importance of an aromatic residue at this position. Other mutations throughout the nascent chain did not have an influence on stalling efficiency which is in contrast to former read-through assays (Alderete *et al.*, 1999) revealing an influence for the mutated residues Ser12, Ala8, Ser7 and Val5. Increased incubation time for the translation reaction (from 20 to 40 min) more

sensitively revealed slight amounts of free peptide also for the Lys18Ala and Ser7Ala mutants in our system.

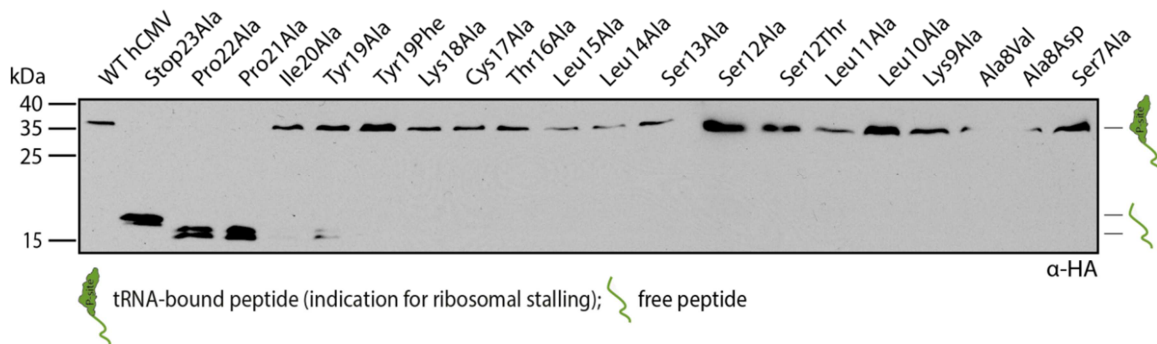


Figure 47: Mutational Scanning of hCMV-peptide Residues to Assess Their Contribution to Ribosomal Stalling.

Anti-hemagglutinin (α -HA) antibody detection of the mutated hCMV-(stalling) peptides. Point mutations from codon 23 (stop) to codon 7 (Ser) were introduced and subsequent *in vitro* translation reactions were performed. The peptidyl-tRNA content represents stalled ribosome-nascent chain complexes, yet the free-peptide content demonstrates to what extend stalling is impeded.

Figure was modified from Matheisl *et al.* (Matheisl *et al.*, 2015).

Interactions of the hCMV-peptide with the Ribosomal Exit Tunnel

As mentioned, the hCMV-peptide was well resolved from the PTC to the central constriction comprising all residues (from Ser7 to Pro22) previously reported to be important for stalling (see Figure 48). All modeling efforts to place an extended polypeptide chain into the density were to no avail. Strikingly, the density revealed an α -helical hCMV-peptide conformation in the upper part of the tunnel. The peptide was built *de novo* and contacting rRNA bases in the tunnel wall (contacts see Table 23) were adjusted from the initial model (Behrmann *et al.*, 2015) to fit the electron density and therefore their position during hCMV-peptide mediated stalling. Henceforth, the residue numbering of *Homo sapiens* (*Hs*) will be used according to Behrmann *et al.* (Behrmann *et al.*, 2015).

The resolution allowed us to model side-chains especially for the two C-terminal prolines (Pro21/22) which are indispensable for stalling (Degnin *et al.*, 1993). Their geometrical verification via PHENIX and Coot proved rather difficult highlighting their introduced tension to the whole chain. The penultimate Pro21 is stabilized by interactions with the shifted base *Hs* U4414 (*Ec* U2506) apparent by density fusion.

The shifted C-terminal peptide path, which deviates from the paths observed so far, is likely accompanied with the interaction of Ile20 and *Hs* U4494 (*Ec* U2586) which, however, according to our mutational scanning analysis, can also be established with Ala at position 20 or is non-essential for stalling. The aromatic Tyr19 is in close proximity to nucleotides *Hs* A3879 (*Ec* A2062) and *Hs* C3880 (*Ec* C2063) whereof the latter is shifted to allow for such close positioning. The contribution of an aromatic residue at position 19 to stalling becomes apparent by slight diminishing when replaced by Ala, but not by Phe during the mutational scanning. On the opposite side of the α -helix Lys18 and Leu15 are in hydrogen bonding distance to *Hs* A4411 (*Ec* A2503) and *Hs* A3876 (*Ec* A2059), respectively. Progressing down the tunnel density fusion suggests that the 28S rRNA might interact

with the nascent chain by contacting Leu14 with the *Hs* G3875 (*Ec* G2058) base, Leu11 with its sugar and Ser13 with *Hs* U4517 (*Ec* U2609).

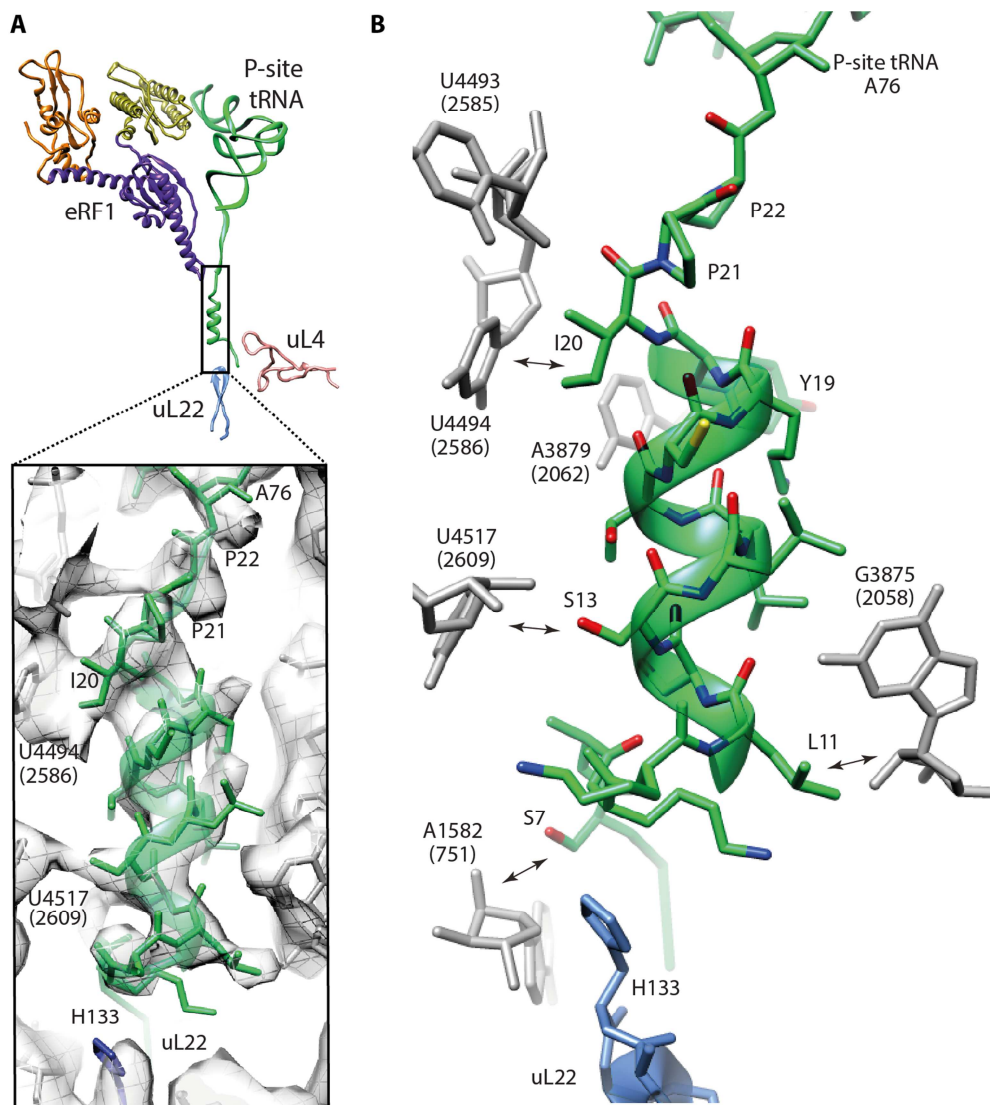


Figure 48: The hCMV-stalling Peptide.

(A) Overview of the tRNA bound to the peptidyl-tRNA binding site (P-site) (green) and of the eRF1 protein with its domains colored distinctively (N domain: light green, M domain: purple, C domain: orange). The central constriction at the ribosomal proteins uL22 (light blue) and uL4 (light pink) is also shown. The close up of the hCMV-stalling peptide (green) density (gray mesh) reveals its α -helical conformation. **(B)** Selected contacts of the hCMV-stalling peptide to the ribosome exit tunnel are indicated by double arrows.

Escherichia coli numbering of ribosomal components is given in parentheses. Figures were modified from Matheisl *et al.* (Matheisl *et al.*, 2015).

The central constriction is formed \sim 30 Å from the PTC by the ribosomal proteins uL4 and uL22 narrowing the tunnel to 10 Å. This tight passage and the surrounding area has been described as monitor in several prokaryotic stalling peptides before (Bischoff *et al.*, 2014; Nakatogawa and Ito, 2002; Sohmen *et al.*, 2015; Yap and Bernstein, 2009) which respond to certain interactions of the peptide chain with the tunnel wall. For the hCMV-stalling peptide, contacts to the base *Hs* A1582 (*Ec* A751) of the 28S rRNA near the central constriction can be observed at the height of Ser7 - Val5. The peptide helix ends at the most distal *Hs* His133 (*Ec* Lys90) of uL22. After a sharp kink of the

peptide-chain, when passing the central constriction, the peptide is less well resolved implying a certain degree of flexibility. From here on (Leu6) only a backbone trace of the peptide was placed.

Table 23: Interactions of the hCMV-peptide with Tunnel Wall Components.

Homo sapiens (*Hs*) numbering of ribosomal components is given. Additionally *Escherichia coli* (*Ec*) numbering is provided in parentheses.

hCMV-peptide Residue	Tunnel Wall Component
Pro21	<i>Hs</i> U4414 (<i>Ec</i> U2506)
Ile20	<i>Hs</i> U4494 (<i>Ec</i> U2586)
Tyr19	<i>Hs</i> A3879 (<i>Ec</i> A2062), <i>Hs</i> C3880 (<i>Ec</i> C2063)
Lys18	<i>Hs</i> A4411 (<i>Ec</i> A2503)
Leu15	<i>Hs</i> A3876 (<i>Ec</i> A2059)
Leu14	<i>Hs</i> G3875 (<i>Ec</i> G2058)
Ser13	<i>Hs</i> U4517 (<i>Ec</i> U2609)
Leu11	<i>Hs</i> G3875 (<i>Ec</i> G2058)
Ser7 - Val5	<i>Hs</i> A1582 (<i>Ec</i> A751)
Leu6 - Leu4	<i>Hs</i> Arg71 (<i>Ec</i> Thr65) of uL4

Comparison of a nascent chain harboring tunnel between *E. coli* (Bischoff *et al.*, 2014) and *H. sapiens* revealed *Hs* Arg71 (*Ec* Thr65) of uL4 to protrude much further into the tunnel in *H. sapiens* possibly contacting Leu6 - Leu4. Besides, the human uL4 protein possesses an extending loop from *Hs* Ile76 to *Hs* Phe92 at its tip which, along with the shifted base *Hs* C2773 (*Ec* C1614), narrows the tunnel down to ~10 Å. Contacts to the nascent chain at this narrowing on both sides indicate the ability to monitor peptide conformation in the tunnel even more closely in the human ribosome. Displacement of *Hs* C2773 (*Ec* C1614) might further influence the bases *Hs* A1582 (*Ec* A751) and A1583 (*Ec* A752) due to joint Mg²⁺ coordination via their backbone phosphates contributing to signal propagation. Mutation of Val5 was shown to moderately influence stalling efficiency (Alderete *et al.*, 1999). Particularly such slighter influence could render the mutation important to not completely abolish stalling, however, upregulate gp48/UL4 expression and therefore obtain altered gp48 levels in the host cell.

In brief, the hCMV-peptide heavily interacts with the ribosome exit tunnel. Considering the increased diameter of an α-helix (compared to an extended peptide chain) exceeding interactions with the narrow environment are allegable to not all contribute to ribosomal stalling. Mutational screening revealed major importance for the stop codon in the A-site as well as the ultimate and the penultimate Pro residues in silencing of the PTC and therefore mediating hCMV-stalling.

Silencing of the Peptidyl Transferase Center

Due to the presence of a stop codon in the A-site, eRF1 binding is enabled and even was demonstrated to leverage the regulatory mechanism by direct interaction with the hCMV-stalling peptide (Janzen *et al.*, 2002). To unravel the molecular interplay of eRF1 and especially its inability to efficiently hydrolyze the peptidyl-tRNA ester-bond while being bound to the ribosome, analysis of critical bases in the PTC and comparisons to the prokaryotic RF2-bound 70S ribosomal structure (Jin *et al.*, 2010) were made (see Figure 49):

Despite considerable functional and structural variations between eRF1 and the bacterial release factors RF1/RF2, their mediated release mechanisms via their GGQ motifs are thought to be

conserved. Positioning of the universally conserved GGQ motif in close proximity to the peptidyl-tRNA ester-bond in the *Thermus* and *H. sapiens* structures (Jin *et al.*, 2010) and the involvement of this motif in peptide release in both organisms as suggested by biochemical analyses (Muhs *et al.*, 2015; Seit-Nebi *et al.*, 2001; Song *et al.*, 2000) support this assumption. In our human termination complex the distance between the conserved GGQ motif and the carbonyl carbon of the ester-bond is ~ 5.2 Å (see Figures 49A, B) which is in accordance with the ability to properly coordinate a catalytic H₂O molecule being involved in the nucleophilic attack of the ester-bond. Moreover, comparison to RF2 GGQ motif and P-site tRNA CCA-end positioning in the 70S ribosome revealed high similarities (see Figure 49C). Therefore, the positioning of the human GGQ motif, as well as the tRNA CCA-end, particularly the 2'OH, which was suggested to participate in the coordination of the catalytic H₂O (Brunelle *et al.*, 2008), is assumed to be canonical during hCMV-peptide mediated stalling. Other key players for the catalytic H₂O coordination are thought to be the side-chain (Song *et al.*, 2000) or rather the backbone nitrogen of Gln185 (Korostelev *et al.*, 2008, 2010; Laurberg *et al.*, 2008; Weixlbaumer *et al.*, 2008) which is also positioned fairly canonically.

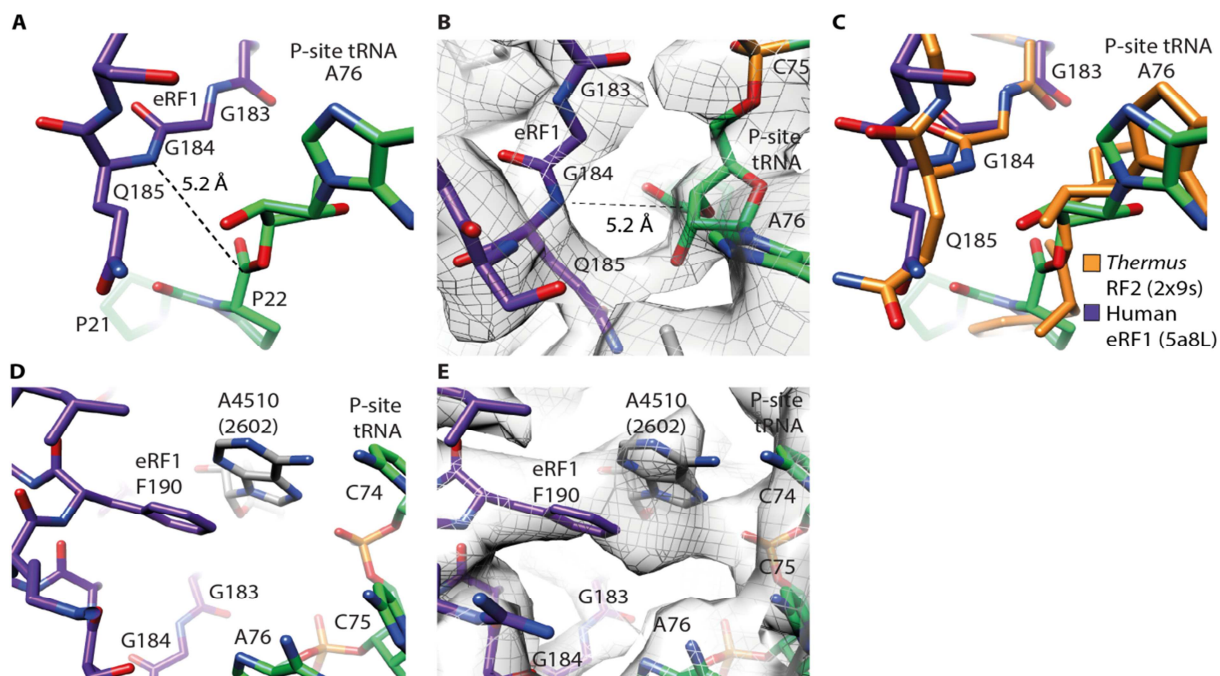


Figure 49: GGQ Motif Positioning.

The peptidyl-tRNA is indicated in green, the eRF1 C domain in orange and the ribosomal RNA in gray. All heteroatoms are colored distinctively. **(A)** The distance between the eRF1 GGQ motif (Gln185 (Q185), backbone N) and the carbonyl carbon of the tRNA ester bond is ~ 5.2 Å. **(B)** Electron density (gray mesh) for the eRF1 GGQ motif and the CCA-end of the peptidyl-tRNA. **(C)** Overlay of the conserved release factor (RF2 and eRF1) GGQ motifs and the peptidyl-tRNA CCA-ends from *Thermus thermophilus* (*Thermus*) (orange) (PDB-code: 2x9s) and human (purple/green) (PDB-code: 5a8L) revealing their nearly identical positions. **(D)** Positioning of *Hs* A4510 (*Ec* A2602) which stabilizes the GGQ-containing loop via the interaction with heRF1 Phe190 (F190). **(E)** View as in (D) showing the corresponding electron density (gray mesh).

Escherichia coli numbering of ribosomal components is given in parentheses. Figures were modified from Mattheisl *et al.* (Mattheisl *et al.*, 2015).

Further universally conserved nucleotides postulated to be critical for proper peptide release are *Hs* A4359 (*Ec* A2451) and *Hs* U4414 (*Ec* U2506) (Youngman *et al.*, 2004) which were found to be similarly positioned in our structure compared to the prokaryotic termination complex and therefore are most likely able to fulfill their intended role in the reaction. Mutational analyses revealed substantial contribution of two more PTC nucleotides to peptide-hydrolysis: *Hs* A4510 (*Ec* A2602) and *Hs* U4493 (*Ec* U2585). Nucleotide *Hs* A4510 (*Ec* A2602), which was reported to stabilize the RFs' GGQ-loops in prokaryotes, is differently positioned in the human termination complex. However, such displacement of the base is in accordance with an equally stabilizing role of *Hs* A4510 (*Ec* A2602) since its shift allows stacking on heRF1 Phe190 (see Figures 49D, E) why this movement rather demonstrates adjustment of the eukaryotic eRF1 - rRNA interaction for efficient peptide-hydrolysis mediated by this otherwise unrelated release factor.

The most remarkable difference was observed for *Hs* U4493 (*Ec* U2585) positioning which is rotated by 90° when compared to its canonical position in the human POST state (see Figures 50A, B) (Behrmann *et al.*, 2015) or the reported position before (Jin *et al.*, 2010) and subsequent (Korostelev *et al.*, 2008; Laurberg *et al.*, 2008) to peptide-release mediated by RF2 (see Figure 50C) in prokaryotes. This *Hs* U4493 (*Ec* U2585) position would be incompatible with the observed hCMV-peptide conformation owing to a sterical clash with Pro21 suggesting to be the cause for the 90° flip of *Hs* U4493 (*Ec* U2585). Such displacement most likely renders the base unable to still participate in the release reaction leading to PTC silencing and hindered translation termination. This model is consistent with mutational substitution of the penultimate Pro21 which results in complete abolishment of the stalling mechanism. This distinct *Hs* U4493 (*Ec* U2585) conformation has only been observed in ErmCL-type stalling before (see Figure 50D) where by contrast however, translation elongation is inhibited.

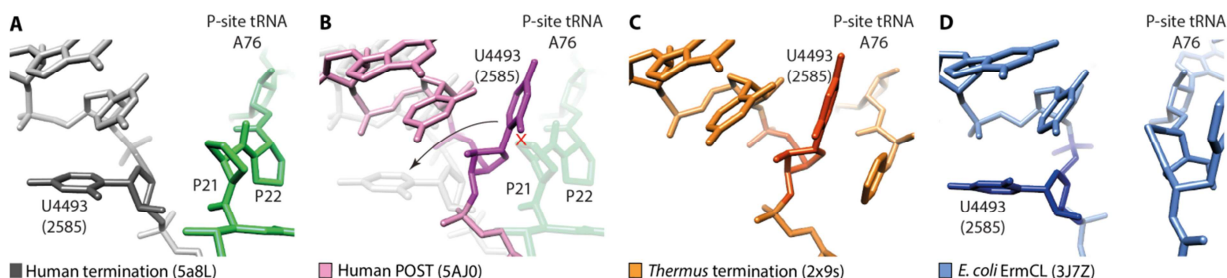


Figure 50: Flipping of the Nucleotide *Hs* U4493 (*Ec* U2585).

(A) The human termination complex (PDB-code: 5a8L) reveals a 90° flipped orientation of *Hs* U4493 (*Ec* U2585) when compared to **(B)** the human post-translocation (POST) state (pink) (PDB-code: 5AJ0). The canonical POST position of *Hs* U4493 would clash (indicated by a red cross) with the hCMV-stalling peptide Pro21 (P21) position likely being the cause for base flipping. **(C)** Position of *Hs* U4493 (*Ec* U2585) in the *Thermus Thermophilus* (*Thermus*) termination complex (PDB-code: 2x9s). **(D)** Similarly flipped position of *Hs* U4493 (*Ec* U2585) in the *Escherichia coli* (*E. coli*) ErmCL-stalled 70S complex (PDB-code: 3J7Z).

E. coli numbering of ribosomal components is given in parentheses. Figures were modified from Mattheisl *et al.* (Mattheisl *et al.*, 2015).

3.3.4 Involvement of Known heRF1 Motifs in Interactions with the Messenger and Ribosomal RNAs

Up until now, attention has been drawn to the heRF1 M domain containing the universally conserved GQQ motif involved in peptide-release. In striking contrast, stop codon recognition, which is the critical step for accurate performance of translation termination upon stop codon encounter, has evolved uniquely. This complex process is mediated via the heRF1 N domain and known to be functional during hCMV-mediated stalling. In this matter well known, repeatedly identified and confirmed motifs (albeit with different emphases and proposed interaction patterns) are the TAS-NIKS (residues 58 - 64), YxCxxxF (residues 125 - 131) and GTS (residues 31 - 33) motifs. Consequently, we analyzed positioning and interactions of such heRF1 motifs with the UAA(A) stop codon and ribosomal components (see Figures 51 and 52A).

Starting with the TAS-NIKS motif (residues 58 - 64) (see Figure 51A), it interacts with the UAA(A) stop codon from the 'top' side (the side from which the A-site tRNA anticodon approaches the mRNA during decoding). The Thr58 is in hydrogen bonding distance to adenine at position 2 (A₂). Ala59, Ile62 and Ser64 are more likely to be involved in the stabilization of the TAS-NIKS containing loop connecting the two α -helices α 2 and α 3. Ile62 seems to be important for proper uracil at position 1 (U₁) positioning via its backbone rather than for pivotal discrimination via its side-chain. Lys63 is in hydrogen bonding distance to U₁ most likely being the key residue of heRF1 to discriminate position 1 during eukaryotic stop codon recognition. Arg65 and Arg68, which were reported critical for heRF1's function on the ribosome (Blanchet *et al.*, 2015), seem to interact with h34 and h31 of the 18S rRNA rather contributing to heRF1 binding itself. In brief, the TAS-NIKS motif facilitates stop codon recognition by direct interaction with U₁ and A₂ and by stabilizing residues that make a substantial contribution to proper heRF1 binding.

The nearby positioned YxCxxxF motif (residues 125 - 131) (see Figure 51B) is likewise located in a loop region whereof the aromatic residues Tyr125 and Phe131 seem to be important for accurate positioning of the region. While Tyr125 seems to interact with Glu55 of the opposite α -helix, Phe131 stacks on Tyr96 conferring structural stability. Cys127 is likely directly involved in interactions with A₂, while Asp128 is likely to contribute to the stabilization of *Hs* A1825 (*Ec* A1493) in h44 in the anticipated flipped out position where the base is able to form stacking interactions with A₂. Therefore, Asp128 seems to indirectly engage in A₂ discrimination. Asn129 and Lys130 do not participate in stop codon decoding interactions being directed to the opposite site.

Across the tip of the YxCxxxF motif, another loop region, containing the GTS motif (residues 31 - 33) (see Figure 51C), is located. Obviously, the Gly31 cannot contribute by side-chain interactions, however, since this aa can engage in extreme ϕ - ψ torsion angles of its protein backbone and therefore a wide range of unique conformations, it seems to rather contribute to proper positioning of the whole GTS motif. Thr32 lies opposite to the adenine at position 3 (A₃) likely forming a hydrogen bond to the otherwise non-hydrogen bonded base. Ser33 likely interacts with Asn67, which neighbors the TAS-NIKS motif, facilitating the correct positioning of the participating motifs in close proximity to the UAA(A) stop codon and to each other.

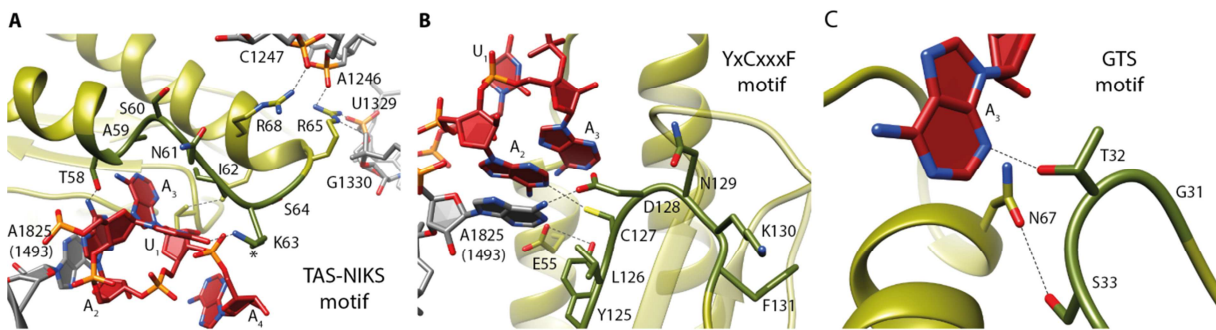


Figure 51: Interactions of Known eRF1 Motifs with the UAA(A) Stop Codon.

Overview of the interactions of: (A) The TAS-NIKS motif (dark green, residues 58 - 64) with uracil at position 1 (U_1) and adenine at position 2 (A_2) of the UAA(A) stop codon (red). The hydroxylation-site on the Lys63 (K63) side-chain C4 is indicated by *. (B) The YxCxxxF motif (dark green, residues 125 - 131) with A_2 of the UAA(A) stop codon (red) as well as with the ribosomal RNA base *Hs* A1825 (*Ec* A1493) (gray) and (C) the GTS motif (dark green, residues 31 - 33) with adenine at position 3 (A_3) of the UAA(A) stop codon (red).

H-bonds are indicated by dotted lines. Figures taken from Mattheisl *et al.* (Mattheisl *et al.*, 2015).

In addition, the adenine at position 4 (A_4), located directly 3' of the stop codon, stacks on *Hs* G626 (*Ec* G530) of h18.

Taken together, the three different motifs in the heRF1 N domain together with the rRNA bases *Hs* G626 (*Ec* G530) and *Hs* A1825 (*Ec* A1493) provide a tight binding pocket for the UAA(A) stop codon. Such cavity formation (see Figure 52B) seems to facilitate close monitoring of the right A-site codon in a three dimensional manner likely contributing to heRF1's accuracy in the stop codon decoding mechanism.

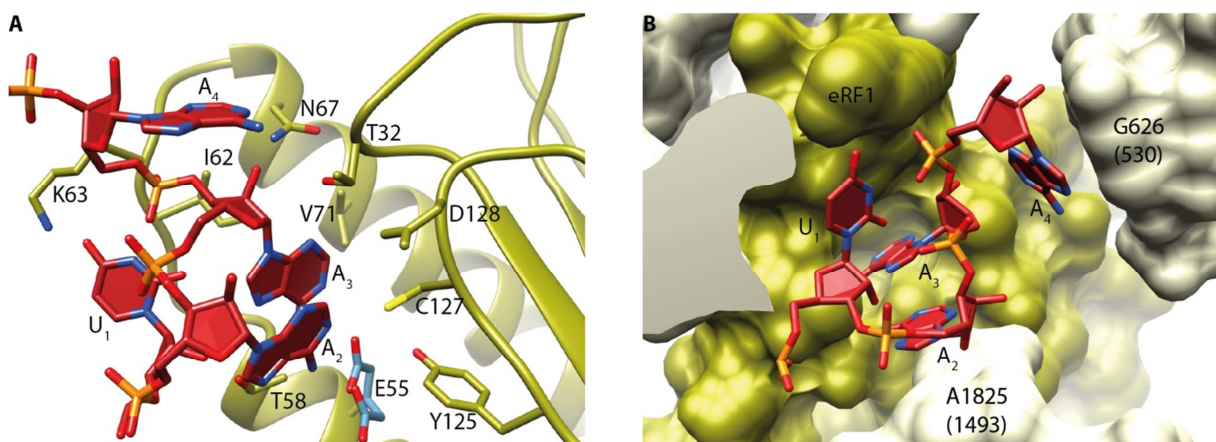


Figure 52: The UAA(A) Stop Codon Interacts with heRF1 and Ribosomal RNA.

(A) Overview of the heRF1 region (light green) in close proximity to the UAA(A) stop codon (red). (B) Cavity formed by heRF1 (light green) and the ribosomal RNA (*Hs* G626 (*Ec* G530) and *Hs* A1825 (*Ec* A1493)) (gray) which accommodates the UAA(A) stop codon (red).

Escherichia coli numbering of ribosomal components is given in parentheses. Figures taken from Mattheisl *et al.* (Mattheisl *et al.*, 2015).

3.3.5 The Stop Codon Resembles a UNR-type U-turn Geometry

As yet, a remarkable feature during the decoding mechanism of the human stop codon has been disregarded. Strikingly, the UAA(A) stop codon itself seems to participate in the accuracy of its discrimination. The adopted UAA geometry (see Figure 53A) resembles the geometry of a UNR-type U-turn motif (see Figure 53B) when heRF1 is bound whereby it significantly differs from known mRNA structures of sense codons or of the bacterial stop codons in the A-site (see Figures 53C - F). Its characteristic interaction pattern consists of an H-bond between the U_1 and the phosphate of the nucleotide at position 3 as well as an H-bond between the 2' OH of the ribose at position 1 and N7 of the purine base at position 3 (see Figures 53G, J). Such RNA conformation has not been observed for mRNA yet, however, in tRNA anticodon loops (see Figure 53H) or in parts of the 23S rRNA (see Figure 53I).

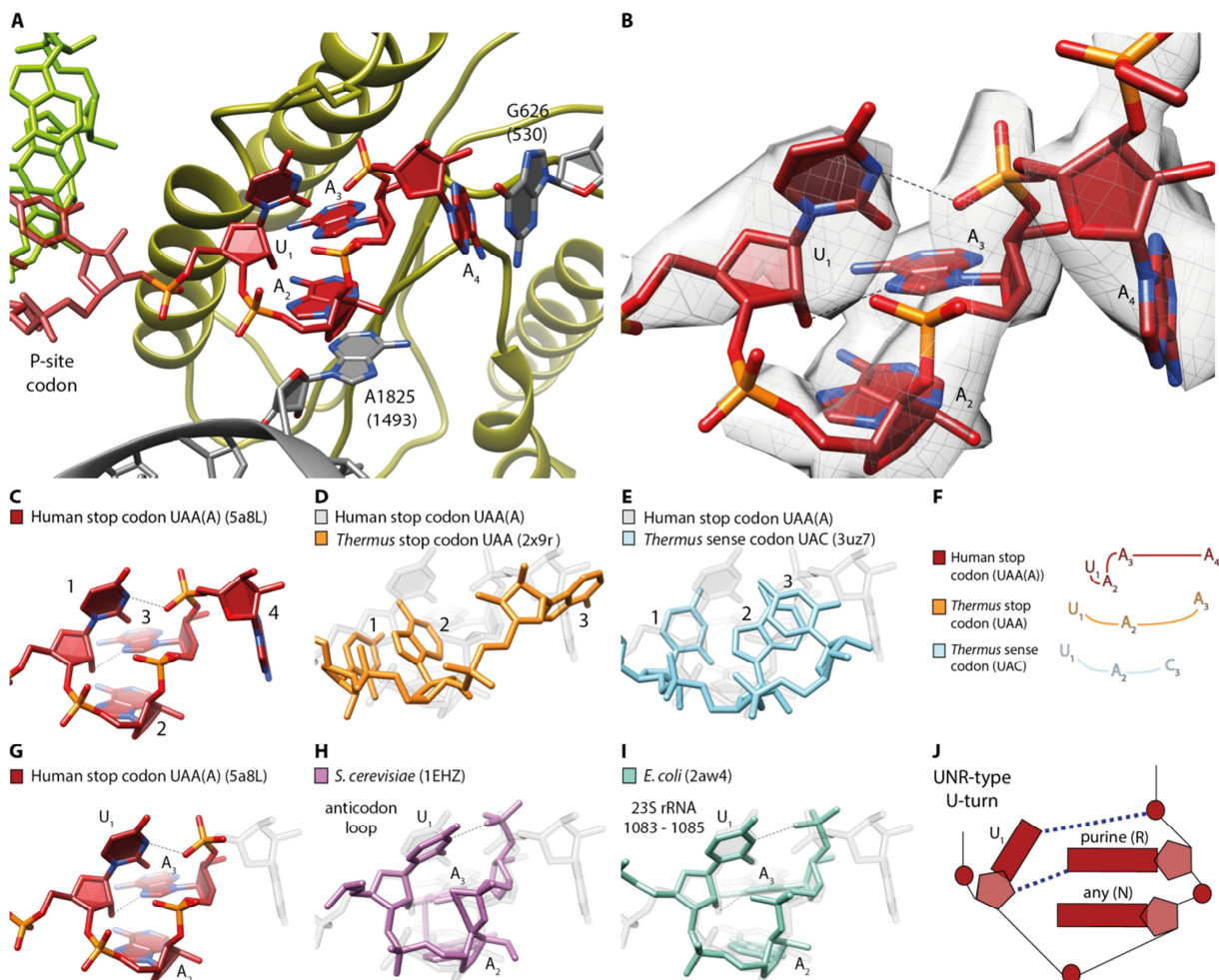


Figure 53: UNR-type U-turn Geometry.

(A) Positioning of the mRNA (red) in between heRF1 (light green), as well as in between the ribosomal RNA (rRNA) bases *Hs* A1825 (*Ec* A1493) and *Hs* G626 (*Ec* G530) (gray), reveals its unique geometry. **(B)** Electron density (gray mesh) of the UAA(A) stop codon forming a UNR-type U-turn geometry. H-bonds are indicated by dotted lines. Comparison of the A-site mRNA geometry in **(C)** the human termination complex (red) (PDB-code: 5a8L), **(D)** the *Thermus thermophilus* (*Thermus*) termination complex (orange) (PDB-code: 2x9s) and **(E)** the *Thermus* UAC decoding complex (light blue) (PDB-code: 38z7). **(F)** Schematic depiction of (C) - (E). Comparison of the UNR-type U-turn geometry in **(G)** the human termination complex stop codon (red) (PDB-code: 5a8L), **(H)** the *Saccharomyces cerevisiae* (*S. cerevisiae*) anticodon loop (light purple) (PDB-code: 1EHZ) and **(I)** the *Escherichia coli* (*E. coli*) 23S rRNA residues U1083 - A1085 (turquoise) (PDB-code: 2aw4). **(J)** Schematic depiction of (G) - (I).

Figures were modified from Mattheis *et al.* (Mattheis *et al.*, 2015).

Formation of such stop codon geometry is accompanied by further restraints on the participating base identities. Position 1 of an UNR-type U-turn has to be occupied by an uracil in order to allow for motif formation. The adenosine at position 2 is pulled into a sandwiched stacking position between the bases *Hs* A1825 (*Ec* A1493) and A₃ in addition to the direct interactions with the heRF1 motifs as described above. The UNR-type U-turn geometry provides a further constrain on position 3: Only a purine base can be positioned here which could explain why extensive discrimination via heRF1 hydrogen bonding remains absent for A₃ for the UAA(A) stop codon. The mRNA re-arrangement further propagates by pulling of A₄ into the A-site DC. Here, A₄ also engages in stacking interactions with *Hs* G626 (*Ec* G530) of h18 which contributes to the formation of the mRNA binding pocket and likely to the stabilization of the UNR-type U-turn geometry.

In conclusion, not only the discriminatory effect of the heRF1 H-bonding interaction pattern ensures the right codon identity, but also the mRNA geometry itself since such intrinsically provided constraint can offer a whole other layer of verification. Hence, stop codon decoding is dependent, but not solely reliable on heRF1. Occurring U-turn formation accompanied by stacking interactions positively contributes to the energy balance and can provide a steric frame-work for stop codon decoding which results in the high accuracy of the crucial, non-reversible process of translation termination.

4 Discussion

4.1 Sample Generation

4.1.1 Establishment of a Human *in vitro* Translation System

Groundwork for the biochemical sample preparation of the human translation termination complex was the establishment and optimization of a human *in vitro* translation extract. Even though such extract has been commercially available (by *Thermo Scientific*) its reliability and reproducibility left a lot to be desired when tested, why the development of an optimized system was indispensable.

Extract preparation was based on the protocol by Mikami *et al.* (Mikami *et al.*, 2010a), yet had to be significantly altered in context of translation initiation and accessory material. The efficiency of hCMV-peptide mediated translational stalling was monitored via Western blotting and antibody detection of the tagged product revealing sufficient material for cryo-EM sample preparation even after affinity purification. In the future, our *in vitro* translation system not only provides hCMV-stalled ribosomes for the reconstruction of the translation termination complex like in this study, but offers a wide variety to analyze translation-related events in the human system. For example, further complexes could be *in vitro* reconstituted in the context of NGD, NSD or NMD. Besides, new developments for targeted genome editing like the clustered, regularly interspaced, short palindromic repeat (CRISPR)-Cas system (reviewed in Sander and Joung, 2014) could be exploited for generating knock-out or mutated human cell-lines resulting in modified extracts which could be supplemented by separately purified factors or directly be used for the enrichment of particular functional states. Not only the purification of stalled ribosomes, but also of expressed PTM-containing proteins, is a valuable option for the application of our newly developed, robust *in vitro* translation system. Depending on the object of the study, yields could be increased by optimization of the buffer conditions, utilization of a different linker sequence between the CrPV IGR IRES and the start codon or testing various IRES elements for efficient initiation.

Wheat germ and yeast translation extracts have been abundant for years, but the complexity of the human system prohibits direct transfer of many research results. Especially in the context of human diseases, an accurate model is desirable when it comes to drug development, increasing the drugs' chances to successfully help patients and to prevent possible side effects. To this end, it is particularly useful to now be able to exploit the human *in vitro* translation system.

4.1.2 Utilization of Viral mRNA Sequences for Modulating Initiation and Stalling in the Human *in vitro* Translation System

Commonly, host infection by viral particles is detrimental for the attacked cell. Upon infection, a virus hijacks the host's replication and metabolic systems to efficiently proliferate itself. To successfully outcompete cellular processes, viruses have evolved measures to circumvent and manipulate the host's regulatory and defense systems which can be exploited as molecular research tools.

A long standing problem during human extract preparation has been the resulting reduced translation efficiency due to the phosphorylation of eIF2 α on Ser51. Such modification causes decreased canonical translation initiation of 5'-m⁷G capped mRNAs (reviewed in Kaufman, 2004). Subsequent to successful Met-tRNA_i^{Met} delivery by GTP-bound eIF2 and start-codon encounter during scanning, GTP hydrolysis results in eIF2-GDP and P_i (also see 1.2.1) (Huang *et al.*, 1997). If eIF2 α is phosphorylated, its affinity towards GDP is increased (Zeenko *et al.*, 2008) rendering its GEF eIF2B

unable to catalyze nucleotide exchange while even being sequestered. Due to its lower abundance, free eIF2B concentration can be dramatically reduced in this manner to efficiently block canonical translation initiation (Clemens, 2001; Oldfield *et al.*, 1994). Such general initiation shut down usually is employed by the cells to cope with various cellular stress conditions (see Figure 54). Four mammalian kinases are known for eIF2 α phosphorylation: Heme-regulated inhibitor (HRI) is activated by heme deficiency or oxidative stress (e.g. due to a heat shock, arsenite or osmotic stress) (Lu *et al.*, 2001; reviewed in Wek *et al.*, 2006)). Further, pancreatic eIF2 α kinase (PKR) catalyzes phosphorylation upon dsRNA presence due to viral infection. Protein kinase RNA-like endoplasmic reticulum kinase (PERK) acts upon unfolded proteins in the ER (ER stress) and general control non-derepressible 2 (GCN2) is activated upon aa deficiency, proteasome inhibition or UV irradiation.

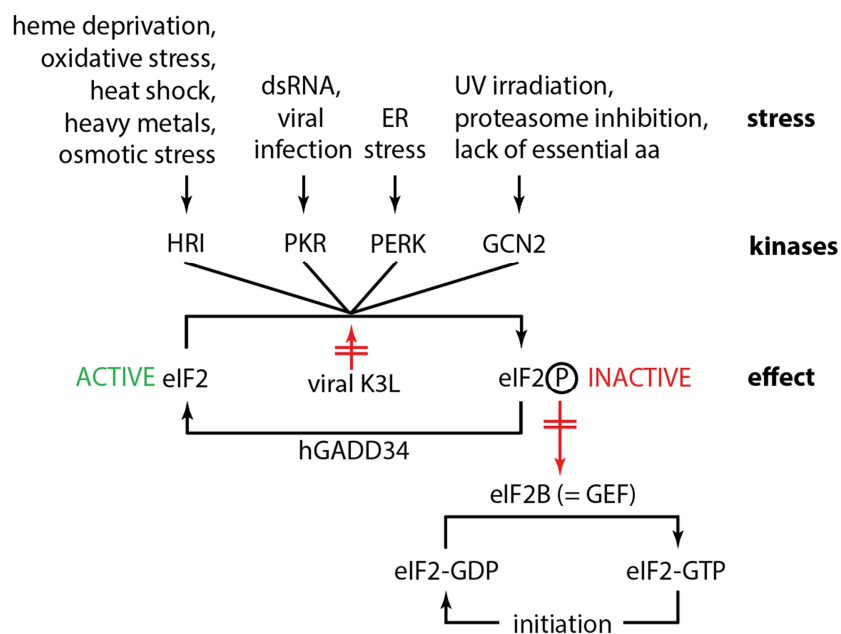


Figure 54: eIF2 Phosphorylation upon Cellular Stress.

The activating stress stimuli for the eIF2 kinases heme-regulated inhibitor (HRI), pancreatic eIF2 α kinase (PKR), protein kinase RNA-like endoplasmic reticulum kinase (PERK) and general control non-derepressible 2 (GCN2) are depicted. Kinase activity phosphorylates (P) eIF2 α on Ser51 rendering it inactive. Its guanine nucleotide exchange factor (GEF) eIF2B cannot act on the phosphorylated eIF2, why eIF2 remains in the GDP-bound state. This state is inactive in translation initiation. The viral K3L or the human growth-arrest- and DNA-damage-induced transcript 34 (hGADD34) proteins can be used to prevent eIF2 phosphorylation or activate the eIF2 phosphatase, respectively.

Also, proteins have been identified to antagonize eIF2 α phosphorylation for returning back to canonical protein synthesis or in the case of viruses to counteract the cellular defense mechanism: As first example, the human growth-arrest- and DNA-damage-induced transcript 34 (hGADD34) protein interacts with the catalytic subunit of the serine/threonine protein phosphatase 1 (PP1) comprising the holoenzyme which acts as phosphatase on eIF2 α (Ron and Harding, 2006). Second, the vaccinia virus K3L protein is an example for structural mimicry of eIF2 α (Ramelot *et al.*, 2002) consequently serving as pseudo substrate for PKR catalyzed phosphorylation competing with eIF2 α for PKR binding (Carroll *et al.*, 1993). Both, K3L and hGADD34 were attempted to be purified and supplemented as accessory proteins to the extract in this study to reduce initiation inhibition by eIF2 phosphorylation which has been shown successfully by Mikami *et al.* (Mikami *et al.*, 2006) before. Hereby, the usage of the more efficient EMCV IRES or 5' capped mRNAs might have become possible. Yet, protein

purification proved to be challenging, resulting in low yields for K3L and aggregation for hGADD34. Even hGADD34 truncation by the N-terminal 120 or 240 aa, which was reported to increase stability (Mikami *et al.*, 2010b), only decreased aggregation marginally. Additionally, no increase in translation efficiency upon EMCV IRES containing mRNA translation was noted upon the supplementation of any purified accessory protein(s) to the *in vitro* translation extract demanding for further remedial measures.

eIF2-independent initiation was anticipated in the translation extract by utilizing the viral IGR IRES mRNA element of the type IV cricket paralysis virus (construct see Figure 55) (Wilson *et al.*, 2000). With this 5' mRNA sequence translation initiation was completely independent of any eukaryotic IFs whereby the cellular defense mechanism of eIF2 phosphorylation was bypassed. Exploiting such viral initiation mechanism allowed successful target translation in the human extract even though eIF2 α -phosphorylation couldn't be prevented during extract preparation. The initiation efficiency of the CrPV IGR IRES is known to be \sim 4x less than of the EMCV IRES (Isken *et al.*, 2008), which is used in the commercial system (by *Thermo Scientific*), yet especially for stalling and therefore the absence of multiple rounds of initiation per transcript such drawback is worth the gain. Analysis of the supplementary solution that is provided in addition to the commercial translation extract revealed the abundance of multiple purified accessory proteins illustrating the complexity to circumvent eIF2 phosphorylation and to successfully perform EMCV IRES-mediated mRNA translation in the human extract.



Figure 55: Schematic of the Construct Used for *in vitro* Translation in the Human Extract.

The mRNA contained a cricket paralysis virus (CrPV) intergenic region (IGR) internal ribosome entry site (IRES) sequence for initiation, a sequence encoding for a hexahistidine ((His)₆)-tag for affinity purification, for a human influenza hemagglutinin (HA)-tag (aa 98 - 106) for Western blot detection, for parts of the dipeptidyl aminopeptidase B (DP75) and for the human hCMV-stalling sequence with a UAA(A) stop codon (stop). This was followed by a linker sequence and a 26 nucleotide poly(A) tail (p(A)₂₆). The stop codon that is relevant for UAA(A) stop codon deficient constructs during mutational scanning analysis is underlined.

Figure was modified from Matheisl *et al.* (Matheisl *et al.*, 2015).

For obtaining the translation termination complex, another viral feature besides the CrPV IGR IRES was utilized. Ribosomes were stalled at their own translation termination which is known to successfully take place upon translation of the human hCMV-peptide. hCMV-peptide mediated stalling has effectively been demonstrated before in WG and RRL extracts (Bhushan *et al.*, 2010b; Brown *et al.*, 2015; Gogala *et al.*, 2014; Preis *et al.*, 2014). As the human organism serves as natural host of the cytomegalovirus, its adaption to the human system was assumed to result in highly efficient stalling. Effectively, in the developed translation extract robust hCMV-mediated stalling could be observed generating RNCs with a stop codon in the A-site that beneficially accumulated herF1.

Stalling efficiency could be monitored via Western blotting, which mostly revealed only one single band for the peptidyl-tRNA and virtually no abundance of the free peptide, stressing stalling stability. In some RNC preparations, higher molecular weight bands at ~55 kDa and/or ~70 kDa were abundant which could represent a PTM of the peptide that does not seem to influence tRNA binding. Considering the increase in size of ~20 kDa and ~35 kDa, N- or O-linked glycosylation might be a possibility. Labeling of the nascent chain by ubiquitin for degradation as consequence of human surveillance mechanisms is rather unlikely as several chain lengths of ubiquitin would be added (Peng *et al.*, 2003) which would result in a range of bands and not in one or two defined bands. Here, mass-spectrometry analysis or PTM-specific antibodies could deliver helpful insights. As control, truncated hCMV mRNA was used for generating truncated RNCs. They contained less stably bound peptidyl-tRNA, yet such mRNA still represents a valuable option for RNC preparation in the human system. Here, the two aforementioned additional bands also occurred sporadically in the Western blots. Another possibility for these two bands could be their unspecific cross-reaction with the detecting anti-HA antibody.

Calculation of the final amount of purified, hCMV-stalled RNCs identified ~1 % of the ribosomes present in the initial translation reaction. Such limited yields highlight the drawback of the human *in vitro* translation system. For this reason, a subsequent sucrose-gradient purification was omitted as it was associated with too high material loss due to handling of low RNC amounts.

Primarily, the hCMV-peptide was exploited to successfully reconstitute a termination complex. Simultaneously though, its high-resolution structure could also reveal the molecular interaction network of the hCMV-peptide and the tunnel wall residues shedding light onto the causes of hindered peptide-release. Of course, other eukaryotic-specific stalling mechanisms like the 2A peptide, AdoMetDC, XBP1 or CPS-A could be investigated similarly in the established translation system.

In *E. coli* or lower eukaryotes RNC generation has been successfully demonstrated over the past years (Becker *et al.*, 2012; Beckmann *et al.*, 2001; Bhushan *et al.*, 2011; Halic *et al.*, 2004; Preis *et al.*, 2014; Seidelt *et al.*, 2009). Taken together, for the human system the utilization of the viral CrPV IGR IRES and the viral hCMV sequences as well as contriving the ideal buffer conditions resulted in a robust expression system from which RNCs could be successfully purified after protocol adaption for human 80S ribosomes. Consequently, as from now, the human system can be added to the list of functional home-made *in vitro* translation systems.

4.1.3 Protein Purification, Complex Formation and Ribosomal Binding

Translation termination is comprised of several steps. The GTPase eRF3 was reported to deliver eRF1 to the ribosomal A-site in a ternary complex contributing to termination efficiency (pre-termination complex) (Salas-Marco and Bedwell, 2004). After stop codon recognition by eRF1 in the DC, GTP hydrolysis is followed by eRF3 release, resulting in the elongated eRF1 conformation (Alkalaeva *et al.*, 2006; Salas-Marco and Bedwell, 2004) reaching into the PTC. Subsequently, eRF1 solely resides on the ribosome (termination complex) which was shown to be sufficient for stop codon decoding and peptide-release (Alkalaeva *et al.*, 2006; Muhs *et al.*, 2015). ABCE1 binding (pre-recycling complex) further enhances peptide-release activity whereupon ribosome recycling is initiated (Shoemaker and Green, 2011). Consequently, in all three described complexes eRF1 is bound to the A-site likely interacting with the DC and the displayed stop codon.

Purification of all participating protein factors was anticipated in parallel to reconstitute all three termination-involved complexes. Two genes (GSPT1 and GSPT2) encode two eRF3 isoforms: eRF3a and eRF3b both of which contain differences in their N-terminus (Hoshino *et al.*, 1998; Jakobsen *et al.*, 2001). eRF3b depletion was demonstrated to not affect termination efficiency in human cells. Yet, eRF3a depletion negatively influences termination efficiency and can be compensated by eRF3b which is not the case *vice versa* (Chauvin *et al.*, 2005). Furthermore, eRF3a seems to be ubiquitously expressed whereas eRF3b expression is tissue-specific (Chauvin *et al.*, 2005). For this reason, eRF3a was used for complex formation. It has proven difficult to express and purify human eRF3a from *E. coli* cells (Frolova *et al.*, 1998), why additional purification of an N-terminally truncated heRF3a protein ($\Delta(1-138)$ heRF3a) was aimed at. Since heRF1, heRF3 and GTP form a ternary complex before ribosome encounter, their complex formation was sought before conducting ribosomal binding studies. For their complex formation, one option was the co-expression and co-purification of heRF1 with heRF3a fl or $\Delta(1-138)$ heRF3a. The co-purification of heRF1 and $\Delta(1-138)$ heRF3a resulted in a clean, stoichiometric and well-concentrated complex that was shown to efficiently bind to the prepared human RNCs in binding studies and low-resolution cryo-EM reconstructions, yet only upon extensive optimization of appropriate buffer conditions. However, with adequate controls of human truncated hCMV-RNCs and RRL hCMV-stalled RNCs, specific binding could be assured under the final chosen buffers. With such conditions cryo-grid preparation did not result in the clumpy, aggregated samples as observed before for the wheat-germ/yeast pre-termination/pre-recycling complexes (Thomas Becker, personal communication) or the yeast Dom34:Hbs1 complex (Becker *et al.*, 2011). One drawback of the co-purification strategy was potential GTP-binding by heRF3a and its co-purification in the ternary complex. As precaution, high GMPPCP excess buffers were applied to displace the initially bound nucleotide. Instead of GMPPCP, guanosine 5'-[β , γ -imido]triphosphate trisodium salt hydrate (GMPPNP) (contains non-hydrolysable imido-group instead of a methylene group) was supplemented in several studies involving eRF3 before (Alkalaeva *et al.*, 2006; des Georges *et al.*, 2014; Preis *et al.*, 2014; Susorov *et al.*, 2015; Taylor *et al.*, 2012). However, GMPPNP was observed to represent a poor GTP-resembling analog for eRF3-binding (Hauryliuk *et al.*, 2006). For the truncated heRF3a protein, also individual purification could be performed successfully. For the heRF3a full length protein, however, the co-purification approach did not result in a stable complex. Here, a thioredoxin-fusion construct was crucial for individual purification (Kononenko *et al.*, 2010) which was followed by *in vitro* complex formation of the components. Final yields were low, yet sufficient for the preparation of cryo-EM samples.

eRF1 was shown to be post-translationally modified by the 2-oxoglutarate and Fe(II)-dependent oxygenase Jmjd4 (Feng *et al.*, 2014). Since the hydroxylation site resides in the TAS-NIKS Lys63 side-chain C4 and was shown to influence termination efficiency (Feng *et al.*, 2014), *in vitro* and *in vivo* hydroxylation assays were performed to obtain hydroxylated human eRF1. Even though at the possible resolution by cryo-EM the hydroxylation itself likely cannot be assigned, its influence on proper Lys63 or even TAS-NIKS loop positioning couldn't be excluded. Published results reveal an ~60 % hydroxylation efficiency by *in vitro* hydroxylation via incubation of purified eRF1, purified Jmjd4 and its co-factors (Feng *et al.*, 2014). Here, we proved an alternative *in vivo* co-expression of the two proteins which led to an ~100 % hydroxylation efficiency of Lys63 whereas no secondary hydroxylation sites could be identified via mass spectrometry.

hABCE1 could not be successfully purified from *E. coli* cells why it was expressed and purified from human HEK293T cells. Its high affinity to the plastic wall of the Eppendorf tube resulted in limitation

of the biochemical experiments conducted. Therefore, binding conditions to the 80S ribosome were transferred from the ternary heRF1:Δ(1-138)heRF3a:GMPPCP complex. heRF1 and hABCE1 were individually added to the RNCs together with adenosine 5'-(β,γ -imido)triphosphate lithium salt hydrate (AMPPNP) since during termination eRF1 binding to the 80S ribosome occurs previous to ABCE1. The two [4Fe-4S]²⁺ clusters of ABCE1 from *Pyrococcus abyssi* were reported to be inefficiently formed and oxidized during purification for which reason they were reconstituted under anaerobic conditions prior to crystallization (Karcher *et al.*, 2008). Such instability could also be possible for the human ABCE1 explaining its adherence to the tube rather than engaging in its native conformation. Its purification under anaerobic conditions could provide remedy.

For the termination complex which only contains heRF1, purified hCMV-RNCs were successfully analyzed for their natively bound heRF1 content via Western blotting and mass spectrometry. Native eRF1 abundance has already been observed before for hCMV-stalled RRL 80S ribosomes (Janzen *et al.*, 2002). Since removal of heRF1 could not be conducted by high salt washes of up to 1 M KOAc to more quantitatively bind the heRF1:heRF3 complex, this stably bound ligand was taken advantage of by directly applying the sample to cryo-EM analysis.

Capitulatory, each termination or recycling involved protein could be purified and analyzed via low-resolution cryo-EM. Ideal binding conditions were tested with the ternary heRF1:Δ(1-138)heRF3a:GMPPCP complex. In low-resolution cryo-EM, the pre-termination complex with eRF1:Δ(1-138)eRF3a:GMPPCP, the termination complex with eRF1 only and the pre-recycling complex with heRF1, hABCE1 and AMPPNP each revealed additional densities corresponding to the respective protein factors. Hereof, the termination complex was chosen for high-resolution cryo-EM studies and the application of the novel DDD technology.

4.2 Cryo-Electron Microscopy as Method of Choice

In the context of eukaryotic translation termination there have been innumerable biochemical approaches to determine the molecular details of stop codon decoding. Multitudinous mutational studies of eRF1 (and eRF3) including loss-of-function (Kolosov *et al.*, 2005; Kryuchkova *et al.*, 2013), gain-of-function (Hatin *et al.*, 2009) or inter-species domain swapping (Ito *et al.*, 2002; Seit-Nebi *et al.*, 2002) were conducted in several eukaryotic organisms all with varying read-outs. Besides, eRF1 mutations appear to differently affect codon recognition for each of the three stop codons. Such studies account for contradictory results as they virtually all presented varying outcomes, why various mechanistic models of how eRF1 recognizes and distinguishes stop codons from sense codons are existent. Here, structural data could provide the missing insights to ascertain the inconsistent results. For biological samples, basically three established methods are widely used for structural studies: NMR spectroscopy, x-ray crystallography or cryo-EM. Crystal structures of human unbound eRF1 and eRF3-bound eRF1 were already obtained in 2000 and 2009, respectively (Cheng *et al.*, 2009; Song *et al.*, 2000). The high-resolution structures of 2.8 Å and 3.8 Å, respectively allowed structural comparisons to the prokaryotic class-I RFs (Song *et al.*, 2000) and revealed eRF1's tRNA resembling shape only upon eRF3 interaction (Cheng *et al.*, 2009). Further, mapping of eRF1 interactions with eRF3 and its stimulatory effect on the eRF3 GTPase could be analyzed (Cheng *et al.*, 2009). Crystallographic studies *per se* don't suffer from a specimen size limit, however, they are associated with several challenges: The resulting resolution is dependent on well-ordered crystal packing which often requires unphysiological buffer conditions in addition to a highly homogenous,

concentrated sample. Large quantities of specimen or their inherent reluctance to crystal packing imposes further limits, not to mention the associated artefacts of crystal packing.

For detailed insight into the dynamics of eRF1, each of its three domains was determined by NMR spectroscopy (Ivanova *et al.*, 2007; Mantysyzov *et al.*, 2010; Polshakov *et al.*, 2012) analyzing peptide-hydrolysis or signal propagation from the DC in the ribosomal SSU where the stop codon is recognized to the PTC in the LSU where peptide-hydrolysis takes place (Ivanova *et al.*, 2007). Furthermore, solving stop codon recognition and the presentation of structural data on flexible regions that could not be crystallized properly was anticipated. Commonly, NMR is only applicable for molecules smaller than ~100 kDa of which likewise large quantities are required.

The main drawback of all presented eRF1 structures is their isolation from the ribosome. According to distance measurements, eRF1's ribosome-bound domain arrangement must be significantly altered for peptide-hydrolysis. Moreover, the underlying molecular mechanism for stop codon decoding can only be convincingly determined by a complex actually presenting the interaction with ribosome-bound mRNA. To this end, already several medium-resolution cryo-EM structures of the ribosome-bound eRF1:eRF3 and eRF1:Rli complexes were solved with resolutions ranging from 8.75 Å to 17 Å (des Georges *et al.*, 2014; Preis *et al.*, 2014; Taylor *et al.*, 2012). Biochemical studies revealed eRF1's capability to decode the stop codon in the ribosomal A-site as well as to subsequently hydrolyze the peptidyl-tRNA ester-bond without eRF3 (Alkalaeva *et al.*, 2006). Its stable binding was confirmed by another medium-resolution cryo-EM study of an eRF1-bound RRL 80S ribosome at 8.7 Å (Muhs *et al.*, 2015). Nevertheless, for the visualization of the intricate molecular interaction pattern that is applied for stop codon decoding, near-atomic resolution is required. To this end, cryo-EM is the method of choice as the new technological and computational advances (also see 1.4) render it superior to other methods for structural investigations of the human termination complex.

4.3 Molecular Mechanism of hCMV-peptide Mediated Stalling of the Human Ribosome

With the application of the in-house DDD equipped microscope as well as SPIDER-based computational refinement and sorting, it was possible to reconstruct the cryo-EM volume of the heRF1 containing hCMV-stalled 80S ribosome complex to an average resolution of 3.8 Å with a final set of 33,165 particles. The homogeneous dataset revealed a comparable resolution for heRF1 which was only slightly less well resolved at the C-terminus owing to a missing stability providing interaction partner like heRF3 or hABCE1.

The obtained cryo-EM volume sheds light on the molecular changes which the ribosome undergoes upon heRF1 binding and on the stop codon decoding process. Additionally, due to the utilization of the hCMV-stalling sequence, the molecular mechanism underlying the hindrance of peptide-release, even though heRF1 can stably bind to the ribosomal A-site, can be anticipated. Since here ester-bond hydrolysis is considered as conserved, differences to prokaryotic termination complexes can provide a hint concerning participating PTC components in a process which is still not completely understood.

The nascent peptide chain was modeled *de novo*. Any attempts to fit an extended peptide conformation into the cryo-EM density have failed, yet modeling an α-helix between the PTC and the central constriction revealed its proper fit. Helix formation in the exit tunnel was suggested

biochemically and computationally before (also see 1.2.5), however, its actual formation has only been observed by cryo-EM in the lower exit tunnel parts so far (Bhushan *et al.*, 2010a).

In 2010, a medium-resolution cryo-EM structure (6.7 Å) of a CMV-stalled WG ribosome was published. Here, differences in the PTC, when compared to the archaeal LSU (Ban, 2000) or to helix-RNCs (Bhushan *et al.*, 2010a), included the tip of the loop of uL16 (L10e) which connects the CCA-end of the P-site tRNA with H89. This could not be observed in the human hCMV-stalled structure. Here, the uL16 (L10e) loop is delocalized from position 103 to 113, why it most likely does not directly engage in any interactions. Notably, its position in the POST state (Behrmann *et al.*, 2015), which was used as initial fit, would have clashed with heRF1 around uL16 (L10e) positions 108/109. Since in the human hCMV-stalled structure the CCA-end is positioned rather canonically (also see Figures 49A - C), it is unlikely that uL16 (L10e) influences hCMV-peptide mediated stalling.

Further, main rRNA interaction partners in the exit tunnel were described for the hCMV-stalled WG ribosome: *Hs* 3879 (*Ec* A2062), *Hs* 4493 (*Ec* U2585), *Hs* 4517 (*Ec* U2609) and *Hs* 2875 (*Ec* A2058). In our cryo-EM structure main rRNA interaction partners for the nascent chain are *Hs* 3879 (*Ec* A2062), *Hs* 4494 (*Ec* U2586), *Hs* 4517 (*Ec* U2609) and *Hs* 2875 (*Ec* A2058) nearly matching. However, interestingly at the lower resolution of 6.5 Å an extended nascent chain conformation was modeled into the density of the WG RNC. Using PSIPRED, helical propensity was predicted after the central constriction for the midgut region around residues Ala8 to Leu14 (Bhushan *et al.*, 2010b). Such helix formation was indeed observed in our structure, however, reached up to Pro22 in the PTC whereas in the WG CMV-stalled RNC structure no density was identified at all for residues 13 - 14. Further, the nascent chain was suggested to be stabilized around residues 10 - 12 by the interaction with uL4 and uL22 forming the constriction. In our cryo-EM reconstruction residue Lys9 interacts with uL22. The following residues which constitute the N-terminal end of the α-helix reside in the constriction area. Further down in the midgut region and lower tunnel, the density gets less well resolved which is also in stark contrast to the well resolved CMV-peptide observed in the WG RNC. Notably though, in the human structure, the peptide residues here already belong to the DP75 encoding sequence.

Another apparent difference is the position of *Ec* A2602 (*Hs* A4510). The base was described as flexible in the WG CMV-stalled RNC complex. In our structure, by contrast, density could be observed for the base. This difference is reasonable as we reported stabilization of *Ec* A2602 (*Hs* A4510) by direct interaction with heRF1 Phe190. A similar interaction of *Ec* A2602 was observed in prokaryotes where it is stabilized in a pocket formed by the respective RF for correct positioning of the GGQ-loop in the PTC (Amort *et al.*, 2007; Polacek *et al.*, 2003; Youngman *et al.*, 2004). It would be particularly interesting to directly compare both molecular models of the hCMV-peptide chains, yet no PDB entry is available for the WG CMV-stalled RNC structure.

An important observation of our cryo-EM structure is the proper positioning of the heRF1 GGQ motif when compared to the crystal structure of the RF2-bound 70S ribosome (Jin *et al.*, 2010). In the human structure the distance between the carbonyl carbon of the ester-bond and the GGQ motif (Gln185, backbone N) is similar to the RF2-containing structure. For this part of the RF, inter-species comparisons are reasonable since the GGQ motif is the only highly conserved motif. Consequently, hCMV-peptide mediated stalling does not interfere in any way with GGQ motif positioning and therefore heRF1 conformation. If this was the case, one could argue conformational influence and even propagation of changes in heRF1 to the DC due to hCMV-stalling. Especially in the context of

the molecular stop codon decoding mechanism it is noteworthy that hCMV-stalling is not influential on the heRF1 conformation itself.

Closer examination of the PTC reveals a 90° flip of *Hs* U4493 (*Ec* U2585) away from the nascent chain. Since the nascent chain engages a shifted path in the PTC region, which interferes with the usual position of *Ec* U2585, this is assumed to be the cause for base evasion during hCMV-stalling. In its back flipped position, *Hs* U4493 (*Ec* U2585) likely cannot participate in ester-bond hydrolysis, why peptide-release is hindered. By contrast, in ErmCL stalling peptide-bond formation is prevented also due to a 90° flip of *Ec* U2585. Mutational studies revealed that also termination can be inhibited during ErmCL translation demonstrating a role of *Ec* U2585 in hindering termination in both stalling mechanisms. Since translation elongation is possible upon stop codon to sense codon mutation of the hCMV-peptide, it is likely that the *Ec* U2585 flip is necessary, yet not sufficient for ErmCL elongation stalling.

In contrast to the elucidation of prokaryotic stalling mechanisms, no mutational studies of tunnel wall components have been conducted so far in the human ribosome. Only a mutational screening of the nascent chain residues revealed important aa for hCMV-peptide mediated stalling (Alderete *et al.*, 1999; Degnin *et al.*, 1993; Janzen *et al.*, 2002). Here, stalling was not monitored directly however, the expression level of a downstream β-gal ORF was measured. Similarly to our mutational screening where stalling efficiency was tested in the *in vitro* translation extract for several point mutations, mutation of the ultimate and penultimate proline residues effected stalling most efficiently. This biochemical evidence perfectly correlates to our cryo-EM structure where the C-terminal peptide path of both prolines and particularly the position of the Pro21 are responsible for the *Hs* U4493 (*Ec* U2585) flip and consequently for the prevention of peptide-hydrolysis. On the contrary, the effects for the mutations of Ser7, Ala8 and Ser12 were different. The mutations Ser7Phe, Ala8Arg and Ser12Pro all showed strong impediment of stalling, resulting in read-through activity and β-gal expression (Alderete *et al.*, 1999). However, no tremendous effect was observed in our mutational screening for the Ser12Ala, Ser12Thr, Ala8Val, Ala8Asp or Ser7Ala mutations. With the structure in hands this discrepancy can be explained. The mutation by Alderete *et al.* (Alderete *et al.*, 1999) introduces the bulky residue Phe at position 7 which likely clashes with *Hs* A1582 (*Ec* A751). Since Ser12 is part of the α-helix, mutation to Pro, which is known to be a helix breaker, most likely disturbs the secondary structure of the stalling peptide which is propagated to the PTC. The Ala8 side-chain is positioned rather freely why the introduced Arg residue might influence positioning due to its highly increased length and positively charged side-chain. By contrast, the mutations conducted in our study seem to be more conservative and therefore don't seem to influence proper peptide conformation for stalling.

When modeling the peptide chain *de novo*, finding the proper conformation of Pro21/22 to fit the density and simultaneously meet geometrical restraints proved rather difficult. Here, the introduction of one or two cis-prolines could provide remedial measures however, their tautomeric state cannot be determined at this resolution. The presence of an ultimate cis-peptide could further contribute to ribosomal stalling solely at termination. Termination is known to be slower than elongation (Freistroffer *et al.*, 2000). If the time-consuming cis-proline formation is only allowed previous to peptide-release, this could explain why solely ester-bond hydrolysis cannot take place anymore. If elongation is fast enough to hinder trans-cis isomerization, the peptide-path may be altered and peptide-bond formation could still occur. At present resolution however, involvement of

isomerization is rather speculation. Furthermore, termination inhibition cannot be caused in general by two C-terminal proline residues because if so, their occurrence would be infrequent. A Swiss-Prot search by Janzen *et al.* (Janzen *et al.*, 2002) however, demonstrated a 70 % occurrence, when compared to random distribution, arguing for additional features that cause stalling at termination.

Taken together, several residues of the hCMV nascent chain might be influential on stalling as documented in other studies. Yet, in our mutational screening, stable stalling is still existent upon most mutations. Maybe the varying introduced side-chains or differences in the experimental read-out can explain the contradictory conclusions here. In general, the α -helix, with its greater diameter than an elongated nascent chain, contacts many residues of the tunnel wall. Mutations could not only influence such contacts, but also be accountable for different secondary structure formation. Certainly the ultimate and penultimate proline residues (Pro21/22) play a pivotal role as shown biochemically and structurally. The 90° flip of *Hs* U4493 (*Ec* U2585) seems to be the major reason for the inhibition of termination and is caused by the deviant peptide path taken due to the two C-terminal prolines. *Hs* U4493 (*Ec* U2585) flipping only seems to contribute to termination as compared to elongation stalling, also rendering the stop codon in the A-site indispensable. For the future, rRNA mutations of the tunnel wall would be one possibility to identify other important contact sides.

4.4 Molecular Mechanism of UAA(A) Stop Codon Decoding

Prior to peptide release, accurate stop codon decoding has to be efficiently performed to ascertain release only upon stop codon encounter. In eukaryotes, the molecular basis of stop codon discrimination by the omnipotent factor eRF1 has remained elusive for long. In prokaryotes, an H-bonding pattern between the RFs and the stop codons contributes to their discrimination (see 1.2.3). Also, during human stop codon decoding, an H-bonding network is established between the UAA(A) stop codon and heRF1 residues of the TAS-NIKS (58 - 64), YxCxxxF (125 - 131) and GTS (31 - 33) motifs contributing to decoding accuracy.

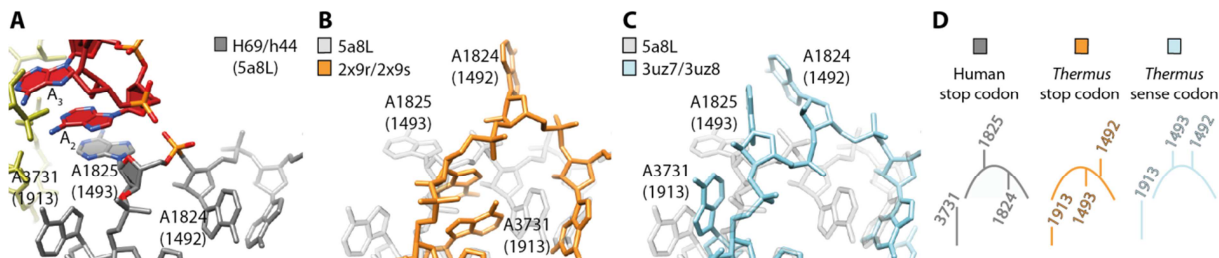


Figure 56: The Ribosome Senses the A-site mRNA Codon.

Positions of the ribosomal RNA residues *Hs* A3731 (*Ec* A1913) as part of Helix 69 (*Ec* h69) (*Hs* A1824 (*Ec* A1492) and *Hs* A1825 (*Ec* A1493) both part of helix 44 (h44) in (A) the human termination complex (gray) (PDB-code: 5a8L), (B) the *Thermus thermophilus* (*Thermus*) termination complex (orange) (PDB-codes: 2x9r and 2x9s) and (C) the *Thermus* UAC sense codon decoding ribosomal complex (light blue) (PDB-codes: 3uz7 and 3uz8). (D) Schematic depiction of (A) - (C).

Yet surprisingly, compared to prokaryotic stop codon decoding, in the human termination complex a special geometry of the A-site $U_1A_2A_3(A_4)$ stop codon is sensed: Two ribosomal bases *Hs* A1825 (*Ec* A1493) and *Hs* G626 (*Ec* G530) are employed for stacking interactions with A_2 and A_4 , respectively, stabilizing a UNR-type U-turn like conformation of the UAA stop codon. While *Hs* A1824 (*Ec* A1492) remains in h44, *Hs* A1825 (*Ec* A1493) bulges out to engage in the stacking interaction (see

Figures 56A, D). By contrast, in the *Thermus* termination complex *Ec* A1492 (*Hs* A1824) flips out of h44 and forms an H-bond with the also flipped out *Ec* G530 (*Hs* G626) (in h18) which interacts with the base at position 3 (and not 4) (see Figures 56B, D). The conformation of *Hs* A1824 (*Ec* A1492) and *Hs* A1825 (*Ec* A1493) were also reported to be important for tRNA discrimination in the A-site during elongation (also see 1.2.2). Here, however, both bases flip out of h44 (see Figures 56C, D) and interact with the displayed anticodon.

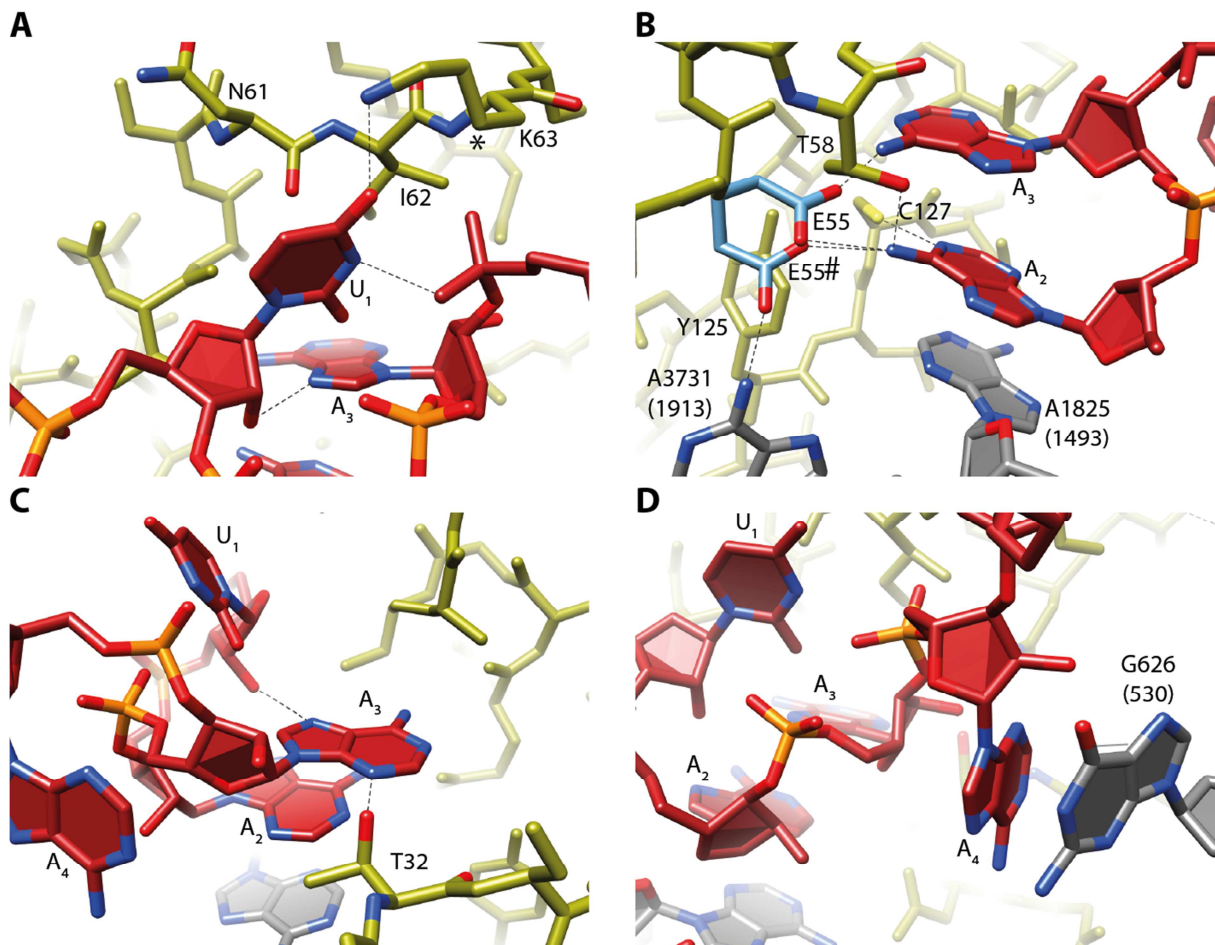


Figure 57: Close Monitoring of Each Stop Codon Residue.

(A) The uridine at position 1 engages in interactions with the TAS-NIKS motif, especially with Lys63 (K63) via its base (U₁), as well as with N7 and the backbone phosphate of adenosine 3. The hydroxylation of Lys63 (K63) is indicated by a ‘*’. **(B)** Adenine 2 (A₂) interacts with Cys127 (C127) in the YxCxxxF motif and participates in stacking interactions with A₃ and the ribosomal RNA (rRNA) residue *Hs* A1825 (*Ec* A1493). Possible rotamer conformations of Glu55 (E55) for base discrimination are depicted in light blue (E55 and E55#). **(C)** A₃ interacts with the Thr32 (T32) of the GTS motif and U₁ for U-turn formation. **(D)** Adenine 4 (A₄) stacks on the rRNA base *Hs* G626 (*Ec* G530).

Hydrogen-bonds are indicated by dotted lines. Figures were modified from Matheisl *et al.* (Matheisl *et al.*, 2015).

Unlike sense codons, where the third (wobble) position is of less importance, all three bases (and even the fourth base) contribute to stop codon decoding in the case of UAA(A). Due to U-turn formation, the fourth base is pulled into the A-site consequently participating in the decoding process. According to toe-print analyses (Alkalaeva *et al.*, 2006), a 2 nt shift occurs upon eRF1 binding to the ribosome which can be explained by further propagation of the mRNA compaction. Since such

shift is not observable without eRF1 addition, one could speculate that eRF1 actively induces U-turn conformation rather than its spontaneous formation upon A-site encounter.

The distinction between a stop and a sense codon is largely realized for position 1 (see Figure 57A) by demanding for the UNR-type U-turn conformation. This restraint excludes already all sense codons, but five (UGG, UCG, UUG, UCA and UUA). In addition, the mRNA geometry has to fit in a tight pocket formed by the rRNA residues *Hs* A1825 (*Ec* A1493) and *Hs* G626 (*Ec* G530) and by heRF1. Furthermore, Lys63 (of the TAS-NIKS motif), which was shown to cross-link to U₁ (Chavatte *et al.*, 2002), is found in H-bonding distance to U₁. The hydroxylation at the side-chain C4 of Lys63 might be involved in ideal positioning of the Lys63 side-chain for such H-bonding. Owing to size constrictions, purines would be too bulky for the binding pocket and cytosine could neither participate in U-turn formation nor in the interaction with Lys63. Consequently, several layers of verification seem to be employed to ascertain the right base identity at position 1. H-bonds of protein structures typically contribute to the energy balance by approximately 6 - 8.5 kJ/mol (1.5 - 2 kcal/mol) (Sheu *et al.*, 2003). U-turn formation is accompanied by the additional development of 2 H-bonds between U₁ and the third phosphate group of the stop codon as well as between the 2' OH group of the U₁ ribose and the N7 of the third base. Stacking interactions of *Hs* A1825 (*Ec* A1493) with A₂ and A₃ as well as of *Hs* G626 (*Ec* G530) with A₄ (see Figures 57B - D) significantly contribute in an energetic manner as stacking provides even higher Gibbs free energy (G) than H-bond formation.

The base at stop codon position 2 (here: A₂) is not directly subjected to constraints by the UNR-type U-turn conformation why it can in principle be occupied by any base. The engaged stacking interaction however, is of higher energy when formed between two purine bases (Friedman and Honig, 1995). The YxCxxF motif is localized in H-bonding distance to A₂, likely to interact with Cys127 (see Figure 57A). This interaction can only be realized with an A or G in position 2. The third position again is defined by UNR-type geometry which only allows purines. In addition, A₃ seems to interact with Thr32 of the GTS motif which would also be possible for a G in this position (see Figure 57C).

As indicated, excluding sense codons is ensured in multiple layers likely accounting for the observed high accuracy of stop codon decoding. In cross-linking experiments (Chavatte *et al.*, 2002) eRF1 was also found to interact with the near-cognate codon UGG arguing for at least transient eRF1 interaction. Since G can be found either in position 2 for UGA or position 3 for UAG, discriminating UGG as sense codon supposedly is particularly challenging possibly explaining why eRF1 interaction shortly takes place. Although no density could be observed for the Glu55 side-chain, which could derive from its flexibility, its favored rotamer conformations are positioned in H-bonding distance to the amino groups of A₂ or A₃. Therefore, it would be possible that Glu55 interacts with either of them leading to its flexibility. Negatively charged side-chains are known to be prone for early e⁻ damage and loss of their visibility (Allegretti *et al.*, 2014) which could also explain the lack of side-chain information for Glu55 in the cryo-EM density. If a UAG or a UGA stop codon is decoded, an H-bond can still be established with one A, yet, if two Gs are present simultaneously in both positions 2 and 3, Glu55 cannot form any H-bonding interaction leading to eRF1 destabilization. This would render Glu55 of major importance for the discrimination of two consecutive Gs in positions 2 and 3.

Why the identity of the base at position 4 is of such major influence on termination efficiency has been under investigation for long, however, no clear picture could be drawn. It was even shown specifically for eukaryotes that a tetra-nucleotide is necessary for successful termination (Caskey *et al.*, 1974) whereas in prokaryotes a trinucleotide is sufficient. Our cryo-EM structure reveals base 4

stacking on the purine base *Hs* G626 (*Ec* G530) for compaction and stabilization of the mRNA conformation. As mentioned, stacking is energetically more favorable for purines with purines (see Figure 58A) explaining higher efficiency and frequency of occurrence for purines at position 4 in eukaryotes (see Figure 58B). Since it is base 3 which stacks on *Ec* G530 in the case of prokaryotes, here the greatest preference for position 4 is an uridine (Tate and Mannering, 1996). Taken together, the resulting energy, when performing eukaryotic stop codon decoding, is composed of H-bonding interactions and is considerably increased by the additional utilization of several stacking interactions due to mRNA compaction and U-turn formation.

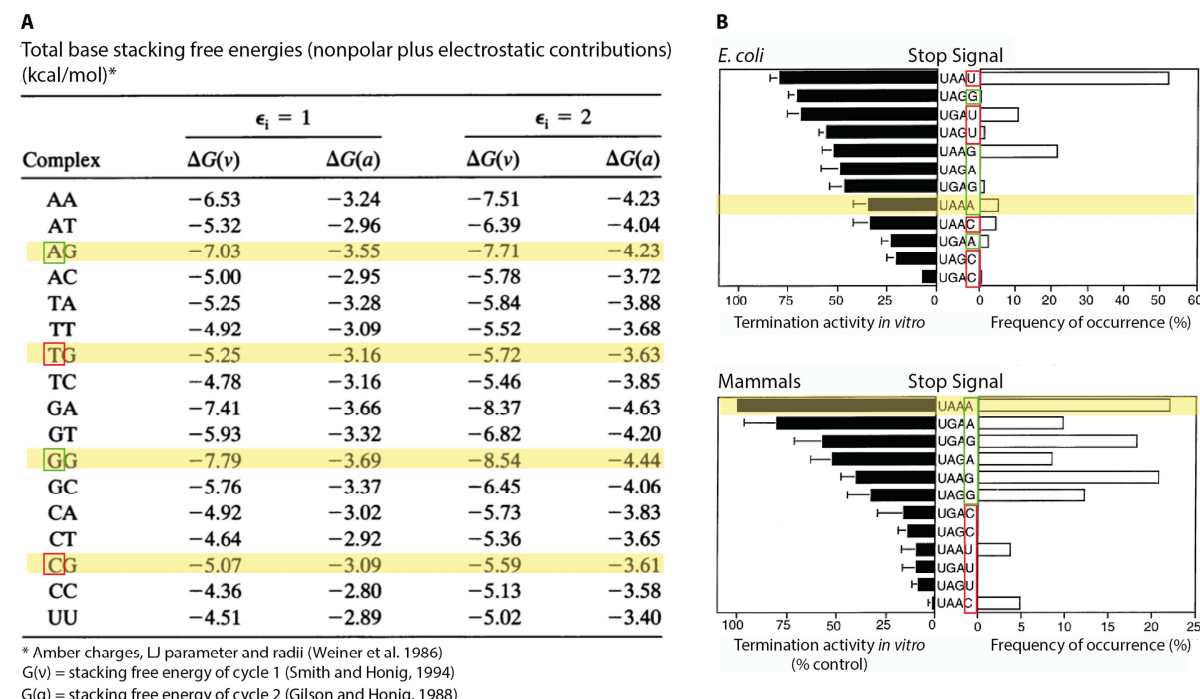


Figure 58: The Following Base (at Position 4) Influences Stop Codon Decoding.

(A) Base stacking free energies as calculated in Friedman *et al.* (Friedman and Honig, 1995) for the DNA bases adenine (A), cytosine (C), guanine (G) and thymine (T). Highlighted in yellow are the possible combinations for position 4 (boxed) when the stacking base is considered to be *Hs* G626. (T and uracil (U) are assumed to similarly contribute to base stacking energy). The pyrimidine bases C and T are boxed in red whereas the purine bases G and A are boxed in green. Cycle 1 ($\Delta G(v)$) is according to Smith *et al.* (Smith and Honig, 1994) and cycle 2 ($\Delta G(a)$) according to Gilson *et al.* (Gilson and Honig, 1988). Base stacking free energies are higher for purine-purine stacking. **(B)** Different termination activities and frequencies of occurrence for stop signals in *Escherichia coli* (*E. coli*) or mammalian cells depicting class-specific differences as reported in Tate *et al.* (Tate and Mannering, 1996). The investigated UAA(A) stop codon is highlighted in yellow. Fourth position pyrimidine and purine bases are boxed in red and green, respectively.

Figure (A) was modified from Friedman *et al.* and Figure (B) from Tate *et al.* (Friedman and Honig, 1995; Tate and Mannering, 1996).

As mentioned, the numerous mutational studies on eRF1 termination efficiency were conducted under various experimental conditions and with different stop codons. Mutated eRF1 residues could be specifically responsible for the direct recognition of either a G or an A in a particular position 2 or 3, leading to influenced termination efficiency. However, a different stop codon could also result in structural rearrangements in eRF1 that particularly occur for each stop codon. Hence, eRF1 might harbor the two different RFs that are present in prokaryotes in one single protein by alternating its

conformation in the A-site. Therefore, the essential question remains, whether mRNA and eRF1 interactions are differently mediated for the UAG and UGA stop codons than what could be observed for the UAA(A) stop codon in this study.

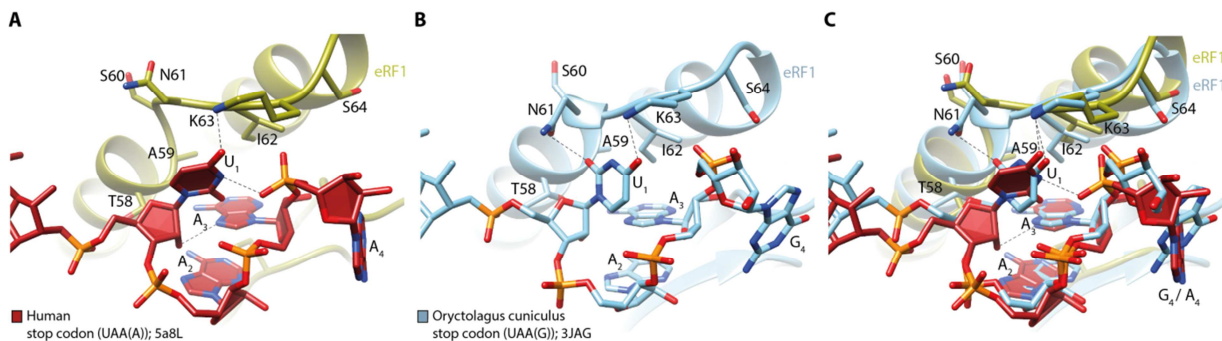


Figure 59: U-turn Like Conformation (or Maybe Not).

(A) U-turn conformation of the UAA(A) stop codon (red) in our cryo-electron microscopy (cryo-EM) derived model of the human termination complex (PDB-code: 5a8L). **(B)** Compacted geometry of the UAA(G) stop codon (light blue) in the cryo-EM derived model of the *Oryctolagus cuniculus* AAQ mutant eRF1- and ABCE1-containing termination complex (PDB-code: 3JAG) (Brown *et al.*, 2015). **(C)** Overlay of (A) and (B) revealing a ~90° turn of U₁ between the two conformations.

Hydrogen bonds are depicted via dotted lines.

Almost simultaneously to the publication of our study, Ramakrishnan and co-workers (Brown *et al.*, 2015) also revealed a cryo-EM reconstruction of the *Oryctolagus cuniculus* (*Oc*) termination complex. The experimental design allowed stalling of termination by the addition of a GGQ to AAQ mutant eRF1 protein to an RRL *in vitro* translation reaction. In this case, the extract-contained ABCE1 protein also assembled on the stalled 80S complex, however, no detailed insights were given for its interactions. An apparent discrepancy concerning stop codon decoding is the missing U-turn conformation in their molecular model (see Figure 59). Here instead, Asn61 of the TAS-NIKS motif was suggested to interact with O2 and N4 of the U₁ base which is turned by ~90°. Consequently, such U₁ positioning results in the loss of the two H-bonds due to U-turn conformation (see Figure 60A), yet allows the Asn61 side-chain to engage in H-bonding (see Figure 60B). To ascertain the precise conformation of U₁, higher resolution would be beneficial. Further, the influence of ABCE1 binding has to be analyzed carefully as it was reported to change eRF1 N domain conformation before (Preis *et al.*, 2014).

The eRF1 AAQ mutation hinders any conclusion about GGQ motif interactions and loop positioning, yet the cryo-EM reconstructions of all three stop codons by Brown *et al.* (Brown *et al.*, 2015) allowed comparison of the eRF1 conformation while decoding each kind of stop codon: The eRF1 TAS-NIKS motif is quite similarly positioned in all three molecular models while decoding UAA(G), UGA(G) or UAG(G). Interestingly, in the termination complexes of the UAA(G) and UAG(G) codons, both harboring an A at position 2, positioning of the YxCxxxF (125 - 131) and GTS (31 - 33) motifs are indistinguishable. Yet, for decoding the UGA(G) codon, both motifs adopt a different conformation. The G at position 2 causes a movement of the YxCxxxF motif towards the mRNA by ~1 Å. This movement is intertwined with a ~4 Å shift of the whole GTS loop which coincides with a turn of the Thr32 side-chain away from the stop codon (see Figure 61A). This indeed presents two varying conformations of eRF1 for the three stop codons. Mutational studies on the eRF3 GTPase function revealed different effects on termination efficiency of the three stop codons when GTP hydrolysis is

impaired (Salas-Marco and Bedwell, 2004). It appears that GTP hydrolysis is most important for UGA stop codon decoding rendering it more dependent on eRF3. Since it was shown that eRF1 engages a slightly different conformation for UGA(G) decoding (Brown *et al.*, 2015), such structural fine-tuning could gain its energy from GTP hydrolysis by eRF3.

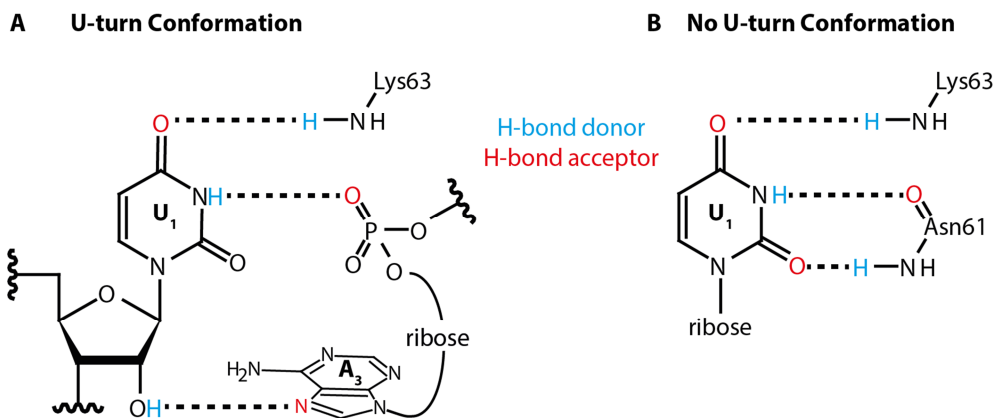


Figure 60: Potential Hydrogen bonding Patterns for the Uridine at Position 1 of the Stop Codon.

(A) Hydrogen bonding (H-bonding) pattern for uridine at position 1 with Lys63 and the adenosine at position 3 which occurs if the stop codon engages in a UNR-type U-turn conformation. Here, three hydrogen bonds (H-bonds) are formed. **(B)** H-bonding pattern for uracil at position 1 (U₁) with Lys63 and Asn61 based on the cryo-EM structure by Brown *et al.* (Brown *et al.*, 2015). Here, also three H-bonds are formed. H-bonds are depicted via dotted lines. H-bond donors are depicted in blue, H-bond acceptors in red.

Ser33Ala mutation (in the GTS motif) was analyzed via NMR spectroscopy (Blanchet *et al.*, 2015) revealing local shifts that also influence the YxCxxxF motif and particularly diminish UGA decoding. Therefore, Ser33 was interpreted to be required for G₂ read-out, yet its ability to participate in eRF1 N domain rearrangement necessary for UGA decoding could also explain its importance when a G is at position 2. Ser70Ala mutation did not introduce NMR shifts (Blanchet *et al.*, 2015), yet Ser70's H-bonding capacity is required for UGA decoding. Comparison of the three stop codon structures revealed closer positioning of Ser70 to the backbone N of Ser33 in the UGA stop codon containing structure. Maybe the H-bonding capacity of Ser70 is also necessary for the stabilization of structural rearrangements occurring in the GTS loop during proper UGA decoding.

Further, the slightly better resolved cryo-EM reconstructions of all three stop codons (Brown *et al.*, 2015) could validate a major role for the Glu55 side-chain in UGG sense codon discrimination. Together with Tyr125 the Glu55 side-chain is positioned to H-bond with the N6 of either A₂ or A₃. Interestingly, close inspection of the cryo-EM densities could not reveal side-chain density for Glu55 in the UAG(G) stop codon containing reconstruction which is best resolved (3.45 Å) (see Figure 61B). Yet, in the less well resolved UGA(G) stop codon containing reconstruction (3.83 Å) (see Figure 61C) density fusion to Tyr125 and A₃ are both prominent. Notably, for the UAA(G) stop codon containing reconstruction (3.65 Å) (see Figure 61D) the Glu55 side-chain seems to be placed slightly different which leads to density fusion rather with A₂. Nonetheless, a guanine base harbors an oxygen at position 6 (O6) which cannot engage in a similar H-bond with Glu55. The UGG sense codon however only contains 2Gs. Not only would their repulsion with each other, but also with Glu55 hinder engagement in similar conformations as observed for any of the three stop codons (see Figure 61E).

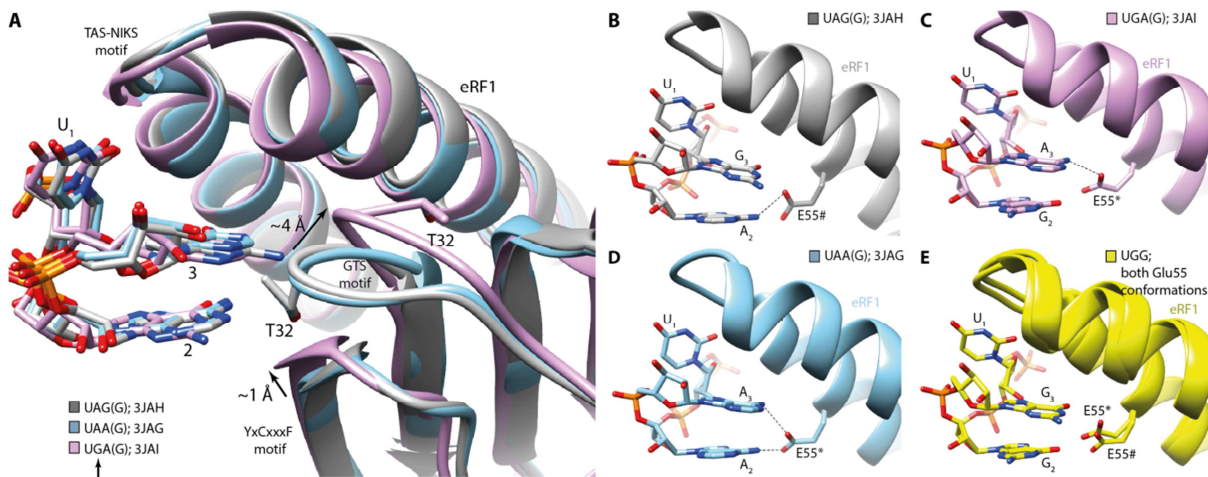


Figure 61: Alternating eRF1 Conformations During Different Stop Codon Decoding.

(A) According to Brown *et al.* (Brown *et al.*, 2015) eRF1 engages in different conformations depending on the base identity at position 2 of the stop codon. During UAG (gray) and UAA (light blue) decoding the YxCxxxF and the GTS motifs are positioned similarly. However, during UGA (light pink) decoding the YxCxxxF motif is shifted by ~ 1 angstrom (\AA) towards the stop codon which causes a shift of ~ 4 \AA in the GTS motif containing loop combined with a flip of the Thr32 (T32) side-chain. Also according to Brown *et al.* (Brown *et al.*, 2015) Glu55 (E55) is the key player in stop codon discrimination always interacting with **(B - D)** an adenine (A) base at position 2 and/or at position 3, explaining why **(E)** UGG is not recognized as stop codon. Here, both Glu55 rotamers are depicted (E55# and E55*) neither capable of hydrogen bonding to the guanine at position 2 or 3.

Two-step models have been suggested before for stop codon decoding by eRF1 (Blanchet *et al.*, 2015; Bulygin *et al.*, 2011; Kryuchkova *et al.*, 2013), however, were rather speculated in a time-wise manner. Initial ribosome engagement of eRF1 in the ternary complex could specifically recognize the three stop codons and upon structural rearrangements to move the M domain into the PTC also the N domain could engage in altered interactions. Such movement would be energy consuming yet, could serve as additional layer of control. Certainly, it could account for the various results during mutational studies. To ascertain the initial interaction of eRF1 with the mRNA stop codon, a high-resolution structure of the ternary complex on the ribosome would be clarifying.

Taken together, due to all acquired cryo-EM structures, novel invaluable insights have been gained of how one omnipotent factor can accomplish decoding of all three stop codons. If the mRNA simply undergoes compaction to engage in the H-bonding interactions with eRF1 or forms a UNR-type U-turn to contribute to its recognition remains to be elucidated. For any scenario, it is likely that the stop codon capacity to form the right geometry is monitored by eRF1 and the ribosome. The knowledge whether the mRNA codon forms compaction by itself or only upon eRF1 binding could particularly help to better understand the phenomenon of stop codon read-through. Analysis of the cryo-EM particles which harbor the stop codon in the A-site yet did not bind eRF1 might provide answers. It is questionable however, if the stop codon is sufficiently stabilized by its rRNA contacts to reveal density of high resolution. The mentioned toe-print assay, which only revealed a 2 nt shift upon eRF1 binding (Alkalaeva *et al.*, 2006), argues against an mRNA compaction by mere presence of the stop codon in the A-site.

The idea of including geometry for increasing fidelity in biological processes has been demonstrated before where precise and rapid progression is of high importance. For example, during translation elongation the A-site mRNA codon and any bound tRNA anticodon form a short A-helix whose

Watson-Crick geometry (for the first 2 nucleotides) is enforced by the aforementioned rRNA bases *Ec* G530 (*Hs* G626), *Ec* A1492 (*Hs* A1824) and *Ec* A1493 (*Hs* A1825) (Demeshkina *et al.*, 2012; Ogle *et al.*, 2003) together with constraints imposed by a P/A kink in the mRNA coordinated by a Mg²⁺ ion and the r-protein S12 (see Figures 62A, B). It was suggested that near- or non-cognate tRNA binding is accompanied by high energy loss due to their restricted geometry, therefore leading to anticodon discrimination (see Figure 62C and 1.2.2). Here, the right geometry formation is not actively sensed, yet enforced geometry is utilized for high fidelity discrimination (Demeshkina *et al.*, 2012).

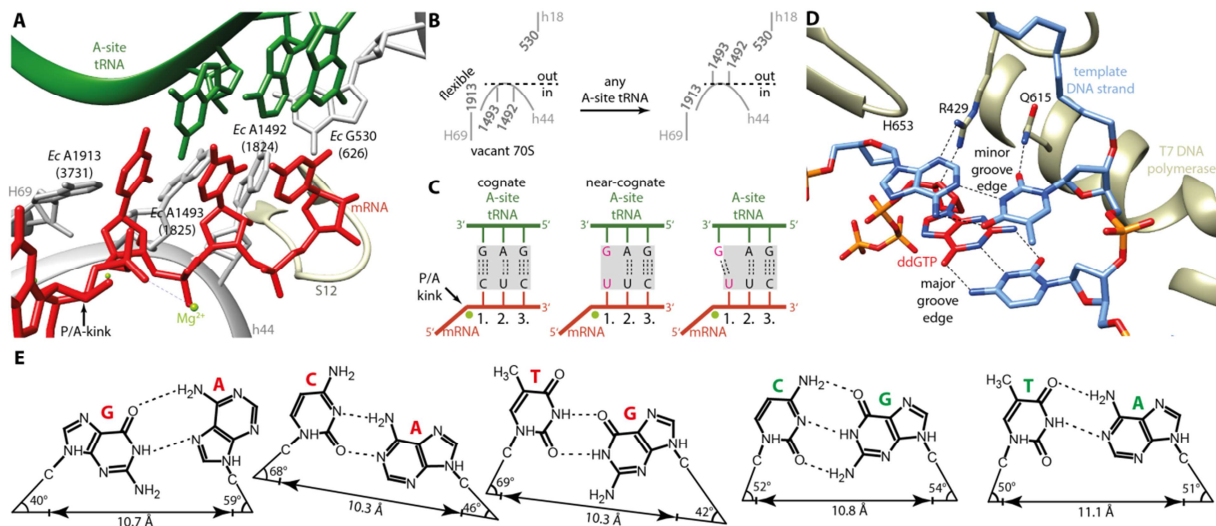


Figure 62: Specific Geometry Formation Contributes to High Fidelity Processes.

(A) In the aminoacyl-tRNA binding site (A-site): Enforcing geometry of the mRNA codon (red) - tRNA anticodon (green) A-minor helix by the ribosomal RNA (rRNA) bases *Ec* G530 (*Hs* G626), *Ec* A1492 (*Hs* A1824) and *Ec* A1493 (*Hs* A1825) (gray) contributes to accuracy of translation elongation. Cognate and non-cognate A-site tRNA binding reveal similar Watson-Crick geometry. In the case of near- or non-cognate tRNAs the required energy for tautomerization or repulsion to fit the enforced geometry leads to tRNA dissociation (PDB-codes: 3TVE and 3TVF). *Escherichia coli* (*Ec*) numbering is given. Human numbering is in parentheses. **(B)** Schematic representation of the rRNA bases *Ec* G530 (*Hs* G626), *Ec* A1492 (*Hs* A1824), *Ec* A1493 (*Hs* A1825) and *Ec* A1913 (*Hs* A3731) (gray) in the decoding center (DC) of a vacant 70S (left) ribosome or during A-site occupation by any cognate, near-cognate or non-cognate tRNA (right). **(C)** Schematic representation of the A-site interactions: The geometry of the first two codons is restricted by the DC (h18, h44, H69 and S12) together with the P/A kink (indicated on the left) which is coordinated by a Mg²⁺ ion (light green). Cognate tRNA binding (left) leads to hydrogen bonding (H-bonding) between the codon and the anticodon. Near-cognate tRNA binding (non-matching bases indicated in pink) leads to enforced Watson-Crick geometry (middle) whereas its geometrically favored wobble base pair geometry (right) would have resulted in two hydrogen bonds if its formation had been possible. **(D)** Active geometry sensing mediated by the T7 DNA polymerase (beige) which contributes to the accuracy of replication. Arg429 (R429) and Gln615 (Q615) of the polymerase form H-bonding interactions to the DNA minor groove (PDB-code: 1T7P) (Doublie *et al.*, 1998). A mismatch, resulting from nucleotide (ddGTP) miss-incorporation by the polymerase, introduces distortions that might lead to the loss of H-bonding. **(E)** Geometry of DNA base pairs according to Hunter *et al.* (Hunter *et al.*, 1986). Distances are given for both C1' atoms and angles are given between the C1' – C1' distance vector and the C1' – N1 (N9) bond showing differences for the Watson-Crick base pairs (green) and non-Watson-Crick base pairs (red).

Figure (C) based on Demeshkina *et al.* (Demeshkina *et al.*, 2012) and Figure (E) on Hunter *et al.* (Hunter *et al.*, 1986).

The concept of enclosing geometric shapes is not only restricted to the ribosome. Another process where a molecular machine examines geometry to add to its high fidelity is applied during DNA synthesis. Here, the DNA polymerase incorporates dNTPs with error frequencies of $\sim 10^{-5}$ to $\sim 10^{-6}$

(Doublié *et al.*, 1998) essential for accurate genome replication. The correct selection of the Watson-Crick base pair is favored by the formation of H-bonds of the incoming dNTP with the DNA template base. Yet, in this high fidelity process, base-pairing and concomitant H-bonding is not enough to account for the great accuracy. Liu *et al.* (Liu *et al.*, 1997) designed a study where a dTTP with a non-standard difluorotoluene (dF) base was incorporated. Its isosterity to the thymine (T) pyrimidine ring combined with its poor base-pairing capacity to any DNA base still allowed its successful incorporation in lieu of T with only slightly diminished fidelity. Consequently, this experiment demonstrated the importance of size and shape of the base pair rather than solely the H-bonding network. In subsequent studies, interactions of the polymerase to the minor groove of the DNA proved crucial for the geometric selection (Brown and Kennard, 1992; Seeman *et al.*, 1976). More specifically, based on crystal structures (Doublié *et al.*, 1998; Kiefer *et al.*, 1998; Li, 1998), the DNA polymerase residues Arg429 and Gln615 interact with the minor groove N3 of the primer 3' end and O3 of the corresponding template base, respectively (see Figure 62D) (Doublié *et al.*, 1998). A mismatch, resulting from dNTP miss-incorporation by the polymerase, introduces distortion in three geometric parameters: The width of the base pair and the two angles between the C1' – C1' distance vector and the C1' – N1 (N9) bonds of the two nucleotides (see Figure 62E) (Hunter *et al.*, 1986). Such distortion might be sensed as loss of one or both of these minor groove interactions of the DNA polymerase. Furthermore, upon nucleotide binding, a large conformational change in the DNA polymerase defines tightness of the active site and determines strictness of the geometric restraints. Here again, the conformational change can only accommodate a properly fitting base-pair.

Accordingly, to also include geometry formation in the irreversible process of translation termination would be reasonable considering its high fidelity and importance in protein synthesis. Whether mRNA compaction is monitored or specifically the capability of U-turn conformation cannot be surely determined at present resolutions. Yet, the acquired cryo-EM reconstructions present the basis for more specifically designed mutational and biochemical assays which can assist in unraveling remaining questions in the context of stop codon decoding.

5 Summary and Outlook

This dissertation presents a high-resolution cryo-EM structure of the human translation termination complex, unraveling the stop codon recognition mechanism during translation termination.

Due to the absence and costliness of reliable commercial human *in vitro* translation systems, we optimized our own enhanced HeLa cell based *in vitro* translation extract. This extract was utilized to obtain hCMV-stalled human 80S ribosomes which harbor an mRNA stop codon (UAA(A)) in the A-site and allow efficient binding of human eRF1. Affinity purification of the complex revealed homogenously and stably stalled ribosomes with a Pro-tRNA bound to the P-site and heRF1 bound to the A-site. Subsequent cryo-EM recording of 245,253 particles with a Titan Krios equipped with a DDD and *in silico* sorting to 33,165 particles resulted in the reconstruction of the termination complex with an overall resolution of 3.8 Å (FSC_{0.143}). The local resolution determination revealed similarly resolved heRF1. Rigid body fitting of the human POST state ribosome (Behrmann *et al.*, 2015) demonstrated its large accordance with our cryo-EM density. Single nucleotides and aa, especially in the PTC, the exit tunnel region and at the DC could be identified to harbor a different conformation due to stalling or heRF1 binding and were adapted accordingly. As expected at this resolution, the pitch of alpha helices, beta-stand separation and most bulky side-chains could be visualized. This allowed modeling of heRF1 based on the ribosome-unbound crystal structure (Cheng *et al.*, 2009) which had to be heavily adjusted for the ribosome-bound state. Further, our density allowed *de novo* modeling of the C-terminal part of the hCMV-stalling peptide and the localization of the two for stalling indispensable ultimate and penultimate prolines which cause flipping of *Hs* U4493 (*Ec* U2585) by 90° hindering its participation in the chemical reaction of peptide-bond hydrolysis therefore being the cause for termination stalling. Surprisingly, from the PTC to the central constriction, the nascent chain engages in an α-helical conformation. Starting from Leu6, positioned at the central constriction, to the N-terminus a backbone trace of the nascent chain could be followed through the exit tunnel. Overall, the α-helix numerously contacts the tunnel wall, yet not all contacting residues seem to be essential for stalling which was demonstrated by mutational scanning analysis.

eRF1 itself was bound in its elongated state reaching from the DC to the PTC. Conformations of the conserved eRF1 GGQ motif in the PTC, as well as the P-site tRNA CCA end, were comparable to their prokaryotic counterparts. In the DC, however, the RFs from prokaryotes and eukaryotes as well as their influence on the ribosome differ greatly. The afore identified TAS-NIKS, YxCxxxF and GTS motifs of eRF1 indeed play a crucial role for stop codon decoding by H-bonding to the three bases UAA. Furthermore, heRF1, as well as the rRNA bases *Hs* A1825 (*Ec* A1493) and *Hs* G626 (*Ec* G530), is involved in cavity formation into which the UAA(A) stop codon is pulled. The mRNA conformation is stabilized by base stacking interactions with A₂ and A₄ accounting for energy gain. Strikingly, the UAA bases engage in a hitherto unique mRNA geometry which has, however, been observed for tRNA and rRNA elements before. More precisely, utilizing the stop codon's capacity to form a UNR-type U-turn geometry as read-out element introduces an additional layer of accuracy by putting restraints on the three involved bases. Position 1 can only be taken by a uracil base and position 3 has to be a purine base. Consequently, such U-turn geometry can only be formed by eight existing codons already omitting 56 sense codons from mistakenly being interpreted as termination signal. The formation of the tight cavity, base stacking and specific H-bonding patterns further confer high fidelity to stop codon decoding by heRF1.

For the future, the established *in vitro* translation extract lays the groundwork for the purification of other eukaryote-specific stalling complexes and for the *in vitro* reconstitution of other human 80S complexes. As always, highest possible resolution of the human termination complex to provide more detailed insights on the molecular mechanism of stop codon decoding or for example to account for the contribution of the Lys63 hydroxylation will be further aspired. Yet, this cryo-EM structure already provides various novelties, aspects and insights to the long-standing question of stop codon decoding in eukaryotes which can now be used as inspiration for skillfully designed prospective research assays in this context.

6 References

Abaeva, I.S., Marintchev, A., Pisareva, V.P., Hellen, C.U.T., and Pestova, T. V (2011). Bypassing of stems versus linear base-by-base inspection of mammalian mRNAs during ribosomal scanning. *EMBO J.* **30**, 115–129.

Acker, M.G., Shin, B.-S., Dever, T.E., and Lorsch, J.R. (2006). Interaction between eukaryotic initiation factors 1A and 5B is required for efficient ribosomal subunit joining. *J. Biol. Chem.* **281**, 8469–8475.

Adams, P.D., Afonine, P. V, Bunkóczki, G., Chen, V.B., Davis, I.W., Echols, N., Headd, J.J., Hung, L.-W., Kapral, G.J., Grosse-Kunstleve, R.W., et al. (2010). PHENIX: a comprehensive Python-based system for macromolecular structure solution. *Acta Crystallogr. D. Biol. Crystallogr.* **66**, 213–221.

Adrian, M., Dubochet, J., Lepault, J., and McDowall, A.W. (1984). Cryo-electron microscopy of viruses. *Nature* **308**, 32–36.

Agirrezabala, X., Lei, J., Brunelle, J.L., Ortiz-Meoz, R.F., Green, R., and Frank, J. (2008). Visualization of the hybrid state of tRNA binding promoted by spontaneous ratcheting of the ribosome. *Mol. Cell* **32**, 190–197.

Agrawal, R.K., Penczek, P., Grassucci, R.A., and Frank, J. (1998). Visualization of elongation factor G on the *Escherichia coli* 70S ribosome: the mechanism of translocation. *Proc. Natl. Acad. Sci. U. S. A.* **95**, 6134–6138.

Aitken, C.E., and Lorsch, J.R. (2012). A mechanistic overview of translation initiation in eukaryotes. *Nat. Struct. Mol. Biol.* **19**, 568–576.

Alderete, J.P., Jarrahian, S., and Geballe, A.P. (1999). Translational effects of mutations and polymorphisms in a repressive upstream open reading frame of the human cytomegalovirus UL4 gene. *73*, 8330–8337.

Algire, M.A., Maag, D., Savio, P., Acker, M.G., Tarun, S.Z., Sachs, A.B., Asano, K., Nielsen, K.H., Olsen, D.S., Phan, L., et al. (2002). Development and characterization of a reconstituted yeast translation initiation system. *RNA* **8**, 382–397.

Algire, M.A., Maag, D., and Lorsch, J.R. (2005). Pi release from eIF2, not GTP hydrolysis, is the step controlled by start-site selection during eukaryotic translation initiation. *Mol. Cell* **20**, 251–262.

Alhebshi, A., Sideri, T.C., Holland, S.L., and Avery, S. V (2012). The essential iron-sulfur protein Rli1 is an important target accounting for inhibition of cell growth by reactive oxygen species. *Mol. Biol. Cell* **23**, 3582–3590.

Alkalaeva, E.Z., Pisarev, A. V, Frolova, L.Y., Kisseelev, L.L., and Pestova, T. V (2006). In vitro reconstitution of eukaryotic translation reveals cooperativity between release factors eRF1 and eRF3. *Cell* **125**, 1125–1136.

Allegretti, M., Mills, D.J., McMullan, G., Kühlbrandt, W., and Vonck, J. (2014). Atomic model of the F420-reducing [NiFe] hydrogenase by electron cryo-microscopy using a direct electron detector. *Elife* **3**, e01963.

Alone, P. V, and Dever, T.E. (2006). Direct binding of translation initiation factor eIF2gamma-G domain to its GTPase-activating and GDP-GTP exchange factors eIF5 and eIF2B epsilon. *J. Biol. Chem.* **281**, 12636–12644.

Amort, M., Wotzel, B., Bakowska-Zywicka, K., Erlacher, M.D., Micura, R., and Polacek, N. (2007). An intact ribose moiety at A2602 of 23S rRNA is key to trigger peptidyl-tRNA hydrolysis during translation termination. *Nucleic Acids Res.* **35**, 5130–5140.

Amunts, A., Brown, A., Bai, X., Llácer, J.L., Hussain, T., Emsley, P., Long, F., Murshudov, G., Scheres, S.H.W., and Ramakrishnan, V. (2014). Structure of the yeast mitochondrial large ribosomal subunit. *Science* **343**, 1485–1489.

Amunts, A., Brown, A., Toots, J., Scheres, S.H.W., and Ramakrishnan, V. (2015). Ribosome. The structure of the human mitochondrial ribosome. *Science* **348**, 95–98.

Andersen, D.S., and Leever, S.J. (2007). The essential *Drosophila* ATP-binding cassette domain protein, pixie, binds the 40 S ribosome in an ATP-dependent manner and is required for translation initiation. *J. Biol. Chem.* **282**, 14752–14760.

Andersen, C.B.F., Ballut, L., Johansen, J.S., Chamieh, H., Nielsen, K.H., Oliveira, C.L.P., Pedersen, J.S., Séraphin, B., Le Hir, H., and Andersen, G.R. (2006). Structure of the exon junction core complex with a trapped DEAD-box ATPase bound to RNA. *Science* **313**, 1968–1972.

Anderson, K., Bhat, M., Kiehart, D., Fehon, R., Cavener, D., Oda, H., Petitt, M., Ito, K., Uno, M., and Nakamura, Y. (2000). A tripeptide “anticodon” deciphers stop codons in messenger RNA. *Nature* **403**, 680–684.

Anfinsen, C.B., and Haber, E. (1961). Studies on the Reduction and Re-formation of Protein Disulfide Bonds. *J. Biol. Chem.* **236**, 1361–1363.

Anfinsen, C.B., Redfield, R.R., Choate, W.L., Page, J., and Carroll, W.R. (1954). Studies on the gross structure, cross-linkages, and terminal sequences in ribonuclease. *J. Biol. Chem.* **207**, 201–210.

Anger, A.M., Armache, J.-P., Berninghausen, O., Habeck, M., Subklewe, M., Wilson, D.N., and Beckmann, R. (2013). Structures of the human and *Drosophila* 80S ribosome. *Nature* **497**, 80–85.

Apiyo, D., and Wittung-Stafshede, P. (2002). Presence of the cofactor speeds up folding of *Desulfovibrio desulfuricans* flavodoxin. *Protein Sci.* **11**, 1129–1135.

Arenz, S., Meydan, S., Starosta, A.L., Berninghausen, O., Beckmann, R., Vázquez-Laslop, N., and Wilson, D.N. (2014a). Drug sensing by the ribosome induces translational arrest via active site perturbation. *Mol. Cell* **56**, 446–452.

Arenz, S., Ramu, H., Gupta, P., Berninghausen, O., Beckmann, R., Vázquez-Laslop, N., Mankin, A.S., and Wilson, D.N. (2014b). Molecular basis for erythromycin-dependent ribosome stalling during translation of the ErmBL leader peptide. *Nat. Commun.* **5**, 3501.

Armache, J.-P., Jarasch, A., Anger, A.M., Villa, E., Becker, T., Bhushan, S., Jossinet, F., Habeck, M., Dindar, G., Franckenberg, S., et al. (2010a). Localization of eukaryote-specific ribosomal proteins in a 5.5-Å cryo-EM map of the 80S eukaryotic ribosome. *Proc. Natl. Acad. Sci. U. S. A.* **107**, 19754–19759.

Armache, J.-P., Jarasch, A., Anger, A.M., Villa, E., Becker, T., Bhushan, S., Jossinet, F., Habeck, M., Dindar, G., Franckenberg, S., et al. (2010b). Cryo-EM structure and rRNA model of a translating eukaryotic 80S ribosome at 5.5-Å resolution. *Proc. Natl. Acad. Sci. U. S. A.* **107**, 19748–19753.

Artimo, P., Jonnalagedda, M., Arnold, K., Baratin, D., Csardi, G., de Castro, E., Duvaud, S., Flegel, V., Fortier, A., Gasteiger, E., et al. (2012). ExPASy: SIB bioinformatics resource portal. *Nucleic Acids Res.* **40**, W597–W603.

Asano, K., Krishnamoorthy, T., Phan, L., and Pavitt, G.D. & Hinnebusch, A.G. (1999). Conserved bipartite motifs in yeast eIF5 and eIF2B ϵ , GTPase-activating and GDP–GTP exchange factors in translation initiation, mediate binding to their common substrate eIF2. *EMBO J.* **18**, 2670–2670.

Asano, K., Clayton, J., Shalev, A., and Hinnebusch, A.G. (2000). A multifactor complex of eukaryotic initiation factors, eIF1, eIF2, eIF3, eIF5, and initiator tRNA(Met) is an important translation initiation intermediate in vivo. *Genes Dev.* **14**, 2534–2546.

Asano, K., Shalev, A., Phan, L., Nielsen, K., Clayton, J., Valásek, L., Donahue, T.F., and Hinnebusch, A.G. (2001). Multiple roles for the C-terminal domain of eIF5 in translation initiation complex assembly and GTPase activation. *EMBO J.* **20**, 2326–2337.

Atkins, J.F., Wills, N.M., Loughran, G., Wu, C.-Y., Parsawar, K., Ryan, M.D., Wang, C.-H., and Nelson, C.C. (2007). A case for “StopGo”: reprogramming translation to augment codon meaning of GGN by promoting unconventional termination (Stop) after addition of glycine and then allowing continued translation (Go). *RNA* **13**, 803–810.

Auld, D.S., Thorne, N., Maguire, W.F., and Inglese, J. (2009). Mechanism of PTC124 activity in cell-based luciferase assays of nonsense codon suppression. *Proc. Natl. Acad. Sci. U. S. A.* **106**, 3585–3590.

Auluck, P.K., Chan, H.Y.E., Trojanowski, J.Q., Lee, V.M.Y., and Bonini, N.M. (2002). Chaperone suppression of alpha-synuclein toxicity in a *Drosophila* model for Parkinson’s disease. *Science* **295**, 865–868.

Bai, X., McMullan, G., and Scheres, S.H. (2014). How cryo-EM is revolutionizing structural biology. *Trends Biochem. Sci.* **40**, 49–57.

Bai, X.-C., Fernandez, I.S., McMullan, G., and Scheres, S.H.W. (2013). Ribosome structures to near-atomic resolution from thirty thousand cryo-EM particles. *Elife* **2**, e00461.

Baker, L.A., and Rubinstein, J.L. (2010). Radiation damage in electron cryomicroscopy. *Methods Enzymol.* **481**, 371–388.

Balagopal, V., and Parker, R. (2011). Smt1 modulates translation after 80S formation in *Saccharomyces cerevisiae*. *RNA* **17**, 835–842.

Ban, N. (2000). The complete atomic structure of the large ribosomal subunit at 2.4 Å resolution. *Science* **289**, 905–920.

Barat, C., Datta, P.P., Raj, V.S., Sharma, M.R., Kaji, H., Kaji, A., and Agrawal, R.K. (2007). Progression of the ribosome recycling factor through the ribosome dissociates the two ribosomal subunits. *Mol. Cell* **27**, 250–261.

Barthelme, D., Scheele, U., Dinkelaker, S., Janoschka, A., Macmillan, F., Albers, S.-V., Driessens, A.J.M., Stagni, M.S., Bill, E., Meyer-Klaucke, W., et al. (2007). Structural organization of essential iron-sulfur clusters in the evolutionarily highly conserved ATP-binding cassette protein ABCE1. *J. Biol. Chem.* **282**, 14598–14607.

Barthelme, D., Dinkelaker, S., Albers, S.-V., Londei, P., Ermler, U., and Tampé, R. (2011). Ribosome recycling depends on a mechanistic link between the FeS cluster domain and a conformational switch of the twin-ATPase ABCE1. *Proc. Natl. Acad. Sci. U. S. A.* **108**, 3228–3233.

Batey, S., Nickson, A.A., and Clarke, J. (2008). Studying the folding of multidomain proteins. *HFSP J.* **2**, 365–377.

Becker, T., Armache, J.-P., Jarasch, A., Anger, A.M., Villa, E., Sieber, H., Motaal, B.A., Mielke, T., Berninghausen, O., and Beckmann, R. (2011). Structure of the no-go mRNA decay complex Dom34-Hbs1 bound to a stalled 80S ribosome. *Nat. Struct. Mol. Biol.* **18**, 715–720.

Becker, T., Franckenberg, S., Wickles, S., Shoemaker, C.J., Anger, A.M., Armache, J.-P., Sieber, H., Ungewickell, C., Berninghausen, O., Daberkow, I., et al. (2012). Structural basis of highly conserved ribosome recycling in eukaryotes and archaea. *Nature* **482**, 501–506.

Beckmann, R., Spahn, C.M., Eswar, N., Helmers, J., Penczek, P.A., Sali, A., Frank, J., and Blobel, G. (2001). Architecture of the protein-conducting channel associated with the translating 80S ribosome. *Cell* **107**, 361–372.

Behrmann, E., Loerke, J., Budkevich, T. V., Yamamoto, K., Schmidt, A., Penczek, P.A., Vos, M.R., Bürger, J., Mielke, T., Scheerer, P., et al. (2015). Structural snapshots of actively translating human ribosomes. *Cell* **161**, 845–857.

Bengtson, M.H., and Joazeiro, C.A.P. (2010). Role of a ribosome-associated E3 ubiquitin ligase in protein quality control. *Nature* **467**, 470–473.

Ben-Shem, A., Jenner, L., Yusupova, G., and Yusupov, M. (2010). Crystal structure of the eukaryotic ribosome. *Science* **330**, 1203–1209.

Ben-Shem, A., Garreau de Loubresse, N., Melnikov, S., Jenner, L., Yusupova, G., and Yusupov, M. (2011). The structure of the eukaryotic ribosome at 3.0 Å resolution. *Science* **334**, 1524–1529.

Berchtold, H., Reshetnikova, L., Reiser, C.O., Schirmer, N.K., Sprinzl, M., and Hilgenfeld, R. (1993). Crystal structure of active elongation factor Tu reveals major domain rearrangements. *Nature* **365**, 126–132.

Berg, P., and Offengand, E.J. (1958). An enzymatic mechanism for linking amino acids to RNA. *Proc. Natl. Acad. Sci. U. S. A.* **44**, 78–86.

Beringer, M., and Rodnina, M. V (2007). The ribosomal peptidyl transferase. *Mol. Cell* **26**, 311–321.

Bernabeu, C., and Lake, J.A. (1982). Nascent polypeptide chains emerge from the exit domain of the large ribosomal subunit: immune mapping of the nascent chain. *Proc. Natl. Acad. Sci. U. S. A.* **79**, 3111–3115.

Berndt, U., Oellerer, S., Zhang, Y., Johnson, A.E., and Rospert, S. (2009). A signal-anchor sequence stimulates signal recognition particle binding to ribosomes from inside the exit tunnel. *Proc. Natl. Acad. Sci. U. S. A.* **106**, 1398–1403.

Berthelot, K., Muldoon, M., Rajkowitsch, L., Hughes, J., and McCarthy, J.E.G. (2004). Dynamics and processivity of 40S ribosome scanning on mRNA in yeast. *Mol. Microbiol.* **51**, 987–1001.

Bertram, G., Bell, H. a, Ritchie, D.W., Fullerton, G., and Stansfield, I. (2000). Terminating eukaryote translation: domain 1 of release factor eRF1 functions in stop codon recognition. *RNA* **6**, 1236–1247.

Bhushan, S., Gartmann, M., Halic, M., Armache, J.-P., Jarasch, A., Mielke, T., Berninghausen, O., Wilson, D.N., and Beckmann, R. (2010a). alpha-Helical nascent polypeptide chains visualized within distinct regions of the ribosomal exit tunnel. *Nat. Struct. Mol. Biol.* **17**, 313–317.

Bhushan, S., Meyer, H., Starosta, A.L., Becker, T., Mielke, T., Berninghausen, O., Sattler, M., Wilson, D.N., and Beckmann, R. (2010b). Structural basis for translational stalling by human cytomegalovirus and fungal arginine attenuator peptide. *Mol. Cell* **40**, 138–146.

Bhushan, S., Hoffmann, T., Seidel, B., Frauenfeld, J., Mielke, T., Berninghausen, O., Wilson, D.N., and Beckmann, R. (2011). SecM-stalled ribosomes adopt an altered geometry at the peptidyl transferase center. *PLoS Biol.* **9**, e1000581.

Bi, X., Ren, J., and Goss, D.J. (2000). Wheat germ translation initiation factor eIF4B affects eIF4A and eIFiso4F helicase activity by increasing the ATP binding affinity of eIF4A. *Biochemistry* **39**, 5758–5765.

Bidou, L., Allamand, V., Rousset, J.-P., and Namy, O. (2012). Sense from nonsense: therapies for premature stop codon diseases. *Trends Mol. Med.* **18**, 679–688.

Binshtain, E., and Ohi, M.D. (2015). Cryo-electron microscopy and the amazing race to atomic resolution. *Biochemistry* **54**, 3133–3141.

Bischoff, L., Berninghausen, O., and Beckmann, R. (2014). Molecular basis for the ribosome functioning as an L-tryptophan sensor. *Cell Rep.* **9**, 469–475.

Blanchard, S.C., Gonzalez, R.L., Kim, H.D., Chu, S., and Puglisi, J.D. (2004). tRNA selection and kinetic proofreading in translation. *Nat. Struct. Mol. Biol.* **11**, 1008–1014.

Blanchet, S., Rowe, M., Von der Haar, T., Fabret, C., Demais, S., Howard, M.J., and Namy, O. (2015). New insights into stop codon recognition by eRF1. *Nucleic Acids Res.* **1–11**.

Blomberg, C., Ehrenberg, M., and Kurland, C.G. (2009). Free-energy dissipation constraint on the accuracy of enzymatic selections. *Q. Rev. Biophys.* **13**, 231.

Bornemann, T., Jöckel, J., Rodnina, M. V., and Wintermeyer, W. (2008). Signal sequence-independent membrane targeting of ribosomes containing short nascent peptides within the exit tunnel. *Nat. Struct. Mol. Biol.* **15**, 494–499.

Böttcher, B., Wynne, S.A., and Crowther, R.A. (1997). Determination of the fold of the core protein of hepatitis B virus by electron cryomicroscopy. *Nature* **386**, 88–91.

Brandt, F., Etchells, S.A., Ortiz, J.O., Elcock, A.H., Hartl, F.U., and Baumeister, W. (2009). The native 3D organization of bacterial polysomes. *Cell* **136**, 261–271.

Brenner, S., Stretton, A.O., and Kaplan, S. (1965). Genetic code: the “nonsense” triplets for chain termination and their suppression. *Nature* **206**, 994–998.

Bretscher, M.S. (1968). Translocation in Protein Synthesis: A Hybrid Structure Model. *Nature* **218**, 675–677.

Brilot, A.F., Chen, J.Z., Cheng, A., Pan, J., Harrison, S.C., Potter, C.S., Carragher, B., Henderson, R., and Grigorieff, N. (2012). Beam-induced motion of vitrified specimen on holey carbon film. *J. Struct. Biol.* **177**, 630–637.

Brina, D., Grosso, S., Miluzio, A., and Biffo, S. (2011). Translational control by 80S formation and 60S availability: the central role of eIF6, a rate limiting factor in cell cycle progression and tumorigenesis. *Cell Cycle* **10**, 3441–3446.

Brockwell, D.J., Smith, D.A., and Radford, S.E. (2000). Protein folding mechanisms: new methods and emerging ideas. *Curr. Opin. Struct. Biol.* **10**, 16–25.

Brödel, A.K., Sonnabend, A., Roberts, L.O., Stech, M., Wüstenhagen, D. a, and Kubick, S. (2013). IRES-mediated translation of membrane proteins and glycoproteins in eukaryotic cell-free systems. *PLoS One* **8**, e82234.

Brown, T., and Kennard, O. (1992). Structural basis of DNA mutagenesis. *Curr. Opin. Struct. Biol.* **2**, 354–360.

Brown, A., Shao, S., Murray, J., Hegde, R.S., and Ramakrishnan, V. (2015). Structural basis for stop codon recognition in eukaryotes. *Nature* **524**, 493–496.

Brunelle, J.L., Shaw, J.J., Youngman, E.M., and Green, R. (2008). Peptide release on the ribosome depends critically on the 2' OH of the peptidyl-tRNA substrate. *RNA* **14**, 1526–1531.

Bryngelson, J.D., Onuchic, J.N., Soccia, N.D., and Wolynes, P.G. (1995). Funnels, pathways, and the energy landscape of protein folding: a synthesis. *Proteins* **21**, 167–195.

Budkevich, T. V., Giesebricht, J., Behrmann, E., Loerke, J., Ramrath, D.J.F., Mielke, T., Ismer, J., Hildebrand, P.W., Tung, C.-S., Nierhaus, K.H., et al. (2014). Regulation of the mammalian elongation cycle by subunit rolling: a eukaryotic-specific ribosome rearrangement. *Cell* **158**, 121–131.

Bulygin, K.N., Khairulina, Y.S., Kolosov, P.M., Ven'yaminova, A.G., Graifer, D.M., Vorobjev, Y.N., Frolova, L.Y., Kisseelev, L.L., and Karpova, G.G. (2010). Three distinct peptides from the N domain of translation termination factor eRF1 surround stop codon in the ribosome. *RNA* **16**, 1902–1914.

Bulygin, K.N., Khairulina, Y.S., Kolosov, P.M., Ven'yaminova, A.G., Graifer, D.M., Vorobjev, Y.N., Frolova, L.Y., and Karpova, G.G. (2011). Adenine and guanine recognition of stop codon is mediated by different N domain conformations of translation termination factor eRF1. *Nucleic Acids Res.* **39**, 7134–7146.

Bushmarina, N.A., Blanchet, C.E., Vernier, G., and Forge, V. (2006). Cofactor effects on the protein folding reaction: acceleration of alpha-lactalbumin refolding by metal ions. *Protein Sci.* **15**, 659–671.

Byers, P.H. (2004). Determination of the molecular basis of Marfan syndrome: a growth industry. *J. Clin. Invest.* **114**, 161–163.

Cabrita, L.D., Hsu, S.-T.D., Launay, H., Dobson, C.M., and Christodoulou, J. (2009). Probing ribosome-nascent chain complexes produced in vivo by NMR spectroscopy. *Proc. Natl. Acad. Sci. U. S. A.* **106**, 22239–22244.

Calvo, S.E., Pagliarini, D.J., and Mootha, V.K. (2009). Upstream open reading frames cause widespread reduction of protein expression and are polymorphic among humans. *Proc. Natl. Acad. Sci. U. S. A.* **106**, 7507–7512.

Campbell, M.G., Cheng, A., Brilot, A.F., Moeller, A., Lyumkis, D., Veesler, D., Pan, J., Harrison, S.C., Potter, C.S., Carragher, B., et al. (2012). Movies of ice-embedded particles enhance resolution in electron cryo-microscopy. *Structure* 20, 1823–1828.

Cannone, J.J., Subramanian, S., Schnare, M.N., Collett, J.R., D’Souza, L.M., Du, Y., Feng, B., Lin, N., Madabusi, L.V., Müller, K.M., et al. (2002). The comparative RNA web (CRW) site: an online database of comparative sequence and structure information for ribosomal, intron, and other RNAs. *BMC Bioinformatics* 3, 2.

Cao, J., and Geballe, A.P. (1995). Translational inhibition by a human cytomegalovirus upstream open reading frame despite inefficient utilization of its AUG codon. *J. Virol.* 69, 1030–1036.

Cao, J., and Geballe, A.P. (1998). Ribosomal release without peptidyl tRNA hydrolysis at translation termination in a eukaryotic system. Ribosomal release without peptidyl tRNA hydrolysis at translation termination in a eukaryotic system. 181–188.

Capechi, M.R. (1967). Polypeptide chain termination in vitro: isolation of a release factor. *Proc. Natl. Acad. Sci. U. S. A.* 58, 1144–1151.

Carlberg, U., Nilsson, A., and Nygard, O. (1990). Functional properties of phosphorylated elongation factor 2. *Eur. J. Biochem.* 191, 639–645.

Carlson, E.D., Gan, R., Hodgman, C.E., and Jewett, M.C. (2011). Cell-free protein synthesis: applications come of age. *Biotechnol. Adv.* 30, 1185–1194.

Carroll, K., Elroy-Stein, O., Moss, B., Jagus, R., Elroy-Stein, O., Moss, B., and Jagus, R. (1993). Recombinant vaccinia virus K3L gene product prevents activation of double-stranded RNA-dependent, initiation factor 2 alpha-specific protein kinase. *J. Biol. Chem.* 268, 12837–12842.

Carter, A.P. (2001). Crystal structure of an initiation factor bound to the 30S ribosomal subunit. *Science* 291, 498–501.

Caskey, C.T., Beaudet, A.L., and Tate, W.P. (1974). Mammalian release factor; in Vitro Assay and Purification (Elsevier).

Castelló, A., Franco, D., Moral-López, P., Berlanga, J.J., Alvarez, E., Wimmer, E., and Carrasco, L. (2009). HIV-1 protease inhibits Cap- and poly(A)-dependent translation upon eIF4GI and PABP cleavage. *PLoS One* 4, e7997.

Cech, T.R. (2000). Structural biology. The ribosome is a ribozyme. *Science* 289, 878–879.

Ceci, M., Gaviraghi, C., Gorrini, C., Sala, L.A., Offenhäuser, N., Marchisio, P.C., and Biffo, S. (2003). Release of eIF6 (p27BBP) from the 60S subunit allows 80S ribosome assembly. *Nature* 426, 579–584.

Ceci, M., Welshhans, K., Ciotti, M.T., Brandi, R., Parisi, C., Paoletti, F., Pistillo, L., Bassell, G.J., and Cattaneo, A. (2012). RACK1 is a ribosome scaffold protein for β-actin mRNA/ZBP1 complex. *PLoS One* 7, e35034.

Chambers, I., Frampton, J., Goldfarb, P., Affara, N., McBain, W., and Harrison, P.R. (1986). The structure of the mouse glutathione peroxidase gene: the selenocysteine in the active site is encoded by the “termination” codon, TGA. *EMBO J.* 5, 1221–1227.

Chang, C., Vesole, D.H., Nelson, J.A.Y., Oldstone, M.B.A., and Stinskil, M.F. (1989). Identification and Expression of a Human Cytomegalovirus Early Glycoprotein. *63*, 3330–3337.

Chattopadhyay, S., Das, B., and Dasgupta, C. (1996). Reactivation of denatured proteins by 23S ribosomal RNA: role of domain V. *Proc. Natl. Acad. Sci. U. S. A.* 93, 8284–8287.

Chau, D.H.W., Yuan, J., Zhang, H., Cheung, P., Lim, T., Liu, Z., Sall, A., and Yang, D. (2007). Coxsackievirus B3 proteases 2A and 3C induce apoptotic cell death through mitochondrial injury and cleavage of eIF4GI but not DAP5/p97/NAT1. *Apoptosis* 12, 513–524.

Chaudhuri, J., Chowdhury, D., and Maitra, U. (1999). Distinct functions of eukaryotic translation initiation factors eIF1A and eIF3 in the formation of the 40S ribosomal preinitiation complex. *J. Biol. Chem.* 274, 17975–17980.

Chauvin, C., Salhi, S., Le Goff, C., Viranaicken, W., Diop, D., and Jean-Jean, O. (2005). Involvement of human release factors eRF3a and eRF3b in translation termination and regulation of the termination complex formation. *Mol. Cell. Biol.* 25, 5801–5811.

Chavatte, L., Seit-Nebi, A., Dubovaya, V., and Favre, A. (2002). The invariant uridine of stop codons contacts the conserved NIKSR loop of human eRF1 in the ribosome. *EMBO J.* 21, 5302–5311.

Chen, C.-M., and Behringer, R.R. (2004). Ovca1 regulates cell proliferation, embryonic development, and tumorigenesis. *Genes Dev.* 18, 320–332.

Chen, J.Z., and Grigorieff, N. (2007). SIGNATURE: a single-particle selection system for molecular electron microscopy. *J. Struct. Biol.* **157**, 168–173.

Chen, C., Stevens, B., Kaur, J., Smilansky, Z., Cooperman, B.S., and Goldman, Y.E. (2011). Allosteric vs. spontaneous exit-site (E-site) tRNA dissociation early in protein synthesis. *Proc. Natl. Acad. Sci. U. S. A.* **108**, 16980–16985.

Chen, J., Lu, G., Lin, J., Davidson, A.L., and Quiocho, F.A. (2003). A tweezers-like motion of the ATP-binding cassette dimer in an ABC transport cycle. *Mol. Cell* **12**, 651–661.

Chen, Y., Feng, S., Kumar, V., Ero, R., and Gao, Y.-G. (2013). Structure of EF-G-ribosome complex in a pretranslocation state. *Nat. Struct. Mol. Biol.* **20**, 1077–1084.

Cheng, S., Sultana, S., Goss, D.J., and Gallie, D.R. (2008). Translation initiation factor 4B homodimerization, RNA binding, and interaction with Poly(A)-binding protein are enhanced by zinc. *J. Biol. Chem.* **283**, 36140–36153.

Cheng, Z., Saito, K., Pisarev, A. V., Wada, M., Pisareva, V.P., Pestova, T. V., Gajda, M., Round, A., Kong, C., Lim, M., et al. (2009). Structural insights into eRF3 and stop codon recognition by eRF1. *Genes Dev.* **23**, 1106–1118.

Chiba, Y. (1999). Evidence for autoregulation of cystathionine-synthase mRNA stability in arabidopsis. *Science* **286**, 1371–1374.

Chiba, S., and Ito, K. (2012). Multisite ribosomal stalling: a unique mode of regulatory nascent chain action revealed for MifM. *Mol. Cell* **47**, 863–872.

Chiba, S., Lamsa, A., and Pogliano, K. (2009). A ribosome-nascent chain sensor of membrane protein biogenesis in *Bacillus subtilis*. *EMBO J.* **28**, 3461–3475.

Chiti, F., and Dobson, C.M. (2006). Protein misfolding, functional amyloid, and human disease. *Annu. Rev. Biochem.* **75**, 333–366.

Chiu, W.-L., Wagner, S., Herrmannová, A., Burela, L., Zhang, F., Saini, A.K., Valásek, L., and Hinnebusch, A.G. (2010). The C-terminal region of eukaryotic translation initiation factor 3a (eIF3a) promotes mRNA recruitment, scanning, and, together with eIF3j and the eIF3b RNA recognition motif, selection of AUG start codons. *Mol. Cell. Biol.* **30**, 4415–4434.

Chow, C.C., Chow, C., Raghunathan, V., Huppert, T.J., Kimball, E.B., and Cavagnero, S. (2003). Chain length dependence of apomyoglobin folding: structural evolution from misfolded sheets to native helices. *Biochemistry* **42**, 7090–7099.

Chu, C.S., Trapnell, B.C., Curristin, S.M., Cutting, G.R., and Crystal, R.G. (1992). Extensive posttranscriptional deletion of the coding sequences for part of nucleotide-binding fold 1 in respiratory epithelial mRNA transcripts of the cystic fibrosis transmembrane conductance regulator gene is not associated with the clinical manifestati. *J. Clin. Invest.* **90**, 785–790.

Clarke, T.F., and Clark, P.L. (2008). Rare codons cluster. *PLoS One* **3**, e3412.

Clemens, M.J. (2001). Initiation factor eIF2 alpha phosphorylation in stress responses and apoptosis. *Prog. Mol. Subcell. Biol.* **27**, 57–89.

Conard, S.E., Buckley, J., Dang, M., Bedwell, G.J., Carter, R.L., Khass, M., and Bedwell, D.M. (2012). Identification of eRF1 residues that play critical and complementary roles in stop codon recognition. *RNA* **18**, 1210–1221.

Connell, S.R., Takemoto, C., Wilson, D.N., Wang, H., Murayama, K., Terada, T., Shirouzu, M., Rost, M., Schüler, M., Giesebricht, J., et al. (2007). Structural basis for interaction of the ribosome with the switch regions of GTP-bound elongation factors. *Mol. Cell* **25**, 751–764.

Cosson, B., Berkova, N., Couturier, A., Chabelskaya, S., Philippe, M., and Zhouravleva, G. (2002). Poly(A)-binding protein and eRF3 are associated in vivo in human and Xenopus cells. *Biol. Cell* **94**, 205–216.

Crick, F. (1970). Central dogma of molecular biology. *Nature* **227**, 561–563.

Crick, F.H. (1966). Codon-anticodon pairing: the wobble hypothesis. *J. Mol. Biol.* **19**, 548–555.

Crick, F.H., Barnett, L., Brenner, S., and Watts-Tobin, R.J. (1961). General nature of the genetic code for proteins. *Nature* **192**, 1227–1232.

Cruz-Vera, L.R., and Yanofsky, C. (2008). Conserved residues Asp16 and Pro24 of TnaC-tRNAPro participate in tryptophan induction of Tna operon expression. *J. Bacteriol.* **190**, 4791–4797.

Cruz-Vera, L.R., Rajagopal, S., Squires, C., and Yanofsky, C. (2005). Features of ribosome-peptidyl-tRNA interactions essential for tryptophan induction of tna operon expression. *Mol. Cell* **19**, 333–343.

Cruz-Vera, L.R., Gong, M., and Yanofsky, C. (2006). Changes produced by bound tryptophan in the ribosome peptidyl transferase center in response to TnaC, a nascent leader peptide. *Proc. Natl. Acad. Sci. U. S. A.* **103**, 3598–3603.

Cruz-Vera, L.R., New, A., Squires, C., and Yanofsky, C. (2007). Ribosomal features essential for tna operon induction: tryptophan binding at the peptidyl transferase center. *J. Bacteriol.* **189**, 3140–3146.

Cuéllar, J., Martín-Benito, J., Scheres, S.H.W., Sousa, R., Moro, F., López-Viñas, E., Gómez-Puertas, P., Muga, A., Carrascosa, J.L., and Valpuesta, J.M. (2008). The structure of CCT-Hsc70 NBD suggests a mechanism for Hsp70 delivery of substrates to the chaperonin. *Nat. Struct. Mol. Biol.* **15**, 858–864.

Das, B., Chattopadhyay, S., and Das Gupta, C. (1992). Reactivation of denatured fungal glucose 6-phosphate dehydrogenase and *E. coli* alkaline phosphatase with *E. coli* ribosome. *Biochem. Biophys. Res. Commun.* **183**, 774–780.

Das, S., Ghosh, R., and Maitra, U. (2001). Eukaryotic translation initiation factor 5 functions as a GTPase-activating protein. *J. Biol. Chem.* **276**, 6720–6726.

David, D.C., Ollikainen, N., Trinidad, J.C., Cary, M.P., Burlingame, A.L., and Kenyon, C. (2010). Widespread protein aggregation as an inherent part of aging in *C. elegans*. *PLoS Biol.* **8**, e1000450.

Daviter, T., Wieden, H.-J., and Rodnina, M. V. (2003). Essential role of histidine 84 in elongation factor Tu for the chemical step of GTP hydrolysis on the ribosome. *J. Mol. Biol.* **332**, 689–699.

Dean, M., and Annilo, T. (2005). Evolution of the ATP-binding cassette (ABC) transporter superfamily in vertebrates. *Annu. Rev. Genomics Hum. Genet.* **6**, 123–142.

Degnini, C.R., Schleiss, M.R., Cao, J., and Geballe, A.P. (1993). Translational inhibition mediated by a short upstream open reading frame in the human cytomegalovirus gpUL4 (gp48) transcript. *J. Virol.* **67**, 5514–5521.

Demeshkina, N., Jenner, L., Westhof, E., Yusupov, M., and Yusupova, G. (2012). A new understanding of the decoding principle on the ribosome. *Nature* **484**, 256–259.

Demontis, F., and Perrimon, N. (2010). FOXO/4E-BP signaling in *Drosophila* muscles regulates organism-wide proteostasis during aging. *Cell* **143**, 813–825.

Deuerling, E., and Bukau, B. (2004). Chaperone-assisted folding of newly synthesized proteins in the cytosol. *Crit. Rev. Biochem. Mol. Biol.* **39**, 261–277.

Devaraneni, P.K., Conti, B., Matsumura, Y., Yang, Z., Johnson, A.E., and Skach, W.R. (2011). Stepwise insertion and inversion of a type II signal anchor sequence in the ribosome-Sec61 translocon complex. *Cell* **146**, 134–147.

Diaconu, M., Kothe, U., Schlünzen, F., Fischer, N., Harms, J.M., Tonevitsky, A.G., Stark, H., Rodnina, M. V., and Wahl, M.C. (2005). Structural basis for the function of the ribosomal L7/12 stalk in factor binding and GTPase activation. *Cell* **121**, 991–1004.

Dill, K.A., Bromberg, S., Yue, K., Fiebig, K.M., Yee, D.P., Thomas, P.D., and Chan, H.S. (1995). Principles of protein folding--a perspective from simple exact models. *Protein Sci.* **4**, 561–602.

Dimitrova, L.N., Kuroha, K., Tatematsu, T., and Inada, T. (2009). Nascent peptide-dependent translation arrest leads to Not4p-mediated protein degradation by the proteasome. *J. Biol. Chem.* **284**, 10343–10352.

Dintzis, H.M. (1961). Assembly of the peptide chains of hemoglobin. *Proc. Natl. Acad. Sci. U. S. A.* **47**, 247–261.

Doma, M.K., and Parker, R. (2006). Endonucleolytic cleavage of eukaryotic mRNAs with stalls in translation elongation. *Nature* **440**, 561–564.

Dong, J., Lai, R., Nielsen, K., Fekete, C.A., Qiu, H., and Hinnebusch, A.G. (2004). The essential ATP-binding cassette protein RLI1 functions in translation by promoting preinitiation complex assembly. *J. Biol. Chem.* **279**, 42157–42168.

Doublie, S., Tabor, S., Long, A.M., Richardson, C.C., and Ellenberger, T. (1998). Crystal structure of a bacteriophage T7 DNA replication complex at 2.2 Å resolution. *Nature* **391**, 251–258.

Dreyfus, M., and Régnier, P. (2002). The Poly(A) Tail of mRNAs. *Cell* **111**, 611–613.

Dubochet, J., Lepault, J., Freeman, R., Berriman, J.A., and Homo, J.-C. (1982). Electron microscopy of frozen water and aqueous solutions. *J. Microsc.* **128**, 219–237.

Duncan, R., Milburn, S.C., and Hershey, J.W. (1987). Regulated phosphorylation and low abundance of HeLa cell initiation factor eIF-4F suggest a role in translational control. Heat shock effects on eIF-4F. *J. Biol. Chem.* **262**, 380–388.

Dunkle, J.A., Wang, L., Feldman, M.B., Pulk, A., Chen, V.B., Kapral, G.J., Noeske, J., Richardson, J.S., Blanchard, S.C., and Cate, J.H.D. (2011). Structures of the bacterial ribosome in classical and hybrid states of tRNA binding. *Science* **332**, 981–984.

De Duve, C. (1988). Transfer RNAs: the second genetic code. *Nature* **333**, 117–118.

Dvorak, H.F., Brockman, R.W., and Heppel, L.A. (1967). Purification and properties of two acid phosphatase fractions isolated from osmotic shock fluid of *Escherichia coli*. *Biochemistry* **6**, 1743–1751.

Ebihara, K., and Nakamura, Y. (1999). C-terminal interaction of translational release factors eRF1 and eRF3 of fission yeast: G-domain uncoupled binding and the role of conserved amino acids. *RNA* **5**, 739–750.

Eckmann, C.R., Rammelt, C., and Wahle, E. (2010). Control of poly(A) tail length. *Wiley Interdiscip. Rev. RNA* **2**, 348–361.

Eichmann, C., Preissler, S., Riek, R., and Deuerling, E. (2010). Cotranslational structure acquisition of nascent polypeptides monitored by NMR spectroscopy. *Proc. Natl. Acad. Sci. U. S. A.* **107**, 9111–9116.

Elad, N., Clare, D.K., Saibil, H.R., and Orlova, E. V (2008). Detection and separation of heterogeneity in molecular complexes by statistical analysis of their two-dimensional projections. *J. Struct. Biol.* **162**, 108–120.

Eldadah, Z.A., Brenn, T., Furthmayr, H., and Dietz, H.C. (1995). Expression of a mutant human fibrillin allele upon a normal human or murine genetic background recapitulates a Marfan cellular phenotype. *J. Clin. Invest.* **95**, 874–880.

Ellis, R.J., and Minton, A.P. (2006). Protein aggregation in crowded environments. *Biol. Chem.* **387**, 485–497.

Ellis, J.P., Culviner, P.H., and Cavagnero, S. (2009). Confined dynamics of a ribosome-bound nascent globin: Cone angle analysis of fluorescence depolarization decays in the presence of two local motions. *Protein Sci.* **18**, 2003–2015.

Emsley, P., and Cowtan, K. (2004). Coot: Model-building tools for molecular graphics. *Acta Crystallogr. Sect. D Biol. Crystallogr.* **60**, 2126–2132.

Ermolenko, D.N., and Noller, H.F. (2011). mRNA translocation occurs during the second step of ribosomal intersubunit rotation. *Nat. Struct. Mol. Biol.* **18**, 457–462.

Etchison, D., Milburn, S.C., Edery, I., Sonenberg, N., and Hershey, J.W. (1982). Inhibition of HeLa cell protein synthesis following poliovirus infection correlates with the proteolysis of a 220,000-dalton polypeptide associated with eucaryotic initiation factor 3 and a cap binding protein complex. *J. Biol. Chem.* **257**, 14806–14810.

Evans, M.S., Sander, I.M., and Clark, P.L. (2008a). Cotranslational folding promotes beta-helix formation and avoids aggregation in vivo. *J. Mol. Biol.* **383**, 683–692.

Evans, R.N., Blaha, G., Bailey, S., and Steitz, T.A. (2008b). The structure of LepA, the ribosomal back translocase. *Proc. Natl. Acad. Sci. U. S. A.* **105**, 4673–4678.

Ezure, T., Suzuki, T., Higashide, S., Shintani, E., Endo, K., Kobayashi, S., Shikata, M., Ito, M., Tanimizu, K., and Nishimura, O. (2006). Cell-free protein synthesis system prepared from insect cells by freeze-thawing. *Biotechnol. Prog.* **22**, 1570–1577.

Ezure, T., Suzuki, T., Shikata, M., Ito, M., Ando, E., Utsumi, T., Nishimura, O., and Tsunasawa, S. (2010). Development of an insect cell-free system. *Curr. Pharm. Biotechnol.* **11**, 279–284.

Fang, P., Spevak, C.C., Wu, C., and Sachs, M.S. (2004). A nascent polypeptide domain that can regulate translation elongation. *Proc. Natl. Acad. Sci. U. S. A.* **101**, 4059–4064.

Feigenblum, D., and Schneider, R.J. (1993). Modification of eukaryotic initiation factor 4F during infection by influenza virus. *J. Virol.* **67**, 3027–3035.

Feng, T., Yamamoto, A., Wilkins, S.E.E., Sokolova, E., Yates, L.A. a, Münzel, M., Singh, P., Hopkinson, R.J.J., Fischer, R., Cockman, M.E.E., et al. (2014). Optimal translational termination requires C4 lysyl hydroxylation of eRF1. *Mol. Cell* **53**, 645–654.

Ferbitz, L., Maier, T., Patzelt, H., Bukau, B., Deuerling, E., and Ban, N. (2004). Trigger factor in complex with the ribosome forms a molecular cradle for nascent proteins. *Nature* **431**, 590–596.

Fernández, I.S., Bai, X.-C., Hussain, T., Kelley, A.C., Lorsch, J.R., Ramakrishnan, V., and Scheres, S.H.W. (2013). Molecular architecture of a eukaryotic translational initiation complex. *Science* **342**, 1240585.

Fernández, I.S., Bai, X.-C., Murshudov, G., Scheres, S.H.W., and Ramakrishnan, V. (2014). Initiation of translation by cricket paralysis virus IRES requires its translocation in the ribosome. *Cell* **157**, 823–831.

Fernández, J.J., Luque, D., Castón, J.R., and Carrascosa, J.L. (2008). Sharpening high resolution information in single particle electron cryomicroscopy. *J. Struct. Biol.* **164**, 170–175.

Fernández-Miragall, O., López de Quinto, S., and Martínez-Salas, E. (2009). Relevance of RNA structure for the activity of picornavirus IRES elements. *Virus Res.* **139**, 172–182.

Fischer, N., Neumann, P., Konevega, A.L., Bock, L.V., Ficner, R., Rodnina, M.V., and Stark, H. (2015). Structure of the *E. coli* ribosome–EF-Tu complex at <3 Å resolution by Cs-corrected cryo-EM. *Nature* **520**, 567–570.

François, B., Russell, R.J.M., Murray, J.B., Aboul-ela, F., Masquida, B., Vicens, Q., and Westhof, E. (2005). Crystal structures of complexes between aminoglycosides and decoding A site oligonucleotides: role of the number of rings and positive charges in the specific binding leading to miscoding. *Nucleic Acids Res.* **33**, 5677–5690.

Frank, J. (2012). Intermediate states during mRNA-tRNA translocation. *Curr. Opin. Struct. Biol.* **22**, 778–785.

Frank, J., and Agrawal, R.K. (2000). A ratchet-like inter-subunit reorganization of the ribosome during translocation. *Nature* **406**, 318–322.

Frank, J., and Gonzalez, R.L. (2010). Structure and dynamics of a processive Brownian motor: the translating ribosome. *Annu. Rev. Biochem.* **79**, 381–412.

Frank, J., Zhu, J., Penczek, P., Li, Y., Srivastava, S., Verschoor, A., Radermacher, M., Grassucci, R., Lata, R.K., and Agrawal, R.K. (1995). A model of protein synthesis based on cryo-electron microscopy of the *E. coli* ribosome. *Nature* **376**, 441–444.

Frank, J., Radermacher, M., Penczek, P., Zhu, J., Li, Y., Ladjadj, M., and Leith, A. (1996). SPIDER and WEB: processing and visualization of images in 3D electron microscopy and related fields. *J Struct Biol* **116**, 190–199.

Frauenfeld, J., Gumbart, J., Sluis, E.O. van der, Funes, S., Gartmann, M., Beatrix, B., Mielke, T., Berninghausen, O., Becker, T., Schulten, K., et al. (2011). Cryo-EM structure of the ribosome-SecYE complex in the membrane environment. *Nat. Struct. Mol. Biol.* **18**, 614–621.

Freistroffer, D.V., Pavlov, M.Y., MacDougall, J., Buckingham, R.H., and Ehrenberg, M. (1997). Release factor RF3 in *E. coli* accelerates the dissociation of release factors RF1 and RF2 from the ribosome in a GTP-dependent manner. *EMBO J.* **16**, 4126–4133.

Freistroffer, D.V., Kwiatkowski, M., Buckingham, R.H., and Ehrenberg, M. (2000). The accuracy of codon recognition by polypeptide release factors. *Proc. Natl. Acad. Sci. U. S. A.* **97**, 2046–2051.

Friedman, R.A., and Honig, B. (1995). A free energy analysis of nucleic acid base stacking in aqueous solution. *Biophys. J.* **69**, 1528–1535.

Frischmeyer, P.A. (1999). Nonsense-mediated mRNA decay in health and disease. *Hum. Mol. Genet.* **8**, 1893–1900.

Frischmeyer, P.A., van Hoof, A., O'Donnell, K., Guerriero, A.L., Parker, R., and Dietz, H.C. (2002). An mRNA surveillance mechanism that eliminates transcripts lacking termination codons. *Science* **295**, 2258–2261.

Frolova, L., Le Goff, X., Rasmussen, H.H., Cheperegin, S., Drugeon, G., Kress, M., Arman, I., Haenni, A.L., Celis, J.E., Philippe, M., et al. (1994). A highly conserved eukaryotic protein family possessing properties of polypeptide chain release factor. *Nature* **372**, 701–703.

Frolova, L., Le Goff, X., Zhouravleva, G., Davydova, E., Philippe, M., and Kisseelev, L. (1996). Eukaryotic polypeptide chain release factor eRF3 is an eRF1- and ribosome-dependent guanosine triphosphatase. *RNA* **2**, 334–341.

Frolova, L., Seit-Nebi, A., and Kisseelev, L. (2002). Highly conserved NIKS tetrapeptide is functionally essential in eukaryotic translation termination factor eRF1. *RNA* **8**, 129–136.

Frolova, L.Y., Simonsen, J.L., Merkulova, T.I., Litvinov, D.Y., Martensen, P.M., Rechinsky, V.O., Camonis, J.H., Kisseelev, L.L., and Justesen, J. (1998). Functional expression of eukaryotic polypeptide chain release factors 1 and 3 by means of baculovirus/insect cells and complex formation between the factors. *Eur. J. Biochem.* **256**, 36–44.

Frolova, L.Y., Tsivkovskii, R.Y., Sivolobova, G.F., Oparina, N.Y., Serpinsky, O.I., Blinov, V.M., Tatkov, S.I., and Kisseelev, L.L. (1999). Mutations in the highly conserved GGQ motif of class 1 polypeptide release factors abolish ability of human eRF1 to trigger peptidyl-tRNA hydrolysis. *RNA* **5**, 1014–1020.

Frolova, L.Y., Merkulova, T.I., and Kisseelev, L.L. (2000). Translation termination in eukaryotes: Polypeptide release factor eRF1 is composed of functionally and structurally distinct domains. *RNA* **6**, 381–390.

Frydman, J. (2001). Folding of newly translated proteins in vivo: the role of molecular chaperones. *Annu. Rev. Biochem.* **70**, 603–647.

Fulle, S., and Gohlke, H. (2009). Statics of the ribosomal exit tunnel: implications for cotranslational peptide folding, elongation regulation, and antibiotics binding. *J. Mol. Biol.* **387**, 502–517.

Gaba, A., Jacobson, A., and Sachs, M.S. (2005). Ribosome occupancy of the yeast CPA1 upstream open reading frame termination codon modulates nonsense-mediated mRNA decay. *Mol. Cell* **20**, 449–460.

Gabdulkhakov, A., Nikonorov, S., and Garber, M. (2013). Revisiting the *Haloarcula marismortui* 50S ribosomal subunit model. *Acta Crystallogr. D. Biol. Crystallogr.* **69**, 997–1004.

Gagnon, M.G., Lin, J., Bulkley, D., and Steitz, T.A. (2014). Crystal structure of elongation factor 4 bound to a clockwise ratcheted ribosome. *Science* **345**, 684–687.

Gale, E.F., and Folkes, J.P. (1954). Effect of nucleic acids on protein synthesis and amino-acid incorporation in disrupted staphylococcal cells. *Nature* **173**, 1223–1227.

Gao, H., Zhou, Z., Rawat, U., Huang, C., Bouakaz, L., Wang, C., Cheng, Z., Liu, Y., Zavialov, A., Gursky, R., et al. (2007). RF3 induces ribosomal conformational changes responsible for dissociation of class I release factors. *Cell* **129**, 929–941.

Gao, Y.-G., Selmer, M., Dunham, C.M., Weixlbaumer, A., Kelley, A.C., and Ramakrishnan, V. (2009). The structure of the ribosome with elongation factor G trapped in the posttranslocational state. *Science* **326**, 694–699.

Gartmann, M., Blau, M., Armache, J.-P., Mielke, T., Topf, M., and Beckmann, R. (2010). Mechanism of eIF6-mediated inhibition of ribosomal subunit joining. *J. Biol. Chem.* **285**, 14848–14851.

Gautschi, M., Lilie, H., Fünfschilling, U., Mun, A., Ross, S., Lithgow, T., Rücknagel, P., and Rospert, S. (2001). RAC, a stable ribosome-associated complex in yeast formed by the DnaK-DnaJ homologs Ssz1p and zuotin. *Proc. Natl. Acad. Sci. U. S. A.* **98**, 3762–3767.

Geballe, A.P. (1996). Inhibition of Nascent-Peptide Release at Translation Termination. *16*, 7109–7114.

Geballe, A.P., Spaete, R.R., and Mocarski, E.S. (1986). A cis-acting element within the 5' leader of a cytomegalovirus beta transcript determines kinetic class. *Cell* **46**, 865–872.

Des Georges, A., Hashem, Y., Unbehaun, A., Grassucci, R. a, Taylor, D., Hellen, C.U.T., Pestova, T. V, and Frank, J. (2014). Structure of the mammalian ribosomal pre-termination complex associated with eRF1.eRF3.GDPNP. *Nucleic Acids Res.* **42**, 3409–3418.

Giegé, R. (2006). The early history of tRNA recognition by aminoacyl-tRNA synthetases. *J. Biosci.* **31**, 477–488.

Gilson, M.K., and Honig, B. (1988). Calculation of the total electrostatic energy of a macromolecular system: solvation energies, binding energies, and conformational analysis. *Proteins* **4**, 7–18.

Glaeser, R. (2004). Historical background: why is it important to improve automated particle selection methods? *J. Struct. Biol.* **145**, 15–18.

Glaeser, R.M., Typke, D., Tiemeijer, P.C., Pulokas, J., and Cheng, A. (2011). Precise beam-tilt alignment and collimation are required to minimize the phase error associated with coma in high-resolution cryo-EM. *J. Struct. Biol.* **174**, 1–10.

Goedken, E.R., Keck, J.L., Berger, J.M., and Marqusee, S. (2000). Divalent metal cofactor binding in the kinetic folding trajectory of *Escherichia coli* ribonuclease HI. *Protein Sci.* **9**, 1914–1921.

Gogala, M., Becker, T., Beatrix, B., Armache, J.-P., Barrio-Garcia, C., Berninghausen, O., and Beckmann, R. (2014). Structures of the Sec61 complex engaged in nascent peptide translocation or membrane insertion. *Nature* **506**, 107–110.

Gollnick, P., and Yanofsky, C. (1990). tRNA(Trp) translation of leader peptide codon 12 and other factors that regulate expression of the tryptophanase operon. *J. Bacteriol.* **172**, 3100–3107.

Gong, F., and Yanofsky, C. (2002). Instruction of translating ribosome by nascent peptide. *Science* **297**, 1864–1867.

Gong, F., and Yanofsky, C. (2003). A transcriptional pause synchronizes translation with transcription in the tryptophanase operon leader region. *J. Bacteriol.* **185**, 6472–6476.

Gong, F., Ito, K., Nakamura, Y., and Yanofsky, C. (2001). The mechanism of tryptophan induction of tryptophanase operon expression: tryptophan inhibits release factor-mediated cleavage of TnaC-peptidyl-tRNA(Pro). *Proc. Natl. Acad. Sci. U. S. A.* **98**, 8997–9001.

Grassucci, R. a, Taylor, D.J., and Frank, J. (2007). Preparation of macromolecular complexes for cryo-electron microscopy. *Nat. Protoc.* **2**, 3239–3246.

Greber, B.J., Boehringer, D., Godinic-Mikulcic, V., Crnkovic, A., Ibba, M., Weygand-Durasevic, I., and Ban, N. (2012). Cryo-EM structure of the archaeal 50S ribosomal subunit in complex with initiation factor 6 and implications for ribosome evolution. *J. Mol. Biol.* **418**, 145–160.

Grentzmann, G., Kelly, P.J., Laalami, S., Shuda, M., Firpo, M.A., Cenatiempo, Y., and Kaji, A. (1998). Release factor RF-3 GTPase activity acts in disassembly of the ribosome termination complex. *RNA* **4**, 973–983.

Gromadski, K.B., and Rodnina, M. V. (2004). Kinetic determinants of high-fidelity tRNA discrimination on the ribosome. *Mol. Cell* **13**, 191–200.

Guo, Z., and Noller, H.F. (2012). Rotation of the head of the 30S ribosomal subunit during mRNA translocation. *Proc. Natl. Acad. Sci. U. S. A.* **109**, 20391–20394.

Hajnsdorf, E., and Boni, I. V (2012). Multiple activities of RNA-binding proteins S1 and Hfq. *Biochimie* **94**, 1544–1553.

Halic, M., Becker, T., Pool, M.R., Spahn, C.M.T., Grassucci, R.A., Frank, J., and Beckmann, R. (2004). Structure of the signal recognition particle interacting with the elongation-arrested ribosome. *Nature* **427**, 808–814.

Halic, M., Becker, T., Frank, J., Spahn, C.M.T., and Beckmann, R. (2005). Localization and dynamic behavior of ribosomal protein L30e. *Nat. Struct. Mol. Biol.* **12**, 467–468.

Hall, G.W., and Thein, S. (1994). Nonsense codon mutations in the terminal exon of the beta-globin gene are not associated with a reduction in beta-mRNA accumulation: a mechanism for the phenotype of dominant beta-thalassemia. *Blood* **83**, 2031–2037.

Hamosh, A., Rosenstein, B.J., and Cutting, G.R. (1992). CFTR nonsense mutations G542X and W1282X associated with severe reduction of CFTR mRNA in nasal epithelial cells. *Hum. Mol. Genet.* **1**, 542–544.

Hansen, J.L., Schmeing, T.M., Moore, P.B., and Steitz, T.A. (2002). Structural insights into peptide bond formation. *Proc. Natl. Acad. Sci. U. S. A.* **99**, 11670–11675.

Hanson, P.J., Zhang, H.M., Hemida, M.G., Ye, X., Qiu, Y., and Yang, D. (2012). IRES-Dependent Translational Control during Virus-Induced Endoplasmic Reticulum Stress and Apoptosis. *Front. Microbiol.* **3**, 92.

Haraguchi, Y., Kadokura, Y., Nakamoto, M., Onouchi, H., and Naito, S. (2008). Ribosome stacking defines CGS1 mRNA degradation sites during nascent peptide-mediated translation arrest. *Plant Cell Physiol.* **49**, 314–323.

Harms, J., Schlüzen, F., Zarivach, R., Bashan, A., Gat, S., Agmon, I., Bartels, H., Franceschi, F., and Yonath, A. (2001). High resolution structure of the large ribosomal subunit from a mesophilic eubacterium. *Cell* **107**, 679–688.

Hartl, F.U. (1996). Molecular chaperones in cellular protein folding. *Nature* **381**, 571–579.

Hartl, F.U., and Hayer-Hartl, M. (2009). Converging concepts of protein folding in vitro and in vivo. *Nat. Struct. Mol. Biol.* **16**, 574–581.

Hartl, F.U., Bracher, A., and Hayer-Hartl, M. (2011). Molecular chaperones in protein folding and proteostasis. *Nature* **475**, 324–332.

Hashem, Y., des Georges, A., Dhote, V., Langlois, R., Liao, H.Y., Grassucci, R.A., Hellen, C.U.T., Pestova, T. V, and Frank, J. (2013). Structure of the mammalian ribosomal 43S preinitiation complex bound to the scanning factor DHX29. *Cell* **153**, 1108–1119.

Hatin, I., Fabret, C., Rousset, J.-P., and Namy, O. (2009). Molecular dissection of translation termination mechanism identifies two new critical regions in eRF1. *Nucleic Acids Res.* **37**, 1789–1798.

Hauriyliuk, V., Zavialov, A., Kisilev, L., and Ehrenberg, M. (2006). Class-1 release factor eRF1 promotes GTP binding by class-2 release factor eRF3. *Biochimie* **88**, 747–757.

He, F., and Jacobson, A. (2015). Nonsense-Mediated mRNA Decay: Degradation of Defective Transcripts Is Only Part of the Story. *Annu. Rev. Genet.* **49**, 339–366.

Herbein, G., and Kumar, A. (2014). The oncogenic potential of human cytomegalovirus and breast cancer. *Front. Oncol.* **4**, 230.

Herbst, R., Schafer, U., and Seckler, R. (1997). Equilibrium Intermediates in the Reversible Unfolding of Firefly (*Photinus pyralis*) Luciferase. *J. Biol. Chem.* **272**, 7099–7105.

Hill, J.R., and Morris, D.R. (1993). Cell-specific translational regulation of S-adenosylmethionine decarboxylase mRNA. Dependence on translation and coding capacity of the cis-acting upstream open reading frame. *J. Biol. Chem.* **268**, 726–731.

Hiller, D.A., Singh, V., Zhong, M., and Strobel, S.A. (2011). A two-step chemical mechanism for ribosome-catalysed peptide bond formation. *Nature* **476**, 236–239.

Hinnebusch, A.G. (2014). The scanning mechanism of eukaryotic translation initiation. *Annu. Rev. Biochem.* *83*, 779–812.

Hirashima, A., and Kaji, A. (1973). Role of elongation factor G and a protein factor on the release of ribosomes from messenger ribonucleic acid. *J. Biol. Chem.* *248*, 7580–7587.

Hiremath, L.S., Webb, N.R., and Rhoads, R.E. (1985). Immunological detection of the messenger RNA cap-binding protein. *J. Biol. Chem.* *260*, 7843–7849.

Hirokawa, G., Iwakura, N., Kaji, A., and Kaji, H. (2008). The role of GTP in transient splitting of 70S ribosomes by RRF (ribosome recycling factor) and EF-G (elongation factor G). *Nucleic Acids Res.* *36*, 6676–6687.

Hoffmann, A., Merz, F., Rutkowska, A., Zachmann-Brand, B., Deuerling, E., and Bukau, B. (2006). Trigger factor forms a protective shield for nascent polypeptides at the ribosome. *J. Biol. Chem.* *281*, 6539–6545.

Holcik, M., and Sonenberg, N. (2005). Translational control in stress and apoptosis. *Nat. Rev. Mol. Cell Biol.* *6*, 318–327.

Van Hoof, A. (2002). Exosome-Mediated Recognition and Degradation of mRNAs Lacking a Termination Codon. *Science* *295*, 2262–2264.

Hopfner, K. (2003). Rad50/SMC proteins and ABC transporters: unifying concepts from high-resolution structures. *Curr. Opin. Struct. Biol.* *13*, 249–255.

Horwich, A.L., and Fenton, W.A. (2009). Chaperonin-mediated protein folding: using a central cavity to kinetically assist polypeptide chain folding. *Q. Rev. Biophys.* *42*, 83–116.

Hoshino, S.-i., Imai, M., Mizutani, M., Kikuchi, Y., Hanaoka, F., Ui, M., and Katada, T. (1998). Molecular Cloning of a Novel Member of the Eukaryotic Polypeptide Chain-Releasing Factors (eRF): its identification as eRF3 interacting with eRF1. *J. Biol. Chem.* *273*, 22254–22259.

Hoshino, S.-i., Imai, M., Kobayashi, T., Uchida, N., and Katada, T. (1999). The eukaryotic polypeptide chain releasing factor (eRF3/GSPT) carrying the translation termination signal to the 3'-Poly(A) tail of mRNA. Direct association of eRF3/GSPT with polyadenylate-binding protein. *J. Biol. Chem.* *274*, 16677–16680.

Houge, G., Døskeland, S.O., Bøe, R., and Lanotte, M. (1993). Selective cleavage of 28S rRNA variable regions V3 and V13 in myeloid leukemia cell apoptosis. *FEBS Lett.* *315*, 16–20.

Houge, G., Robaye, B., Eikhom, T.S., Golstein, J., Mellgren, G., Gjertsen, B.T., Lanotte, M., and Døskeland, S.O. (1995). Fine mapping of 28S rRNA sites specifically cleaved in cells undergoing apoptosis. *Mol. Cell. Biol.* *15*, 2051–2062.

Huang, H.-k., Yoon, H., Hannig, E.M., and Donahue, T.F. (1997). GTP hydrolysis controls stringent selection of the AUG start codon during translation initiation in *Saccharomyces cerevisiae*. *Genes Dev.* *11*, 2396–2413.

Humes, H.D. (1988). Aminoglycoside nephrotoxicity. *Kidney Int.* *33*, 900–911.

Hung, L.W., Wang, I.X., Nikaido, K., Liu, P.Q., Ames, G.F., and Kim, S.H. (1998). Crystal structure of the ATP-binding subunit of an ABC transporter. *Nature* *396*, 703–707.

Hunter, W.N., Brown, T., Anand, N.N., and Kennard, O. (1986). Structure of an adenine-cytosine base pair in DNA and its implications for mismatch repair. *Nature* *320*, 552–555.

Ishii, E., Chiba, S., Hashimoto, N., Kojima, S., Homma, M., Ito, K., Akiyama, Y., and Mori, H. (2015). Nascent chain-monitored remodeling of the Sec machinery for salinity adaptation of marine bacteria. *Proc. Natl. Acad. Sci. U. S. A.* *112*, 5513–5522.

Isken, O., Kim, Y.K., Hosoda, N., Mayeur, G.L., Hershey, J.W.B., and Maquat, L.E. (2008). Upf1 phosphorylation triggers translational repression during nonsense-mediated mRNA decay. *Cell* *133*, 314–327.

Ito, K., and Chiba, S. (2013). Arrest peptides: cis-acting modulators of translation. *Annu. Rev. Biochem.* *82*, 171–202.

Ito, K., Frolova, L., Seit-Nebi, A., Karamyshev, A., Kisseelev, L., and Nakamura, Y. (2002). Omnipotent decoding potential resides in eukaryotic translation termination factor eRF1 of variant-code organisms and is modulated by the interactions of amino acid sequences within domain 1. *Proc. Natl. Acad. Sci. U. S. A.* *99*, 8494–8499.

Ito-Harashima, S., Kuroha, K., Tatematsu, T., and Inada, T. (2007). Translation of the poly(A) tail plays crucial roles in nonstop mRNA surveillance via translation repression and protein destabilization by proteasome in yeast. *Genes Dev.* *21*, 519–524.

Ivanov, P. V., Gehring, N.H., Kunz, J.B., Hentze, M.W., and Kulozik, A.E. (2008). Interactions between UPF1, eRFs, PABP and the exon junction complex suggest an integrated model for mammalian NMD pathways. *EMBO J.* *27*, 736–747.

Ivanova, E. V., Kolosov, P.M., Birdsall, B., Kelly, G., Pastore, A., Kisseelev, L.L., and Polshakov, V.I. (2007). Eukaryotic class 1 translation termination factor eRF1—the NMR structure and dynamics of the middle domain involved in triggering ribosome-dependent peptidyl-tRNA hydrolysis. *FEBS J.* **274**, 4223–4237.

Jackson, R.J., and Hunt, T. (1983). Preparation and use of nuclease-treated rabbit reticulocyte lysates for the translation of eukaryotic messenger RNA. *Methods Enzymol.* **96**, 50–74.

Jackson, R.J., Howell, M.T., and Kaminski, A. (1990). The novel mechanism of initiation of picornavirus RNA translation. *Trends Biochem. Sci.* **15**, 477–483.

Jackson, R.J., Hellen, C.U.T., and Pestova, T. V (2010). The mechanism of eukaryotic translation initiation and principles of its regulation. *Nat. Rev. Mol. Cell Biol.* **11**, 113–127.

Jackson, R.J., Hellen, C.U.T., and Pestova, T. V (2012). Termination and post-termination events in eukaryotic translation. *Adv. Protein Chem. Struct. Biol.* **86**, 45–93.

Jakobsen, C.G., Søgaard, T.M.M., Frolova, L.Y., and Justesen, J. (2001). Identification of eRF3b, a Human Polypeptide Chain Release Factor with eRF3 Activity in vitro and in vivo. *35*, 575–583.

Janert, K.P. (2009). *Gnuplot in Action - Understanding Data with Graph.* (Manning Public.).

Jang, S.K., Kräusslich, H.G., Nicklin, M.J., Duke, G.M., Palmenberg, A.C., and Wimmer, E. (1988). A segment of the 5' nontranslated region of encephalomyocarditis virus RNA directs internal entry of ribosomes during in vitro translation. *J. Virol.* **62**, 2636–2643.

Janosi, L., Hara, H., Zhang, S., and Kaji, A. (1996). Ribosome recycling by ribosome recycling factor (RRF) ? An important but overlooked step of protein biosynthesis. *Adv. Biophys.* **32**, 121–201.

Janzen, D.M.M., Frolova, L., and Geballe, A.P.P. (2002). Inhibition of translation termination mediated by an interaction of eukaryotic release factor 1 with a nascent peptidyl-tRNA. *Mol. Cell. Biol.* **22**, 8562–8570.

Jenner, L.B., Demeshkina, N., Yusupova, G., and Yusupov, M. (2010). Structural aspects of messenger RNA reading frame maintenance by the ribosome. *Nat. Struct. Mol. Biol.* **17**, 555–560.

Jin, H., Kelley, A.C., Loakes, D., and Ramakrishnan, V. (2010). Structure of the 70S ribosome bound to release factor 2 and a substrate analog provides insights into catalysis of peptide release. *Proc. Natl. Acad. Sci. U. S. A.* **107**, 8593–8598.

Jomaa, A., Boehringer, D., Leibundgut, M., and Ban, N. (2016). Structures of the *E. coli* translating ribosome with SRP and its receptor and with the translocon. *Nat. Commun.* **7**, 10471.

Julián, P., Konevega, A.L., Scheres, S.H.W., Lázaro, M., Gil, D., Wintermeyer, W., Rodnina, M. V, and Valle, M. (2008). Structure of ratcheted ribosomes with tRNAs in hybrid states. *Proc. Natl. Acad. Sci. U. S. A.* **105**, 16924–16927.

Kaminishi, T., Wilson, D.N., Takemoto, C., Harms, J.M., Kawazoe, M., Schlüzen, F., Hanawa-Suetsugu, K., Shirouzu, M., Fucini, P., and Yokoyama, S. (2007). A snapshot of the 30S ribosomal subunit capturing mRNA via the Shine-Dalgarno interaction. *Structure* **15**, 289–297.

Kapp, L.D., and Lorsch, J.R. (2004). The molecular mechanics of eukaryotic translation. *Annu. Rev. Biochem.* **73**, 657–704.

Karcher, A., Schele, A., and Hopfner, K.-P. (2008). X-ray structure of the complete ABC enzyme ABCE1 from *Pyrococcus abyssi*. *J. Biol. Chem.* **283**, 7962–7971.

Karimi, R., Pavlov, M.Y., Buckingham, R.H., and Ehrenberg, M. (1999). Novel Roles for Classical Factors at the Interface between Translation Termination and Initiation. *Mol. Cell* **3**, 601–609.

Kaufman, R.J. (2004). Regulation of mRNA translation by protein folding in the endoplasmic reticulum. *Trends Biochem. Sci.* **29**, 152–158.

Kavran, J.M., Gundlapalli, S., O'Donoghue, P., Englert, M., Soll, D., and Steitz, T.A. (2007). Structure of pyrrolysyl-tRNA synthetase, an archaeal enzyme for genetic code innovation. *Proc. Natl. Acad. Sci.* **104**, 11268–11273.

Kayed, R., Head, E., Thompson, J.L., McIntire, T.M., Milton, S.C., Cotman, C.W., and Glabe, C.G. (2003). Common structure of soluble amyloid oligomers implies common mechanism of pathogenesis. *Science* **300**, 486–489.

Keeling, K.M., Xue, X., Gunn, G., and Bedwell, D.M. (2014). Therapeutics based on stop codon readthrough. *Annu. Rev. Genomics Hum. Genet.* **15**, 371–394.

Keiler, K.C., Waller, P.R.H., and Sauer, R.T. (1996). Role of a peptide tagging system in degradation of proteins synthesized from damaged messenger RNA. *Science* **271**, 990–993.

Kerem, E., Konstan, M.W., De Boeck, K., Accurso, F.J., Sermet-Gaudelus, I., Wilschanski, M., Elborn, J.S., Melotti, P., Bronsveld, I., Fajac, I., et al. (2014). Ataluren for the treatment of nonsense-mutation cystic fibrosis: a randomised, double-blind, placebo-controlled phase 3 trial. *Lancet Respir. Med.* 2, 539–547.

Kerr, I.D. (2004). Sequence analysis of twin ATP binding cassette proteins involved in translational control, antibiotic resistance, and ribonuclease L inhibition. *Biochem. Biophys. Res. Commun.* 315, 166–173.

Kervestin, S., and Jacobson, A. (2012). NMD: a multifaceted response to premature translational termination. *Nat. Rev. Mol. Cell Biol.* 13, 700–712.

Khade, P.K., Shi, X., and Joseph, S. (2013). Steric complementarity in the decoding center is important for tRNA selection by the ribosome. *J. Mol. Biol.* 425, 3778–3789.

Khatter, H., Myasnikov, A.G., Mastio, L., Billas, I.M.L., Birck, C., Stella, S., and Klaholz, B.P. (2014). Purification, characterization and crystallization of the human 80S ribosome. *Nucleic Acids Res.* 42, e49.

Khatter, H., Myasnikov, A.G., Natchiar, S.K., and Klaholz, B.P. (2015). Structure of the human 80S ribosome. *Nature* 520, 640–645.

Kiefer, J.R., Mao, C., Braman, J.C., and Beese, L.S. (1998). Visualizing DNA replication in a catalytically active *Bacillus* DNA polymerase crystal. *Nature* 391, 304–307.

Kim, K.K., Min, K., and Suh, S.W. (2000). Crystal structure of the ribosome recycling factor from *Escherichia coli*. *EMBO J.* 19, 2362–2370.

Klaholz, B.P. (2011). Molecular recognition and catalysis in translation termination complexes. *Trends Biochem. Sci.* 36, 282–292.

Klinge, S., Voigts-Hoffmann, F., Leibundgut, M., Arpagaus, S., and Ban, N. (2011). Crystal structure of the eukaryotic 60S ribosomal subunit in complex with initiation factor 6. *Science* 334, 941–948.

Klinge, S., Voigts-Hoffmann, F., Leibundgut, M., and Ban, N. (2012). Atomic structures of the eukaryotic ribosome. *Trends Biochem. Sci.* 37, 189–198.

Klug, A. (2010). From virus structure to chromatin: X-ray diffraction to three-dimensional electron microscopy. *Annu. Rev. Biochem.* 79, 1–35.

Knebel, A., Morrice, N., and Cohen, P. (2001). A novel method to identify protein kinase substrates: eEF2 kinase is phosphorylated and inhibited by SAPK4/p38delta. *EMBO J.* 20, 4360–4369.

Knudsen, C., Wieden, H.J., and Rodnina, M. V (2001). The importance of structural transitions of the switch II region for the functions of elongation factor Tu on the ribosome. *J. Biol. Chem.* 276, 22183–22190.

Koh, C.S., Brilot, A.F., Grigorieff, N., and Korostelev, A.A. (2014). Taura syndrome virus IRES initiates translation by binding its tRNA-mRNA-like structural element in the ribosomal decoding center. *Proc. Natl. Acad. Sci. U. S. A.* 111, 9139–9144.

Kolitz, S.E., and Lorsch, J.R. (2010). Eukaryotic initiator tRNA: finely tuned and ready for action. *FEBS Lett.* 584, 396–404.

Kolosov, P., Frolova, L., Seit-Nebi, A., Dubovaya, V., Kononenko, A., Oparina, N., Justesen, J., Efimov, A., and Kisselov, L. (2005). Invariant amino acids essential for decoding function of polypeptide release factor eRF1. *Nucleic Acids Res.* 33, 6418–6425.

Kolupaeva, V.G., Unbehaun, A., Lomakin, I.B., Hellen, C.U.T., and Pestova, T. V (2005). Binding of eukaryotic initiation factor 3 to ribosomal 40S subunits and its role in ribosomal dissociation and anti-association. *RNA* 11, 470–486.

Konevga, A.L., Fischer, N., Semenkov, Y.P., Stark, H., Wintermeyer, W., and Rodnina, M. V (2007). Spontaneous reverse movement of mRNA-bound tRNA through the ribosome. *Nat. Struct. Mol. Biol.* 14, 318–324.

Kong, C., Ito, K., Walsh, M.A., Wada, M., Liu, Y., Kumar, S., Barford, D., Nakamura, Y., and Song, H. (2004). Crystal structure and functional analysis of the eukaryotic class II release factor eRF3 from *S. pombe*. *Mol. Cell* 14, 233–245.

Kononenko, A. V, Mitkevich, V. a, Atkinson, G.C., Tenson, T., Dubovaya, V.I., Frolova, L.Y., Makarov, A. a, and Hauryliuk, V. (2010). GTP-dependent structural rearrangement of the eRF1:eRF3 complex and eRF3 sequence motifs essential for PABP binding. *Nucleic Acids Res.* 38, 548–558.

Korostelev, A.A. (2011). Structural aspects of translation termination on the ribosome. *RNA* 17, 1409–1421.

Korostelev, A., Asahara, H., Lancaster, L., Laurberg, M., Hirschi, A., Zhu, J., Trakhanov, S., Scott, W.G., and Noller, H.F. (2008). Crystal structure of a translation termination complex formed with release factor RF2. *Proc. Natl. Acad. Sci. U. S. A.* **105**, 19684–19689.

Korostelev, A., Zhu, J., Asahara, H., and Noller, H.F. (2010). Recognition of the amber UAG stop codon by release factor RF1. *EMBO J.* **29**, 2577–2585.

Kosolapov, A., Tu, L., Wang, J., and Deutsch, C. (2004). Structure acquisition of the T1 domain of Kv1.3 during biogenesis. *Neuron* **44**, 295–307.

Kozak, M. (1986). Point mutations define a sequence flanking the AUG initiator codon that modulates translation by eukaryotic ribosomes. *Cell* **44**, 283–292.

Kozak, M. (1991). An analysis of vertebrate mRNA sequences: intimations of translational control. *J. Cell Biol.* **115**, 887–903.

Kryuchkova, P., Grishin, A., Eliseev, B., Karyagina, A., Frolova, L., and Alkalaeva, E. (2013). Two-step model of stop codon recognition by eukaryotic release factor eRF1. *Nucleic Acids Res.* **41**, 4573–4586.

Kubelka, J., Hofrichter, J., and Eaton, W.A. (2004). The protein folding “speed limit”. *Curr. Opin. Struct. Biol.* **14**, 76–88.

Kucukelbir, A., Sigworth, F.J., and Tagare, H.D. (2014). Quantifying the local resolution of cryo-EM density maps. *Nat. Methods* **11**, 63–65.

Kudlicki, W., Coffman, A., Kramer, G., and Hardesty, B. (1997). Ribosomes and ribosomal RNA as chaperones for folding of proteins. *Fold. Des.* **2**, 101–108.

Kuhlenkoetter, S., Wintermeyer, W., and Rodnina, M. V (2011). Different substrate-dependent transition states in the active site of the ribosome. *Nature* **476**, 351–354.

Kuroha, K., Tatematsu, T., and Inada, T. (2009). Upf1 stimulates degradation of the product derived from aberrant messenger RNA containing a specific nonsense mutation by the proteasome. *EMBO Rep.* **10**, 1265–1271.

Kushnirov, V. V., Ter-Avanesyan, M.D., Telckov, M. V., Surguchov, A.P., Smirnov, V.N., and Inge-Vechtomov, S.G. (1988). Nucleotide sequence of the SUP2 (SUP35) gene of *Saccharomyces cerevisiae*. *Gene* **66**, 45–54.

Lagerkvist, U. (1978). “Two out of three”: an alternative method for codon reading. *Proc. Natl. Acad. Sci.* **75**, 1759–1762.

Langlois, R., Pallesen, J., and Frank, J. (2011). Reference-free particle selection enhanced with semi-supervised machine learning for cryo-electron microscopy. *J. Struct. Biol.* **175**, 353–361.

Laurberg, M., Asahara, H., Korostelev, A., Zhu, J., Trakhanov, S., and Noller, H.F. (2008). Structural basis for translation termination on the 70S ribosome. *Nature* **454**, 852–857.

Lawless, C., Pearson, R.D., Selley, J.N., Smirnova, J.B., Grant, C.M., Ashe, M.P., Pavitt, G.D., and Hubbard, S.J. (2009). Upstream sequence elements direct post-transcriptional regulation of gene expression under stress conditions in yeast. *BMC Genomics* **10**, 7.

Lawrence, M.G., Lindahl, L., and Zengel, J.M. (2008). Effects on translation pausing of alterations in protein and RNA components of the ribosome exit tunnel. *J. Bacteriol.* **190**, 5862–5869.

Leapman, R.D., and Sun, S. (1995). Cryo-electron energy loss spectroscopy: observations on vitrified hydrated specimens and radiation damage. *Ultramicroscopy* **59**, 71–79.

Leeds, P., Peltz, S.W., Jacobson, A., and Culbertson, M.R. (1991). The product of the yeast UPF1 gene is required for rapid turnover of mRNAs containing a premature translational termination codon. *Genes Dev.* **5**, 2303–2314.

LeFebvre, A.K., Korneeva, N.L., Trutschl, M., Cvek, U., Duzan, R.D., Bradley, C.A., Hershey, J.W.B., and Rhoads, R.E. (2006). Translation initiation factor eIF4G-1 binds to eIF3 through the eIF3e subunit. *J. Biol. Chem.* **281**, 22917–22932.

Leidig, C., Bange, G., Kopp, J., Amlacher, S., Aravind, A., Wickles, S., Witte, G., Hurt, E., Beckmann, R., and Sinning, I. (2013). Structural characterization of a eukaryotic chaperone—the ribosome-associated complex. *Nat. Struct. Mol. Biol.* **20**, 23–28.

Lengyel, P. (1966). Problems in protein biosynthesis. *J. Gen. Physiol.* **49**, 305–330.

Li, Y. (1998). Crystal structures of open and closed forms of binary and ternary complexes of the large fragment of *Thermus aquaticus* DNA polymerase I: structural basis for nucleotide incorporation. *EMBO J.* **17**, 7514–7525.

Li, W., Liu, Z., Korpella, R.K., Langlois, R., Sanyal, S., and Frank, J. (2015). Activation of GTP hydrolysis in mRNA-tRNA translocation by elongation factor G. *Sci. Adv.* **1**, e1500169.

Li, X., Mooney, P., Zheng, S., Booth, C.R., Braunfeld, M.B., Gubbens, S., Agard, D.A., and Cheng, Y. (2013). Electron counting and beam-induced motion correction enable near-atomic-resolution single-particle cryo-EM. *Nat. Methods* **10**, 584–590.

Liao, S., Lin, J., Do, H., and Johnson, A.E. (1997). Both luminal and cytosolic gating of the aqueous ER translocon pore are regulated from inside the ribosome during membrane protein integration. *Cell* **90**, 31–41.

Lin, J., Gagnon, M.G., Bulkley, D., and Steitz, T.A. (2015). Conformational changes of elongation factor G on the ribosome during tRNA translocation. *Cell* **160**, 219–227.

Lin, K.-F., Sun, C.-S., Huang, Y.-C., Chan, S.I., Koubek, J., Wu, T.-H., and Huang, J.J.-T. (2012). Cotranslational protein folding within the ribosome tunnel influences trigger-factor recruitment. *Biophys. J.* **102**, 2818–2827.

Lin, P.-J., Jongsma, C.G., Liao, S., and Johnson, A.E. (2011). Transmembrane segments of nascent polytopic membrane proteins control cytosol/ER targeting during membrane integration. *J. Cell Biol.* **195**, 41–54.

Linde, L., and Kerem, B. (2008). Introducing sense into nonsense in treatments of human genetic diseases. *Trends Genet.* **24**, 552–563.

Liu, D., Moran, S., and Kool, E.T. (1997). Bi-stranded, multisite replication of a base pair between difluorotoluene and adenine: confirmation by “inverse” sequencing. *Chem. Biol.* **4**, 919–926.

Liu, F., Putnam, A., and Jankowsky, E. (2008). ATP hydrolysis is required for DEAD-box protein recycling but not for duplex unwinding. *Proc. Natl. Acad. Sci. U. S. A.* **105**, 20209–20214.

Liu, H., Jin, L., Koh, S.B.S., Atanasov, I., Schein, S., Wu, L., and Zhou, Z.H. (2010). Atomic structure of human adenovirus by cryo-EM reveals interactions among protein networks. *Science* **329**, 1038–1043.

Liu, S., Wiggins, J.F., Sreenath, T., Kulkarni, A.B., Ward, J.M., and Leppla, S.H. (2006). Dph3, a small protein required for diphthamide biosynthesis, is essential in mouse development. *Mol. Cell. Biol.* **26**, 3835–3841.

Llácer, J.L., Hussain, T., Marler, L., Aitken, C.E., Thakur, A., Lorsch, J.R., Hinnebusch, A.G., and Ramakrishnan, V. (2015). Conformational differences between open and closed states of the eukaryotic translation initiation complex. *Mol. Cell* **59**, 399–412.

Lomakin, I.B., and Steitz, T.A. (2013). The initiation of mammalian protein synthesis and mRNA scanning mechanism. *Nature* **500**, 307–311.

Lomakin, I.B., Kolupaeva, V.G., Marintchev, A., Wagner, G., and Pestova, T. V (2003). Position of eukaryotic initiation factor eIF1 on the 40S ribosomal subunit determined by directed hydroxyl radical probing. *Genes Dev.* **17**, 2786–2797.

Lomakin, I.B., Shirokikh, N.E., Yusupov, M.M., Hellen, C.U.T., and Pestova, T. V (2006). The fidelity of translation initiation: reciprocal activities of eIF1, IF3 and YciH. *EMBO J.* **25**, 196–210.

Lorsch, J.R., and Herschlag, D. (1998). The DEAD box protein eIF4A. 1. A minimal kinetic and thermodynamic framework reveals coupled binding of RNA and nucleotide. *Biochemistry* **37**, 2180–2193.

Lovett, P.S., and Rogers, E.J. (1996). Ribosome regulation by the nascent peptide. *Microbiol. Rev.* **60**, 366–385.

Lu, J., and Deutsch, C. (2005). Folding zones inside the ribosomal exit tunnel. *Nat. Struct. Mol. Biol.* **12**, 1123–1129.

Lu, J., and Deutsch, C. (2008). Electrostatics in the ribosomal tunnel modulate chain elongation rates. *J. Mol. Biol.* **384**, 73–86.

Lu, J., Kobertz, W.R., and Deutsch, C. (2007). Mapping the electrostatic potential within the ribosomal exit tunnel. *J. Mol. Biol.* **371**, 1378–1391.

Lu, J., Hua, Z., Kobertz, W.R., and Deutsch, C. (2011). Nascent peptide side chains induce rearrangements in distinct locations of the ribosomal tunnel. *J. Mol. Biol.* **411**, 499–510.

Lu, L., Han, A.P., and Chen, J.J. (2001). Translation initiation control by heme-regulated eukaryotic initiation factor 2alpha kinase in erythroid cells under cytoplasmic stresses. *Mol. Cell. Biol.* **21**, 7971–7980.

Lu, P., Bai, X., Ma, D., Xie, T., Yan, C., Sun, L., Yang, G., Zhao, Y., Zhou, R., Scheres, S.H.W., et al. (2014). Three-dimensional structure of human γ -secretase. *Nature* **512**, 166–170.

Luo, Z., and Sachs, M.S. (1996). Role of an upstream open reading frame in mediating arginine-specific translational control in *Neurospora crassa*. *J. Bacteriol.* **178**, 2172–2177.

Lykke-Andersen, J., and Bennett, E.J. (2014). Protecting the proteome: Eukaryotic cotranslational quality control pathways. *J. Cell Biol.* **204**, 467–476.

Lyumkis, D., Brilot, A.F., Theobald, D.L., and Grigorieff, N. (2013). Likelihood-based classification of cryo-EM images using FREALIGN. *J. Struct. Biol.* **183**, 377–388.

Maag, D., Fekete, C.A., Gryczynski, Z., and Lorsch, J.R. (2005). A conformational change in the eukaryotic translation preinitiation complex and release of eIF1 signal recognition of the start codon. *Mol. Cell* **17**, 265–275.

Maag, D., Algire, M.A., and Lorsch, J.R. (2006). Communication between eukaryotic translation initiation factors 5 and 1A within the ribosomal pre-initiation complex plays a role in start site selection. *J. Mol. Biol.* **356**, 724–737.

Majumdar, R., Bandyopadhyay, A., and Maitra, U. (2003). Mammalian translation initiation factor eIF1 functions with eIF1A and eIF3 in the formation of a stable 40 S preinitiation complex. *J. Biol. Chem.* **278**, 6580–6587.

Majzoub, K., Hafirassou, M.L., Meignin, C., Goto, A., Marzi, S., Fedorova, A., Verdier, Y., Vinh, J., Hoffmann, J.A., Martin, F., et al. (2014). RACK1 controls IRES-mediated translation of viruses. *Cell* **159**, 1086–1095.

Mandal, A., Mandal, S., and Park, M.H. (2014). Genome-wide analyses and functional classification of proline repeat-rich proteins: potential role of eIF5A in eukaryotic evolution. *PLoS One* **9**, e111800.

Mantsyzov, A.B., Ivanova, E. V., Birdsall, B., Alkalaeva, E.Z., Kryuchkova, P.N., Kelly, G., Frolova, L.Y., and Polshakov, V.I. (2010). NMR solution structure and function of the C-terminal domain of eukaryotic class 1 polypeptide chain release factor. *FEBS J.* **277**, 2611–2627.

Maquat, L.E. (2004). Nonsense-mediated mRNA decay: splicing, translation and mRNP dynamics. *Nat. Rev. Mol. Cell Biol.* **5**, 89–99.

Marcotrigiano, J., Gingras, A.-C., Sonenberg, N., and Burley, S.K. (1999). Cap-dependent translation initiation in eukaryotes is regulated by a molecular mimic of eIF4G. *Mol. Cell* **3**, 707–716.

Mariappan, M., Li, X., Stefanovic, S., Sharma, A., Mateja, A., Keenan, R.J., and Hegde, R.S. (2010). A ribosome-associating factor chaperones tail-anchored membrane proteins. *Nature* **466**, 1120–1124.

Marintchev, A., Kolupaeva, V.G., Pestova, T. V., and Wagner, G. (2003). Mapping the binding interface between human eukaryotic initiation factors 1A and 5B: a new interaction between old partners. *Proc. Natl. Acad. Sci. U. S. A.* **100**, 1535–1540.

Mattheisl, S., Berninghausen, O., Becker, T., and Beckmann, R. (2015). Structure of a human translation termination complex. *Nucleic Acids Res.* **43**, 8615–8626.

Matsuda, R., Ikeuchi, K., Nomura, S., and Inada, T. (2014). Protein quality control systems associated with no-go and nonstop mRNA surveillance in yeast. *Genes Cells* **19**, 1–12.

Matthaei, J.H., and Nirenberg, M.W. (1961). Characteristics and stabilization of DNAase-sensitive protein synthesis in *E. coli* extracts. *Proc. Natl. Acad. Sci. U. S. A.* **47**, 1580–1588.

Mayer, M.P., and Bukau, B. (2005). Hsp70 chaperones: cellular functions and molecular mechanism. *Cell. Mol. Life Sci.* **62**, 670–684.

McInerney, G.M., Kedersha, N.L., Kaufman, R.J., Anderson, P., and Liljeström, P. (2005). Importance of eIF2alpha phosphorylation and stress granule assembly in alphavirus translation regulation. *Mol. Biol. Cell* **16**, 3753–3763.

McMullan, G., Faruqi, A.R., Henderson, R., Guerrini, N., Turchetta, R., Jacobs, A., and van Hoften, G. (2009a). Experimental observation of the improvement in MTF from backthinning a CMOS direct electron detector. *Ultramicroscopy* **109**, 1144–1147.

McMullan, G., Clark, A.T., Turchetta, R., and Faruqi, A.R. (2009b). Enhanced imaging in low dose electron microscopy using electron counting. *Ultramicroscopy* **109**, 1411–1416.

McMullan, G., Faruqi, A.R., Clare, D., and Henderson, R. (2014). Comparison of optimal performance at 300keV of three direct electron detectors for use in low dose electron microscopy. *Ultramicroscopy* **147**, 156–163.

Melnikov, S., Ben-Shem, A., Garreau de Loubresse, N., Jenner, L., Yusupova, G., and Yusupov, M. (2012). One core, two shells: bacterial and eukaryotic ribosomes. *Nat. Struct. Mol. Biol.* **19**, 560–567.

Mendell, J.T., Sharifi, N.A., Meyers, J.L., Martinez-Murillo, F., and Dietz, H.C. (2004). Nonsense surveillance regulates expression of diverse classes of mammalian transcripts and mutes genomic noise. *Nat. Genet.* **36**, 1073–1078.

Meyuhas, O., and Dreazen, A. (2009). Ribosomal protein S6 kinase from TOP mRNAs to cell size. *Prog. Mol. Biol. Transl. Sci.* **90**, 109–153.

Mikami, S., Kobayashi, T., Yokoyama, S., and Imataka, H. (2006). A hybridoma-based in vitro translation system that efficiently synthesizes glycoproteins. *J. Biotechnol.* **127**, 65–78.

Mikami, S., Kobayashi, T., and Imataka, H. (2010a). Cell-free protein synthesis systems with extracts from cultured human cells. *Methods Mol. Biol.* **607**, 43–52.

Mikami, S., Kobayashi, T., Machida, K., Masutani, M., Yokoyama, S., and Imataka, H. (2010b). N-terminally truncated GADD34 proteins are convenient translation enhancers in a human cell-derived in vitro protein synthesis system. *Biotechnol. Lett.* **32**, 897–902.

Miyazaki, K. (2011). MEGAWHOP cloning: a method of creating random mutagenesis libraries via megaprimer PCR of whole plasmids. (Elsevier Inc.).

Moazed, D., and Noller, H.F. (1989). Intermediate states in the movement of transfer RNA in the ribosome. *Nature* **342**, 142–148.

Morley, S.J., Coldwell, M.J., and Clemens, M.J. (2005). Initiation factor modifications in the preapoptotic phase. *Cell Death Differ.* **12**, 571–584.

Morris, D.R., and Geballe, A.P. (2000). Upstream open reading frames as regulators of mRNA translation. *Mol. Cell. Biol.* **20**, 8635–8642.

Mort, M., Ivanov, D., Cooper, D.N., and Chuzhanova, N.A. (2008). A meta-analysis of nonsense mutations causing human genetic disease. *Hum. Mutat.* **29**, 1037–1047.

Mu, T.-W., Ong, D.S.T., Wang, Y.-J., Balch, W.E., Yates, J.R., Segatori, L., and Kelly, J.W. (2008). Chemical and biological approaches synergize to ameliorate protein-folding diseases. *Cell* **134**, 769–781.

Muhs, M., Hilal, T., Mielke, T., Skabkin, M.A.A., Sanbonmatsu, K.Y.Y., Pestova, T.V. V, and Spahn, C.M.T.M.T. (2015). Cryo-EM of ribosomal 80S complexes with termination factors reveals the translocated cricket paralysis virus IRES. *Mol. Cell* **25**, 1–11.

Mulvey, M., Poppers, J., Sternberg, D., and Mohr, I. (2003). Regulation of eIF2alpha phosphorylation by different functions that act during discrete phases in the herpes simplex virus type 1 life cycle. *J. Virol.* **77**, 10917–10928.

Muth, G.W. (2000). A single adenosine with a neutral pKa in the ribosomal peptidyl transferase center. *Science* **289**, 947–950.

Muto, H., Nakatogawa, H., and Ito, K. (2006). Genetically encoded but nonpolypeptide prolyl-tRNA functions in the A site for SecM-mediated ribosomal stall. *Mol. Cell* **22**, 545–552.

Nakamura, Y., and Ito, K. (2011). tRNA mimicry in translation termination and beyond. *Wiley Interdiscip. Rev. RNA* **2**, 647–668.

Nakamura, Y., Ito, K., and Isaksson, L.A. (1996). Emerging Understanding of Translation Termination. *Cell* **87**, 147–150.

Nakatogawa, H., and Ito, K. (2002). The ribosomal exit tunnel functions as a discriminating gate. *Cell* **108**, 629–636.

Nanda, J.S., Cheung, Y.-N., Takacs, J.E., Martin-Marcos, P., Saini, A.K., Hinnebusch, A.G., and Lorsch, J.R. (2009). eIF1 controls multiple steps in start codon recognition during eukaryotic translation initiation. *J. Mol. Biol.* **394**, 268–285.

Nickell, S., Förster, F., Linaroudis, A., Net, W., Del, Beck, F., Hegerl, R., Baumeister, W., and Plitzko, J.M. (2005). TOM software toolbox: acquisition and analysis for electron tomography. *J. Struct. Biol.* **149**, 227–234.

Nilsson, J., Sengupta, J., Frank, J., and Nissen, P. (2004). Regulation of eukaryotic translation by the RACK1 protein: a platform for signalling molecules on the ribosome. *EMBO Rep.* **5**, 1137–1141.

Nissen, P., Kjeldgaard, M., Thirup, S., Polekhina, G., Reshetnikova, L., Clark, B.F., and Nyborg, J. (1995). Crystal structure of the ternary complex of Phe-tRNAPhe, EF-Tu, and a GTP analog. *Science* **270**, 1464–1472.

Nissen, P., Hansen, J., Ban, N., Moore, P.B., and Steitz, T.A. (2000). The structural basis of ribosome activity in peptide bond synthesis. *Science* **289**, 920–930.

Noeske, J., Wasserman, M.R., Terry, D.S., Altman, R.B., Blanchard, S.C., and Cate, J.H.D. (2015). High-resolution structure of the *Escherichia coli* ribosome. *Nat. Struct. Mol. Biol.* **22**, 336–341.

Nomoto, A., Lee, Y.F., and Wimmer, E. (1976). The 5' end of poliovirus mRNA is not capped with m7G(5')ppp(5')Np. *Proc. Natl. Acad. Sci. U. S. A.* **73**, 375–380.

Nürenberg, E., and Tampé, R. (2013). Tying up loose ends: ribosome recycling in eukaryotes and archaea. *Trends Biochem. Sci.* **38**, 64–74.

Ogle, J.M., Brodersen, D.E., Clemons, W.M., Tarry, M.J., Carter, A.P., and Ramakrishnan, V. (2001). Recognition of cognate transfer RNA by the 30S ribosomal subunit. *Science* **292**, 897–902.

Ogle, J.M., Murphy, F. V., Tarry, M.J., and Ramakrishnan, V. (2002). Selection of tRNA by the Ribosome Requires a Transition from an Open to a Closed Form. *Cell* **111**, 721–732.

Ogle, J.M., Carter, A.P., and Ramakrishnan, V. (2003). Insights into the decoding mechanism from recent ribosome structures. *Trends Biochem. Sci.* **28**, 259–266.

Oldfield, S., Jones, B.L., Tanton, D., and Proud, C.G. (1994). Use of monoclonal antibodies to study the structure and function of eukaryotic protein synthesis initiation factor eIF-2B. *Eur. J. Biochem.* **221**, 399–410.

Olofsson, S.-O., Bjursell, G., Boström, K., Carlsson, P., Elovson, J., Protter, A.A., Reuben, M.A., and Bondjers, G. (1987). Apolipoprotein B: structure, biosynthesis and role in the lipoprotein assembly process. *Atherosclerosis* **68**, 1–17.

Olsen, D.S., Savner, E.M., Mathew, A., Zhang, F., Krishnamoorthy, T., Phan, L., and Hinnebusch, A.G. (2003). Domains of eIF1A that mediate binding to eIF2, eIF3 and eIF5B and promote ternary complex recruitment in vivo. *EMBO J.* **22**, 193–204.

Olzscha, H., Schermann, S.M., Woerner, A.C., Pinkert, S., Hecht, M.H., Tartaglia, G.G., Vendruscolo, M., Hayter-Hartl, M., Hartl, F.U., and Vabulas, R.M. (2011). Amyloid-like aggregates sequester numerous metastable proteins with essential cellular functions. *Cell* **144**, 67–78.

Ominato, K., Akita, H., Suzuki, A., Kijima, F., Yoshino, T., Yoshino, M., Chiba, Y., Onouchi, H., and Naito, S. (2002). Identification of a short highly conserved amino acid sequence as the functional region required for posttranscriptional autoregulation of the cystathionine gamma-synthase gene in *Arabidopsis*. *J. Biol. Chem.* **277**, 36380–36386.

Onouchi, H., Nagami, Y., Haraguchi, Y., Nakamoto, M., Nishimura, Y., Sakurai, R., Nagao, N., Kawasaki, D., Kadokura, Y., and Naito, S. (2005). Nascent peptide-mediated translation elongation arrest coupled with mRNA degradation in the CGS1 gene of *Arabidopsis*. *Genes Dev.* **19**, 1799–1810.

Ortiz, P.A., Ulloque, R., Kihara, G.K., Zheng, H., and Kinzy, T.G. (2006). Translation elongation factor 2 anticodon mimicry domain mutants affect fidelity and diphtheria toxin resistance. *J. Biol. Chem.* **281**, 32639–32648.

Özeş, A.R., Feoktistova, K., Avanzino, B.C., and Fraser, C.S. (2011). Duplex unwinding and ATPase activities of the DEAD-box helicase eIF4A are coupled by eIF4G and eIF4B. *J. Mol. Biol.* **412**, 674–687.

Palade, G.E. (1955). A small particulate component of the cytoplasm. *J. Biophys. Biochem. Cytol.* **1**, 59–68.

Pallesen, J., Hashem, Y., Korkmaz, G., Korpella, R.K., Huang, C., Ehrenberg, M., Sanyal, S., and Frank, J. (2013). Cryo-EM visualization of the ribosome in termination complex with apo-RF3 and RF1. *Elife* **2**, e00411.

Pan, D., Kirillov, S. V., and Cooperman, B.S. (2007). Kinetically competent intermediates in the translocation step of protein synthesis. *Mol. Cell* **25**, 519–529.

Pape, T., Wintermeyer, W., and Rodnina, M. (1999). Induced fit in initial selection and proofreading of aminoacyl-tRNA on the ribosome. *EMBO J.* **18**, 3800–3807.

Park, M.H., Nishimura, K., Zanelli, C.F., and Valentini, S.R. (2010). Functional significance of eIF5A and its hypusine modification in eukaryotes. *Amino Acids* **38**, 491–500.

Parker, R. (2012). RNA degradation in *Saccharomyces cerevisiae*. *Genetics* **191**, 671–702.

Parola, A.L., and Kobilka, B.K. (1994). The peptide product of a 5' leader cistron in the beta 2 adrenergic receptor mRNA inhibits receptor synthesis. *J. Biol. Chem.* **269**, 4497–4505.

Passmore, L.A., Schmeing, T.M., Maag, D., Applefield, D.J., Acker, M.G., Algire, M.A., Lorsch, J.R., and Ramakrishnan, V. (2007). The eukaryotic translation initiation factors eIF1 and eIF1A induce an open conformation of the 40S ribosome. *Mol. Cell* **26**, 41–50.

Paulin, F.E., Campbell, L.E., O'Brien, K., Loughlin, J., and Proud, C.G. (2001). Eukaryotic translation initiation factor 5 (eIF5) acts as a classical GTPase-activator protein. *Curr. Biol.* **11**, 55–59.

Pauling, L., and Corey, R.B. (1953). A Proposed Structure For The Nucleic Acids. *Proc. Natl. Acad. Sci. U. S. A.* **39**, 84–97.

Pavitt, G.D., and Ron, D. (2012). New insights into translational regulation in the endoplasmic reticulum unfolded protein response. *Cold Spring Harb. Perspect. Biol.* **4**, 1–13.

Pavlov, M.Y., Watts, R.E., Tan, Z., Cornish, V.W., Ehrenberg, M., and Forster, A.C. (2009). Slow peptide bond formation by proline and other N-alkylamino acids in translation. *Proc. Natl. Acad. Sci. U. S. A.* **106**, 50–54.

Pelletier, J., and Sonenberg, N. (1988). Internal initiation of translation of eukaryotic mRNA directed by a sequence derived from poliovirus RNA. *Nature* **334**, 320–325.

Peltz, S.W., Brown, A.H., and Jacobson, A. (1993). mRNA destabilization triggered by premature translational termination depends on at least three cis-acting sequence elements and one trans-acting factor. *Genes Dev.* **7**, 1737–1754.

Peltz, S.W., Welch, E.M., Jacobson, A., Trotta, C.R., Naryshkin, N., Sweeney, H.L., and Bedwell, D.M. (2009). Nonsense suppression activity of PTC124 (ataluren). *Proc. Natl. Acad. Sci. U. S. A.* **106**, E64; author reply E65.

Peng, J., Schwartz, D., Elias, J.E., Thoreen, C.C., Cheng, D., Marsischky, G., Roelofs, J., Finley, D., and Gygi, S.P. (2003). A proteomics approach to understanding protein ubiquitination. *Nat. Biotechnol.* **21**, 921–926.

Peske, F., Rodnina, M. V., and Wintermeyer, W. (2005). Sequence of steps in ribosome recycling as defined by kinetic analysis. *Mol. Cell* **18**, 403–412.

Pestova, T. V., and Kolupaeva, V.G. (2002). The roles of individual eukaryotic translation initiation factors in ribosomal scanning and initiation codon selection. *Genes Dev.* **16**, 2906–2922.

Pestova, T. V., Borukhov, S.I., and Hellen, C.U. (1998). Eukaryotic ribosomes require initiation factors 1 and 1A to locate initiation codons. *Nature* **394**, 854–859.

Pestova, T. V., Lomakin, I.B., Lee, J.H., Choi, S.K., Dever, T.E., and Hellen, C.U. (2000). The joining of ribosomal subunits in eukaryotes requires eIF5B. *Nature* **403**, 332–335.

Pettersen, E.F., Goddard, T.D., Huang, C.C., Couch, G.S., Greenblatt, D.M., Meng, E.C., and Ferrin, T.E. (2004). UCSF Chimera-a visualization system for exploratory research and analysis. *J Comput Chem* **25**, 1605–1612.

Phillips, D.C. (1967). Symposium on three-dimensional structure of macromolecules of biological origin. By invitation of the committee on arrangements for the autumn meeting. Presented before the Academy on October 19, 1966. Chairman, Walter Kauzmann: THE HEN EGG-WHITE LYSOZYME. *Proc. Natl. Acad. Sci.* **57**, 483–495.

Pisarev, A. V., Kolupaeva, V.G., Pisareva, V.P., Merrick, W.C., Hellen, C.U.T., and Pestova, T. V (2006). Specific functional interactions of nucleotides at key -3 and +4 positions flanking the initiation codon with components of the mammalian 48S translation initiation complex. *Genes Dev.* **20**, 624–636.

Pisarev, A. V., Kolupaeva, V.G., Yusupov, M.M., Hellen, C.U., and Pestova, T. V (2008). Ribosomal position and contacts of mRNA in eukaryotic translation initiation complexes. *EMBO J.* **27**, 1609–1621.

Pisarev, A. V., Skabkin, M. a, Pisareva, V.P., Skabkina, O. V., Rakotondrafara, A.M., Hentze, M.W., Hellen, C.U.T., and Pestova, T. V (2010). The role of ABCE1 in eukaryotic posttermination ribosomal recycling. *Mol. Cell* **37**, 196–210.

Pisarev, A. V., Hellen, C.U.T., and Pestova, T. V. (2007). Recycling of Eukaryotic Posttermination Ribosomal Complexes. *Cell* **131**, 286–299.

Pisareva, V.P., Pisarev, A. V., Hellen, C.U.T., Rodnina, M. V., and Pestova, T. V (2006). Kinetic analysis of interaction of eukaryotic release factor 3 with guanine nucleotides. *J. Biol. Chem.* **281**, 40224–40235.

Pisareva, V.P., Pisarev, A. V., Komar, A.A., Hellen, C.U.T., and Pestova, T. V (2008). Translation initiation on mammalian mRNAs with structured 5'UTRs requires DExH-box protein DHX29. *Cell* **135**, 1237–1250.

Polacek, N., Gomez, M.J., Ito, K., Xiong, L., Nakamura, Y., and Mankin, A. (2003). The critical role of the universally conserved A2602 of 23S ribosomal RNA in the release of the nascent peptide during translation termination. *Mol. Cell* **11**, 103–112.

Polshakov, V.I., Eliseev, B.D., Birdsall, B., and Frolova, L.Y. (2012). Structure and dynamics in solution of the stop codon decoding N-terminal domain of the human polypeptide chain release factor eRF1. *Protein Sci.* **21**, 896–903.

Pool, M.R. (2009). A trans-membrane segment inside the ribosome exit tunnel triggers RAMP4 recruitment to the Sec61p translocase. *J. Cell Biol.* **185**, 889–902.

Pozdnyakova, I., Guidry, J., and Wittung-Stafshede, P. (2000). Copper-triggered β -hairpin formation: Initiation site for azurin folding? *J. Am. Chem. Soc.* **122**, 6337–6338.

Preis, A., Heuer, A., Barrio-Garcia, C., Hauser, A., Eyler, D.E., Berninghausen, O., Green, R., Becker, T., and Beckmann, R. (2014). Cryoelectron microscopic structures of eukaryotic translation termination complexes containing eRF1-eRF3 or eRF1-ABCE1. *Cell Rep.* **8**, 59–65.

Proshkin, S., Rahmouni, A.R., Mironov, A., and Nudler, E. (2010). Cooperation between translating ribosomes and RNA polymerase in transcription elongation. *Science* **328**, 504–508.

Pulak, R., and Anderson, P. (1993). mRNA surveillance by the *Caenorhabditis elegans* smg genes. *Genes Dev.* **7**, 1885–1897.

Quade, N., Boehringer, D., Leibundgut, M., van den Heuvel, J., and Ban, N. (2015). Cryo-EM structure of hepatitis C virus IRES bound to the human ribosome at 3.9-Å resolution. *Nat. Commun.* **6**, 7646.

Querol-Audi, J., Sun, C., Vogan, J.M., Smith, M.D., Gu, Y., Cate, J.H.D., and Nogales, E. (2013). Architecture of human translation initiation factor 3. *Structure* **21**, 920–928.

Rabl, J., Leibundgut, M., Ataide, S.F., Haag, A., and Ban, N. (2011). Crystal structure of the eukaryotic 40S ribosomal subunit in complex with initiation factor 1. *Science* **331**, 730–736.

Ramakrishnan, V. (2002). Ribosome structure and the mechanism of translation. *Cell* **108**, 557–572.

Ramelot, T.A., Cort, J.R., Yee, A.A., Liu, F., Goshe, M.B., Edwards, A.M., Smith, R.D., Arrowsmith, C.H., Dever, T.E., and Kennedy, M.A. (2002). Myxoma virus immunomodulatory protein M156R is a structural mimic of eukaryotic translation initiation factor eIF2α. *J. Mol. Biol.* **322**, 943–954.

Ramu, H., Mankin, A., and Vazquez-Laslop, N. (2009). Programmed drug-dependent ribosome stalling. *Mol. Microbiol.* **71**, 811–824.

Ramu, H., Vázquez-Laslop, N., Klepacki, D., Dai, Q., Piccirilli, J., Micura, R., and Mankin, A.S. (2011). Nascent peptide in the ribosome exit tunnel affects functional properties of the A-site of the peptidyl transferase center. *Mol. Cell* **41**, 321–330.

Ratje, A.H., Loerke, J., Mikolajka, A., Brünner, M., Hildebrand, P.W., Starosta, A.L., Dönhöfer, A., Connell, S.R., Fucini, P., Mielke, T., et al. (2010). Head swivel on the ribosome facilitates translocation by means of intra-subunit tRNA hybrid sites. *Nature* **468**, 713–716.

Raught, B., and Gingras, A.-C. (1999). eIF4E activity is regulated at multiple levels. *Int. J. Biochem. Cell Biol.* **31**, 43–57.

Redpath, N.T., Foulstone, E.J., and Proud, C.G. (1996). Regulation of translation elongation factor-2 by insulin via a rapamycin-sensitive signalling pathway. *EMBO J.* **15**, 2291–2297.

Rennie, M.J. (2005). Why muscle stops building when it's working. *J. Physiol.* **569**, 3.

Reynolds, K., Zimmer, A.M., and Zimmer, A. (1996). Regulation of RAR beta 2 mRNA expression: evidence for an inhibitory peptide encoded in the 5'-untranslated region. *J. Cell Biol.* **134**, 827–835.

Roberto Gambari, G.B.F.S.A.F. and M.B. (2015). Cystic Fibrosis in the Light of New Research (InTech).

Robinson, P.J., Findlay, J.E., and Woolhead, C.A. (2012). Compaction of a prokaryotic signal-anchor transmembrane domain begins within the ribosome tunnel and is stabilized by SRP during targeting. *J. Mol. Biol.* **423**, 600–612.

Rodnina, M. V (2013). The ribosome as a versatile catalyst: reactions at the peptidyl transferase center. *Curr. Opin. Struct. Biol.* **23**, 595–602.

Rodnina, M. V, and Wintermeyer, W. (2009). Recent mechanistic insights into eukaryotic ribosomes. *Curr. Opin. Cell Biol.* **21**, 435–443.

Rodnina, M. V., Pape, T., Fricke, R., Kuhn, L., and Wintermeyer, W. (1996). Initial binding of the elongation factor Tu-GTP-aminoacyl-tRNA complex preceding codon recognition on the ribosome. *J. Biol. Chem.* **271**, 646–652.

Rogers, G.W., Richter, N.J., Lima, W.F., and Merrick, W.C. (2001). Modulation of the helicase activity of eIF4A by eIF4B, eIF4H, and eIF4F. *J. Biol. Chem.* **276**, 30914–30922.

Rogers, G.W., Komar, A.A., and Merrick, W.C. (2002). eIF4A: the godfather of the DEAD box helicases. *Prog. Nucleic Acid Res. Mol. Biol.* **72**, 307–331.

Ron, D., and Harding, P.H. (2006). eIF2alpha Phosphorylation in Cellular Stress Responses and Disease. *T Ranslational Control Biol. Med.* ©2007 Cold Spring Harb. Lab. Press 349–372.

Rozovsky, N., Butterworth, A.C., and Moore, M.J. (2008). Interactions between eIF4AI and its accessory factors eIF4B and eIF4H. *RNA* **14**, 2136–2148.

Ruskin, R.S., Yu, Z., and Grigorieff, N. (2013). Quantitative characterization of electron detectors for transmission electron microscopy. *J. Struct. Biol.* **184**, 385–393.

Russo, C.J., and Passmore, L.A. (2014). Ultrastable gold substrates for electron cryomicroscopy. *Science* **346**, 1377–1380.

Ruvinsky, I., and Meyuhas, O. (2006). Ribosomal protein S6 phosphorylation: from protein synthesis to cell size. *Trends Biochem. Sci.* **31**, 342–348.

Saini, A.K., Nanda, J.S., Lorsch, J.R., and Hinnebusch, A.G. (2010). Regulatory elements in eIF1A control the fidelity of start codon selection by modulating tRNA(i)(Met) binding to the ribosome. *Genes Dev.* **24**, 97–110.

Salas-Marco, J., and Bedwell, D.M. (2004). GTP hydrolysis by eRF3 facilitates stop codon decoding during eukaryotic translation termination. *Mol. Cell. Biol.* **24**, 7769–7778.

Sander, J.D., and Joung, J.K. (2014). CRISPR-Cas systems for editing, regulating and targeting genomes. *Nat. Biotechnol.* **32**, 347–355.

Sasaki, Y., Welshhans, K., Wen, Z., Yao, J., Xu, M., Goshima, Y., Zheng, J.Q., and Bassell, G.J. (2010). Phosphorylation of zipcode binding protein 1 is required for brain-derived neurotrophic factor signaling of local-actin synthesis and growth cone turning. *J. Neurosci.* **30**, 9349–9358.

Savelsbergh, A., Katunin, V.I., Mohr, D., Peske, F., Rodnina, M. V., and Wintermeyer, W. (2003). An elongation factor G-induced ribosome rearrangement precedes tRNA-mRNA translocation. *Mol. Cell* **11**, 1517–1523.

Scheres, S.H. (2014). Beam-induced motion correction for sub-megadalton cryo-EM particles. *Elife* **3**, e03665.

Scheres, S.H.W. (2010). Classification of structural heterogeneity by maximum-likelihood methods. *Methods Enzymol.* **482**, 295–320.

Scheres, S.H.W. (2012a). RELION: implementation of a Bayesian approach to cryo-EM structure determination. *J. Struct. Biol.* **180**, 519–530.

Scheres, S.H.W. (2012b). A Bayesian view on cryo-EM structure determination. *J. Mol. Biol.* **415**, 406–418.

Scheres, S.H.W., and Chen, S. (2012). Prevention of overfitting in cryo-EM structure determination. *Nat. Methods* **9**, 853–854.

Scheres, S.H.W., Gao, H., Valle, M., Herman, G.T., Eggernmont, P.P.B., Frank, J., and Carazo, J.-M. (2007). Disentangling conformational states of macromolecules in 3D-EM through likelihood optimization. *Nat. Methods* **4**, 27–29.

Schleiss, M.R., Degn, C.R., and Geballe, A.P. (1991). Translational control of human cytomegalovirus gp48 expression. *65*, 6782–6789.

Schmeing, T.M., Huang, K.S., Strobel, S. a, and Steitz, T.A. (2005a). An induced-fit mechanism to promote peptide bond formation and exclude hydrolysis of peptidyl-tRNA. *Nature* **438**, 520–524.

Schmeing, T.M., Huang, K.S., Kitchen, D.E., Strobel, S.A., and Steitz, T.A. (2005b). Structural insights into the roles of water and the 2' hydroxyl of the P site tRNA in the peptidyl transferase reaction. *Mol. Cell* **20**, 437–448.

Schmeing, T.M., Voorhees, R.M., Kelley, A.C., Gao, Y.-G., Murphy, F. V., Weir, J.R., and Ramakrishnan, V. (2009). The crystal structure of the ribosome bound to EF-Tu and aminoacyl-tRNA. *Science* **326**, 688–694.

Schmitt, E., Naveau, M., and Mechulam, Y. (2010). Eukaryotic and archaeal translation initiation factor 2: a heterotrimeric tRNA carrier. *FEBS Lett.* **584**, 405–412.

Schröder, R.R. (2015). Advances in electron microscopy: A qualitative view of instrumentation development for macromolecular imaging and tomography. *Arch. Biochem. Biophys.* **581**, 25–38.

Schuette, J.-C., Murphy, F. V., Kelley, A.C., Weir, J.R., Giesebricht, J., Connell, S.R., Loerke, J., Mielke, T., Zhang, W., Penczek, P.A., et al. (2009). GTPase activation of elongation factor EF-Tu by the ribosome during decoding. *EMBO J.* **28**, 755–765.

Schüler, M., Connell, S.R., Lescoute, A., Giesebricht, J., Dabrowski, M., Schroeer, B., Mielke, T., Penczek, P.A., Westhof, E., and Spahn, C.M.T. (2006). Structure of the ribosome-bound cricket paralysis virus IRES RNA. *Nat. Struct. Mol. Biol.* **13**, 1092–1096.

Schütz, P., Bumann, M., Oberholzer, A.E., Bieniossek, C., Trachsel, H., Altmann, M., and Baumann, U. (2008). Crystal structure of the yeast eIF4A-eIF4G complex: an RNA-helicase controlled by protein-protein interactions. *Proc. Natl. Acad. Sci. U. S. A.* **105**, 9564–9569.

Schuwirth, B.S., Borovinskaya, M.A., Hau, C.W., Zhang, W., Vila-Sanjurjo, A., Holton, J.M., and Cate, J.H.D. (2005). Structures of the bacterial ribosome at 3.5 Å resolution. *Science* **310**, 827–834.

Scolnick, E., Tompkins, R., Caskey, T., and Nirenberg, M. (1968). Release factors differing in specificity for terminator codons. *Proc. Natl. Acad. Sci. U. S. A.* **61**, 768–774.

Seeman, N.C., Rosenberg, J.M., and Rich, A. (1976). Sequence-specific recognition of double helical nucleic acids by proteins. *Proc. Natl. Acad. Sci. U. S. A.* **73**, 804–808.

Seidelt, B., Innis, C.A., Wilson, D.N., Gartmann, M., Armache, J.-P., Villa, E., Trabuco, L.G., Becker, T., Mielke, T., Schulten, K., et al. (2009). Structural insight into nascent polypeptide chain-mediated translational stalling. *Science* **326**, 1412–1415.

Seit-Nebi, A., Frolova, L., Justesen, J., and Kisseelev, L. (2001). Class-1 translation termination factors: invariant GGQ minidomain is essential for release activity and ribosome binding but not for stop codon recognition. *Nucleic Acids Res.* **29**, 3982–3987.

Seit-Nebi, A., Frolova, L., and Kisseelev, L. (2002). Conversion of omnipotent translation termination factor eRF1 into ciliate-like UGA-only unipotent eRF1. *EMBO Rep.* **3**, 881–886.

Selimoglu, E. (2007). Aminoglycoside-induced ototoxicity. *Curr. Pharm. Des.* **13**, 119–126.

Selmer, M. (1999). Crystal structure of *thermotoga maritima* ribosome recycling factor: A tRNA mimic. *Science* **286**, 2349–2352.

Selmer, M. (2006). Structure of the 70S Ribosome Complexed with mRNA and tRNA. *Science* **313**, 1935–1942.

Semenkov, Y.P., Rodnina, M. V., and Wintermeyer, W. (2000). Energetic contribution of tRNA hybrid state formation to translocation catalysis on the ribosome. *Nat. Struct. Biol.* **7**, 1027–1031.

Sengoku, T., Nureki, O., Nakamura, A., Kobayashi, S., and Yokoyama, S. (2006). Structural basis for RNA unwinding by the DEAD-box protein *Drosophila* Vasa. *Cell* **125**, 287–300.

Sengupta, J., Nilsson, J., Gursky, R., Spahn, C.M.T., Nissen, P., and Frank, J. (2004). Identification of the versatile scaffold protein RACK1 on the eukaryotic ribosome by cryo-EM. *Nat. Struct. Mol. Biol.* **11**, 957–962.

Sengupta, J., Nilsson, J., Gursky, R., Kjeldgaard, M., Nissen, P., and Frank, J. (2008). Visualization of the eEF2-80S ribosome transition-state complex by cryo-electron microscopy. *J. Mol. Biol.* **382**, 179–187.

Shaikh, T.R., Gao, H., Baxter, W.T., Asturias, F.J., Boisset, N., Leith, A., and Frank, J. (2008). SPIDER image processing for single-particle reconstruction of biological macromolecules from electron micrographs. *Nat. Protoc.* **3**, 1941–1974.

Sharma, D., R, S.D., and and Green, R. (2004). EF-G-independent reactivity of a pre-translocation-state ribosome complex with the aminoacyl tRNA substrate puromycin supports an intermediate (hybrid) state of tRNA binding. *RNA* **10**, 102–113.

Sharma, P., Yan, F.F., Doronina, V.A., Escuin-Ordinas, H., Ryan, M.D., and Brown, J.D. (2012). 2A peptides provide distinct solutions to driving stop-carry on translational recoding. *Nucleic Acids Res.* **40**, 3143–3151.

Sheppard, D.N., Ostedgaard, L.S., Rich, D.P., and Welsh, M.J. (1994). The amino-terminal portion of CFTR forms a regulated Cl⁻ channel. *Cell* **76**, 1091–1098.

Sheu, S.-Y., Yang, D.-Y., Selzle, H.L., and Schlag, E.W. (2003). Energetics of hydrogen bonds in peptides. *Proc. Natl. Acad. Sci. U. S. A.* **100**, 12683–12687.

Shimizu, Y., Inoue, A., Tomari, Y., Suzuki, T., Yokogawa, T., Nishikawa, K., and Ueda, T. (2001). Cell-free translation reconstituted with purified components. *Nat. Biotechnol.* **19**, 751–755.

Shimizu, Y., Kanamori, T., and Ueda, T. (2005). Protein synthesis by pure translation systems. *Methods* **36**, 299–304.

Shin, B.-S., Maag, D., Roll-Mecak, A., Arefin, M.S., Burley, S.K., Lorsch, J.R., and Dever, T.E. (2002). Uncoupling of initiation factor eIF5B/IF2 GTPase and translational activities by mutations that lower ribosome affinity. *Cell* **111**, 1015–1025.

Shine, J., and Dalgarno, L. (1974). The 3'-terminal sequence of *Escherichia coli* 16S ribosomal RNA: complementarity to nonsense triplets and ribosome binding sites. *Proc. Natl. Acad. Sci. U. S. A.* **71**, 1342–1346.

Shoemaker, C.J., and Green, R. (2011). Kinetic analysis reveals the ordered coupling of translation termination and ribosome recycling in yeast. *Proc. Natl. Acad. Sci. U. S. A.* **108**, E1392–E1398.

Shoemaker, C.J., and Green, R. (2012). Translation drives mRNA quality control. *Nat. Struct. Mol. Biol.* **19**, 594–601.

Shoji, S., Walker, S.E., and Fredrick, K. (2006). Reverse translocation of tRNA in the ribosome. *Mol. Cell* **24**, 931–942.

Sievers, A., Beringer, M., Rodnina, M. V., and Wolfenden, R. (2004). The ribosome as an entropy trap. *Proc. Natl. Acad. Sci. U. S. A.* **101**, 7897–7901.

Sigworth, F.J. (1998). A maximum-likelihood approach to single-particle image refinement. *J. Struct. Biol.* **122**, 328–339.

Sigworth, F.J., Doerschuk, P.C., Carazo, J.-M., and Scheres, S.H.W. (2010). An introduction to maximum-likelihood methods in cryo-EM. *Methods Enzymol.* **482**, 263–294.

Singh, C.R., Lee, B., Udagawa, T., Mohammad-Qureshi, S.S., Yamamoto, Y., Pavitt, G.D., and Asano, K. (2006). An eIF5/eIF2 complex antagonizes guanine nucleotide exchange by eIF2B during translation initiation. *EMBO J.* **25**, 4537–4546.

Singh, C.R., Udagawa, T., Lee, B., Wassink, S., He, H., Yamamoto, Y., Anderson, J.T., Pavitt, G.D., and Asano, K. (2007). Change in nutritional status modulates the abundance of critical pre-initiation intermediate complexes during translation initiation in vivo. *J. Mol. Biol.* **370**, 315–330.

Siridechadilok, B., Fraser, C.S., Hall, R.J., Doudna, J.A., and Nogales, E. (2005). Structural roles for human translation factor eIF3 in initiation of protein synthesis. *Science* **310**, 1513–1515.

Skabkin, M.A., Skabkina, O. V., Dhote, V., Komar, A.A., Hellen, C.U.T., and Pestova, T. V (2010). Activities of Ligatin and MCT-1/DENR in eukaryotic translation initiation and ribosomal recycling. *Genes Dev.* **24**, 1787–1801.

Smith, K.C., and Honig, B. (1994). Evaluation of the conformational free energies of loops in proteins. *Proteins* **18**, 119–132.

Sohmen, D., Chiba, S., Shimokawa-Chiba, N., Innis, C.A., Berninghausen, O., Beckmann, R., Ito, K., and Wilson, D.N. (2015). Structure of the *Bacillus subtilis* 70S ribosome reveals the basis for species-specific stalling. *Nat. Commun.* **6**, 6941.

Sonenberg, N., and Hinnebusch, A.G. (2009). Regulation of translation initiation in eukaryotes: mechanisms and biological targets. *Cell* **136**, 731–745.

Song, H., Mugnier, P., Das, A.K., Webb, H.M., Evans, D.R., Tuite, M.F., Hemmings, B.A., and Barford, D. (2000). The crystal structure of human eukaryotic release factor eRF1 - mechanism of stop codon recognition and peptidyl-tRNA hydrolysis. *Cell* **100**, 311–321.

Sorzano, C.O.S., Recarte, E., Alcorlo, M., Bilbao-Castro, J.R., San-Martín, C., Marabini, R., and Carazo, J.M. (2009). Automatic particle selection from electron micrographs using machine learning techniques. *J. Struct. Biol.* **167**, 252–260.

Spahn, C.M.T., and Penczek, P.A. (2009). Exploring conformational modes of macromolecular assemblies by multiparticle cryo-EM. *Curr. Opin. Struct. Biol.* **19**, 623–631.

Spahn, C.M.T., Beckmann, R., Eswar, N., Penczek, P.A., Sali, A., Blobel, G., and Frank, J. (2001). Structure of the 80S Ribosome from *Saccharomyces cerevisiae* - tRNA-Ribosome and Subunit-Subunit Interactions. *Cell* **107**, 373–386.

Spevak, C.C., Ivanov, I.P., and Sachs, M.S. (2010). Sequence requirements for ribosome stalling by the arginine attenuator peptide. *J. Biol. Chem.* **285**, 40933–40942.

Stansfield, I., Jones, K.M., Herbert, P., Lewendon, A., Shaw, W. V, and Tuite, M.F. (1998). Missense translation errors in *Saccharomyces cerevisiae*. *J. Mol. Biol.* **282**, 13–24.

Stark, H., Rodnina, M. V, Rinke-Appel, J., Brimacombe, R., Wintermeyer, W., and van Heel, M. (1997). Visualization of elongation factor Tu on the *Escherichia coli* ribosome. *Nature* **389**, 403–406.

Studer, S.M., Feinberg, J.S., and Joseph, S. (2003). Rapid kinetic analysis of EF-G-dependent mRNA translocation in the ribosome. *J. Mol. Biol.* **327**, 369–381.

Suloway, C., Pulokas, J., Fellmann, D., Cheng, A., Guerra, F., Quispe, J., Stagg, S., Potter, C.S., and Carragher, B. (2005). Automated molecular microscopy: the new Leginon system. *J. Struct. Biol.* **151**, 41–60.

Sun, C., Todorovic, A., Querol-Audí, J., Bai, Y., Villa, N., Snyder, M., Ashchyan, J., Lewis, C.S., Hartland, A., Gradia, S., et al. (2011). Functional reconstitution of human eukaryotic translation initiation factor 3 (eIF3). *Proc. Natl. Acad. Sci. U. S. A.* **108**, 20473–20478.

Susorov, D., Mikhailova, T., Ivanov, a., Sokolova, E., and Alkalaeva, E. (2015). Stabilization of eukaryotic ribosomal termination complexes by deacylated tRNA. *Nucleic Acids Res.* **1–12**.

Sweeney, R., Chen, L., and Yao, M.C. (1994). An rRNA variable region has an evolutionarily conserved essential role despite sequence divergence. *Mol. Cell. Biol.* **14**, 4203–4215.

Taniuchi, H., and Anfinsen, C.B. (1969). An experimental approach to the study of the folding of staphylococcal nuclease. *J. Biol. Chem.* **244**, 3864–3875.

Tate, W.P., and Mannerling, S.A. (1996). MicroReview Three, four or more: The translational stop signal at length. *Mol. Microbiol.* **21**, 213–219.

Taylor, D., Unbehaun, A., Li, W., Das, S., Lei, J., Liao, H.Y., Grassucci, R. a, Pestova, T. V, and Frank, J. (2012). Cryo-EM structure of the mammalian eukaryotic release factor eRF1-eRF3-associated termination complex. *Proc. Natl. Acad. Sci. U. S. A.* **109**, 18413–18418.

Taylor, D.J., Nilsson, J., Merrill, A.R., Andersen, G.R., Nissen, P., and Frank, J. (2007). Structures of modified eEF2 80S ribosome complexes reveal the role of GTP hydrolysis in translocation. *EMBO J.* **26**, 2421–2431.

Taylor, D.J., Devkota, B., Huang, A.D., Topf, M., Narayanan, E., Sali, A., Harvey, S.C., and Frank, J. (2009). Comprehensive molecular structure of the eukaryotic ribosome. *Structure* **17**, 1591–1604.

Thein, S.L. (2013). The molecular basis of β-thalassemia. *Cold Spring Harb. Perspect. Med.* **3**, a011700.

Thompson, R.C., and Stone, P.J. (1977). Proofreading of the codon-anticodon interaction on ribosomes. *Proc. Natl. Acad. Sci. U. S. A.* **74**, 198–202.

Tomic, S., Johnson, A.E., Hartl, F.U., and Etchells, S.A. (2006). Exploring the capacity of trigger factor to function as a shield for ribosome bound polypeptide chains. *FEBS Lett.* **580**, 72–76.

Tourigny, D.S., Fernández, I.S., Kelley, A.C., and Ramakrishnan, V. (2013). Elongation factor G bound to the ribosome in an intermediate state of translocation. *Science* **340**, 1235490.

Toyoda, T., Tin, O.F., Ito, K., Fujiwara, T., Kumasaka, T., Yamamoto, M., Garber, M.B., and Nakamura, Y. (2000). Crystal structure combined with genetic analysis of the *Thermus thermophilus* ribosome recycling factor shows that a flexible hinge may act as a functional switch. *RNA* **6**, 1432–1444.

Tsai, A., Uemura, S., Johansson, M., Puglisi, E.V., Marshall, R.A., Aitken, C.E., Korlach, J., Ehrenberg, M., and Puglisi, J.D. (2013). The impact of aminoglycosides on the dynamics of translation elongation. *Cell Rep.* **3**, 497–508.

Tu, L.W., and Deutsch, C. (2010). A folding zone in the ribosomal exit tunnel for Kv1.3 helix formation. *J. Mol. Biol.* **396**, 1346–1360.

Tu, L., Wang, J., and Deutsch, C. (2007). Biogenesis of the T1-S1 linker of voltage-gated K⁺ channels. *Biochemistry* **46**, 8075–8084.

Tuller, T., Carmi, A., Vestsigian, K., Navon, S., Dorfan, Y., Zaborske, J., Pan, T., Dahan, O., Furman, I., and Pilpel, Y. (2010). An evolutionarily conserved mechanism for controlling the efficiency of protein translation. *Cell* **141**, 344–354.

Uchida, N., Hoshino, S.-I., Imataka, H., Sonenberg, N., and Katada, T. (2002). A novel role of the mammalian GSPT/eRF3 associating with poly(A)-binding protein in Cap/Poly(A)-dependent translation. *J. Biol. Chem.* **277**, 50286–50292.

Uemura, S., Aitken, C.E., Korlach, J., Flusberg, B.A., Turner, S.W., and Puglisi, J.D. (2010). Real-time tRNA transit on single translating ribosomes at codon resolution. *Nature* **464**, 1012–1017.

Valasek, L. (2003). The yeast eIF3 subunits TIF32/a, NIP1/c, and eIF5 make critical connections with the 40S ribosome in vivo. *Genes Dev.* **17**, 786–799.

Valle, M., Sengupta, J., Swami, N.K., Grassucci, R.A., Burkhardt, N., Nierhaus, K.H., Agrawal, R.K., and Frank, J. (2002). Cryo-EM reveals an active role for aminoacyl-tRNA in the accommodation process. *EMBO J.* **21**, 3557–3567.

Vassilenko, K.S., Alekhina, O.M., Dmitriev, S.E., Shatsky, I.N., and Spirin, A.S. (2011). Unidirectional constant rate motion of the ribosomal scanning particle during eukaryotic translation initiation. *Nucleic Acids Res.* **39**, 5555–5567.

Vazquez-Laslop, N., Thum, C., and Mankin, A.S. (2008). Molecular mechanism of drug-dependent ribosome stalling. *Mol. Cell* **30**, 190–202.

Vázquez-Laslop, N., Ramu, H., Klepacki, D., Kannan, K., and Mankin, A.S. (2010). The key function of a conserved and modified rRNA residue in the ribosomal response to the nascent peptide. *EMBO J.* **29**, 3108–3117.

Veesler, D., Ng, T.-S., Sendamarai, A.K., Eilers, B.J., Lawrence, C.M., Lok, S.-M., Young, M.J., Johnson, J.E., and Fu, C. (2013). Atomic structure of the 75 MDa extremophile *Sulfolobus* turreted icosahedral virus determined by CryoEM and X-ray crystallography. *Proc. Natl. Acad. Sci. U. S. A.* **110**, 5504–5509.

Villa, E., Sengupta, J., Trabuco, L.G., LeBarron, J., Baxter, W.T., Shaikh, T.R., Grassucci, R.A., Nissen, P., Ehrenberg, M., Schulten, K., et al. (2009). Ribosome-induced changes in elongation factor Tu conformation control GTP hydrolysis. *Proc. Natl. Acad. Sci. U. S. A.* **106**, 1063–1068.

Vogeley, L., Palm, G.J., Mesters, J.R., and Hilgenfeld, R. (2001). Conformational change of elongation factor Tu (EF-Tu) induced by antibiotic binding. Crystal structure of the complex between EF-Tu.GDP and aurodox. *J. Biol. Chem.* **276**, 17149–17155.

Voigt-Hoffmann, F., Klinge, S., and Ban, N. (2012). Structural insights into eukaryotic ribosomes and the initiation of translation. *Curr. Opin. Struct. Biol.* **22**, 768–777.

Voorhees, R.M., and Hegde, R.S. (2015). Structures of the scanning and engaged states of the mammalian SRP-ribosome complex. *Elife* **4**, e07975.

Voorhees, R.M., and Ramakrishnan, V. (2013). Structural basis of the translational elongation cycle. *Annu. Rev. Biochem.* **82**, 203–236.

Voorhees, R.M., Weixlbaumer, A., Loakes, D., Kelley, A.C., and Ramakrishnan, V. (2009). Insights into substrate stabilization from snapshots of the peptidyl transferase center of the intact 70S ribosome. *Nat. Struct. Mol. Biol.* **16**, 528–533.

Voorhees, R.M., Schmeing, T.M., Kelley, A.C., and Ramakrishnan, V. (2010). The mechanism for activation of GTP hydrolysis on the ribosome. *Science* **330**, 835–838.

Voss, N.R., Gerstein, M., Steitz, T.A., and Moore, P.B. (2006). The geometry of the ribosomal polypeptide exit tunnel. *J. Mol. Biol.* **360**, 893–906.

Voss, N.R., Yoshioka, C.K., Radermacher, M., Potter, C.S., and Carragher, B. (2009). DoG Picker and TiltPicker: software tools to facilitate particle selection in single particle electron microscopy. *J. Struct. Biol.* **166**, 205–213.

Wagenknecht, T., Grassucci, R., and Frank, J. (1988). Electron microscopy and computer image averaging of ice-embedded large ribosomal subunits from *Escherichia coli*. *J. Mol. Biol.* **199**, 137–147.

Walker, S.E., Shoji, S., Pan, D., Cooperman, B.S., and Fredrick, K. (2008). Role of hybrid tRNA-binding states in ribosomal translocation. *Proc. Natl. Acad. Sci. U. S. A.* **105**, 9192–9197.

Wang, Z., and Sachs, M.S. (1997a). Arginine-specific regulation mediated by the *neurospora crassa* arg-2 upstream open reading frame in a homologous, cell-free in vitro translation system. *J. Biol. Chem.* **272**, 255–261.

Wang, Z., and Sachs, M.S. (1997b). Ribosome stalling is responsible for arginine-specific translational attenuation in *Neurospora crassa*. *Mol. Cell. Biol.* **17**, 4904–4913.

Wang, X., Li, W., Williams, M., Terada, N., Alessi, D.R., and Proud, C.G. (2001). Regulation of elongation factor 2 kinase by p90(RSK1) and p70 S6 kinase. *EMBO J.* **20**, 4370–4379.

Webb, T.R., Cross, S.H., McKie, L., Edgar, R., Vizor, L., Harrison, J., Peters, J., and Jackson, I.J. (2008). Diphthamide modification of eEF2 requires a J-domain protein and is essential for normal development. *J. Cell Sci.* **121**, 3140–3145.

Wegrzyn, R.D., and Deuerling, E. (2005). Molecular guardians for newborn proteins: ribosome-associated chaperones and their role in protein folding. *Cell. Mol. Life Sci.* **62**, 2727–2738.

Weigert, M.G., and Garen, A. (1965). Base composition of nonsense codons in *E. coli*. Evidence from amino-acid substitutions at a tryptophan site in alkaline phosphatase. *Nature* **206**, 992–994.

Weisser, M., Voigt-Hoffmann, F., Rabl, J., Leibundgut, M., and Ban, N. (2013). The crystal structure of the eukaryotic 40S ribosomal subunit in complex with eIF1 and eIF1A. *Nat. Struct. Mol. Biol.* **20**, 1015–1017.

Weixlbaumer, A., Jin, H., Neubauer, C., Voorhees, R.M., Petry, S., Kelley, A.C., and Ramakrishnan, V. (2008). Insights into translational termination from the structure of RF2 bound to the ribosome. *Science* **322**, 953–956.

Wek, R.C., Jiang, H.-Y., and Anthony, T.G. (2006). Coping with stress: eIF2 kinases and translational control. *Biochem. Soc. Trans.* **34**, 7–11.

Welch, E.M., Barton, E.R., Zhuo, J., Tomizawa, Y., Friesen, W.J., Trifillis, P., Paushkin, S., Patel, M., Trotta, C.R., Hwang, S., et al. (2007). PTC124 targets genetic disorders caused by nonsense mutations. *Nature* **447**, 87–91.

Wiedmann, B., Sakai, H., Davis, T.A., and Wiedmann, M. (1994). A protein complex required for signal-sequence-specific sorting and translocation. *Nature* **370**, 434–440.

Wilson, C.J., Apiyo, D., and Wittung-Stafshede, P. (2004). Role of cofactors in metalloprotein folding. *Q. Rev. Biophys.* **37**, 285–314.

Wilson, J.E., Pestova, T. V., Hellen, C.U., and Sarnow, P. (2000). Initiation of Protein Synthesis from the A Site of the Ribosome. *Cell* **102**, 511–520.

Wilson, M.A., Meaux, S., and van Hoof, A. (2007). A genomic screen in yeast reveals novel aspects of nonstop mRNA metabolism. *Genetics* **177**, 773–784.

Wimberly, B.T., Brodersen, D.E., Clemons, W.M., Morgan-Warren, R.J., Carter, A.P., Vonrhein, C., Hartsch, T., and Ramakrishnan, V. (2000). Structure of the 30S ribosomal subunit. *Nature* **407**, 327–339.

Witt, S.N. (2009). Tethering creates unusual kinetics for ribosome-associated chaperones with nascent chains. *Protein Pept. Lett.* **16**, 631–634.

Wittung-Stafshede, P. (2002). Role of cofactors in protein folding. *Acc. Chem. Res.* **35**, 201–208.

Wong, L.E., Li, Y., Pillay, S., Frolova, L., and Pervushin, K. (2012). Selectivity of stop codon recognition in translation termination is modulated by multiple conformations of GTS loop in eRF1. *Nucleic Acids Res.* **40**, 5751–5765.

Wong, W., Bai, X., Brown, A., Fernandez, I.S., Hanssen, E., Condon, M., Tan, Y.H., Baum, J., and Scheres, S.H.W. (2014). Cryo-EM structure of the *Plasmodium falciparum* 80S ribosome bound to the anti-protozoan drug emetine. *Elife* **3**, e03080.

Wu, C., Wei, J., Lin, P.-J., Tu, L., Deutsch, C., Johnson, A.E., and Sachs, M.S. (2012). Arginine changes the conformation of the arginine attenuator peptide relative to the ribosome tunnel. *J. Mol. Biol.* **416**, 518–533.

Yamamoto, Y., Singh, C.R., Marintchev, A., Hall, N.S., Hannig, E.M., Wagner, G., and Asano, K. (2005). The eukaryotic initiation factor (eIF) 5 HEAT domain mediates multifactor assembly and scanning with distinct interfaces to eIF1, eIF2, eIF3, and eIF4G. *Proc. Natl. Acad. Sci. U. S. A.* **102**, 16164–16169.

Yanagisawa, T., Ishii, R., Fukunaga, R., Nureki, O., and Yokoyama, S. (2006). Crystallization and preliminary X-ray crystallographic analysis of the catalytic domain of pyrrolysyl-tRNA synthetase from the methanogenic archaeon *Methanosarcina mazei*. *Acta Crystallogr. Sect. F. Struct. Biol. Cryst. Commun.* **62**, 1031–1033.

Yang, J.-R., Chen, X., and Zhang, J. (2014). Codon-by-codon modulation of translational speed and accuracy via mRNA folding. *PLoS Biol.* **12**, e1001910.

Yap, M.-N., and Bernstein, H.D. (2009). The plasticity of a translation arrest motif yields insights into nascent polypeptide recognition inside the ribosome tunnel. *Mol. Cell* **34**, 201–211.

Yarunin, A., Panse, V.G., Petfalski, E., Dez, C., Tollervey, D., and Hurt, E.C. (2005). Functional link between ribosome formation and biogenesis of iron-sulfur proteins. *EMBO J.* **24**, 580–588.

Yokoyama, T., and Suzuki, T. (2008). Ribosomal RNAs are tolerant toward genetic insertions: evolutionary origin of the expansion segments. *Nucleic Acids Res.* **36**, 3539–3551.

Yoshida, T., Uchiyama, S., Nakano, H., Kashimori, H., Kijima, H., Ohshima, T., Saito, Y., Ishino, T., Shimahara, H., Yoshida, T., et al. (2001). Solution structure of the ribosome recycling factor from *aquifex aeolicus*. *Biochemistry* **40**, 2387–2396.

Youngman, E.M., Brunelle, J.L., Kochaniak, A.B., and Green, R. (2004). The active site of the ribosome is composed of two layers of conserved nucleotides with distinct roles in peptide bond formation and peptide release. *Cell* **117**, 589–599.

Yu, Y., Marintchev, A., Kolupaeva, V.G., Unbehaun, A., Veryasova, T., Lai, S.-C., Hong, P., Wagner, G., Hellen, C.U.T., and Pestova, T. V (2009). Position of eukaryotic translation initiation factor eIF1A on the 40S ribosomal subunit mapped by directed hydroxyl radical probing. *Nucleic Acids Res.* **37**, 5167–5182.

Yuan, J., O'Donoghue, P., Ambrogelly, A., Gundlapalli, S., Sherrer, R.L., Palioura, S., Simonović, M., and Söll, D. (2010). Distinct genetic code expansion strategies for selenocysteine and pyrrolysine are reflected in different aminoacyl-tRNA formation systems. *FEBS Lett.* **584**, 342–349.

Yusupov, M.M. (2001). Crystal structure of the ribosome at 5.5 Å resolution. *Science* **292**, 883–896.

Yusupova, G., and Yusupov, M. (2015). Ribosome biochemistry in crystal structure determination. *RNA* **21**, 771–773.

Yusupova, G.Z., Yusupov, M.M., Cate, J.H., and Noller, H.F. (2001). The path of messenger RNA through the ribosome. *Cell* **106**, 233–241.

Zaher, H.S., and Green, R. (2009). Quality control by the ribosome following peptide bond formation. *Nature* **457**, 161–166.

Zaher, H.S., Shaw, J.J., Strobel, S.A., and Green, R. (2011). The 2'-OH group of the peptidyl-tRNA stabilizes an active conformation of the ribosomal PTC. *EMBO J.* **30**, 2445–2453.

Zavialov, A. V., Hauryliuk, V. V., and Ehrenberg, M. (2005). Splitting of the posttermination ribosome into subunits by the concerted action of RRF and EF-G. *Mol. Cell* **18**, 675–686.

Zavialov, A. V., Buckingham, R.H., and Ehrenberg, M. (2001). A posttermination ribosomal complex is the guanine nucleotide exchange factor for peptide release factor RF3. *Cell* **107**, 115–124.

Zeenko, V. V., Wang, C., Majumder, M., Komar, A.A., Snider, M.D., Merrick, W.C., Kaufman, R.J., and Hatzoglou, M. (2008). An efficient in vitro translation system from mammalian cells lacking the translational inhibition caused by eIF2 phosphorylation. *RNA* **14**, 593–602.

Zhang, D., Yan, K., Liu, G., Song, G., Luo, J., Shi, Y., Cheng, E., Wu, S., Jiang, T., Lou, J., et al. (2016). EF4 disengages the peptidyl-tRNA CCA end and facilitates back-translocation on the 70S ribosome. *Nat. Struct. Mol. Biol.* **23**, 125–131.

Zhang, G., Hubalewska, M., and Ignatova, Z. (2009a). Transient ribosomal attenuation coordinates protein synthesis and co-translational folding. *Nat. Struct. Mol. Biol.* **16**, 274–280.

Zhang, J., Pan, X., Yan, K., Sun, S., Gao, N., and Sui, S.-F. (2015). Mechanisms of ribosome stalling by SecM at multiple elongation steps. *Elife* **4**, e09684.

Zhang, W., Dunkle, J.A., and Cate, J.H.D. (2009b). Structures of the ribosome in intermediate states of ratcheting. *Science* **325**, 1014–1017.

Zhang, W.-X., Xue, W., Lin, J.-B., Zheng, Y.-Z., and Chen, X.-M. (2008). 3D geometrically frustrated magnets assembled by transition metal ion and 1,2,3-triazole-4,5-dicarboxylate as triangular nodes. *CrystEngComm* **10**, 1770.

Zhao, Z., Fang, L.L., Johnsen, R., and Baillie, D.L. (2004). ATP-binding cassette protein E is involved in gene transcription and translation in *Caenorhabditis elegans*. *Biochem. Biophys. Res. Commun.* **323**, 104–111.

Zhou, Z.H., and Chiu, W. (1993). Prospects for using an IVEM with a FEG for imaging macromolecules towards atomic resolution. *Ultramicroscopy* **49**, 407–416.

Zhou, J., Korostelev, A., Lancaster, L., and Noller, H.F. (2012a). Crystal structures of 70S ribosomes bound to release factors RF1, RF2 and RF3. *Curr. Opin. Struct. Biol.* **22**, 733–742.

Zhou, J., Lancaster, L., Trakhanov, S., and Noller, H.F. (2012b). Crystal structure of release factor RF3 trapped in the GTP state on a rotated conformation of the ribosome. *RNA* **18**, 230–240.

Zhou, M., Guo, J., Cha, J., Chae, M., Chen, S., Barral, J.M., Sachs, M.S., and Liu, Y. (2013). Non-optimal codon usage affects expression, structure and function of clock protein FRQ. *Nature* **495**, 111–115.

Zhu, Y., Carragher, B., Glaeser, R.M., Fellmann, D., Bajaj, C., Bern, M., Mouche, F., de Haas, F., Hall, R.J., Kriegman, D.J., et al. (2004). Automatic particle selection: results of a comparative study. *J. Struct. Biol.* **145**, 3–14.

Zinoni, F., Birkmann, A., Stadtman, T.C., and Böck, A. (1986). Nucleotide sequence and expression of the selenocysteine-containing polypeptide of formate dehydrogenase (formate-hydrogen-lyase-linked) from *Escherichia coli*. *Proc. Natl. Acad. Sci. U. S. A.* **83**, 4650–4654.

Ziv, G., Haran, G., and Thirumalai, D. (2005). Ribosome exit tunnel can entropically stabilize alpha-helices. *Proc. Natl. Acad. Sci. U. S. A.* **102**, 18956–18961.

7 Appendix

7.1 Plasmid Constructs for Protein Expression

Color code

 ATG start codon

 3xFLAG-tag

 Sequencing primer binding site

 TAA/TAG stop codon

 (His)₆-(His)₈-tag

 TRX-tag

 3C-/TEV-cleavage site

7.1.1 pCDNA3.1 3xFLAG-hABCE1

1 M D Y K D H D G D Y K D H D I D Y K D D 20
 1 **ATGGACTACAAAGACCATGACGGTATTATAAGATCATGACATCGATTACAAGGATGAC** 60

 21 D D K A G S M A D K L T R I A I V N H D 40
 61 **GATGACAAGGCCGGATCCATGGCAGACAAATTAACAAGAATTGCTATTGTCAACCACGAC** 120

 41 K C K P K K C R Q E C K K S C P V V R M 60
 121 AAATGCAAACCTAAGAAATGTCGACAGGGAGTGCAAAAGAGTTGCCCTGGGTCGGATG 180

 61 G K L C I E V T P Q S K I A W I S E T L 80
 181 GGAAAATTGTGCATAGAAGTTACACCCAGAGCAAAATAGCATGGATTCGAAACTCTC 240

 81 C I G C G I C I K K C P F G A L S I V N 100
 241 TGTATTGGTTGTTGATTAGAAATGTCCTTGGCGCCTATCAATTGTCAAT 300

 101 L P S N L E K E T T H R Y C A N A F K L 120
 301 TTGCCAAGCAACTGGAAAAAGAAACAACACATCGCTACTGTGCCAATGCCCTCAAGCTT 360

 121 H R L P I P R P G E V L G L V G T N G I 140
 361 CACAGGTTGCCTATCCCTCGTCAGGTGAAGTTGGATTAGTTGAACTAATGGTATT 420

 141 G K S T A L K I L A G K Q K P N L G K Y 160
 421 GGAAAGTCAACTGCACTAAAATTAGCAGGAAACAAAGCCAAACCTGGAAAGTAT 480

 161 D D P P D W Q E I L T Y F R G S E L Q N 180
 481 GATGATCCACCTGATTGGCAAGAGATTTGACTTATTCCGTGGATCTGAATTACAAAT 540

 181 Y F T K I L E D D L K A I I K P Q Y V D 200
 541 TACTTACCAAGATTCTCGAAGATGACCTAAAGCCATTATCAAACCTCAATATGTAGAC 600

 201 Q I P K A A K G T V G S I L D R K D E T 220
 601 CAAATTCCCAAGGCTGCAAAGGGACAGTGGCTCTATTCTGGACCGAAAAGATGAAACA 660

 221 K T Q A I V C Q Q L D L T H L K E R N V 240
 661 AAGACACAGGCAATTGTATGTCAGCAGCTGATTAACTCACCTTAAAGAACGAAATGTC 720

 241 E D L S G G E L Q R F A C A V V C I Q K 260
 721 GAAGATCTTCAGGAGGAGTTGCAGAGATTTGCTTGTGCTGTCGTTGCATACAAAG 780

 261 A D I F M F D E P S S Y L D V K Q R L K 280
 781 GCTGATATTGTTGATGAACCTCTAGTTACCTCGATGTCAAGCAACGTTAAAG 840

 281 A A I T I R S L I N P D R Y I I V V E H 300
 841 GCTGCCATTACGATTGATCTCAATAAAATCCAGATAGATATATCATTGTGGTGGAGCAT 900

 301 D L S V L D Y L S D F I C C L Y G V P S 320
 901 GATCTAAGTGTATTAGACTATCTCTCTGACTTCATCTGCTGTCTATATGGGGTACCGAGT 960

 321 A Y G V V T M P F S V R E G I N I F L D 340
 961 GCTTATGGTGTGTCACGATGCCATTAGTGTAAAGAGAAGGCATAATATTTTGAT 1020

341 G Y V P T E N X R F R D A S L V F K V A 360
 1021 GGCTATGTTCCAACAGAGAACNTGAGGTTAGGGATGCGTCGCTTGTAAAGGTAGCT 1080

361 E T A N E E V K K M C M Y K Y P G M K 380
 1081 GAGACAGCAAATGAAGAAGAAGTTAAAAGATGTGCATGTATAATATCCCGGGATGAAG 1140

381 K K M G E F E L A I V A G E F T D S E I 400
 1141 AAAAAGATGGGAGAGTTCGAGCTAGCAATTGTAGCTGGAGAGTCACGGACTCTGAGATC 1200

401 M V M L G E N G T G K T T F I R M L A G 420
 1201 ATGGTGATGCTGGGGAGAACATGGTACAGGTAAAACATTTATCAGAATGCTTGCTGGA 1260

421 R L K P D E G G E V P V L N V S Y K P Q 440
 1261 AGGCTTAAACCAAGATGAAGGAGGAGAAGTGCAGTTCAAATGTCAGTTATAAGCCACAG 1320

441 K I S P K S T G S V R Q L L H E K I R D 460
 1321 AAAATCAGTCCCAAATCAACAGGAAGTGTGCGCAGTTACTGCATGAAAAGATCAGAGAT 1380

461 A Y T H P Q F V T D V M K P L Q I E N I 480
 1381 GCTTACACGCATCCGCAGTTGTGACTGATGTAATGAAGCCCCTACAGATTGAAAACATC 1440

481 I D Q E V Q T L S G G E L Q R V A L A L 500
 1441 ATTGACCAAGAGGTACAGACATTGTCTGGTGGTGAACCTCAGCGAGTAGCTTAGCTCTT 1500

501 C L G K P A D V Y L I D E P S A Y L D S 520
 1501 TGTGTTGGGCAAACCTGCTGACGTCTATTGATTGATGAACCTTCTGCATATTGGATTCT 1560

521 E Q R L M A A R V V K R F I L H A K K T 540
 1561 GAGCAAAGATTAATGGCAGCTCGGGTCGTCAAACGTTTCAATTCTCCATGCAAAGAAC 1620

541 A F V V E H D F I M A T Y L A D R V I V 560
 1621 GCTTTGTTGTAGAACATGACTCATGGCACCTATCTAGCAGATCGCGTCATCGTT 1680

561 F D G V P S K N T V A N S P Q T L L A G 580
 1681 TTTGATGGTGTTCATCAAAGAACACAGTTGCAAACAGTCCTCAGACTCTTGGCTGGC 1740

581 M N K F L S Q L E I T F R R D P N N Y R 600
 1741 ATGAACAAATTGGTCTCAGCTCGAAATTACATTAGAAGAGACCCAAACAACAGG 1800

601 P R I N K L N S I K D V E Q K K S G N Y 620
 1801 CCACGAATAATAAGCTCAATTCAATCAAGGATGTAGAACAAAAGAACAGTAGGGAAACTAC 1860

621 F F L D D * 626
 1861 TTTTCTGGATGAT**TAG** 1878

7.1.2 pET-28a (His)₆-Δ(1-46)Jmjd4

1 M G S S H H H H H H S S G L V P R G S H 20
 1 ATGGGCAGCAGC **CATCATCATCATCATCAC** AGCAGCGGCCTGGTGCCGCGCGCAGCCAT 60

 21 M D R E T R A L A D S H F R G L G V D V 40
 61 ATGGACCGCGAGACGCGCGCCCTGCCGACAGCCACTTCCGAGGCCTGGGGTCGATGTC 120

 41 P G V G Q A P G R V A F V S E P G A F S 60
 121 CCCGGCGTCGGCCAGGCTCCGGGCCGGTAGCCTTCGTCTGGAGGCCGGCGCCTTC 180

 61 Y A D F V R G F L L P N L P C V F S S A 80
 181 TACGCCGACTTGTGCGGGGCTTCTTGCTGCCAACCTGCCCTGCGTGTTCAGCGCC 240

 81 F T Q G W G S R R R W V T P A G R P D F 100
 241 TTACACGCAGGGCTGGGCAGCCGGCGCTGGTAGCAGCCCGGGGAGGCCGACTTC 300

 101 D H L L R T Y G D V V V P V A N C G V Q 120
 301 GACCACCTGCTACGGACCTACGGAGACGTGGTTGTACCAAGTTGCAAACGTGGGTCCAG 360

 121 E Y N S N P K E H M T L R D Y I T Y W K 140
 361 GAATACAACCTCGAACCCAAAGAGACATGACTCTCAGAGACTACATCACCTACTGGAAA 420

 141 E Y I Q A G Y S S P R G C L Y L K D W H 160
 421 GAGTACATACAGGCAGGGCTACTCCTCTCCAGGGCTGTCTCACCTCAAAGACTGGCAC 480

 161 L C R D F P V E D V F T L P V Y F S S D 180
 481 TTGTGCAGGGACTTCCGGTGGAGGACGTTTCAACCTGCCTGTACTTCTCGTCCGAC 540

 181 W L N E F W D A L D V D D Y R F V Y A G 200
 541 TGGCTGAATGAGTTCTGGATGCAGTGGATGTGGATGACTACCGCTTGTCTACGCCGG 600

 201 P A G S W S P F H A D I F R S F S W S V 220
 601 CCTGCGGGCAGCTGGTCCCCGTTCCATGCTGACATCTCCGCTCCTCAGCTGGTCTGTC 660

 221 N V C G R K K W L L F P P G Q E E A L R 240
 661 AATGTCTGTGGAGGAAGAAGTGGCTCCTCTCCCCCAGGGCAGGAAGAGGCCCTGCGG 720

 241 D R H G N L P Y D V T S P A L C D T H L 260
 721 GACCGCCACGGCAACCTGCCCTACGACGTGACCTCCCCAGCAGCTGCGACACACACCTG 780

 261 H P R N Q L A G P P L E I T Q E A G E M 280
 781 CACCCACGGAACCAGCTTGCTGGCCACCCCTGGAGATCACGCAGGAAGCGGGCGAGATG 840

 281 V F V P S G W H H Q V H N L D D T I S I 300
 841 GTGTTGTGCCAGTGGCTGGCACCAACCAGGTGCACAAACCTGGATGACACCATCTCCATC 900

 301 N H N W V N G F N L A N M W R F L Q Q E 320
 901 AACCCACAACCTGGGTCAATGGCTTCAACCTGGCCAACATGTGGCGCTTCTTGCAGCAGGAG 960

 321 L C A V Q E E V S E W R D S M P D W H H 340
 961 CTATGCGCCGTGCAGGAGGAGGTCAAGCGAGTGGAGGGACTCCATGCCGACTGGCACAC 1020

Appendix

41 H C Q V I M R S C S G I N F E E F Y H F 360
1021 CACTGCCAGGTACATCATGAGGTCCCTGCTCGGGCATCAACTTGAAGAGTTTACCACTTC 1080

361 L K V I A E K R L L V L R E A A A E D G 380
1081 CTCAAGGTACCGCTGAGAAGAGGGCTCCTGGTCCTGAGGGAGGCAGCCGCTGAGGACGGT 1140

381 A G L G F E Q A A F D V G R I T E V L A 400
1141 GCTGGGTTGGGTTTCGAACAGGCAGCCTTGATGTTGGCGCATCACAGAGGTGCTGCC 1200

401 S L V A H P D F Q R V D T S A F S P Q P 420
1201 TCCTTGGTTGCGCACCCGACTTCCAGAGAGTGGACACCAGCGCGTTCTCACACAGCCC 1260

421 K E L L Q Q L R E A V D A A A A A P * 438
1261 AAAGAGCTGCTGCAGCAGCTGAGAGAGGCTGTTGATGCTGCTGCCCGCCATAG 1314

7.1.3 pET-32a TRX-(His)₆-TEV-heRF3a Full Length

Appendix

341 P K K E H V N V V F I G H V D A G K S T 360
 1021 CCTAAGAAAGAGCATGTAAATGTAGTATTCAATTGGGCACGTAGATGCTGGCAAGTCAACC 1080

361 I G G Q I M Y L T G M V D K R T L E K Y 380
 1081 ATTGGAGGACAAATAATGTATTGACTGGAATGGTTGACAAAAGGACGCTGAAAAGTAT 1140

381 E R E A K E K N R E T W Y L S W A L D T 400
 1141 GAAAGAGAAGCTAAAGAGAAAACAGAGAACTGGTACTGTCTGGCCTAGACACA 1200

401 N Q E E R D K G K T V E V G R A Y F E T 420
 1201 AATCAGGAAGAACGAGACAAGGGTAAAACAGTAGAAGTGGTCGTGCCTATTGAAACC 1260

421 E K K H F T I L D A P G H K S F V P N M 440
 1261 GAAAAGAACGCATTCAAAATTCTAGATGCCCTGGCCACAAGAGTTTGTCCCAAATATG 1320

441 I G G A S Q A D L A V L V I S A R K G E 460
 1321 ATTGGTGGTGCCTCTCAAGCTGATTGGCTGTGCTGTAATCTCAGCCAGGAAAGGAGAG 1380

461 F E T G F E K G G Q T R E H A M L A K T 480
 1381 TTTGAAACTGGATTGAAAAGGAGGACAGACAAGAGAACATGCAATGTTGGAAAGACA 1440

481 A G V K H L I V L I N K M D D P T V N W 500
 1441 GCAGGTGTAAAACACCTAATTGTGCTAATTAAAGATGGATGCCAACAGTAAATTGG 1500

501 S N E R Y E E C K E K L V P F L K K V G 520
 1501 AGCAATGAGAGATATGAAGAATGTAAGGAGAAACTAGTGCCATTGAAAGTTGGC 1560

521 F N P K K D I H F M P C S G L T G A N L 540
 1561 TTCAATCCAAAAGGACATTCACTTATGCCCTGCTCAGGACTTACTGGAGCAAATCTC 1620

541 K E Q S D F C P W Y I G L P F I P Y L D 560
 1621 AAAGAGCAGTCGGATTCTGTCCTGGTACATTGGATTACCGTTATTCCATATCTGGAT 1680

561 N L P N F N R S V D G P I R L P I V D K 580
 1681 AATTGCCGAACCTCAATAGATCAGTTGATGGACCAATCAGGCTGCCATTGTGGATAAG 1740

581 Y K D M G T V V L G K L E S G S I C K G 600
 1741 TACAAGGATATGGGCACTGTGGCCTGGAAAGCTGGAATCAGGATCTATTGTAAGGC 1800

601 Q Q L V M M P N K H N V E V L G I L S D 620
 1801 CAGCAGCTTGTGATGATGCCAAACAAGCACAACGTGGAAGTTCTTGGAAATCTTCGAT 1860

621 D V E T D T V A P G E N L K I R L K G I 640
 1861 GATGTAGAGACTGATACCGTAGCCCCAGGTGAAAACCTCAAAATCAGACTGAAAGGAATT 1920

641 E E E E I L P G F I L C D P N N L C H S 660
 1921 GAAGAAGAGGAGATTCTCCAGGGTTTACTTGATGCTTAATAATCTTGTCAATTCT 1980

661 G R T F D A Q I V I I E H K S I I C P G 680
 1981 GGACGCACATTGATGCCAGATAGTGTGATTAGAGCACAAATCCATCATGCCAGGC 2040

681 Y N A V L H I H T C I E E V E I T A L I 700
 2041 TATAATGCGGTGCTGCATATTACACCTGTATTGAGGAGGTGAAATAACAGCCTTAATC 2100

701 C L V D K K S G E K S K T R P R F V K Q 720
 2101 TGCTGGTAGACAAAAATCAGGAGAAAAAGTAAGACCCGACCCGTTTGTGAAACAA 2160

Appendix

721 D Q V C I A R L R T A G T I C L E T F K 740
2161 GATCAAGTGTGCATTGCTCGCTTAAGGACAGCAGGAACCATCTGCCTTGAGACCTTAAA 2220

741 D F P Q M G R F T L R D E G K T I A I G 760
2221 GACTTCCCTCAGATGGGTCGTTCACCTTAAGAGATGAGGGTAAGACCATTGCAATTGGA 2280

761 K V L K L V P E K D * 771
2281 AAAGTTCTGAAACTGGTCCAGAGAAAGAC**TAA** 2313

7.1.4 pETDuet-1 heRF1

1 M A D D P S A A D R N V E I W K I K K L 20
 1 **ATGGCGGACGACCCAGTGCCTGCCGACAGGAACGTGGAGATCTGAAAGATCAAGAACGTC** 60

 21 I K S L E A A R G N G T S M I S L I I P 40
 61 **ATTAAGAGCTTGGAGGGCGGCCGCGCAATGGCACCCAGCATGATATCATTGATCATTCT** 120

 41 P K D Q I S R V A K M L A D E F G T A S 60
 121 **CCCAAAGACCAGATTTCACGAGTGGCAAAAATGTTAGCGGATGAGTTGAACTGCATCT** 180

 61 N I K S R V N R L S V L G A I T S V Q Q 80
 181 **AACATTAAGTCACGAGTAAACCGCCTTCAGTCCTGGAGCCATTACATCTGTACAACAA** 240

 81 R L K L Y N K V P P N G L V V Y C G T I 100
 241 **AGACTCAAACTTATAACAAAGTACCTCCAAATGGTCTGGTTGTATACTGTGGAACAATT** 300

 101 V T E E G K E K K V N I D F E P F K P I 120
 301 **GTAACAGAAGAAGGAAAGGAAAAGAAAGTCAACATTGACTTGAACCTTCAAACCAATT** 360

 121 N T S L Y L C D N K F H T E A L T A L L 140
 361 **AATACGTATTGTATTGTGTGACAACAAATTCCATACAGAGGCTTACAGCACTACTT** 420

 141 S D D S K F G F I V I D G S G A L F G T 160
 421 **TCAGATGATAGCAAGTTGGATTCAATTGTAATAGATGGTAGTGGTGCAC** 480

 161 L Q G N T R E V L H K F T V D L P K K H 180
 481 **CTCCAAGGAAACACAAGAGAAGTCCTGCACAAATTCACTGTGGATCTCCAAAGAACAC** 540

 181 G R G G Q S A L R F A R L R M E K R H N 200
 541 **GGTAGAGGAGGTCAGTCAGCCTTGCCTTGCCTTAAAGAATGGAAAAGCGACATAAC** 600

 201 Y V R K V A E T A V O L F I S G D K V N 220
 601 **TATGTTCGAAAGTAGCAGAGACTGCTGTGCAGCTGTTATTCTGGGGACAAAGTGAAT** 660

 221 V A G L V L A G S A D F K T E L S Q S D 240
 661 **GTGGCTGGCTAGTTAGCTGGATCCGCTGACTTAAACTGAAACTAAGTCAATCTGAT** 720

 241 M F D O R L O S K V L K L V D I S Y G G 260
 721 **ATGTTGATCAGAGGTTACAATCAAAGTTAAATTAGTTGATATATCCTATGGTGGT** 780

 261 E N G F N O A I E L S T E V L S N V K F 280
 781 **GAAAATGGATTCAACCAAGCTATTGAGTTATCTACTGAAGTCCTCTCCAACGTGAAATTC** 840

 281 I O E K K L I G R Y F D E I S O D T G K 300
 841 **ATTCAAGAGAAGAAATTAAATAGGACGATACTTGATGAAATCAGGCCAGGACACGGGCAAG** 900

 301 Y C F G V E D T L K A L E M G A V E I L 320
 901 **TACTGTTTGGCGTTGAAGATAACACTAAAGGCTTGGAAATGGGAGCTGTAGAAATTCTA** 960

 321 I V Y E N L D I M R Y V L H C O G T E E 340
 961 **ATAGTCTATGAAAATCTGGATATAATGAGATATGTTCTCATTGCCAAGGCACAGAACAGAG** 1020

Appendix

341 E K I L Y L T P E Q E K D K S H F T D K 360
1021 GAGAAAATTCTCTATCTAACTCCAGAGCAAGAAAAGGATAAATCTCATTACAGACAAA 1080

361 E T G Q E H E L I E S M P L L E W F A N 380
1081 GAGACCGGACAGGAACATGAGCTTATCGAGAGCATGCCCTGTTGGAATGGTTGCTAAC 1140

381 N Y K K F G A T L E I V T D K S Q E G S 400
1141 AACTATAAAAAATTGGAGCTACGTTGAAATTGTCACAGATAAATCACAGAAGGGTCT 1200

401 Q F V K G F G G I G G I L R Y R V D F Q 420
1201 CAGTTTGAAAGGATTGGTGAATTGGAGGTATCTTGCAGTACCGAGTAGATTCCAG 1260

421 G M E Y Q G G D D E F F D L D D Y * 438
1261 GGAATGGAATACCAAGGAGGAGCGATGAATTTTGACCTTGATGACTACTAA 1314

7.1.5 pETDuet-1 (His)₈-3C-heRF1

1 M G H H H H H H H H D Y D I P T T L E V 20
 1 ATGGGT CATCACCATCACCATCAC GATTACGATATTCCAACGACC CTGGAAGTT 60

21 L F Q G P A D D P S A A D R N V E I W K 40
 61 CTGTTCCAGGGGGCCCGCGGACGACCCAGTGCTGCCGACAGGAACGTGGAGATCTGGAAG 120

41 I K K L I K S L E A A R G N G T S M I S 60
 121 ATCAAGAAGCTCATTAAGAGCTTGGAGGCGGCCGCGCAATGGCACCCAGCATGATATCA 180

61 L I I P P K D Q I S R V A K M L A D E F 80
 181 TTGATCATTCTCCAAAGACCAAGACAGATTTCACGAGTGGCAAAAATGTTAGCGGATGAGTT 240

81 G T A S N I K S R V N R L S V L G A I T 100
 241 GGAAC TGCACTAACATTAAGTCACGAGTAAACCGCCTTCAGTCCTGGAGCCATTACA 300

101 S V Q Q R L K L Y N K V P P N G L V V Y 120
 301 TCTGTACAACAAAGACTCAAACATTATAACAAAGTACCTCCAAATGGCTGGTTGTATAC 360

121 C G T I V T E E G K E K K V N I D F E P 140
 361 TGTGGAACAATTGTAACAGAAGAGAAAGGAAAGAAAGTCAACATTGACTTGAACCT 420

141 F K P I N T S L Y L C D N K F H T E A L 160
 421 TTCAAACCAATTAAATACGTCAATTGTATTGTGTGACAACAAATTCCATACAGAGGCTCTT 480

161 T A L L S D D S K F G F I V I D G S G A 180
 481 ACAGCACTACTTCAGATGATAGCAAGTTGGATTCAATTGTAATAGATGGTAGTGGTCA 540

181 L F G T L Q G N T R E V L H K F T V D L 200
 541 CTTTTGGCACACTCCAAGGAAACACAAGAGAAGTCCTGCACAAATTCACTGTGGATCTC 600

201 P K K H G R G G Q S A L R F A R L R M E 220
 601 CCAAAGAAACACGGTAGAGGGAGGTCAAGTCAGCCTGCCTTGCCTTGCCTTAAGAATGGAA 660

221 K R H N Y V R K V A E T A V Q L F I S G 240
 661 AAGCGACATAACTATGTCGGAAAGTAGCAGAGACTGCTGTGCAGCTGTTATTCTGGG 720

241 D K V N V A G L V L A G S A D F K T E L 260
 721 GACAAAGTGAATGTGGCTGGCTAGTTAGCTGGATCCGCTGACTTTAAACTGAACCA 780

261 S Q S D M F D Q R L Q S K V L K L V D I 280
 781 AGTCAATCTGATATGTTGATCAGAGGTTACAATCAAAGTTAAATTAGTTGATATA 840

281 S Y G G E N G F N Q A I E L S T E V L S 300
 841 TCCTATGGTGGTAAAATGGATTCAACCAAGCTATTGAGTTATCTACTGAAGTCCTCTCC 900

301 N V K F I Q E K K L I G R Y F D E I S Q 320
 901 AACGTGAAATTCAAGAGAAGAAATTAAATAGGACGATACTTGTGAAATCAGCCAG 960

321 D T G K Y C F G V E D T L K A L E M G A 340
 961 GACACGGGCAAGTACTGTTGGCGTTGAAGATAACTAAAGGCTTGGAAATGGGAGCT 1020

341 V E I L I V Y E N L D I M R Y V L H C Q 360
1021 GTAGAAATTCTAATAGTCTATGAAAATCTGGATATAATGAGATATGTTCTTCATTGCCAA 1080

361 G T E E E K I L Y L T P E Q E K D K S H 380
1081 GGCACAGAAGAGGAGAAAATTCTCTATCTAACTCCAGAGCAAGAAAAGGATAATCTCAT 1140

381 F T D K E T G Q E H E L I E S M P L L E 400
1141 TTCACAGACAAAGAGACCGGACAGGAACATGAGCTATCGAGAGCATGCCCTGTTGGAA 1200

401 W F A N N Y K K F G A T L E I V T D K S 420
1201 TGGTTTGCTAACAACTATAAAAATTGGAGCTACGTTGGAAATTGTCACAGATAAAATCA 1260

421 Q E G S Q F V K G F G G I G G I L R Y R 440
1261 CAAGAAGGGTCTCAGTTGTGAAAGGATTGGTGGAATTGGAGGTATCTGCGGTACCGA 1320

441 V D F Q G M E Y Q G G D D E F F D L D D 460
1321 GTAGATTCAGGAATGGAATACCAAGGAGGAGACGATGAATTTTGACCTTGATGAC 1380

461 Y * 462
1381 TACTAA 1386

7.1.6 pETDuet-1 Δ(1-138)heRF3a

1 M S E P I E N G E T E M S P E E S W E H 20
 1 ATGTCAGAACCTATTGAAAATGGAGAGACAGAAATGTCTCCAGAAGAACATGGGAGCAC 60

21 K E E I S E A E P G G G S L G D G R P P 40
 61 AAAGAAGAAATAAGTGAAGCAGAGCCAGGGGTGGTCCTGGGAGATGGAAGGCCGCCA 120

41 E E S A H E M M E E E E I P K P K S V 60
 121 GAGGAAAGTGCCTCATGAAATGATGGAGGAGGAAGAGGAAATCCAAAACCTAAGTCTGTG 180

61 V A P P G A P K K E H V N V V F I G H V 80
 181 GTTGCACCGCCAGGTGCTCTAAAGAAAGAGCATGTAAATGTAGTATTCTGGGCACGTA 240

81 D A G K S T I G G Q I M Y L T G M V D K 100
 241 GATGCTGGCAAGTCACCATTGGAGGACAAATAATGTATTTGACTGGAATGGTGACAAA 300

101 R T L E K Y E R E A K E K N R E T W Y L 120
 301 AGGACGCTTGAAAAGTATGAAAGAGAAGCTAAAGAGAAAAACAGAGAACTTGGTACTTG 360

121 S W A L D T N Q E E R D K G K T V E V G 140
 361 TCTTGGGCCTTAGACACAAATCAGGAAGAACGAGACAAGGGTAAACAGTAGAAGTGGGT 420

141 R A Y F E T E K K H F T I L D A P G H K 160
 421 CGTGCCTATTTGAAACCGAAAAGAAGCATTCTAGATGCCCTGGCCACAAG 480

161 S F V P N M I G G A S Q A D L A V L V I 180
 481 AGTTTGTCCAAATATGATTGGTGGTGCCTCTCAAGCTGATTGGCTGTGCTGGTAATC 540

181 S A R K G E F E T G F E K G G Q T R E H 200
 541 TCAGCCAGGAAAGGAGAGTTGAAACTGGATTGAAAAAGGAGGACAGACAAGAGAACAT 600

201 A M L A K T A G V K H L I V L I N K M D 220
 601 GCAATGTTGGCAAAGACAGCAGGTGTAAACACCTAATTGTGCTAATTAAAGATGGAT 660

221 D P T V N W S N E R Y E E C K E K L V P 240
 661 GATCCAACAGTAAATTGGAGCAATGAGAGATATGAAGAATGTAAGGAGAAACTAGTGCA 720

241 F L K K V G F N P K K D I H F M P C S G 260
 721 TTTTGAAAAAAGTTGGCTTCATCCAAAAGACATTCACTTATGCCCTGCTCAGGA 780

261 L T G A N L K E Q S D F C P W Y I G L P 280
 781 CTTACTGGAGCAAATCTCAAAGAGCAGTCGGATTCTGTCCCTGGTACATTGGATTACCG 840

281 F I P Y L D N L P N F N R S V D G P I R 300
 841 TTTATTCCATATCTGGATAATTGCCGAACCTCAATAGATCAGTTGATGGACCAATCAGG 900

301 L P I V D K Y K D M G T V V L G K L E S 320
 901 CTGCCAATTGTGGATAAGTACAAGGATATGGGCACTGTGGCCTGGAAAGCTGGAATCA 960

321 G S I C K G Q Q L V M M P N K H N V E V 340
 961 GGATCTATTGTAAAGGCCAGCAGCTGTGATGATGCCAAACAAGCACACAGTGGAAAGTT 1020

Appendix

341 L G I L S D D V E T D T V A P G E N L K 360
1021 CTTGGAATACTTCCGATGATGATGAGACTGATACCGTAGCCCCAGGTGAAAACCTCAA 1080

361 I R L K G I E E E I L P G F I L C D P 380
1081 ATCAGACTGAAAGGAATTGAAGAAGAGGAGATTCTCCAGGGTTATACTTGTGATCCT 1140

381 N N L C H S G R T F D A Q I V I I E H K 400
1141 AATAATCTTGTCAATTCTGGACGCACATTGATGCCAGATAGTGATTATAGAGCACAAA 1200

401 S I I C P G Y N A V L H I H T C I E E V 420
1201 TCCATCATCTGCCAGGCTATAATGCGGTGCTGCATATTACACCTGTATTGAGGAGGTG 1260

421 E I T A L I C L V D K K S G E K S K T R 440
1261 GAAATAACAGCCTTAATCTGCTGGTAGACAAAAATCAGGAGAAAAAGTAAGACCCGA 1320

441 P R F V K Q D Q V C I A R L R T A G T I 460
1321 CCCCCTTTGTCAAACAAGATCAAGTATGCATTGCTCGCTTAAGGACAGCAGGAACCATC 1380

461 C L E T F K D F P Q M G R F T L R D E G 480
1381 TGCCTTGAGACCTTAAAGACTCCCTCAGATGGTCGTTCACCTTAAGAGATGAGGGT 1440

481 K T I A I G K V L K L V P E K D * 497
1441 AAGACCATTGCAATTGGAAAAGTTCTGAAACTGGTCCAGAGAAAGACTAA 1491

7.1.7 pRSFDuet-1 Δ(1-138)heRF3a-3C-(His)₈

1 M S E P I E N G E T E M S P E E S W E H 20
 1 ATGTCAGAACCTATTGAAAATGGAGAGACAGAAATGTCTCCAGAAGAACATGGGAGCAC 60

21 K E E I S E A E P G G G S L G D G R P P 40
 61 AAAGAAGAAATAAGTGAAGCAGAGCCAGGGGTGGTCTGGAGATGGAAGGCCGCA 120

41 E E S A H E M M E E E E I P K P K S V 60
 121 GAGGAAAGTGCCTCATGAAATGATGGAGGAGGAAGAGGAAATCCAAAACCTAAGTCTGTG 180

61 V A P P G A P K K E H V N V V F I G H V 80
 181 GTTGCACGCCAGGTGCTCTAAGAAAGAGCATGTAAATGTAGTATTCTATTGGCACGTA 240

81 D A G K S T I G G Q I M Y L T G M V D K 100
 241 GATGCTGGCAAGTCAACCATTGGAGGACAAATAATGTATTGACTGGAATGGTGACAAA 300

101 R T L E K Y E R E A K E K N R E T W Y L 120
 301 AGGACGCTTGAAAGTATGAAAGAGAAGCTAAAGAGAAAAACAGAGAAACTTGGTACTTG 360

121 S W A L D T N Q E E R D K G K T V E V G 140
 361 TCTTGGCCTTAGACACAAATCAGGAAGAACGAGACAAGGGTAAACAGTAGAAGTGGGT 420

141 R A Y F E T E K K H F T I L D A P G H K 160
 421 CGTGCCTATTGAAACCGAAAAGAAGCATTCTAGATGCCCTGGCCACAAG 480

161 S F V P N M I G G A S Q A D L A V L V I 180
 481 AGTTTGTCCTAAATATGATTGGTGGTGCCTCTCAAGCTGATTGGCTGTGCTGGTAATC 540

181 S A R K G E F E T G F E K G G Q T R E H 200
 541 TCAGCCAGGAAAGGAGAGTTGAAACTGGATTGAAAAGGAGGACAGACAAGAGAACAT 600

201 A M L A K T A G V K H L I V L I N K M D 220
 601 GCAATGTTGGCAAAGACAGCAGGTGTAAACACCTAATTGTGCTAATTAAAGATGGAT 660

221 D P T V N W S N E R Y E E C K E K L V P 240
 661 GATCCAACAGTAAATTGGAGCAATGAGAGATATGAAGAATGTAAGGAGAAACTAGTGCCA 720

241 F L K K V G F N P K K D I H F M P C S G 260
 721 TTTTGAAAAAGTTGGCTCAATCCAAAAGGACATTCACTTATGCCCTGCTCAGGA 780

261 L T G A N L K E Q S D F C P W Y I G L P 280
 781 CTTACTGGAGCAAATCTCAAAGAGCAGTCGGATTCTGTCCTGGTACATTGGATTACCG 840

281 F I P Y L D N L P N F N R S V D G P I R 300
 841 TTTATTCCATATCTGGATAATTGCCAACTTCATAGATCAGTTGATGGACCAATCAGG 900

301 L P I V D K Y K D M G T V V L G K L E S 320
 901 CTGCCAATTGTGGATAAGTACAAGGATATGGGCACTGTGGCCTGGAAAGCTGGAATCA 960

321 G S I C K G Q Q L V M M P N K H N V E V 340
 961 GGATCTATTGTAAGGCCAGCAGCTGTGATGCCAAACAGCACACGTGGAAGTT 1020

Appendix

341 L G I L S D D V E T D T V A P G E N L K 360
1021 CTTGGAATACTTCCGATGATGTAGAGACTGATACCGTAGCCCCAGGTGAAAACCTCAAA 1080

361 I R L K G I E E E I L P G F I L C D P 380
1081 ATCAGACTGAAAGGAATTGAAGAAGAGGAGATTCTCCAGGGTTATACTTGTGATCCT 1140

381 N N L C H S G R T F D A Q I V I I E H K 400
1141 AATAATCTTGTCAATTCTGGACGCACATTGATGCCAGATAGTGTATTAGAGCACAAA 1200

401 S I I C P G Y N A V L H I H T C I E E V 420
1201 TCCATCATCTGCCAGGCTATAATCGGGTGTGCATATTACCTGTATTGAGGAGGTG 1260

421 E I T A L I C L V D K K S G E K S K T R 440
1261 GAAATAACAGCCTTAATCTGCTGGTAGACAAAAAATCAGGAGAAAAAGTAAGACCCGA 1320

441 P R F V K Q D Q V C I A R L R T A G T I 460
1321 CCCCGTTTGTCAAACAAGATCAAGTATGCATTGCTCGCTTAAGGACAGCAGGAACCATC 1380

461 C L E T F K D F P Q M G R F T L R D E G 480
1381 TGCCTTGAGACCTTAAAGACTCCCTCAGATGGTCGTTCACCTTAAGAGATGAGGGT 1440

481 K T I A I G K V L K L V P E K D L E V L 500
1441 AAGACCATTGCAATTGGAAAAGTTCTGAAACTGGTCCAGAGAAAGACCTGGAAGTTCTG 1500

501 F Q G P D Y D I P T T H H H H H H H H H * 520
1501 TTCCAGGGGCCCGATTACGATATTCCAACGACCCTACCATCACCATCACCTAA 1560

7.1.8 pRSFDuet-1 (His)₈-3C-Δ(1-138)heRF3a

1 M G H H H H H H H H D Y D I P T T L E V 20
 1 ATGGGT **CATCACCATCACCATCAC** GATTACGATATTCCAACGACC **CTGGAAGTT** 60

21 L F Q G P S E P I E N G E T E M S P E E 40
 61 **CTGTTCCAGGGGCC**T CAGAACCTATTGAAAATGGAGAGACAGAAATGTCCTCAGAAGAA 120

41 S W E H K E E I S E A E P G G G S L G D 60
 121 TCATGGGAGCACAAAGAAGAAATAAGTGAAGCAGAGCCAGGGGTGGTCCTGGGAGAT 180

61 G R P P E E S A H E M M E E E E I P K 80
 181 GGAAGGCCGCCAGAGGAAAGTGCCTGAAATGATGGAGGAGGAAGAGGAAATCCCAAAA 240

81 P K S V V A P P G A P K K E H V N V V F 100
 241 CCTAAGTCTGTGGTGCACCGCCAGGTGCTCTAAGAAAGAGCATGTAAATGTAGTATTC 300

101 I G H V D A G K S T I G G Q I M Y L T G 120
 301 ATTGGGCACGTAGATGCTGGCAAGTCACCATTGGAGGACAAATAATGTATTTGACTGGA 360

121 M V D K R T L E K Y E R E A K E K N R E 140
 361 ATGGTTGACAAAAGGACGCTTGAAAGTATGAAAGAGAAGCTAAAGAGAAAAACAGAGAA 420

141 T W Y L S W A L D T N Q E E R D K G K T 160
 421 ACTTGGTACTTGTCTGGCCTTAGACACAAATCAGGAAGAACGACAAGGGTAAACACA 480

161 V E V G R A Y F E T E K K H F T I L D A 180
 481 GTAGAAGTGGTCGTGCCTATTTGAAACCGAAAAGAAGCATTCAACATTCTAGATGCC 540

181 P G H K S F V P N M I G G A S Q A D L A 200
 541 CCTGGCCACAAGAGTTTGTCCAAATATGATTGGTGGTGCCTCTCAAGCTGATTTGGCT 600

201 V L V I S A R K G E F E T G F E K G G Q 220
 601 GTGCTGGTAATCTCAGCCAGGAAAGGAGAGTTGAAACTGGATTGAAAAAGGAGGACAG 660

221 T R E H A M L A K T A G V K H L I V L I 240
 661 ACAAGAGAACATGCAATGTTGGCAAAGACAGCAGGTGTAAACACCTAATTGTGCTAATT 720

241 N K M D D P T V N W S N E R Y E E C K E 260
 721 AATAAGATGGATGATCCAACAGTAAATTGGAGCAATGAGAGATATGAAGAATGTAAGGAG 780

261 K L V P F L K K V G F N P K K D I H F M 280
 781 AAACTAGTGCCATTTGAAAAAGTTGGCTTCAATCCAAAAGGACATTCACTTATG 840

281 P C S G L T G A N L K E Q S D F C P W Y 300
 841 CCCTGCTCAGGACTTACTGGAGCAAATCTCAAAGAGCAGTCGGATTCTGTCCTGGTAC 900

301 I G L P F I P Y L D N L P N F N R S V D 320
 901 ATGGATTACCGTTATTCCATATCTGGATAATTGCCGAACCTCAATAGATCAGTTGAT 960

321 G P I R L P I V D K Y K D M G T V V L G 340
 961 GGACCAATCAGGCTGCCAATTGTGGATAAGTACAAGGATATGGGCACTGTGGTCCTGGGA 1020

Appendix

341 K L E S G S I C K G Q Q L V M M P N K H 360
1021 AAGCTGGAATCAGGATCTATTGTAAAGGCCAGCAGCTGTGATGCCAAACAAGCAC 1080

361 N V E V L G I L S D D V E T D T V A P G 380
1081 AACGTGGAAGTTCTTGGAAATACTTCCGATGATGTAGAGACTGATAACGTAGCCCCAGGT 1140

381 E N L K I R L K G I E E E E I L P G F I 400
1141 GAAAACCTCAAAATCAGACTGAAAGGAATTGAAGAAGAGGAGATTCTCAGGGTTATA 1200

401 L C D P N N L C H S G R T F D A Q I V I 420
1201 CTTTGTGATCCTAATAATCTTGTCAATTCTGGACGCACATTGATGCCAGATACTGATT 1260

421 I E H K S I I C P G Y N A V L H I H T C 440
1261 ATAGAGCACAAATCCATCATCTGCCAGGCTATAATGCGGTGCTGCATATTACACGT 1320

441 I E E V E I T A L I C L V D K K S G E K 460
1321 ATTGAGGAGGTGAAATAACAGCCTTAATCTGCTTGGTAGACAAAAATCAGGAGAAAA 1380

461 S K T R P R F V K Q D Q V C I A R L R T 480
1381 AGTAAGACCCGACCCGTTTGTCAAACAAGATCAAGTATGCATTGCTCGCTTAAGGACA 1440

481 A G T I C L E T F K D F P Q M G R F T L 500
1441 GCAGGAACCATCTGCCTTGAGACCTTAAAGACTTCCCTCAGATGGTCGTTCACCTTA 1500

501 R D E G K T I A I G K V L K L V P E K D 520
1501 AGAGATGAGGGTAAGACCATTGCAATTGGAAAAGTTCTGAAACTGGTCCAGAGAAAGAC 1560

521 * 521
1561 **TAA** 1563

7.1.9 pETDuet-1 heRF3a Full Length

Appendix

341 A K T A G V K H L I V L I N K M D D P T 360
1021 GCAAAGACAGCAGGTGAAACACCTAATTGTGCTAATTAAAGATGGATGATCCAACA 1080

361 V N W S N E R Y E E C K E K L V P F L K 380
1081 GTAAATTGGAGCAATGAGAGATATGAAGAATGTAAGGAGAAACTAGTGCCTTTGAAA 1140

381 K V G F N P K K D I H F M P C S G L T G 400
1141 AAAGTTGGCTTCAATCCAAAAAGGACATTCACTTTATGCCCTGCTCAGGACTTACTGGA 1200

401 A N L K E Q S D F C P W Y I G L P F I P 420
1201 GCAAATCTCAAAGAGCAGTCGGATTCTGCCTTGGTACATTGGATTACCGTTATTCCA 1260

421 Y L D N L P N F N R S V D G P I R L P I 440
1261 TATCTGGATAATTCGCCAACTCAATAGATCAGTTGATGGACCAATCAGGCTGCCATT 1320

441 V D K Y K D M G T V V L G K L E S G S I 460
1321 GTGGATAAGTACAAGGATATGGCACTGTGGCCTGGAAAGCTGGAATCAGGATCTATT 1380

461 C K G Q Q L V M M P N K H N V E V L G I 480
1381 TGTAAAGGCCAGCAGCTGTGATGATGCCAAACAAGCACACGTGGAAGTTCTGGAATA 1440

481 L S D D V E T D T V A P G E N L K I R L 500
1441 CTTTCCGATGATGTAGAGACTGATACCGTAGCCCCAGGTGAAAACCTCAAATCAGACTG 1500

501 K G I E E E I L P G F I L C D P N N L 520
1501 AAAGGAATTGAAAGAGGAGATTCTCCAGGGTTATACTTGATCCTAATAATCTT 1560

521 C H S G R T F D A Q I V I I E H K S I I 540
1561 TGTCAATTCTGGACGCACATTGATGCCAGATAGTGATTAGAGCACAAATCCATCATC 1620

541 C P G Y N A V L H I H T C I E E V E I T 560
1621 TGCCCAGGCTATAATGCGGTGCTGCATATTACACCTGTATTGAGGAGGTGGAAATAACA 1680

561 A L I C L V D K K S G E K S K T R P R F 580
1681 GCCTTAATCTGCTTGGTAGACAAAAATCAGGAGAAAAAGTAAGACCCGACCCGTTTT 1740

581 V K Q D Q V C I A R L R T A G T I C L E 600
1741 GTCAAACAAGATCAAGTATGCATTGCTCGCTTAAGGACAGCAGGAACCCTGCTTGAG 1800

601 T F K D F P Q M G R F T L R D E G K T I 620
1801 ACCTTAAAGACTTCCCTCAGATGGGTCGTTCACCTAAGAGATGAGGGTAAGACCATT 1860

621 A I G K V L K L V P E K D * 634
1861 GCAATTGGAAAAGTTCTGAAACTGGTCCAGAGAAAGAC TAA 1902

7.1.10 pETDuet-1 heRF3a Full Length-3C-(His)₈

Appendix

341 A K T A G V K H L I V L I N K M D D P T 360
1021 GCAAAGACAGCAGGTGTAAAACACCTAATTGTGCTAATTAAAGATGGATGATCCAACA 1080

361 V N W S N E R Y E E C K E K L V P F L K 380
1081 GTAAATTGGAGCAATGAGAGATATGAAGAATGTAAGGAGAAACTAGTGCCATTGGAAA 1140

381 K V G F N P K K D I H F M P C S G L T G 400
1141 AAAGTTGGCTTCAATCCCAAAAAGGACATTCACTTATGCCCTGCTCAGGACTTACTGGA 1200

401 A N L K E Q S D F C P W Y I G L P F I P 420
1201 GCAAATCTCAAAGAGCAGTCGGATTCTGTCTGGTACATTGGATTACCGTTATTCCA 1260

421 Y L D N L P N F N R S V D G P I R L P I 440
1261 TATCTGGATAATTGCCGAACCTCAATAGATCAGTTGATGGACCAATCAGGCTGCCAATT 1320

441 V D K Y K D M G T V V L G K L E S G S I 460
1321 GTGGATAAGTACAAGGATATGGGCACTGTGGCCTGGAAAGCTGGAATCAGGATCTATT 1380

461 C K G Q Q L V M M P N K H N V E V L G I 480
1381 TGTAAAGGCCAGCAGCTTGTGATGATGCCAACAGCACAACTGGAAAGTTCTTGGAAATA 1440

481 L S D D V E T D T V A P G E N L K I R L 500
1441 CTTCCGATGATGTAGAGACTGATACCGTAGCCCCAGGTGAAAACCTCAAAATCAGACTG 1500

501 K G I E E E I L P G F I L C D P N N L 520
1501 AAAGGAATTGAAGAAGAGGAGATTCTCAGGGTTATACTTGTGATCCTAATAATCTT 1560

521 C H S G R T F D A Q I V I I E H K S I I 540
1561 TGTCAATTCTGGACGCACATTGATGCCAGATACTGATTATAGAGCACAAATCCATCATC 1620

541 C P G Y N A V L H I H T C I E E V E I T 560
1621 TGCCCAGGCTATAATCGGGTGCATATTACCTGTATTGAGGAGGTGGAAATAACA 1680

561 A L I C L V D K K S G E K S K T R P R F 580
1681 GCCTTAATCTGCTTGGTAGACAAAAATCAGGAGAAAAAGTAAGACCCGACCCGTTTT 1740

581 V K Q D Q V C I A R L R T A G T I C L E 600
1741 GTCAAACAAGATCAAGTATGCATTGCTCGCTTAAGGACAGCAGGAACCCTGAG 1800

601 T F K D F P Q M G R F T L R D E G K T I 620
1801 ACCTTAAAGACTTCCTCAGATGGTCGTTCACCTTAAGAGATGAGGGTAAGACCATT 1860

621 A I G K V L K L V P E K D L E V L F Q G 640
1861 GCAATTGGAAAAGTTCTGAAACTGGTCCAGAGAAAGACCTGGAAGTTCTGTTCCAGGG 1920

641 P D Y D I P T T H H H H H H H H H H * 657
1921 CCCGATTACGATATTCAACGACCCTCACCATCACCATCAC TAA 1971

7.1.11 pETDuet-1 (His)₈-3C-heRF3a Full Length

1 M G H H H H H H H H D Y D I P T T L E V 20
 1 ATGGGT CATCACCATCACCATCAC GATTACGATATTCCAACGACC CTGGAAGTT 60

21 L F Q G P D P G S G G G G G G G G S S S 40
 61 CTGTTCCAGGGGCCCCGATCCGGGCAGTGGCGGCAGGCGGTGGGAGCAGCAGC 120

41 G S S S S D S A P D C W D Q A D M E A P 60
 121 GGCAGCAGCAGCAGCGACTCGGCGCCTGACTGCTGGGACCAGGCGGACATGGAAGCCCC 180

61 G P G P C G G G S L A A A A E A Q R E 80
 181 GGGCCGGGCCCTTGCGGCAGGCGCTCCCTGGCGCGGGCAGGCCCAGCGGGAG 240

81 N L S A A F S R Q L N V N A K P F V P N 100
 241 AACCTCAGCGCGGCCTTCAGCCGGCAACTCAACGTCAACGCCAGGCC TTCGTGCCAAC 300

101 V H A A E F V P S F L R C P A A P P P P 120
 301 GTCCACGCCGCCAGTTCTGCGCCCTTCAGGGCAGCGGCCAGCGGCCACCCCA 360

121 A G G A A N N H G A G S G A G G R A A P 140
 361 GCTGGCGGCCGCCAATAACCACGGAGCCGGCAGCGCGCGGGAGGCCGTGCGGCACCT 420

141 V E S S Q E E Q S L C E G S N S A V S M 160
 421 GTGGAATCCTCTCAAGAGGAACAGTCATTGTGTGAAGGTTCAAATTCAAGCTGTTAGCATG 480

161 E L S E P I E N G E T E M S P E E S W E 180
 481 GAACTTCAAGAACCTATTGAAAATGGAGAGACAGAAATGTCTCCAGAAGAACATGGAG 540

181 H K E E I S E A E P G G G S L G D G R P 200
 541 CACAAAGAAGAAATAAGTGAAGCAGAGCCAGGGGTGGTCCTGGGAGATGGAAGGCCG 600

201 P E E S A H E M M E E E E I P K P K S 220
 601 CCAGAGGAAAGTGCCATGAAATGATGGAGGAGGAAGAGGAATCCCACCTAAGTCT 660

221 V V A P P G A P K K E H V N V V F I G H 240
 661 GTGGTTGCACCGCCAGGTGCTCTAAGAAAGAGCATGTAAATGTAGTATTCAATTGGCAC 720

241 V D A G K S T I G G Q I M Y L T G M V D 260
 721 GTAGATGCTGGCAAGTCAACCATTGGAGGACAAATAATGTATTGACTGGAATGGTTGAC 780

261 K R T L E K Y E R E A K E K N R E T W Y 280
 781 AAAAGGACGCTTGAAGATGAAAGAGAGCTAAAGAGAAAAACAGAGAAACTGGTAC 840

281 L S W A L D T N Q E E R D K G K T V E V 300
 841 TTGTCTTGGGCCTTAGACACAAATCAGGAAGAACGAGACAAGGGTAAACAGTAGAAGTG 900

301 G R A Y F E T E K K H F T I L D A P G H 320
 901 GGTGCGCTATTGAAACCGAAAAGAACGATTTACAATTCTAGATGCCCTGGCAC 960

321 K S F V P N M I G G A S Q A D L A V L V 340
 961 AAGAGTTTGTCCCAAATATGATTGGTGGTGCCTCTCAAGCTGATTGGCTGTGCTGGTA 1020

Appendix

341 I S A R K G E F E T G F E K G G Q T R E 360
1021 ATCTCAGCCAGGAAAGGAGAGTTGAACTGGATTGAAAAAGGAGGACAGACAAGAGAA 1080

361 H A M L A K T A G V K H L I V L I N K M 380
1081 CATGCAATGTTGGCAAAGACAGCAGGTGTAAAACACCTAATTGTGCTAATTAAAGATG 1140

381 D D P T V N W S N E R Y E E C K E K L V 400
1141 GATGATCCAACAGTAAATTGGAGCAATGAGAGATATGAAGAATGTAAGGAGAAACTAGTG 1200

401 P F L K K V G F N P K K D I H F M P C S 420
1201 CCATTTTGAAAAAGTTGGCTTCAATCCAAAAAGGACATTCACTTATGCCCTGCTCA 1260

421 G L T G A N L K E Q S D F C P W Y I G L 440
1261 GGACTTACTGGAGCAAATCTCAAAGAGCAGTCGGATTTCTGTCCTGGTACATTGGATTA 1320

441 P F I P Y L D N L P N F N R S V D G P I 460
1321 CCGTTTATTCCATATCTGGATAATTGCCGAACCTCAATAGATCAGTTGATGGACCAATC 1380

461 R L P I V D K Y K D M G T V V L G K L E 480
1381 AGGCTGCCAATTGTGGATAAGTACAAGGATATGGCACTGTGGCCTGGAAAGCTGGAA 1440

481 S G S I C K G Q Q L V M M P N K H N V E 500
1441 TCAGGATCTATTGTAAAGGCCAGCAGCTGTGATGATGCCAAACAAGCACACGTGGAA 1500

501 V L G I L S D D V E T D T V A P G E N L 520
1501 GTTCTTGGAAATACTTCCGATGATGTAGAGACTGATACCGTAGCCCCAGGTGAAACCTC 1560

521 K I R L K G I E E E I L P G F I L C D 540
1561 AAAATCAGACTGAAAGGAATTGAAGAAGAGGAGATTCTCAGGGTTTACTTGTGAT 1620

541 P N N L C H S G R T F D A Q I V I I E H 560
1621 CCTAATAATCTTGTCAATTCTGGACGCACATTGATGCCAGATAGTGATTATAGAGCAC 1680

561 K S I I C P G Y N A V L H I H T C I E E 580
1681 AAATCCATCATCTGCCAGGCTATAATGCGGTGCTGCATATTACACCTGTATTGAGGAG 1740

581 V E I T A L I C L V D K K S G E K S K T 600
1741 GTGAAATAACAGCCTTAATCTGCTTGGTAGACAAAAAATCAGGAGAAAAAAGTAAGACC 1800

601 R P R F V K Q D Q V C I A R L R T A G T 620
1801 CGACCCCGTTTGTCAAACAAGATCAAGTATGCATTGCTCGCTTAAGGACAGCAGGAACC 1860

621 I C L E T F K D F P Q M G R F T L R D E 640
1861 ATCTGCCTTGAGACCTTAAAGACTTCCCTCAGATGGTCGTTCACCTTAAGAGATGAG 1920

641 G K T I A I G K V L K L V P E K D * 658
1921 GGTAAGACCATTGCAATTGGAAAAGTTCTGAACTGGTCCAGAGAAAGACTAA 1974

7.2 Plasmid Construct for the Human *in vitro* Translation System

Color code

 CrPV IGR IRES sequence

 linker

 ATG start codon

 (His)₆-tag

 3C-cleavage site

 HA-tag

 hCMV-stalling sequence

 TAA stop codon

 poly(A)-tail

7.2.1 pT7CFE1 CrPV IGR IRES-linker-(His)₆-3C-HA-hCMV-p(A)₂₆ with TAA(A)

Constructs containing the TAG(A), TGA(A) and TAA(G) stop codons were similarly constructed.

1 AAAGCAAAATGTGATCTGCTTGTAAATACAATTGAGAGGTTAATAATTACAAGTA 60

61 GTGCTATTTGTATTAGTTAGCTATTAGCTTACGTTCCAGGATGCCTAGTGGCAG 120

121 CCCCCACAATATCCAGGAAGCCCTCTCTGCGGTTTCAGATTAGGTAGTCGAAAACCTA 60
180

181 AGAAATTTACCTgaaaaacacgatgataatatggccaccaccaccaccacactggcc 240

11 T T H M L E V L F Q G P Y P Y D V P D Y 30
241 accacccatatgCTGGAAGTGCCTGTTCAAGGGCCCGtaccacatacgatgttccagattac 300

31 A E G G E E V E R I P D E L F D T K K 50
301 gctGAAGGTGGCGAAGAAGAAGTTGAGCGCATTCTGATGAACTTTCGATACAAAAAAG 360

51 K H L L D E F H S N T P D Y Q E P N S N 70
361 AAGCATTGTTAGATGAATTCCATTCAAACACACCAGATTATCAAGAACCCAACTCTAAT 420

71 Y T N D G K L K V S F S V V R N N T F Q 90
421 TACACCAATGATGGAAATTAAAGGTGTCGTTCTGTTGTAAGAAACAATACATTCAA 480

91 P K Y H E L Q W I S D N K I E M E P L V 110
481 CCCAAATATCACGAGCTGCAATGGATTAGTGACAATAAAATTGAAATGGAACCGCTGGTG 540

101 L S A K K L S S L L T C K Y I P P * 130
541 CTGAGTGCAGAAAAACTGAGCAGCCTGCTGACCTGCAAATATATTCCCTCCTTAAAcactc 600

601 gagtgagatctgactgaaaaaaaaaaaaaaaaaaaaa 642

8 Acknowledgements

Undertaking this PhD has been a truly life-changing experience accompanied with both painful and enjoyable experiences. The latter would not have been possible without many people who I want to express my sincere gratitude to.

First, I want to thank my supervisor Prof. Dr. Roland Beckmann for convincing me to pursue my PhD in his lab, for the excellent scientific environment by providing any necessary equipment to establish my project from scratch, for the large freedom in my research and for the trust in me to succeed in this competitive field. Also, I want to thank Dr. Thomas Becker here for taking great care of funding for my project and to ensure cluster stability especially in times of required speed-calculations.

Further, I want to thank the International Max Planck Research School for Molecular and Cellular Life Sciences (IMPRS) for supporting me during my PhD by numerous workshops, extracurricular activities and new friendships. Thank you Dr. Hans-Joerg Schaeffer, Dr. Ingrid Wolf and Maximiliane Reif from the IMPRS coordination office for so thoughtfully running the inspiring graduate school. In this context, I also want to thank my Thesis Advisory Committee (TAC) members Dr. Daniel N. Wilson and Prof. Dr. Elena Conti for the annual evaluations and discussions on my research project and I want to thank my lab mates Dr. Stephan Wickles, Dr. Julian Deeng and Dr. Lukas Bischoff for suggesting to also become part of the IMPRS program and always making sure we had an excellent time there.

I am very grateful to Andrea Gilmozzi to work with me throughout this challenging project and to never disbelieve that the enormous hours she spent cloning, pipetting or in the cell culture will lead to a successful project in the end. Working with her made the project much more fun.

Furthermore, I want to acknowledge Dr. Bertrand Becker who has always cared, shared his ideas and was never unwilling to help anyone in the lab. Thank you also Dr. Stefan Arenz, Christian Schmidt and Dr. Stephan Wickles for introducing me to the world of processing and providing help with acquiring my own associated 'Autobahn'.

Also, I greatly appreciate Dr. Eli van der Sluis and Dr. Birgitta Beatrix because I could always come to them with any questions concerning biochemical approaches and realizations. They have always put thought and research in their answers even though it was not directly related to their projects, they never hesitated to support me and provide input.

Further, thank you Dr. Andreas Anger, Dr. Jean-Paul Amarche, Dr. Lukas Bischoff, Dr. Caroline Haas and Dr. Christoph Leidig for saving me from at least some of the pitfalls that science holds and providing me with a welcoming start in the lab.

A very special thanks also to Dr. Otto Berninghausen, Joanna Musial, Susanne Rieder, Heidi Sieber, Charlotte Ungewickell and Ingegerd Walz for keeping the lab and the cryo-EM facility up and running and for always making sure everything is organized properly.

Importantly, I also want to thank my friends and family outside of the lab who were really understanding and supporting (and even sent me CARE packages) throughout the past years even though I could not always set my priorities on them. Finally, I want to thank Dr. Daniel Sohmen not only, but particularly for his moral and action-taking support during the 'scooping time', for never hesitating to help when things became rough and for making sure I always had a supporting (lunch) partner.